UNIVERSITY OF BIRMINGHAM

SEISMIC RESPONSE OF ACCELERATION-SENSITIVE NON-STRUCTURAL COMPONENTS MOUNTED ON IRREGULAR MULTI-STOREY REINFORCED CONCRETE BUILDINGS

by

AYAD BASHEER ALDEKA

A thesis submitted to
The School of Civil Engineering
The University of Birmingham

For the degree of
DOCTOR OF PHILOSOPHY

School of Civil Engineering
College of Engineering and Physical Sciences
University of Birmingham
January 2015

ABSTRACT

This research investigates the seismic response of lightweight acceleration-sensitive non-structural components (NSCs) integrated on sixty four different cases of irregular multi-storey reinforced concrete (RC) structures designed on different ground types. Dynamic nonlinear finite element (FE) analyses of the primary-secondary (P-S) systems were carried out to provide insight into the seismic response of the NSCs and to evaluate the accuracy of Eurocode 8 (EC8) provisions for the design of NSCs. The effects of the plan and/or vertical mass irregularities of the primary structures (P-structures) were investigated to quantify the dynamic amplification of the NSCs induced by the torsional behaviour. Various sets of natural and artificial earthquake records consisting of seventy accelerograms were used. Appropriate constitutive relationships were used to model the behaviour of the RC P-structures. The NSCs were modelled as vertical cantilevers fixed at their bases with masses on the free ends. The lengths of the NSCs were chosen in such a way that the NSCs vibration periods match the vibrations periods of the P-structures. Full dynamic interaction was considered between the NSCs and P-structures. The investigated parameters include the NSC to P-structure vibration period ratio, peak ground acceleration, NSC to P-structure height ratio, P-structure eccentricity ratio, and NSC damping ratio. The effect of ground type (namely ground types A, B, C, D and E as defined in EC8) on the seismic response of NSCs integrated on irregular multi-storey RC structures was also investigated. The numerical results indicate that the seismic behaviour of the NSCs is significantly influenced by the investigated parameters. The results concluded that during earthquakes, the seismic response of NSCs can be amplified by the torsional behaviour of the P-structures to which NSCs are attached. Furthermore, comparison between the FE results and the corresponding predictions of the EC8 for the accelerations of the NSCs at the design

acceleration values, suggests that the recommendations of the EC8 underestimate the NSCs accelerations by up to 43% for NSCs attached to the flexible sides, and in resonance with one of the first three vibration periods of the P-structures. The perceived cause of this discrepancy is that EC8 does not take into account the amplification in the dynamic response of NSCs induced by the torsional behaviour of RC P-structures. Consequently, the current EC8 equation for the design of NSCs was modified, assuming a NSC damping ratio of 3%. The effects of both the torsion and maximum seismic capacity of a P-structure were taken into account in this improvement. The accuracy of the modified expression is also verified against extensive dynamic analyses of simple and complicated cases of P-S systems.

ACKNOWLEDGEMENTS

It is a great pleasure for me to be able to thank and honour Dr Dirar, Professor Chan, and Dr Martinez-Vazquez for their permission when they accepted to be my supervisors and their kindness and helpfulness has followed every development in my research. It is truly that I am impressed with their spacious proficiency in the specialty of earthquakes. I have benefited a lot from their important ideas and original concepts. I am fortunate to have an opportunity to work under their expertise. Respectful thanks for their encouragement during my research. I would like to extend my thanks to Dr Yaser Jemaa for his help and crucial contribution to this dissertation.

I would like to thank Mr Edmund Booth, Fellow of the Royal Academy of Engineering and Chair of BSI Committee B/525/8 for EC8, for his valuable comments on the adopted methodology and the results presented in the current research.

Special thanks go to all academic, administrative and technical staff in the School of Civil Engineering, the University of Birmingham.

This research was funded by the Iraqi Government and their financial support is gratefully acknowledged. Great thanks to the Iraqi Minister of Higher Education and Scientific Research for awarding me an Appreciation Certificate. This certificate was issued to recognise my publications achieved during the PhD study. In addition, I would like to thank all staff of the Iraqi Cultural Attaché in London for their cooperation and support.

I much appreciate the professional 'Janet's Proofreading Service' for editing my thesis as a third party editor.

Finally, warm thanks to my family (parents, brothers, sisters, wife and my sons) for their support and the great help that they gave me and especially for always being close throughout the last few years.

Thanks to everyone who encouraged and supported me, even with a single good word.

- Table of Contents
- List of Figures
- List of Tables
- List of Notations
- List of Abbreviations

TABLE OF CONTENTS

LIST OF FIGURES

LIST OF TABLES

NOTATIONS

A_p^a	the acceleration amplification factor of NSCs estimates as PCA/PGA
A_p^ξ	the acceleration amplification factor of NSCs due to a reduction in the value of damping ratio
a_1	first isotropic hardening parameter of a steel reinforcement
a_2	second isotropic hardening parameter of a steel reinforcement
a_g	the design value of ground acceleration on ground type A
av_g	the design value of vertical acceleration
a_{gR}	the reference peak-ground acceleration on ground type A
b	strain hardening ratio of a steel reinforcement
C_a	horizontal seismic factor for a specific ground type
d_m	the displacement at ultimate strength of a MDOF system
d_m^*	the effective displacement at ultimate strength of a SDOF system
d_t	the target displacement of a MDOF system
d_t^*	the target displacement of the idealised equivalent SDOF system at T^*
d_{et}^*	the target displacement of MDOF system at T^* and unlimited elastic behaviour
d_y	the displacement at yield strength of a MDOF system
d_y^*	the yield displacement of the idealised equivalent SDOF system
E_c	the tangent modulus of elasticity of the concrete
E_m	the actual deformation energy of a MDOF system
E_m^*	the effective deformation energy of the idealised equivalent SDOF system
E_{sec}	the secant modulus of elasticity of the concrete
E_0	the initial tangent stiffness of a steel reinforcement
E_1	the final tangent stiffness of a steel reinforcement
e_x	the eccentricity value in the *x* direction
e_y	the eccentricity value in the *y* direction

F_{Sc}	the maximum seismic capacity of a building
F_p	horizontal seismic design force for non-structural component
F_T	torsional amplification factor of non-structural component
F_y	the ultimate strength of a MDOF system
F_y^*	the ultimate strength of the idealised equivalent SDOF system
f_c	the longitudinal compressive stress of the concrete
f'_{cc}	the ultimate compressive strength of the confined concrete
f'_{co}	the unconfined concrete strength
f'_l	the effective lateral confinement stress of concrete
f'_t	the concrete tensile strength
g_x	coordinate of centre of mass in the *x* direction
g_y	coordinate of centre of mass in the *y* direction
H	total height of a building
I_B	the percentage of the increase in the acceleration of NSC when the mass irregularity occurs at the bottom floors of a building
I_M	the percentage of the increase in the acceleration of NSC when the mass irregularity occurs at the middle floors of a building
I_T	the percentage of the increase in the acceleration of NSC when the mass irregularity occurs at the top floors of a building
I_{TB}	the percentage of the increase in the acceleration of NSC when the mass irregularity occurs at the combination case of top and bottom floors of a building
I_{TM}	the percentage of the increase in the acceleration of NSC when the mass irregularity occurs at the combination case of top and middle floors of a building
K_a	the lateral stiffness of the circular arm of non-structural component
K_R	the torsional stiffness of a storey structural elements of a building
K_x	the lateral stiffness in the *x* direction of a storey structural elements
K_y	the lateral stiffness in the *y* direction of a storey structural elements
L_a	the length of the circular arm of non-structural component
L_m	location of the mass irregularity along the building height
l_s	radius of gyration of the floor mass in plan

l_x	coordinate of centre of rigidity in the *x* direction
l_y	coordinate of centre of rigidity in the *y* direction
Ḿ	total floor masses in three consecutive irregular masses floors
Ms	moment magnitude of a surface seismic wave
m_i	mass value in the *i-th* floor
m_r	the floor mass ratio
m^*	effective mass of an equivalent SDOF system
q	the upper magnitude of the behaviour factor of the structural system
q_o	the primary magnitude of the behaviour factor of the structural system
R	independent parameter which defines the curvature of the transition in a steel reinforcement
R_{ex}	the eccentricity ratio of a floor in the *x* direction
r_x	radius of elasticity of a floor in the *x* direction
R_{ey}	the eccentricity ratio of a floor in the *y* direction
r_y	radius of elasticity of a floor in the *y* direction
R_o	exponential transition elastic-plastic of a steel reinforcement
S_a	the seismic coefficient applicable to non-structural component
S	the soil factor
$S_e(T)$	shape function of elastic response spectral of the seismic action
S_{ay}	acceleration at yield point of a MDOF system
$S_{ae}(T^*)$	elastic acceleration response spectrum at the effective period T^*
S_{ag}	design response spectrum
T_C	natural period of non-structural component
T	vibration period of a system
T^*	effective period of SDOF system
TB	the lower period of the constant horizontal spectral shape
TC	the upper period of the constant horizontal spectral shape

TD	the value which indicates the start point of the constant displacement limit of a spectrum
W	weight of a building
W_p	weight of an equipment
z_c	location of NSC along the height of a building with respect to the location of implementation of the seismic impact
α	the ratio of the design value of ground acceleration for ground type A to the gravity's acceleration g
α_1	a parameter reflecting the initial influence of the flexural resistance in the structural members
α_u	a parameter reflecting the development of the plastic hinges in the structural members
β	Newmark's time integration parameter controls the variation in the acceleration during a time step
γ	Newmark's time integration parameter controls the amount of the artificial damping introduced by a time step
γ_I	importance factor of a structure
γ_{Rd}	over-strength factor of the structural elements
ε_c	the longitudinal concrete compressive strain
ε_{cc}	value of the concrete strain corresponding to the value of the ultimate compressive strength of the confined concrete
ε_{co}	value of the concrete strain corresponding to the value of the unconfined concrete strength
ε_{sp}	value of the concrete spalling strain corresponding to the value of the concrete stress equal to zero
ε_t	concrete tensile strain
ε^*	the effective strain of a steel reinforcement
ε_s	strain of a steel reinforcement
ε_r	strain of a steel reinforcement at unloading point, which is assumed equal to (0) at the initial elastic state
ε_o	strain of a steel reinforcement at point of intersection of two asymptotes, which defines the current loading or unloading path
η	the damping correction factor of elastic response spectrum
$\dot{\eta}$	the number of floors with a mass irregularity

θ	the floor rotation
μ	the value of ductility of a primary structure
ξ_c	the viscous damping ratio of non-structural component
ξ_S	the variance between two values of strains in a steel reinforcement
σ^*	effective stress of a steel reinforcement
σ_s	stress of a steel reinforcement
σ_r	stress of a steel reinforcement at unloading point, which is assumed equal to (0) at the initial elastic state
σ_o	stress of a steel fibre at point of intersection of two asymptotes, which defines the current loading or unloading path
Φ_i	normalised displacements of a MDOF system
Γ	transformation factor between MDOF and SDOF systems

ABBREVIATIONS

BSSC	Building Seismic Safety Council
CM	Centre of Mass
CR	Centre of Rigidity
CQC	Complete Quadratic Combination
DCM	Ductility Class Medium
ESD	European Strong-motion Database
FEA	Finite Element Analysis
FEMA	Federal Emergency Management Agency
FRS	Floor Response Spectrum
ITACA	Italian Accelerometric Archive
MDOF	Multi-Degree-Of-Freedom
NC	Near Collapse
NDOF	Number- Degree-Of-Freedom
NEHRP	National Earthquake Hazards Reduction Program
PCA	Peak Component Acceleration
PGA	Peak Ground Acceleration
PSA	Pseudo Acceleration
PSD	Power Spectral Density
RS	Response Spectrum
SDOF	Single-Degree-Of-Freedom
SIMBAD	Selected Input Motions for displacement-Base Assessment and Design
SQRSS	Square Root of the Sums of the Squares
TMD	Tuned Mass Damper

CHAPTER ONE: INTRODUCTION

1.1 Background

The term "non-structural components" (NSCs) refers to secondary systems (S-systems) attached to a structure but are not considered as part of the main structural elements of the structure. The S-systems can be adversely affected by the seismic response of primary systems (P- systems) under the effect of earthquakes (Villaverde, 1991; Whittaker and Soong, 2003; Mondal and Jain, 2005). Conventionally, NSCs have been classified as the architectural, mechanical and electrical elements and contents of a main structure (Naeim, 2001; Whittaker and Soong, 2003; Griffin, 2006; ASCE, 2010; Kaynia, 2013). Non-loaded walls, cladding elements, and suspended ceilings are examples of the architectural parts; whereas, fire protection elements, air conditioning devices, and boilers are classified as mechanical components. Electric motors, some medical equipment, and computer systems can be classified as electrical components.

According to their nature and performance, as well as their properties, the NSCs can be affected by significant inertia forces, accelerations and/or deformations induced by the primary structures (P-structures) during the effect of base motions (FEMA, 1997a; Villaverde, 1997a). Therefore, based on their behaviour and the primary nature of the damage, NSCs can be divided into three groups: acceleration-sensitive, deformation-sensitive, or acceleration and deformation-sensitive systems (FEMA, 1997a; Gillengerten, 2001; Kaynia, 2013). Non-

structural components can be considered as acceleration-vulnerable when their accelerations are affected by the floor accelerations of the P-structures. Satisfactory functioning of these types of S-systems can be achieved by evaluating the maximum acceleration values which these S-systems may be subjected during their attachments to the P-structures under the effect of the seismic forces. Subsequently, the anchors or braces of the S-systems can be designed to prevent any shifting or overturning during the seismic action (ASCE, 2010). Generally, the fixed-base S-systems, such as most of the mechanical and electrical equipment, can be classified as acceleration-sensitive components (Gillengerten, 2001; Kaynia, 2013). However, the components can be categorised as deformation vulnerable if they are affected by the lateral displacements of the floors that can be estimated typically by the values of the inter-storey drifts (FEMA, 1997a; Gillengerten, 2001). Therefore, damage of these types of components can be controlled by designing the P-structures to fulfil the requirements of the damage limitations of the inter-storey drift ratios (FEMA, 1997a). Restrained S-systems in a building can be considered as deformation-sensitive components (Kaynia, 2013). Most of architectural elements or those components that provide a continuous link between two different floor levels are examples of the deformation-sensitive S-systems.

Furthermore, the components are classified as acceleration and deformation-sensitive S-systems when their failure is controlled by both the amplification in the accelerations and the inter-storey drift of the P-structures (FEMA, 1997a; Gillengerten, 2001). Consequently, the design of the S-systems and the supporting structures, to fulfil the acceleration amplification factors for S-systems and the limitations of the lateral displacement of the P-structures, is the main factor that can be adopted to make these types of S-systems functional during earthquakes. An example of the systems that can be affected by both the floor

accelerations and floor displacements are elevators that consist of walls, doors and in some cases, glass, that are mainly destroyed by the effect of the inter-storey drift. On other hand, electrical motors and counter masses of the elevators can be damaged due to the amplification in the accelerations of the floors along the building height. Based on the above classifications, Figure 1.1 shows various S-systems as presented in FEMA 273/274 (1997a, 1997b).

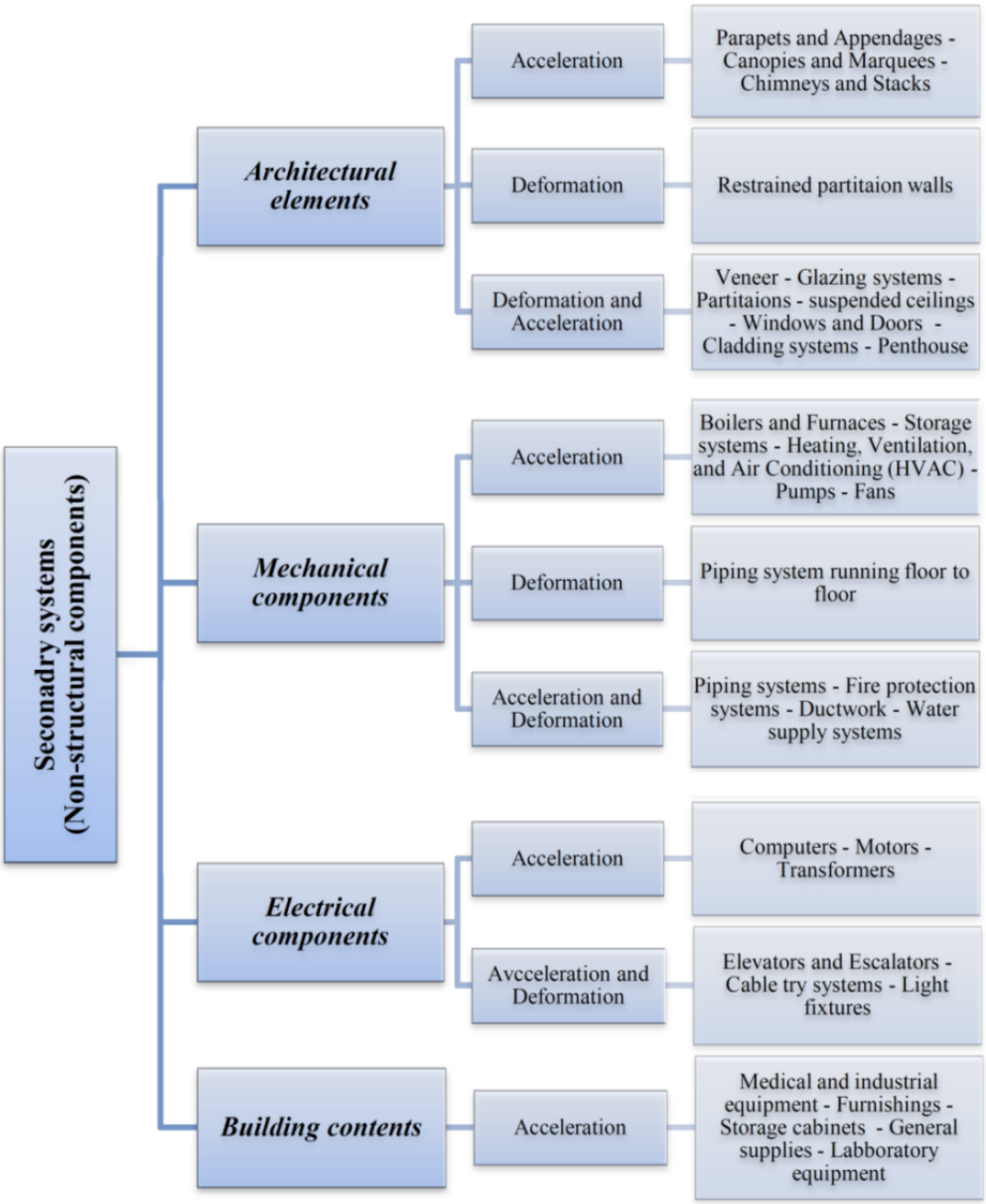

Figure 1.1 Classification of the S-systems as presented in FEMA 273/274 (1997a, 1997b).

After most earthquake events, it was recognised that damage to the S-systems integrated on the P-structures could have a considerable effect on the life of the occupants and the function of some parts of the main structures (McKevitt, 2004). Therefore, based on the losses suffered after the damage to the S-systems during the seismic loading, another classification for the S-systems can be defined. This classification includes failure that denotes as a life risk, failure that characterises the damage of the supporting building function and the damage that relates principally to the economic loss (Watts, 2004). The hazard assessment of the S-systems should also be made based on their location on the floors of the supporting building (i.e. stiff or flexible sides), anchorage condition (i.e. free or fixed-base) and their frequencies (i.e. rigid or flexible S-systems), etc. S-systems should be assessed for one mode of hazard. For priority purposes, when the S-system may be exposed to more than one mode of hazard, then the risk that causes losses in human life should be selected first. The risk due to the losses in the function of the P-structure should be selected second. Lastly, the hazard due to the economic losses should then be chosen (Guragain *et al.*, 2004; FEMA, 2007). The S-systems can be considered as rigid if their periods are less than 0.06 s; however, for periods greater than this value, the NSCs are classified as flexible components (BSSC, 2003). Rigid NSCs are expected to expose the equivalent values of acceleration as the floor of a building at their points of attachment (Rodriguez *et al.*, 2002; Lepage *et al.*, 2012). However, in particular for NSCs having periods matching the fundamental vibration periods of the P-systems, NSCs experience amplification in the accelerations more than those values of the floor at the same points of contact.

In most of the primary-secondary (P-S) systems, the S-systems constitute a considerable percentage of the total cost; accordingly, the economic losses due to failure of

the S-systems can be significant (Segal and Hall 1989; Naeim 2000; Myrtle *et al.*, 2005). Certainly, in recent base motions events, the economic losses accountable to the S-systems have been found generally greater than those losses related to the failure of the main structural elements. Figure 1.2 compares the costs of the NSCs, contents, and the main structural components (Whittaker and Soong, 2003). Obviously, this data demonstrates that the investments in the NSCs and the contents of buildings are far greater than the main structural components. The costs of the maintenance and rehabilitation of the S-systems (i.e. the NSCs and contents) were approximately equal to 82%, 87%, and 92% for those systems attached to or occupying offices, hotels, and hospitals, respectively (Whittaker and Soong, 2003).

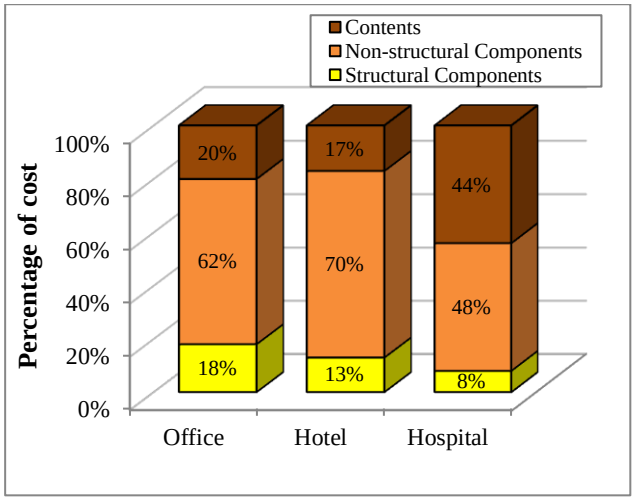

Figure 1.2 Cost comparison for the NSCs, contents, and the main structural components (Whittaker and Soong, 2003).

Owing to the damage to the NSCs and losses of human life during past earthquakes, the guidelines on the NSCs were included for the first time in the appendix of the 1927 Uniform Building Code (UBC, 1927) (cited in Mondal and Jain, 2005). It is stated that both the P-structures and S-systems should be firmly connected together as one part. After that, it was identified that similar to the main elements of the supporting structure; the S-systems

should be designed by accounting for the effect of the lateral seismic loading. Accordingly, in 1935, the approach of the estimation of the design values of the seismic forces for non-structural components as $F_p = C_a\, W_p$ is suggested in the appendix of the UBC, where C_a is a horizontal seismic factor for a specific ground type and W_p is the weight of NSC. However, this expression was not mandatory at that time for the design of the NSCs because it was not presented in the main provisions of the 1935 UBC (UBC, 1935) (cited in Mondal and Jain, 2005). This provision was unchanged until 1961, hence after that the effect of the seismic actions on the NSCs was included in the main provisions instead of the appendix of the UBC.

As the intensity of the seismic loads may increase along the building height, the estimation of the values of the amplification factors of these loads is important for design purposes of the S-systems. Consequently, the earliest formal recommendations for the seismic design of the NSCs based on the amplification of the seismic loading were reported in the main guidelines of the Tentative Provisions for the Development of the Seismic Regulation for the Building (ATC, 1978). These recommendations were also implemented in most of the seismic codes provisions such as UBC (1997), International Building Code (IBC, 2012), National Earthquake Hazards Reduction Program-NEHRP (BSSC, 2003), Eurocode 8 (EC8, 2004), and the standard of American Society of Civil Engineers (ASCE, 2010).

1.2 A Statement of the Current Research Problem

Seismic design of non-structural components is quite essential for important structures and lifeline systems. EC8 (2004) provisions state that *"for NSCs of great importance or of a*

particularly dangerous nature, the seismic analysis shall be based on a realistic model of the relevant structures". Therefore, as it is important for safety and economic purposes, extensive research efforts have been carried out over the last four decades to quantify the effect of seismic loadings and dynamic interaction of the P-S systems on the dynamic response of the NSCs.

The review of the literature on the research that studied the response of NSCs as presented in Chapter 2 has shown that the number of studies on NSC attached to regular 2-Dimensional P-structures has largely exceeded the number of studies on NSC attached to P-structures with significant torsional effects. Moreover, previous research on NSCs integrated on torsional P-structures focused on the seismic response of NSCs mounted on either simple P-structures having eccentricity in one direction between their centre of mass (CM) and centre of rigidity (CR), or single-bay P-structures with the eccentricities in the horizontal directions (X and Y). Furthermore, previous analytical studies on NSCs have produced conflicting results with regards to their seismic behaviour in spite of adopting similar sets of differential equations and modelling assumptions for the P-S system.

In addition, vertical mass irregularity and torsion, in modern structures, are two significant disadvantages in seismic zones. Therefore, it is essential to investigate their influence on the NSCs behaviour. The review of the literature on the response of the S-systems has also revealed that there are no studies dealing with NSCs attached to P-structures with vertical mass irregularities. Even though there were many previous studies as presented later in Chapter 7 that only investigated the behaviour of vertically irregular P-structures; there are conflicting conclusions with regards to their behaviour under the effect of different

cases of vertical mass irregularities. Moreover, past investigations on P-structures with plan and/or vertical irregularities do not vindicate the convenience of the proposed regularity criteria in modern design codes, e.g. EC8 (2004). As regards the NSCs, better and more meaningful comparisons may be obtained if they are attached to P-structures designed to specific code conditions.

Evaluation of the primary systems (P-systems) seismic performance requires either experimental work or analytical and numerical methods. Attributable to the large dimension of civil engineering structures such as multi-storey structures, nuclear power stations, and long-span bridges, physical tests are not usually feasible. Hence, analytical and numerical simulations are most often used for seismic structural assessment. However, due to novel materials, advanced construction techniques and modern architectural requirements, the structural layouts and composite materials used in present-day P-structures are too complicated for an analytical solution to be available. A viable solution to bridge the knowledge gap in the area of seismic response of NSCs mounted on large civil structures is to use numerical methods such as advanced finite element (FE) analysis. Accordingly, this research presents three-dimensional nonlinear dynamic FE analyses of NSCs mounted on inelastic irregular reinforced concrete (RC) multi-storey structures. The originality and innovation of this research is based on the fact that there is no available research, which has studied the seismic behaviour of NSCs mounted on inelastic multi-storey irregular RC structures experiencing significant torsional modes due to the effect of the plan and/or vertical mass irregularities, using a validated FE analysis method. The overall advantage of the present nonlinear dynamic FE analyses is that they can help identify the essential parameters

affecting the global seismic behaviour of the acceleration-sensitive NSCs mounted on different cases of multi-storey RC structures with the torsional effect.

Based on the extensive range of the adopted cases of the P-S systems and the resulting dynamic response of the NSCs in this research study, several analytical relations were developed. These relationships could be used to evaluate the increase in NSCs accelerations due to the increase in rotational displacements, masses along the heights of the P-structures, or due to decreases in damping ratios of the NSCs. Furthermore, it is worth noting that a significant modification is made to the existing formula of the EC8 (2004) for evaluating the values of the amplification in the acceleration of NSCs. The proposed equation can be used to estimate the maximum acceleration amplification factor of NSCs when they are attached to the flexible sides (FS) along the heights of the torsional RC structures. The modified expression is also verified against extensive dynamic analyses of simple and complicated building cases designed as per the modern seismic provisions of the of Eurocode 1 (EC1, 2002), Eurocode 2 (EC2, 2004), and EC8 (2004).

1.3 Aim and Objectives of the Research

The ultimate intention of the current research is to improve the predictions of the EC8 (2004) design formula for NSCs attached to the flexible sides of irregular RC structures. Furthermore, investigating the dynamic behaviour of lightweight acceleration-sensitive NSCs attached to the floors of different cases of irregular multi-storey RC buildings using three-

dimensional dynamic FE analyses is also one of the main aims of the current study. To achieve the aim of the research, the following seven research objectives have been identified:

(1) to identify the effect of different design characteristics of the P-structures on the seismic response of NSCs having different natural frequency values;

(2) to estimate the dependence of the seismic behaviour of the acceleration-sensitive NSCs on the properties of multi-storey RC structures such as their fundamental vibration periods, seismic capacities, and types of ground on which it is assumed they would be constructed. Moreover, the effect of some properties of the NSCs such as their damping ratios, natural frequencies, locations along the building height, and locations on the floors, i.e. the flexible sides and centres of rigidity of the irregular RC buildings, is to be evaluated;

(3) to investigate the influence of different values of eccentricity ratios of the P-structure on the acceleration response of the attached NSCs;

(4) to investigate the effect of P-structure vertical mass irregularity on the seismic response of NSCs;

(5) to propose a relation between the amplification in the accelerations of the NSCs and the top floor rotations of the P-structures;

(6) to compare the predictions of the nonlinear dynamic FE analyses with those of the EC8 (2004) seismic design provisions for the NSCs; and

(7) to extend the current EC8 (2004) design expression for the NSCs to include the structural ductility, maximum seismic capacity and the torsional effects.

It is necessary to achieve the aim and objectives listed above to obtain a solid knowledge base and to understand the real global seismic behaviour of the NSCs mounted on

irregular multi-storey RC buildings with significant torsional effect under bi-directional base motions. The first and second objectives as stated above were studied in detail in Chapter 5, whereas the third objective was amply investigated in Chapter 6. The main intention of Chapter 7 is to study objective number 4. Furthermore, according to the finite element results presented in Chapters 5, 6 and 7, objectives 5 and 6 were also investigated in each of these chapters. Based on the results of the seismic response of the NSCs attached to 64 different cases of P-structures that were investigated according to objectives 1 to 6, a modification to the formula presented in the EC8 (2004) for the design of the NSCs as stated in objective 7, is made in Chapter 8. Therefore, this research can lead to further understanding and development of the current design provisions of the NSCs attached to irregular RC P-structures.

According to the numerical results presented in Chapters 5 to 8, considerable conclusions have been made and several formulae were developed to quantify the effect of torsion on the amplification in the accelerations of the NSCs. The most obvious finding to emerge from this research is that during earthquakes, the seismic response of NSCs attached to the floors of irregular reinforced concrete P-structures can be amplified by the torsional behaviour of the P-structures. Furthermore, amplifications in the values of NSCs accelerations were observed when either the damping ratio of NSC decreases form high (3%) to low (0.01%) values or when the total mass ratio increases along the height of the P-structure with vertical mass irregularity. Based on the three above-mentioned parameters i.e. torsion of the P-structure, damping ratio of the NSC, and total mass ratio of P-structures with vertical mass irregularity, three relationships were developed. The first relationship is between the torsional amplification factor (F_T) of NSC and the top floor rotation (θ) of the P-structure. The second

correlation is between the damping amplification factor (A_p^{ξ}) of NSC and the top floor rotation (θ). The third relationship is between the percentage of increase in NSCs accelerations and the increase in total mass ratio at different locations along the height of the P-structures with vertical irregularity. Based on the first relationship, modification to the EC8 (2004) formula (defined later in Section 1.4 – see Eq. (1-1)) is made for the design of the NSCs when they are attached to the flexible sides of the floors of irregular P-structures (see Eq. (8-3) in Chapter 8). According to the results presented in Chapter 8, the proposed formula provides safer predictions for the NSCs accelerations than those of the current EC8 provisions under the effect of peak ground acceleration (PGA) values corresponding to the maximum seismic capacities of the P-structures. Therefore, for human life safety, as well as functional and economical purposes, it is expected that the NSCs designed using the proposed formula can be functional without damage under the effect of earthquakes having PGA values in the range of 70% to 80% of the maximum seismic capacities of the P-structures.

1.4 Research Methodology

This section summarises the methodology used for carrying out the FE analyses and calculating the dynamic response of the NSCs according to EC8 (2004) provisions. It also sets the basis for the comparison between the FE results and the EC8 (2004) predictions for the seismic response of the considered NSCs. The adopted methodology includes the following steps:

Step 1 (validation of the FE code): in this research, the validation process of the numerical simulations of irregular RC buildings with significant torsional behaviour was

based on the experimental structure SPEAR. The FE code used, MIDAS Gen Ver. 3.1 (2013), was validated using the experimental results presented in the studies by Negro *et al.* (2004) and Fajfar *et al.* (2006). The comparison between the numerical and experimental results included the top floor rotations and top floor displacements in the X and Y directions at the centre of mass. Furthermore, the results of the base shears in the X and Y directions, as well as the base moments about the Z direction were also adopted in the comparison. The results showed that the adopted element type and the material models fully captured the displacements and rotations, as well as the shear forces and moment reactions in the linear and nonlinear ranges of the selected building. Details on the validation of the adopted FE code are provided in Chapter 4 (see Section 4.2).

Step 2 (selection of the RC P-structures): different cases of RC buildings that can be classified as irregular in their plan and/or vertical mass distribution were selected. Any general and widely acceptable methodology should adopt an extensive range of P-structures so that the findings can be generalised and utilised in the wider context for other cases of structures. Therefore, in order to increase the confidence in the results of this research, 64 cases of irregular RC P-structures were adopted. These cases can provide a range of various factors (i.e. maximum seismic capacities, fundamental periods, total heights, floors rotations, ground types and distribution of the masses along their heights, as well as different values of eccentricity ratios) that may have a significant effect on the NSCs attached to the considered P-structures.

Step 3 (selection of the earthquake records): as per the EC8 (2004) provisions (see clause 4.3.3.4.3-3), average effects of at least seven artificial, recorded or simulated earthquake records should be used for nonlinear analysis purposes. So as to increase certainty in the results of the

current investigation, different sets of natural and artificial earthquake records consisting of 70 accelerograms compatible with the EC8 (2004) Type 1 elastic response spectra for ground types A, B, C, D, and E were used. A description of the selected natural and artificial records can be found in Chapter 3 (see Section 3.3).

Step 4 (dynamic properties of the P-structures): modal (eigenvalue) analyses were carried out for the selected RC P-structures in order to determine their vibration periods.

Step 5 (vibration properties of the NSCs): the NSCs considered in this research are lightweight acceleration-sensitive mechanical, electrical, or medical equipment such as those found in industrial, commercial, or healthcare buildings, respectively. The NSCs are designed so as to have natural periods matching the vibration periods of the considered RC P-structures.

Step 6 (push-over analyses): nonlinear static analyses were carried out to calculate the elastic and maximum seismic capacities of the RC P-structures. These values of the seismic capacities were used to explicate the FE results and compare such results with the predictions of the EC8 (2004).

Step 7 (nonlinear dynamic analyses): nonlinear dynamic FE analyses were carried out for different cases of the P-S systems under the effect of peak ground accelerations that cause elastic and inelastic behaviour of the adopted P-structures. Average numerical results of 6755 nonlinear dynamic FE analyses of the P-S systems identifying the influence of the investigated parameters on the seismic response of NSCs were presented and discussed in Chapters 5, 6, and 7.

Step 8 (comparison between FE results and EC8 (2004) predictions): the numerical results presented in each chapter (i.e. Chapters 5, 6, and 7) were compared with those values predicted by the EC8 (2004) for the design of the NSCs. EC8 suggests the following expression for the calculation of the dynamic factor (S_a) applicable to non-structural systems:

$$S_a = \alpha . S \left[\frac{3[1 + (z_c/H)]}{1 + [1 - (T_C/T_1)]^2} - 0.5 \right] \quad (1\text{-}1)$$

where,

α is the ratio of the design ground acceleration a_g, on ground of type A to the gravity acceleration g;

S is the soil factor (for Type 1 elastic response spectrum of EC8 (2004), S is taken as 1.0, 1.2, 1.15, 1.35, or 1.40 for ground types A, B, C, D, or E, respectively);

T_C is the natural period of NSC;

T_1 is the first fundamental vibration period of the P-system;

z_c is the elevation of the NSC above the location of implementation of the seismic impact and,

H is the total height of the P-structure considered from the level of implementation of the seismic impact.

Hence, multiplying S_a, as given by Eq. (1-1), by the acceleration of gravity (g) yields the acceleration for the design of the NSCs which is compared with the peak component acceleration values obtained from the FE analyses. Similar to the main formula of EC8 (2004) for the design of the NSCs as presented in Eq. (1-1), the NSCs in this investigation were assumed to remain within the elastic range. However, the considered cases of the P-structures were subjected to PGA values causing elastic and inelastic deformations in the P-structures.

Step 9 (extension of the EC8 expression for the design of the NSCs): in this research, the current EC8 design provision for the NSCs is extended by taking into consideration the effects of the maximum seismic capacity and torsional behaviour of the supporting structure. The adopted methodology that used to extend the EC8 formula is described in detail in Chapter 8.

1.5 Thesis Layout

This thesis consists of nine chapters; the starting point of Chapter 1 is an explanation of the classifications of the non-structural elements, their response and the primary types of their hazards during earthquakes. Chapter 1 also presents a statement of the current research problem and the aim and objectives of the research. Furthermore, a summary of the research methodology adopted to achieve the ultimate aim and the seven objectives of the current research is also explained.

Previous research on the seismic analysis methods of the NSCs attached to the P-structures is briefly reviewed in Chapter 2. In previous research, the secondary systems were assumed to be mounted on either two-dimensional regular P-structures or three-dimensional torsional systems.

Chapter 3 includes the description of the adopted material models for both the concrete and steel reinforcement. Thereafter, approaches that can be used to generate natural and artificial base motion records using the computer codes REXEL Ver. 3.5 (Iervolino *et al.*,

2010a) and SIMQKE (SIMQKE, 1976; Gelfi, 2007) are explained. Furthermore, the criterion for selecting the type of ground for each group of the considered P-structures in this research is explained. Then, different sets of base motion records consisting of 70 accelerograms that were employed in the dynamic analyses of the P-S systems in this research are detailed in Chapter 3.

A validation of the FE computer code MIDAS Gen (2013) used for the dynamic analysis of P-structures with torsional behaviour is summarised in Chapter 4. According to the comparisons between the numerical and experimental results, it is concluded that the adopted fibre beam-element and the nonlinear material constitutive models can accurately predict the torsional behaviour of irregular buildings. Moreover, the specifications and characteristics of the NSCs are also explained in Chapter 4.

In Chapter 5, three groups of frame structures, consisting of 25 irregular RC buildings, were chosen to investigate the effect of P-structure torsional behaviour and seismic capacity on the NSCs accelerations. The rationale adopted for the selection of the RC P-structures considered in Chapter 5 is explained. Furthermore, the influence of ground type on the seismic response of NSCs integrated on asymmetrical RC P-structures is also investigated in Chapter 5.

Dynamic response of NSCs mounted on one-bay three-storey RC frames having different values of eccentricities between the centre of mass and centre of rigidity were investigated and presented in Chapter 6. Acceleration response of the NSCs attached to the flexible sides and the centres of rigidity of different floors were investigated.

To investigate the influence of vertical mass irregularity of the P-structures on the dynamic performance of lightweight acceleration-sensitive NSCs, thirty cases of vertical mass distributions in addition to a reference case with uniform mass distribution were considered in Chapter 7. A complicated irregular 20-storey, multi-bay RC building was chosen as the P-structure. Based on the results of the extensive FE analyses, expressions that can be used to calculate the percentage increase in the accelerations of the NSCs due to the increase in the masses along the building height were proposed.

In Chapter 8, the current EC8 design equation for the design of the NSCs is modified by taking into consideration the effects of the torsional behaviour and the maximum seismic capacity of the supporting structure. The accuracy of the modified EC8 expression is also validated in Chapter 8.

Conclusions and remarkable findings of the extensive nonlinear dynamic analyses carried out as part of the current research are presented in Chapter 9. Future research and further studies that should be carried out on the NSCs were also recommended.

CHAPTER TWO: LITERATURE REVIEW

2.1 Introduction

The progression of the seismic analysis methods of the NSCs attached to the P-systems started over the past four decades with a particular concentration on critical equipment contained in nuclear power stations (Biggs, 1971). To determine a simplified design method for S-systems and to reduce their damage in earthquakes, the dynamic response of the S-systems within P-structures have been the focus of many research studies as presented in the state of the art reviews (Chen and Soong, 1988; Phan and Taylor, 1996; Villaverde, 1997b; Filiatrault *et al.,* 2002; Whittaker and Soong, 2003).

In this chapter, past and recent studies on the response of S-systems have been divided into two main categories; namely studies on S-systems that assumed to be mounted on regular (i.e. without significant torsional effects) elastic or inelastic P-systems, and the secondary elements were attached to P-systems with torsional effects. It can be easily observed that the number of studies on the S-systems attached to the regular P-systems has largely exceeded the number of those studies on NSCs when they mounted on the P-systems with torsional effects. In the following sections, research studies that were attempted to propose different design approaches for the acceleration-sensitive NSCs and/or investigate their seismic responses are briefly reviewed.

2.2 Studies on NSCs Mounted on Regular Systems

2.2.1 Studies on NSCs Mounted on Elastic Systems

A study by Singh and Ang (1974) can be considered as a one of the earliest studies on the dynamic responses of the NSCs. A theoretical stochastic model was proposed to evaluate the elastic behaviour of lightweight S-systems subjected to base motions. The S-systems were modelled as multi-degree-of-freedom (MDOF) attached at single or multi points to elastic P-systems as shown in Figure 2.1. The behaviour of the S-systems was studied by considering or ignoring their dynamic interaction with the P-systems. The proposed model was compared with the results of the elastic response spectrum (RS) approach. The results of this study (Singh and Ang, 1974) showed that the accounted responses of the NSCs using the proposed model were found more reliable than those responses accounted from the elastic RS method.

Using a transient analysis, Sackman and Kelly (1979) developed a rational analytical approach to evaluate a maximum seismic behaviour of lightweight equipment attached to elastic P-structure under the effect of seismic loading. The equipment was modelled as a single-degree-of-freedom (SDOF) system and their frequencies tuned or slightly un-tuned to the fundamental vibration periods of the P-system, which was modelled as a number-degree-of-freedom (NDOF) as shown in Figure 2.2. The considered S-systems assumed that their masses were very small in comparison with the mass of the P-system. A design RS was used as an input to represent the seismic loading to the P-S system. Maximum values of the accelerations and displacements of the NSCs were evaluated. Sackman and Kelly (1979) concluded that their approach can be used directly to evaluate the seismic response of S-system mounted on a simple two-directional P-system from a given design spectrum.

Perturbation techniques were employed by Sackman *et al.* (1983) to evaluate the modal properties of the combined P-S system, which was composed of lightweight SDOF equipment attached to elastic MDOF P-structure. An example of a P-structure modelled as 10-DOFs as displayed in Figure 2.3, was studied. The results showed that the interaction between the secondary and P-structure had a significant effect on the modal properties of the P-S system when frequencies of the secondary element were in tuned condition with the fundamental vibration periods of the P-structure.

A modal-superposition approach was proposed by Der Kiureghian *et al.* (1983) to determine the seismic behaviour of lightweight S-systems attached to elastic P-structures subjected to random base motions. Dynamic properties of the combined P-S system were estimated using a perturbation technique that was developed by Sackman *et al.* (1983). Furthermore, Der Kiureghian *et al.* (1983) selected a structural model of 10-DOFs that was adopted by Sackman *et al.* (1983) (see Figure 2.3). Two types of base motion inputs were used; the Power Spectral Density (PSD) method for a stationary input and the response spectrum method for an earthquake input. The method included the effects of the dynamic interaction and the resonant condition between the secondary and primary systems. The results in the study by Der Kiureghian *et al.* (1983) demonstrated the precision of the modal-superposition method in evaluating the dynamic behaviour of the S-systems when they are attached to regular two-dimensional P-structures.

Simple approximate expressions were recommended by Villaverde (1991) to estimate the maximum seismic behaviour of lightweight S-systems mounted on elastic P-structures. Three cases of the P-S systems as shown in Figure 2.4, were studied. The combined primary and secondary systems were modelled as 3- and 2-DOFs respectively. Damping ratios equal

to 0.1% and 2% were adopted for the secondary and primary systems respectively. The accuracy of the adopted procedure was verified by using a time-history analysis technique. The results of this study (Villaverde, 1991) showed that the proposed expressions produced mean and maximum errors in the responses of approximately equal to 4% and 22% respectively in comparison with the corresponding responses evaluated by the time-history analysis.

Singh *et al.* (2006a, 2006b) evaluated seismic design forces of rigid and flexible NSCs using the elastic behaviour of a P-structure. Their studies focused on the examination and improving of some formulae in regards to the evaluating of the seismic design forces on the NSCs, which were included in the provisions of the 2003 NEHRP (BSSC, 2003). Two simplified approaches for the determination of the seismic force coefficients of NSCs were proposed using the dynamic characteristics of both the P-structure and NSC. Based on the fundamental vibration period of the P-structure and damping ratios of both the NSCs and the P-structure, new design expressions were proposed. These expressions were restricted to be used for the NSCs attached to the structures in which the mass and stiffness properties do not change largely along the P-structures heights. In addition, the yielding of the P-structures was not taken into account. The results showed that, for the NSCs that were mounted on low height buildings; the design forces estimated by the 2003 NEHRP (BSSC, 2003) provisions were found lower than those calculated using the proposed methods, especially at the uppermost floors. However, due to a decrease in the values of the fundamental vibration periods of the tall buildings, it was found that the acceleration predictions of the 2003 NEHRP (BSSC, 2003) provisions were observed higher than those estimated using the proposed expression.

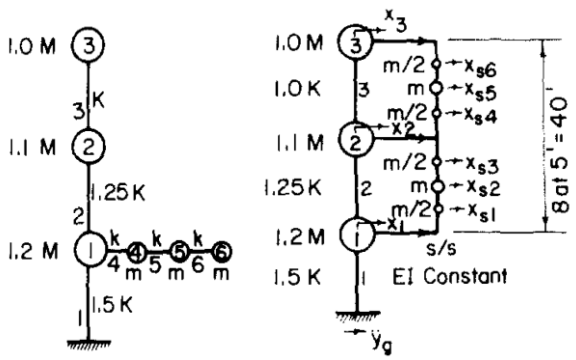

Figure 2.1 Primary-secondary systems proposed by Singh and Ang (1974).

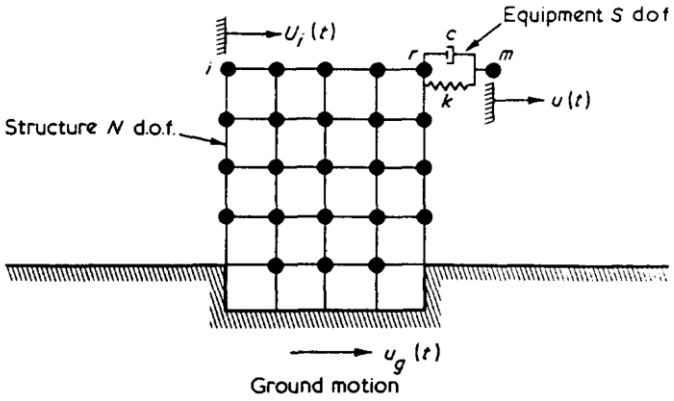

Figure 2.2 Primary-secondary system proposed by Sackman and Kelly (1979).

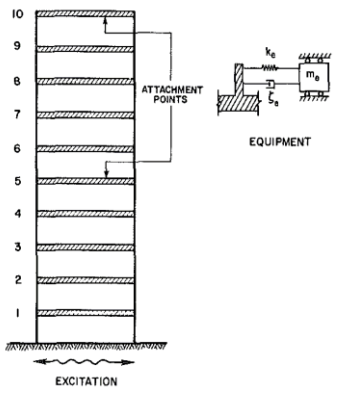

Figure 2.3 Primary-secondary system adopted by Sackman *et al.* (1983).

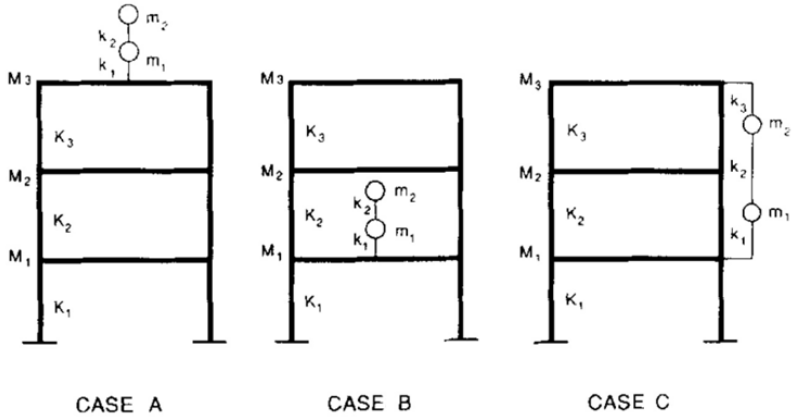

Figure 2.4 Cases of the P-S systems studied by Villaverde (1991).

2.2.2 Studies on NSCs Mounted on Inelastic Systems

Elastic analysis would be appropriate for those P-S systems that can be subjected to low base motions with a maximum value of peak ground acceleration equal to elastic capacity of the P-structure. The P-systems generally go into an inelastic response under moderate or severe earthquakes. In order to minimise the damages to NSCs or to remain functional inside the structures, seismic forces for the design of the NSCs may necessary to be evaluated under the effect of PGA values corresponding to maximum seismic capacities of the P-structures. This section briefly explains the previous studies that were attempted to investigate the seismic behaviour of the NSCs mounted on inelastic P-structures.

Lin and Mahin (1985) implemented the first attempt of investigation the influence of the inelastic behaviour of the P-systems on the seismic response of the S-systems. Preliminary analyses were implemented to evaluate the seismic response of lightweight acceleration sensitive S-systems attached to the P-systems that were experienced inelastic deformations under the effect of strong earthquakes. Both the S-systems and P-systems were modelled as a

SDOF, as displayed in Figure 2.5. Different hysteretic models for the P-systems and different damping values for the S-systems were considered. A floor response spectrum (FRS) method was used to predict the amplification factor of the accelerations and to improve possible design guidelines of the S-systems. The dynamic interaction between the primary and secondary systems was ignored. The results in this study (Lin and Mahin, 1985) showed that the relative displacement between the primary and secondary systems and the absolute acceleration of the S-systems were decreased due to yielding of the P-system when the natural frequency of the S-systems is equal to or larger than the fundamental vibration period of the P-structure.

Using the method of the FRS, a study by Sewell *et al.* (1986) attempted to find approximate formulae to evaluate the seismic behaviour and the factors that influence the equipment supported on inelastic P-structures subjected to severe earthquakes. Amplification of the peak component acceleration was also determined in some studied periods by using the method of the FRS. The P-structure was modelled as a MDOF as shown in Figure 2.6, with one or two arbitrary points of attachment for equipment. It was observed that due to a decrease in the stiffness of the P-structure in the nonlinear range, a reduction in the seismic response of the floors was produced.

Villaverde (1987) presented a simplified approximate method for the evaluating of the dynamic response of lightweight S-systems such as equipment and piping attached to nonlinear P-systems subjected to earthquakes. Shear beam with 5-DOFs was used to model the P-S systems. Three-DOFs were used to model the P-systems having an elasto-plastic load-deformation response whereas the other 2-DOFs were used to model the S-system. It was

considered that the S-system integrated on the P-system as a combined system as shown in Figure 2.7. The procedure was expressed in terms of the dynamic properties of the uncoupled primary and secondary systems. This method was restricted to the cases of the S-systems that had a small mass in comparison with the total weight of the P-system. Different locations of the S-systems along the height of the P-system were studied. In the implemented comparative investigation, this simplified method predicted the numerical integration approaches with minimum and maximum average errors of 2% and 40% respectively. Therefore, this method was found suitable for a rational, quick and inexpensive dynamic analysis of lightweight S-systems at the initial stages of their design.

Chen and Lutes (1990) used analytical approaches to study the dynamic behaviour of an elastic S-system supported on an elasto-plastic P-structure under the effect of ground motion accelerations. A bilinear hysteretic yielding model was used to consider the nonlinearity of the P-structure. Figure 2.8 shows the adopted modelling of the P-S system. The possibility of the damage to the S-system from either first seismic affect or its fatigue due to a plastic behaviour of the P-structure was studied. The results showed that the behaviour of the S-system was found more significantly affected due to first seismic damage than the fatigue damage of the P-system.

In a study by Singh *et al.* (1993), a seismic coefficient represented as a ratio between the elastic and inelastic accelerations was evaluated due to the effect of an inelasticity of the P-system. A simplified approach was used to evaluate the mode shape frequencies of the P-S system. The results concluded that this seismic coefficient could be used in the cases in which the yielding of the P-structure decreases the values of the floor response spectra. The results

also provided a simple method to incorporate the effect of the nonlinearity of the P-system in the computation of the seismic design forces of the S-systems.

Schroeder and Backman (1994) evaluated the effects of the seismic characteristics of the P-system on the dynamic behaviour of the S-systems using nonlinear dynamic analysis. Background information for the advancement of the NSCs provisions of the 1994 NEHRP (BSSC, 1994) was provided. It was concluded that when a NSC located at the upper floors of a P-structure, higher accelerations could be experienced than those attached to the lower floors. Furthermore, the acceleration responses were found linearly distributed along the height of the P-structure.

A simplified approach was suggested by Villaverde (1997a) to obtain an equivalent design force for the S-system attached to the P-structure. The design spectrum that was defined according to the 1994 Uniform Building Code (UBC, 1994) for the design of the P-structure was used as a base motion input to the P-S system. Dynamic interaction between the secondary and primary systems was taken into account. The effect of the nonlinear response of the P-structure on the seismic behaviour of the S-system was considered. To examine the proposed approach, a system consisting of a six-storey structure and a secondary system which represented as three-masses as shown in Figure 2.9, was adopted. Based on the suggested approach, it was concluded that the method is sufficient for the design purpose of the S-systems.

To estimate the dynamic behaviour of the S-systems under the effects of inelastic behaviour and interface conditions of the P-structure, two analytical methods were suggested

by Adam and Fotiu (2000). An iterative synthesis and modal combination approaches of tuned conditions were adopted. A four-storey frame as shown in Figure 2.10, was suggested as a P-structure. The masses of the floors were modelled as lumped masses at the joints of the frame. The S-system is considered as a SDOF attached at the top floor of the P-structure. Values of 0.3% and 3% were adopted for the damping ratios of the secondary and primary systems respectively. The results of the dynamic response of the S-systems produced by the adopted approaches were compared with the corresponding results derived by decoupled analysis. Based on the comparison results, these two adopted methods were found computationally efficient.

Recent studies on NSCs have dealt with the evaluating of the peak floor acceleration (PFA) of the P-structures. Several researchers have studied the procedures of the estimation of the variation in the values of PFAs along the height of the P-structures. For instance, Rodriguez *et al.* (2002) proposed an analytical approach to determine the floor horizontal accelerations that can be produced in regular buildings under the effect of an earthquake. Then, these floors accelerations can be used as input for the determination of the seismic design forces of the NSCs that can be expected to be attached to such buildings. The nonlinear behaviour of the P-structures was evaluated using a modified modal superposition method. Two-dimensional regular buildings with 3-, 6-, and 12-storey that were designed in accordance with the standards of the loadings and concrete structures of New Zealand codes (NZS4203, 1992; NZS3101, 1995), were chosen. Based on the results of the accelerations of different floors, it was concluded that the maximum amplifications of the floors accelerations were occurred at the uppermost floors of the studied buildings. It was also concluded that the

floors acceleration responses were reduced significantly immediately beyond the elastic range of the buildings.

For the evaluation of the dynamic behaviour of NSCs integrated on inelastic structures, Villaverde (2005, 2006) proposed an approximate technique based on an expression presented previously in a study by Villaverde (1991). Several assumptions are made to derive the final expression such as the resonance of the vibration periods between the secondary and primary systems and adopting values of 0% and 5% for the damping ratio of the secondary and primary systems respectively. The proposed technique involved the determination of the maximum value of the lateral seismic loading under the effect of unidirectional base motion. Strength reduction parameters were adopted to account for the nonlinearity of the P-systems. A previously studied frame by Villaverde (1997a) as shown in Figure 2.9, was used to explain the adopted technique. It was concluded that the adopted technique represents a simple but efficient method for evaluating the seismic response of NSCs when they are attached to regular P-systems. However, Villaverde (2005, 2006) recommended that the adequacy of the proposed technique should be investigated under different ground motions and different characteristics of both the primary and secondary systems.

To study the seismic behaviour of the S-systems, Medina *et al.* (2006) adopted primary structures modelled as two-dimensional, single-bay shear frame buildings having different number of storeys. The P-structures had 3-, 6-, 9-, and 18-storey as displayed in Figure 2.11. Using a dynamic analysis method, peak accelerations of the NSCs mounted on the above-mentioned P-structures under the effect of the base motions in one direction were

evaluated. The S-systems were considered as SDOF systems having small masses in comparison with the total weight of the P-structures. The seismic responses of the NSCs were extracted from the floors accelerations during earthquakes. The results observed that the fundamental vibration periods and the stiffness of the P-structures had a significant effect on the values of the floors response spectra. Furthermore, the locations of the NSCs and their damping had a considerable influence on their seismic response. It was concluded that a lower damping ratio produces a higher amplification in the NSCs acceleration. In addition, the acceleration amplification responses were decreased during the nonlinear response of the P-structures. However, Medina *et al.* (2006) concluded that their results were limited to the NSCs attached to the structures and subjected to the ground motions that had similar characteristics to the studied cases.

Pavlou and Constantinou (2006) performed an analytical study that aimed to estimate the dynamic behaviour of the S-system mounted on inelastic P-structures having damping systems as shown in Figure 2.12. Two-dimensional regular steel frames designed according to the provisions of the 2001 NEHRP (BSSC, 2001) were used to perform the nonlinear dynamic analyses. Different parameters such as various energy dissipation systems of the damped frames were adopted. The results showed that the adopted viscous damping systems provided a considerable protection for the S-systems by the reduction of the floors acceleration values during earthquakes. Reductions in acceleration responses of the S-systems by about 50% and 75% were obtained for those having periods equal to the first and second natural frequencies of the P-structures respectively in comparison with the corresponding values when the S-systems were mounted on un-damped structures.

A study by Sankaranarayanan and Medina (2007) quantified the influence of different parameters on the modification factor of the acceleration-sensitive NSCs supported on inelastic frames. The same regular frame structures presented by Medina *et al.* (2006) as shown in Figure 2.11, were used. It was concluded that the modification factor is primarily a function of the location of the component, its damping ratio and frequencies, as well as the level of nonlinearity and the fundamental vibration periods of the P-structures. An additional study by Sankaranarayanan and Medina (2008) proposed a statistical model to evaluate a modification factor of the acceleration for the NSCs that tuned their periods with those of the P-structure. This model was based on inelastic behaviour of two-dimensional regular multi-storey structures subjected to 40 base motions. The proposed modification factor can be employed similarly to the behaviour modification coefficient of the P-systems, by scaling the elastic FRS to obtain the corresponding responses within an inelastic range of the P-systems. In general, the results showed that the proposed model was capable of predicting the modification factors of the accelerations within 20%.

A simple methodology using the equations of motion was proposed by Adam and Furtmüller (2008) to assess the dynamic response of NSCs supported on elastic-plastic load-bearing structures. A value of the floor response spectrum of inelastic P-system was used to evaluate the dynamic behaviour of the NSCs by taking into account the ductility of the P-structure. One-bay, 12-storey P-structure as shown in Figure 2.13, was chosen. The members plastic deformations of the P-structure were represented by the rotational springs at both the base of the structures and the ends of their beams. The results showed that the proposed methodology provided a sufficient accuracy for both the displacement and acceleration floor spectrum of the studied structure.

Chaudhuri and Villaverde (2008) investigated a wide-ranging parametric study to evaluate the dynamic behaviour of NSCs supported on steel regular frame structures experiencing inelasticity under the effect of a set of base motion records. The adopted steel frame structures as displayed in Figure 2.14, were designed for Zone IV according to the provisions of the 1997 Uniform Building Code (UBC, 1997). The effect of the location, damping ratio and natural frequencies of the NSCs, as well as the behaviour of the supporting frames were studied. In general, the results showed that the inelasticity response of the selected steel frames produced a reduction in the amplification value of the seismic behaviour of the NSCs in comparison with the linear cases. In a few cases, when the NSCs were located at the lower levels of the steel frames, their seismic behaviour amplified by a factor of more than 5.2, for those having natural frequencies tuned with the second and third natural frequencies of the P-structures. Chaudhuri and Villaverde (2008) recommended that the conclusions of their study were valid only for the NSCs integrated on the considered structures under the effect of the adopted ground motion records.

An investigation of the seismic response of lightweight subsystem in the presence of the inelastic response of the P-structure was conducted by Oropeza *et al.* (2010) using a FRS methodology. Both the P-structure and NSC modelled as SDOF systems (see Figure 2.15), and subjected to the base motion records extracted from the European Strong-Motion Database (ESD). The influence of a number of parameters such as the initial natural frequency, different hysteretic models, and the decrease in the strength of the P-structure, as well as different natural frequencies of the NSCs, were investigated. The results were presented in terms of the resonance factor of the NSCs. Based on the results of the above parameters; design guidelines of the NSCs according to the provision of the Swiss code (SIA,

2003) (cited in Oropeza *et al.,* 2010), were improved. It was found that both provisions of the Swiss and EC8 codes underestimated the values of the resonance factors of the NSCs. Generally, it was observed that the predictions of the Swiss code underestimated the seismic responses of the NSCs by about 38% - 45% for those NSCs had a period equal to the first period of the P-structures T_1; whereas, the EC8 provisions underestimated the responses by a range of 50% - 55% for the NSCs that tuned with T_1.

Using the generated values of the peak floor accelerations of multi-storey structures, a simple approach was proposed by Lepage *et al.* (2012) to evaluate the values of the peak component accelerations of the NSCs. The formula that is adopted in the ASCE code (2010) for the determination of the design values of the seismic forces for the NSCs was adopted. The approach neglected the interaction between the P-structures and NSCs. Amplification factors equal to 1 and 2.5 were suggested for the rigid and flexible NSCs respectively. A modification parameter was used to define the effect of the inelastic response of the P-structure on the seismic behaviour of the NSCs. Data of the floors accelerations obtained from existing multi-storey regular structures during strong base motion records were adopted to assess the validity of the approach. It was concluded by Lepage *et al.* (2012) that their approach should be calibrated or modified when other cases of P-structures and ground motions are adopted.

In the previously mentioned studies, i.e. studies that explained in Section 2.2, the NSCs were assumed to be attached to only regular P-systems without considering the effect of torsion. Since base motions take place randomly at multi-directions and not necessarily having equal values of intensities along the two horizontal axes at the base of the P-structures,

torsional behaviour may induce in some symmetrical buildings (Rosenblueth, 1980). This fact is detected in most of the building codes, e.g., UBC (1997), IBC (2012), EC8 (2004), and NBCC (2005), where a 5% of the dimensions of the layout is used for accidental torsion of symmetrical buildings. Obviously, when a building is irregular in plan, considerable torsional modes may also be introduced during earthquake actions. Thus, the floors accelerations may increase which can lead to significant effect on the NSCs, especially for those attached to the extreme edges of a building. Based on the provisions of the ASCE (2010), a value ranging between 1 and 3.0 is suggested as a torsional amplification factor for the design purpose that should be multiplying by either the accidental torsion moments or the design seismic forces for the irregular systems. Therefore, considering the torsional effect could be important for the design purposes of the NSCs, which are attached to such extreme flexible locations. It is worth noting that most of the design methods proposed in the studies presented in Section 2.2 are suitable for NSCs attached to regular 2D P-systems. However, the new design formula suggested in the current research can be used for the design of NSCs attached to both regular and irregular 3D P-structures by accounting for the effects of the seismic capacity and torsional behaviour of the P-structures.

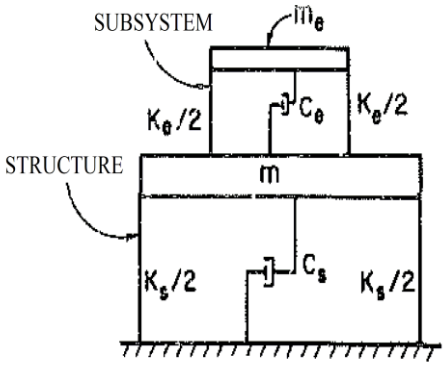

Figure 2.5 Primary-secondary system proposed by Lin and Mahin (1985).

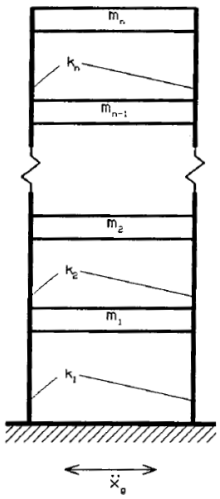

Figure 2.6 Primary system adopted by Sewell *et al.* (1986).

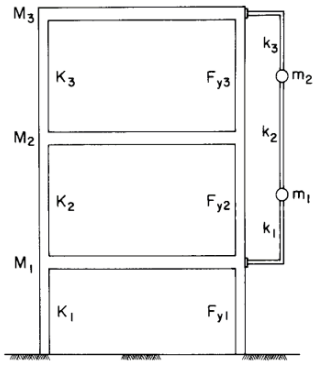

Figure 2.7 Primary-secondary system adopted by Villaverde (1987).

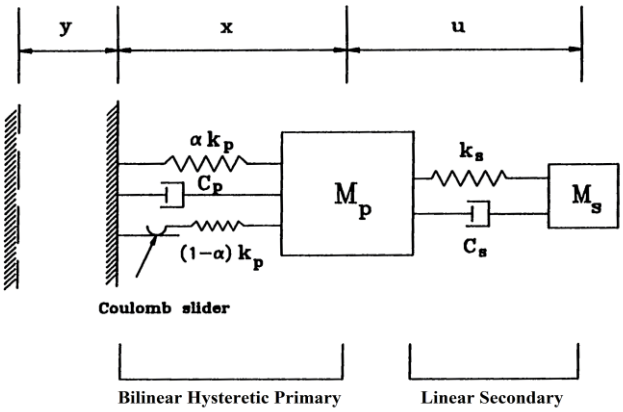

Figure 2.8 Primary-secondary system adopted by Chen and Lutes (1990).

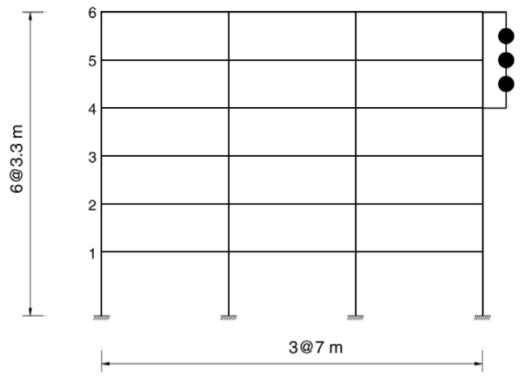

Figure 2.9 Primary-secondary system proposed by Villaverde (1997a).

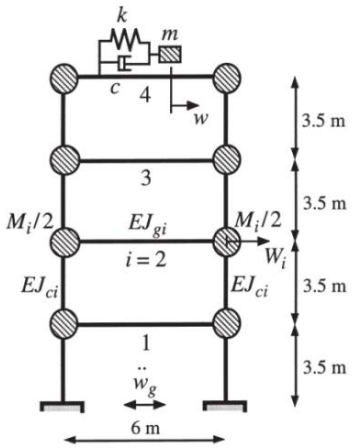

Figure 2.10 Primary-secondary system used by Adam and Fotiu (2000).

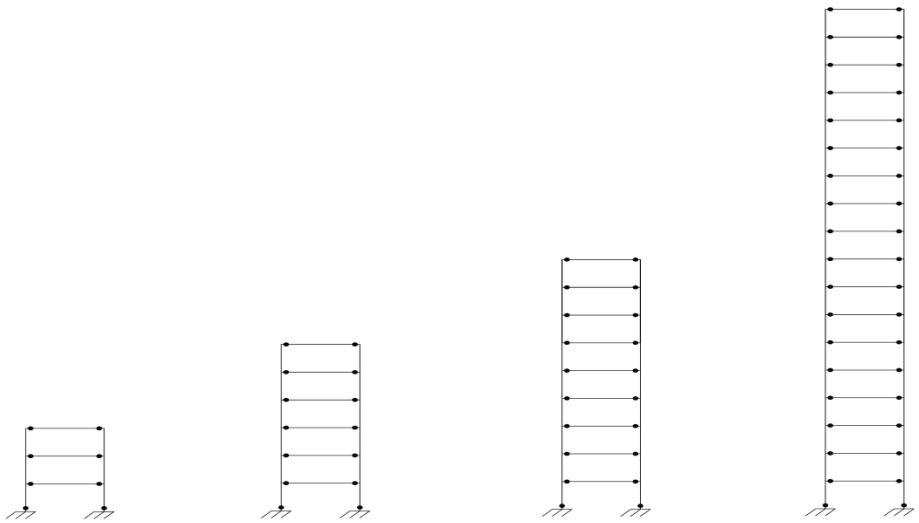

Figure 2.11 Primary structure frames used by Medina *et al.* (2006).

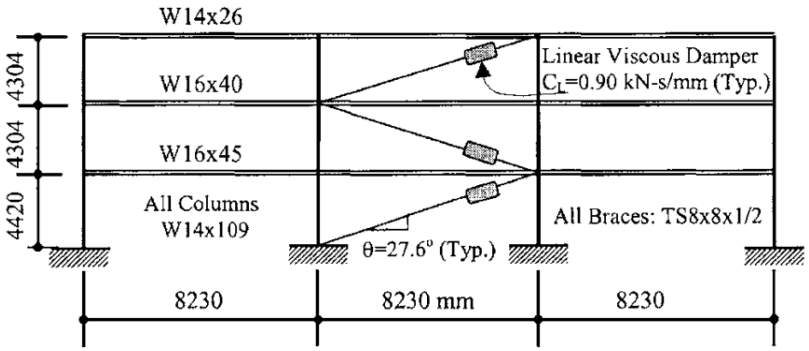

Figure 2.12 Steel frame with damping systems used by Pavlou and Constantinou (2006).

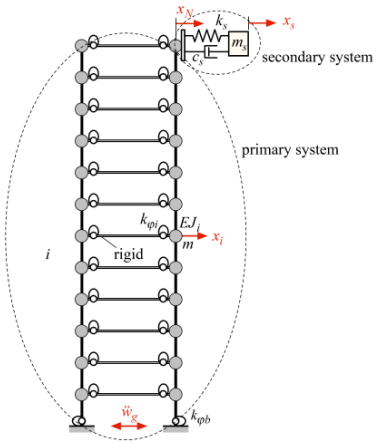

Figure 2.13 Primary-secondary system proposed by Adam and Furtmüller (2008).

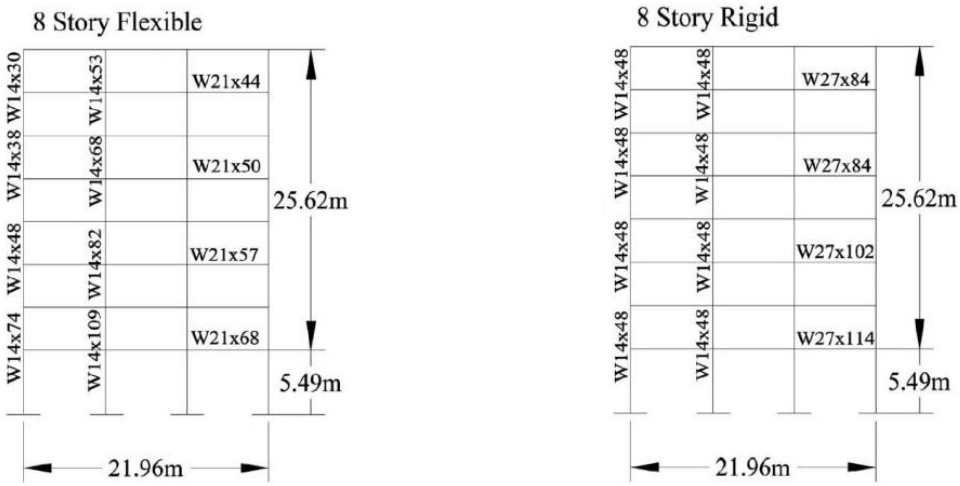

Figure 2.14 Primary structure frames used by Chaudhuri and Villaverde (2008).

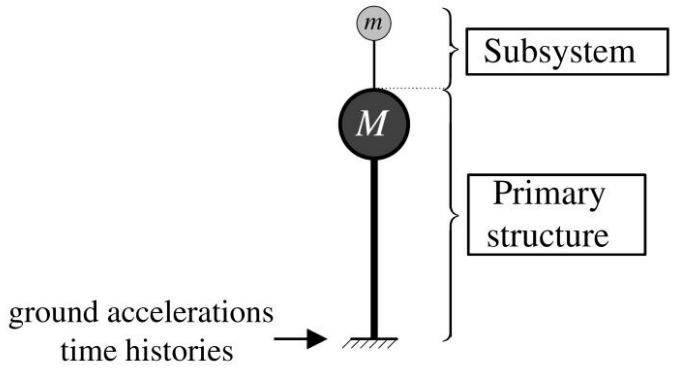

Figure 2.15 Primary-secondary system proposed by Oropeza *et al.* (2010).

2.3 Studies on NSCs Attached to P-systems with Torsional Modes

Realizing that the torsional behaviour of the P-system may have an observable impact, which may increase the seismic behaviour of the NSCs, a number of researchers have attempted to estimate their responses when they attached to such torsional P-systems using either analytical approaches or experimental work. The following sections illustrate most of the past and current studies that attempt to outline a relation between the acceleration response of the S-systems and the torsional modes of the P-structures. In these studies, the NSCs were mounted on either elastic P-systems and the eccentricities were in one direction or inelastic one-bay single or multi-storey systems with eccentricities in the horizontal directions (X and Y). A study by Yang and Huang (1993) can be considered as the first attempt to investigate the effect of the torsional response of fixed base supporting systems on the seismic response of the attached lightweight equipment.

2.3.1 Analytical Studies on NSCs with Torsional Effect

Using the solution of partial differential equations, several analytical studies were carried out to investigate the dynamic response of S-systems mounted on torsional elastic or inelastic P-systems. For example, Yang and Huang (1993, 1998) adopted the solution of the equations of motion to evaluate the acceleration responses of elastic P-S systems. However, in the analytical studies that were presented by Agrawal and Datta (1997, 1998, 1999a, 1999b, 2001) or by Agrawal (1999, 2000a, 2000b), sets of coupled differential equations were used to simulate the linear and nonlinear behaviours of the P-systems. The inelastic response of the P-system was presented by hysteretic force-deformation behaviour. Random ground motions that presented as white-noise seismic waves were subjected to the P-S systems. The dynamic responses of both the secondary and primary systems were obtained by using both the frequency domain spectral and time domain simulation analyses. The response quantities of interest were evaluated in terms of the relative displacement between the primary and secondary systems and the absolute acceleration of the S-system itself. Behaviour of the S-systems was examined under a set of parametric variations. These parameters included the uncoupled lateral frequency, the eccentricity ratio, ratio of uncoupled lateral to rotational frequencies, damping ratio and the hysteretic parameters of the P-structure. Furthermore, properties of the S-systems such as their frequency and damping ratio, as well as the normalised eccentricity of the S-system were investigated.

Having considered the above-mentioned research, it can be classified into two groups of studies; namely, two and three-dimensional (3D) modelling of the P-S systems under the effect of unidirectional and bi-directional base motions respectively, as explained in the following sections.

2.3.1.1 Two-dimensional Modelling of the P-S systems

A number of researchers adopted two-dimensional modelling of P-S systems such as Yang and Huang (1993, 1998), Agrawal and Datta (1997, 1998) and Agrawal (2000a). Each floor of the P-S system was simulated as three-DOFs, one for each of the lateral and rotational modes and the other for the modelling of the S-system. The influence of the elastic and inelastic responses of two-dimensional P-systems, which implemented by the above-mentioned research can be illustrated in the following sections.

2.3.1.1.1 S-systems Attached to Elastic Two-dimensional P-systems

Yang and Huang (1993, 1998) proposed a mathematical two-dimensional model with either fixed base or base isolation systems to evaluate the seismic behaviour of lightweight equipment attached to torsional P-systems. Their approach was restricted to elastic P-S systems with classical damping and the eccentricity of the floors was considered only in one direction as shown in Figure 2.16. Each floor of the P-system was idealised as 2-DOFs, a 1-DOF for each of the translation and torsion to estimate the influence of the translational and torsional modes of the P-system. The mass of the equipment was assumed very small in comparison with the weight of the P-system as it influences slightly the oscillation modes of the P-system. A perturbation approach was used to determine the closed-form formulae for the modal properties of the P-S systems. The dynamic interaction between the secondary and primary systems was investigated in both the tuned and un-tuned conditions. The modal combination results were found using a complete quadratic combination (CQC) approach. Based on their results (Yang and Huang, 1993, 1998), it observed that under the tuned condition with the first transitional mode, the accelerations of the S-systems were found larger

than those the corresponding values when they tuned with the torsional mode of the P-system. Moreover, due to the reduction in the values of the fundamental periods of the isolated system, the dynamic responses of the S-systems attached to the base-isolated torsional system were found much lower than those attached to the fixed base P-system.

In the study by Agrawal and Datta (1997), seismic responses of the S-systems attached to a torsional elastic P-system were studied under the effect of a unidirectional random ground excitation. Two-dimensional P-systems with an eccentricity in one direction between their centre of mass (CM) and centre of rigidity (CR), were adopted. Figure 2.17 displays the model that was adopted by Agrawal and Datta (1997) to investigate the seismic response of a SDOF S-system attached to a 2-DOFs torsional elastic P-system. The results showed that the rotary coupling of the P-system could have a significant influence on the seismic responses of the S-system. The results of the study by Agrawal and Datta (1997) showed that, for S-systems, which were under tuned condition with the P-system, their dynamic responses were increased linearly with the increase in the eccentricity ratios (e/r_e) of the P-system. However, in un-tuned condition, the dynamic responses were observed almost insensitive to the variation of e/r_e; where (e) refers to the eccentricity between the CM and CR of the P-system; and (r_e) represents the value of the radius of elasticity of the P-system.

To mitigate the peak acceleration responses of the S-system attached to elastic P-systems, a passive tuned mass damper (TMD) attached to the S-system was used by Agrawal (2000a). Both the S-system and the TMD were modelled as SDOF; whereas, the P-system was modelled as a 2-DOFs and the eccentricity considered only in one direction as shown in Figure 2.18. The results showed that, for a strong torsional coupled P-system under the tuned

condition and for tuning of the TMD with the first frequency of the combined system, the seismic responses were increased with the increase in the eccentricity ratio of the equipment system. However, the dynamic responses were found almost insensitive to change in the eccentricity ratio of the equipment system for the other cases. Furthermore, the acceleration responses of the equipment were found higher if the TMD is moved from the equipment system. So, the TMD works as an effective vibration control device for the equipment system. In addition, the results showed that the seismic responses were decreased with the increase in the damping ratio of the TMD.

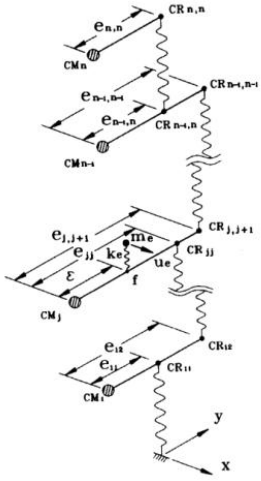

Figure 2.16 Primary system proposed by Yang and Huang (1993, 1998).

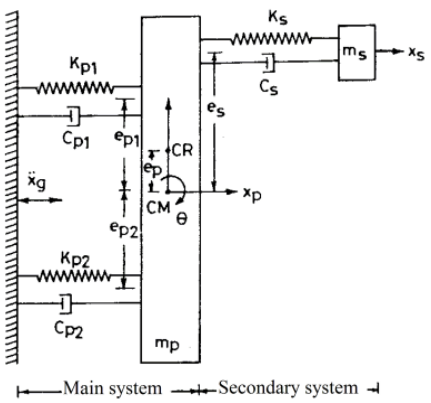

Figure 2.17 Primary-secondary system proposed by Agrawal and Datta (1997).

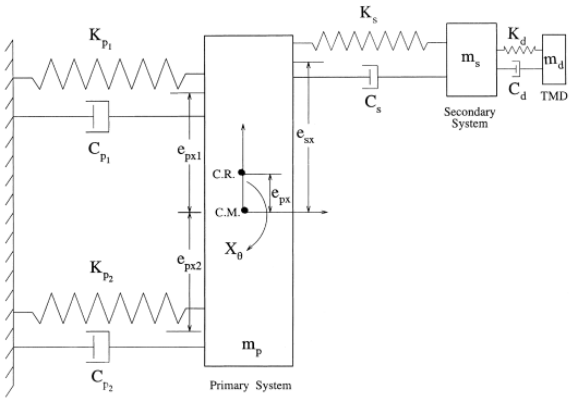

Figure 2.18 Primary-secondary system proposed by Agrawal for the cases of using a passive tuned mass damper (TMD) (Agrawal, 2000a).

2.3.1.1.2 S-systems Attached to Inelastic Two-dimensional P-systems

Agrawal and Datta (1998) selected a P-S system as presented in Figure 2.17, which was adopted in their study (Agrawal and Datta 1997) to evaluate the responses of the S-system mounted on a torsional coupled yielding P-system under the effect of a white-noise excitation. As shown in Figure 2.17, the S-system was modelled as 1-DOF attached to a 2-DOFs torsional inelastic P-system. The results of their study (Agrawal and Datta, 1998) showed that under certain conditions, the yielding of the P-system may cause an increase in the seismic responses of the attached S-system. Furthermore, the results observed that the rotary coupling of the P-system had a significant influence on the dynamic responses of the S-system. For a strong torsional coupled P-system and under tuned conditions, the responses were increased linearly with the increase in the value of e/r_e; however, in an un-tuned condition, the responses were observed almost insensitive to the variation of e/r_e.

2.3.1.2 Three-dimensional Modelling of P-S systems

Most of the models that were adopted to investigate the seismic responses of the S-systems as presented in Section 2.3.1.1 were unable to simulate the effect of the torsion that can be

produced in the orthogonal horizontal directions (X and Y). However, in the studies by Agrawal and Datta (1999a, 1999b, 2001) and Agrawal (1999, 2000b), the eccentricity between the CM and the CR of the P-system was considered in the two horizontal directions. Each storey of the P-system was modelled as 3-DOFs. A 1-DOF was used to simulate the effect of torsion; however the other 2-DOFs were used to represent the transitional modes in the X and Y directions. The effect of the linear and nonlinear behaviour of 3D P-systems that was investigated by the aforementioned studies is explained in the following sections.

2.3.1.2.1 S-systems Attached to Elastic Three-dimensional P-systems

In a study by Agrawal (2000b), the effect of the torsion on the seismic response of an equipment system attached to an elastic single-storey sliding support P-system was studied under the effect of a bi-directional random ground excitation. Figure 2.19 shows the adopted model of the sliding support of the P-system. The S-system was modelled as SDOF; however, the sliding support was modelled as a fictitious spring. A high elastic stiffness was used to represent the rigid friction-force deformation of the sliding base. Seismic responses of the S-systems were calculated by considering the interaction and non-interaction between the primary and equipment systems. The results showed that, for both the strong and weak torsional coupled P-systems in the tuning condition, the seismic responses of the equipment system were increased with the increase in the values of the normalised eccentricities of the P-system. However, for non-tuning condition, an opposite trend of the variation of the dynamic responses of the equipment system was observed. Furthermore, for strong and weak torsional coupled P-systems in the tuning condition, the seismic responses of the S-systems were found higher if interaction was considered between the equipment and the P-systems.

In a study by Agrawal and Datta (2001), seismic behaviour of a multi-supported S-system mounted on a torsional coupled linear single storey P-system was investigated under the effect of bi-directional random seismic waves. The S-systems were considered to be attached to the P-system at multi-points as shown in Figure 2.20. The axial stiffness of the S-system was assumed very high. The normalised eccentricities of the P-system were varied to provide various degrees of a torsional coupling of the P-system. The dynamic behaviours of the S-systems were computed by considering the effect of the interaction or non-interaction between the primary and secondary systems. The results showed that, for the strong torsional coupled P-system and under both tuned and un-tuned conditions, the seismic responses of the S-system were decreased with the increase in value of e/r_e. Moreover, for the same above conditions, the dynamic responses were found higher if interaction is considered. However, an opposite trend was observed for the weak torsional coupled P-system, where the seismic responses were found higher if interaction is not considered.

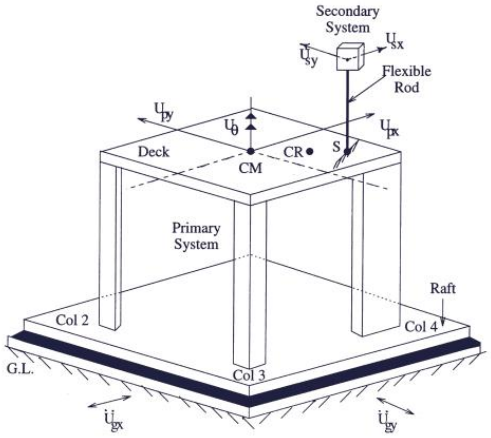

Figure 2.19 Primary-secondary system adopted by Agrawal (2000b) for the cases of using a sliding support.

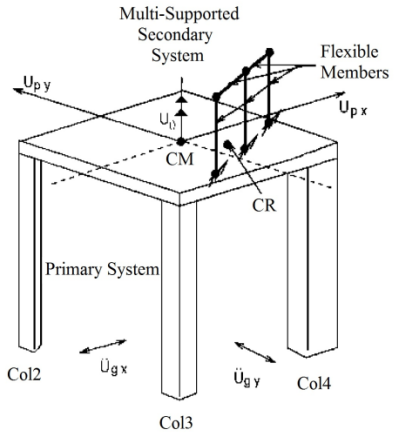

Figure 2.20 Primary-secondary system adopted by Agrawal and Datta (2001) for the case of S-system with a multi support.

2.3.1.2.2 S-systems Attached to Inelastic Three-dimensional P-systems

In the analytical studies by Agrawal and Datta (1999a, 1999b), seismic responses of S-systems attached to 3D P-systems that exhibited non-linearity were investigated during earthquakes. The eccentricity values of the P-system were considered in the two horizontal directions (X and Y), as shown in Figure 2.21. Even though these two studies were used similar sets of the coupled differential equations, modelling for the P-S system, and the same parametric values of the example study case, the results of the seismic response of the S-systems were found to be conflicting. For instance, in the study by Agrawal and Datta (1999a), the results showed that under the tuned condition, the dynamic responses of the S-system were increased with the increase in the normalised eccentricities (e/r_e) of the P-system; whereas, an opposite trend was observed under un-tuned condition. However, in the study by Agrawal and Datta (1999b), the results showed that under the tuned condition, the seismic responses of the S-system were decreased with the increase in the values of e/r_e; whereas, for un-tuned condition, the corresponding responses were found almost insensitive to change in e/r_e value. In most of the results of the above-mentioned studies were observed incompatible or non-similar in spite of adopting the same parameters.

To evaluate the seismic response of the S-systems attached to the floors of a multi-storey inelastic P-system (see Figure 2.22) under the effect of bi-directional random seismic waves, Agrawal (1999) adopted the same sets of the differential equations and modelling of both the primary and secondary systems that were used in the studies presented by Agrawal and Datta (1999a, 1999b). In general, it was concluded that, for strong and weak torsional coupled P-systems under the tuned condition, the dynamic responses of the equipment system attained their peak value if the equipment system is mounted on the 2^{nd} floor level. For low

and high values of eccentricity ratios, the seismic responses of the equipment system were found less when the equipment system located at the top floor level. It seems from the aforementioned conclusions that there were inconsistencies between the results presented in (Agrawal, 1999) and the recommendations of most current provision codes for the seismic design of the S-systems such as UBC (1997), IBC (2012), EC8 (2004), and ASCE (2010). These codes state that the acceleration amplification factors of both the primary and secondary systems would be maximum at the top floors of the P-system.

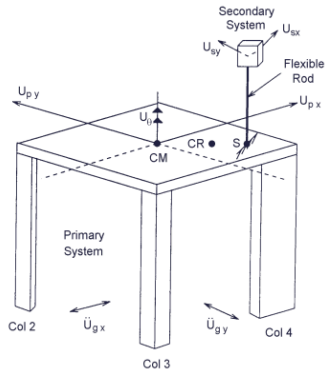

Figure 2.21 Primary-secondary system adopted by Agrawal and Datta (1999a, 1999b) with eccentricities in the X and Y directions.

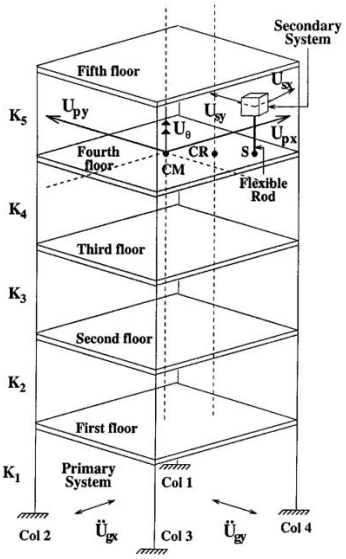

Figure 2.22 Primary-secondary system adopted by Agrawal (1999) with eccentricities in the X and Y directions.

2.3.2 Experimental Studies on NSCs with Torsional Effect

Experimental research studies addressing the seismic response of NSCs attached to torsional P-structures are scarce. An experimental research program by Mohammed *et al.* (2008) was conducted on a limited number of model tests to investigate the effect of both the stiffness eccentric and mass eccentric of the P-system on the seismic response of the NSCs. Figure 2.23 shows the adopted modelling of the P-S systems. This model was subjected to a unidirectional base motion; it was comprised of a square aluminium platform (300 mm × 300 mm) supported at its corners by 3 mm diameter aluminium rods with varied lengths for stiffness adjustment. The NSCs were modelled as a lumped mass and were either rigid or near tuned to the fundamental vibration periods of the P-systems. To simulate the mass's eccentricity in the P-system, additional masses were attached to the side of the platform. The results showed that the nonlinearity behaviour of the P-systems had considerable implications on the de-magnification of the seismic response of near resonant NSCs. Moreover, the experimental results demonstrated that the dynamic responses of the S-systems were increased due to the increase in the stiffness's eccentricity value of the supporting P-system as a result of increase of the torsional behaviour of the P-system; while these responses were decreased with the increase in the mass's eccentricity value as a result of increase in the value of fundamental periods of the P-system. However, Mohammed *et al.* (2008) concluded that their results were valid only for the investigated systems and cannot be generalised to different systems under different ground motions; or when higher numbers of fundamental vibration periods of the P-system are taken into account.

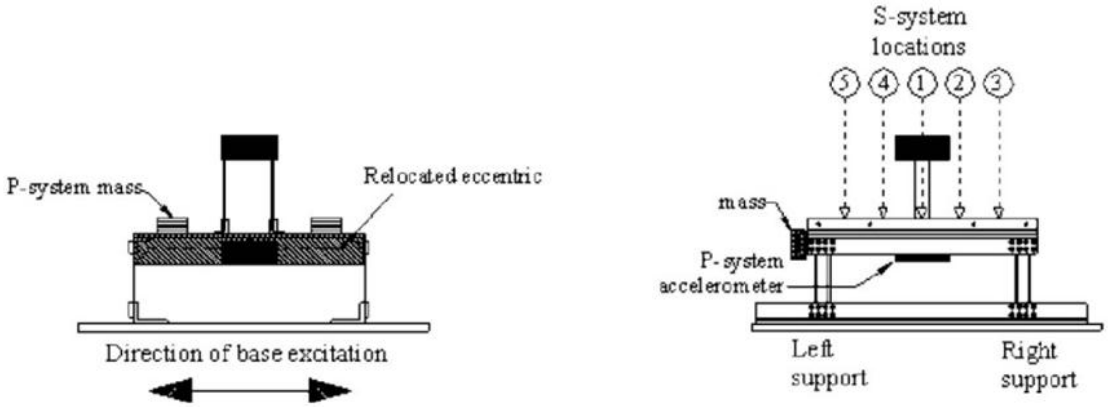

(a) (b)

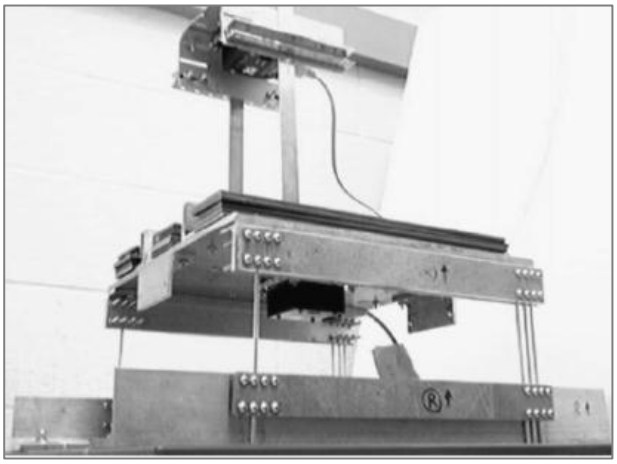

(c)

Figure 2.23 Experimental model details proposed by Mohammed *et al.* (2008) (a) elevation, (b) side view, and (c) three-dimensional view.

A careful evaluation of the research studies presented in Sections 2.3.1 and 2.3.2 suggests that there are limited experimental investigations on NSCs attached to a small scale of steel frame P-system, as well as there are significant conflicting results in the seismic behaviour of NSCs evaluated using analytical solutions. However, the main contributions of the current thesis can be summarised as follows: developing finite element predictive tools which can be used for evaluating the seismic response of NSCs attached to irregular complicated RC P-structures; identifying the essential parameters affecting the global seismic

behaviour of NSCs; developing several analytical relations that can be used to estimate the percentage increase or decrease in the NSCs accelerations due to the effects of rotation, seismic capacity, NSCs damping, and distribution of masses along the buildings heights; as well as evaluating the accuracy of the EC8 recommendation and suggesting a significant modification to improve its predictions.

2.4 Summary

According to the foregoing review of the literatures, it can be seen that much development has been made towards understanding of the seismic responses of the non-structural components when they attached to the supporting structures and subjected to moderate and severe base motions. The majority of the analyses and design methods of the S-systems, as well as the seismic codes were developed to reduce the damage and increase their functionality in the buildings. Notwithstanding these developments, the investigations and surveys on the damage of the S-systems during the recent earthquakes have concluded that the problem is an intricate one and has not been totally solved; therefore, it recommended that further research should be performed. The effect of the torsional behaviour of the P-systems on the seismic response of NSCs is one area of research that was recommended for further studies.

As discussed, torsional modes with the effect of seismic loading may significantly increase the seismic behaviour of the NSC if the primary structure is highly asymmetrical in the plan. Therefore, it may lead to incorrect designs of the NSCs, if the effect of torsion is ignored. This problem has received a little interest in the previous research; some analytical methods and very limited cases of experimental research were attempted to investigate the

dynamic behaviour of the S-systems integrated on either two dimensional P-system with eccentricity in one direction or single-bay P-system with eccentricities in the two horizontal directions (X and Y). Furthermore, despite some of these analytical methods were used similar sets of differential equations, modelling of the P-S systems, and the same parametric values of the example study case, the results of the dynamic responses of the S-systems were found to be conflicting.

Further research is thus needed to investigate the torsional effect and to develop the rational design methods of the NSCs when they housed inside complicated structures, which may behave a combination of lateral-torsional modes during earthquakes. The dynamic behaviour of complicated multi-storey reinforced concrete buildings and their attachments of the secondary elements cannot be formulated analytically considering the inelastic ductile behaviour of reinforced concrete members; it requires to be formulated with help of the numerical methods, in order to assess the torsional effects.

CHAPTER THREE: MATERIALS MODELLING AND GENERATION OF EARTHQUAKE RECORDS

3.1 Introduction

Numerical FE simulations of RC structures for dynamic performance evaluation require a very accurate modelling of the geometrical and mechanical properties of the materials of each structural element so that it can reproduce actual values of the seismic responses. Therefore, modelling of the structural members and the nonlinear material constitutive models should be chosen so that it is able to replicate the seismic behaviours of the structures such as their displacements, rotations, stiffness, fundamental periods, and their inelasticity, when they are subjected to dynamic forces up to failure. In this research, a windows-based computer FE code MIDAS Gen Ver. 3.1 (2013) is employed to perform all nonlinear dynamic analyses of the selected P-S systems. Some of the principle highlights of this software can be described as follows: MIDAS Gen adopts the speediest Multi-Frontal Solver for nonlinear analysis with employing the latest algorithms, which produce accurate results. Moreover, MIDAS Gen can provide design utilising numerous standards such as EC1 (2002), EC2 (2004), and EC8 (2004) of the European countries, as well as standard provisions of other countries to obtain an optimal design. In addition, it contains various ranges of elements and different material constitutive models for the concrete and steel fibres that can be used to model the structural members accurately (MIDAS Gen, 2013).

In this chapter, representative constitutive models, which were adopted to represent the nonlinear behaviour of the RC P-structures, are explained. Moreover, different sets of natural or artificial base motions that extracted or generated by the use of the computer codes, REXEL (Iervolino *et al.*, 2010a) or SIMQKE (SIMQKE, 1976; Gelfi, 2007) are also elucidated.

3.2 Material Modelling

In the present-day, due to the variety of the types of failure modes of the existing buildings during earthquakes, vast numbers of analytical and numerical approaches have been developed to evaluate their seismic nonlinear behaviour. Dynamic numerical analyses of three-dimensional (3D) systems such as multi-storey structures are computationally uneconomical when nonlinearity is considered. Therefore, different modelling methods of the structural elements have been proposed by different researchers (Suidan and Schnobrich, 1973; Ciampi and Carlesimo, 1986; Zeris and Mahin, 1988, 1991; Zienkiewicz and Taylor, 1989, 1991; Neuenhofer and Filippou, 1997; Wilson, 1998; Chen, 2007), to overcome this problem without reduction of the accuracy of the results. A beam-element model proposed by Spacone *et al.* (1996a, 1996b, 1996c) is one of the techniques that computationally very economically for the modelling of the hysteretic response of each member of the 3D structural model. This economy does not cause a reduction in the accuracy of the results of the beams and columns (Spacone *et al.*, 1996c; Neuenhofer and Filippou, 1997). Hence, a beam-element model was adopted in this research for the simulation of the primary structural elements.

As the current research deals with the RC P-structures having different cross-sections and amount of steel reinforcement, a suitable way was needed to model the cross-sections of the beams and columns. Therefore, a distributed inelastic fibre element as shown in Figure 3.1 was used to model the structural members. This modelling approach produces a very accurate simulation of the geometrical and mechanical characteristics of the structural elements to obtain an accurate representation of nonlinear behaviour along the length of the member (D'Ambrisi *et al.*, 2008). A perfect bond between the longitudinal steel bars and the concrete fibre is assumed for the modelling of the RC structural elements. Therefore, the effect of the bond-slip behaviour is not taken into account.

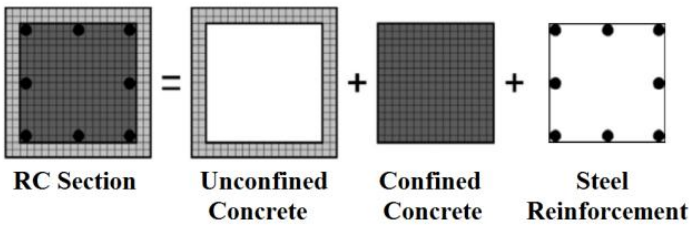

Figure 3.1 Description of a reinforced concrete section as implemented in MIDAS Gen code (2013).

In numerical analysis, the nonlinear behaviour of the structural element can be obtained by adopting the appropriate stress-strain relationships of the selected materials in the cross-section of the structural elements. Consequently, the reliability of the numerical results depends on the accuracy of the models used to describe the materials. In RC structures, the structural members can be composed from two main materials: concrete and steel.

In this research, the confined and unconfined mechanisms of the concrete were considered by adopting the model proposed by Mander *et al.* (1988). However, for steel

reinforcement the relationship developed by Menegotto and Pinto (1973) is employed. These two models are explained in detail in the following sections.

3.2.1 Concrete Constitutive Model

Various past earthquake events have observed that many structural members in existing RC structures that had insufficient shear reinforcements led to significant damage or even failure of these members (Park and Priestley, 1980; Zoghi, 2013). A suitable distribution of such as steel bars can provide a considerable improvement in the strength and ductility of the confined concrete. Therefore, considering the confinement factor of the shear reinforcements of the main structural elements in the case of the dynamic loads is very important.

Different research studies such as (Kent and Park, 1971; Muguruma *et al.*, 1980; Sheikh and Uzumeri, 1982; Mander *et al.*, 1988; Fujii *et al.*, 1988; Saatcioglu and Razvi, 1992) have implemented various tests on the confining effect of the shear reinforcement in the columns and developed a number of analytical models. The Mander *et al.* (1988) model is a widely-used in analysing RC structures under the effect of either static or dynamic loadings (Wu, 2007). This model was developed based on the test results of a full-scale of thirty-one RC columns with circular or rectangular cross-sections having different distributions of steel bars.

The stress-strain relationship model of the concrete material that proposed by Mander *et al.* (1988) is adopted in this research. The main reason of adopting this model is for its significant ability to represent the effect of the shear reinforcements of the structural members

on the global strength and ductility of the P-structures during earthquakes. By using this model as shown in Figure 3.2, the effect of different patterns of the steel confinement can be simulated (Cetisli and Naito, 2003). The shear reinforcement of a structural member can be designed as rectangular stirrups for beams and columns that have a rectangular cross-section. However, circular hoops are used for columns with a circular section. These stirrups or hoops can also have either uniform or non-uniform confinement stresses along the length of each member in the transverse axes. The concrete cover of the cross-section of the concrete may behave unconfined and ultimately becomes ineffective after the stresses reach to the value of the compressive strength of the concrete. Due to the confinement effect, the concrete core will continue in carrying the additional stresses at the high-level of the strains.

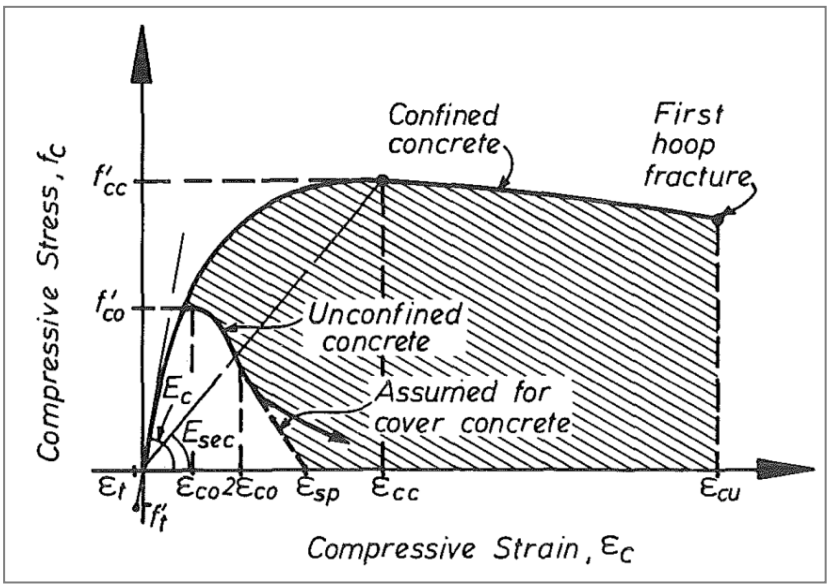

Figure 3.2 Stress-strain model of the confined and unconfined concrete (Mander *et al.*, 1988).

The expression of the stress-strain relationship according to Mander *et al.* (1988) model is based on a formula that was proposed by Popovics (1973). For slow rate of strain,

the compressive stress of the concrete f_c in the longitudinal direction can be estimated as follows:

$$f_c = \frac{f'_{cc}.\acute{x}\acute{r}}{\acute{r} - 1 + \acute{x}^{\acute{r}}} \tag{3-1}$$

in which, f'_{cc} is the ultimate confined compressive strength and can be evaluated based on the solution of the *"multi-axial failure criterion*", which can be expressed as follows (Mander *et al.*, 1988):

$$f'_{cc} = f'_{co}\left(-1.254 + 2.254\sqrt{1 + \frac{7.94\,f'_l}{f'_{co}}} - 2\frac{f'_l}{f'_{co}}\right) \tag{3-2}$$

where f'_{co} is unconfined compressive strength of the concrete; and f'_l is the effective stress due to the effect of the lateral confinement.

The parameter $\acute{x}$ in Eq. (3-1) can be calculated as a ratio between the longitudinal concrete compressive strain ε_c and the value of the strain ε_{cc} that corresponds to the value of f'_{cc}; see Figure 3.2. Therefore, the value of $\acute{x}$ can be expressed as follows:

$$\acute{x} = \frac{\varepsilon_c}{\varepsilon_{cc}} \tag{3-3}$$

where,

$$\varepsilon_{cc} = \varepsilon_{co}\left[1 + 5\left(\frac{f'_{cc}}{f'_{co}} - 1\right)\right] \tag{3-4}$$

in which, ε_{co} refers to the value of the strain at the corresponding value of f'_{co}. As recommended by Richart *et al.* (1928), in general, a value of ε_{co} equal to 0.002 can be adopted for unconfined concrete.

However, the parameter $\acute{r}$ in Eq. (3-1) can be expressed in terms of the concrete modulus of the elasticity as follows:

$$\acute{r} = \frac{E_c}{E_c - E_{sec}} \tag{3-5}$$

where E_c and E_{sec} are the tangent and secant modulus of elasticity of the concrete respectively and may be estimated as follows:

$$E_c = 5000\sqrt{f'_{co}}\ MPa \tag{3-6}$$

and,

$$E_{sec} = \frac{f'_{cc}}{\varepsilon_{cc}} \tag{3-7}$$

To define the relation between the stresses and strains in the cover zone of the concrete, the falling part of the curve at the range of $\varepsilon_c > 2\varepsilon_{co}$ is assumed a straight line as shown in Figure 3.2. Furthermore, it is assumed that the value of the concrete stress is equal to zero at the value of the spalling strain ε_{sp} amount to 0.004 (Sakai and Sheikh, 1989).

Furthermore, the following formulations can be used to estimate the concrete tensile strength f'_t and the corresponding value of the strain ε_t:

$$f'_t = 0.62\sqrt{f'_{co}}\ MPa \tag{3-8}$$

and,

$$\varepsilon_t = \frac{f'_t}{E_c} \tag{3-9}$$

where E_c is previously defined in Eq. (3-6).

To evaluate the effective lateral confinement stress, a similar method that was proposed by Sheikh and Uzumeri (1980, 1982) is implemented in the cross-section of the structural concrete element. The largest value of the transverse stress that can be developed from the effect of the shear reinforcement can only be applied effectively on the core zone of the concrete fibre, where the confinement stress has completely developed, due to the arching action. Figure 3.3 illustrates the arching action that can take place between the successive transverse rectangular stirrups.

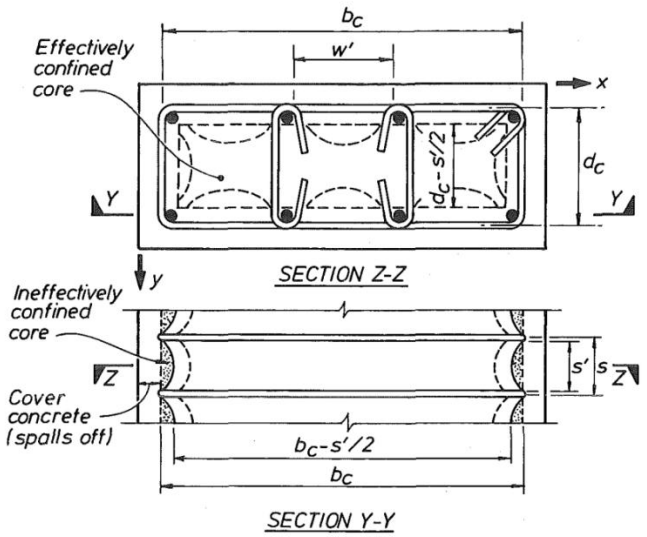

Figure 3.3 Effectively confined core for rectangular shear reinforcement (Mander *et al.*, 1988).

The concept of the confinement of concrete due to the effect of shear reinforcement has been used in most of modern seismic design provisions of the RC structural elements. These provisions provide criteria and limitations to define the length of the critical regions, as well as to specify the diameter and spacing of the transverse steel bars. For example, in the seismic design of the columns within a structure according to clause 5.4.3.2 of EC8 (2004), the critical length from both ends of the column should be equal to the largest value of (the larger dimension of the column cross-section; sixth of its clear height; or 450 mm). However,

the maximum value of the spacing between the hoops in the critical region should be equal to smallest value of (half of the smaller dimension of the stirrup; eight times of the diameter of the longitudinal steel bars; or 175 mm). Furthermore, hoops with diameter less than 6 mm should not be used in these regions.

3.2.2 Steel Constitutive Model

The available models that can be used to consider the nonlinear relationship of the stress-strain in cyclic behaviour of the steel fibre can be classified into two groups. In the first group, the formulations of the history dependent of the behaviour of the steel material is considered; while, the other group is based on the generalisation of the formula that was proposed by Ramberg and Osgood (1943). In the latter group, history dependence is also taken into account, but not in a direct manner. The Petersson and Popov (1977) model is a typical example of the first category; while the model that was suggested by Menegotto and Pinto (1973) is a widely-known model of the second group.

In this research, the model developed by Menegotto and Pinto (1973) is adopted to describe the nonlinear behaviour of longitudinal steel reinforcement. The main characteristics of this model are that is numerically efficient and agrees very well with the results of cyclic tests on steel reinforcement bars. According to the Menegotto and Pinto (1973) model as shown in Figure 3.4, the expression of the nonlinear relation of the stress-strain of the steel reinforcement can be expressed as follows:

$$\sigma^* = b.\varepsilon^* + \frac{(1-b).\varepsilon^*}{(1+\varepsilon^{*R})^{1/R}} \tag{3-10}$$

where the values of the effective stress σ^* and strain ε^* can be expressed in terms of the unload/reload interval as follows:

$$\varepsilon^* = \frac{\varepsilon_s - \varepsilon_r}{\varepsilon_o - \varepsilon_r} \tag{3-11}$$

and,

$$\sigma^* = \frac{\sigma_s - \sigma_r}{\sigma_o - \sigma_r} \tag{3-12}$$

where ε_s and σ_s are, respectively, the strain and stress values of the steel fibre; while the values of $\varepsilon_r, \sigma_r, \varepsilon_o$, and σ_o can be defined as follows:

$(\varepsilon_r, \sigma_r)$: is the unloading point; at the initial linear condition, which is taken equal to (0, 0) and,

$(\varepsilon_o, \sigma_o)$: is the point of the intersection of two asymptotes that describes the loading or unloading curve path.

The reduction factor in the stiffness of steel fibre b in Eq. (3-10) can be defined as the ratio between the final and initial tangent stiffness E_1/E_0, as explained in Figure 3.4. However, the parameter R describes the shape of the unloading curve. Furthermore, this parameter allows good representation of Bauschinger effect, which refers to the changes in the stress-strain characteristics upon the inversion of loading due to changes in the microscopic stress distribution of the material (Kent and Park, 1969; Taucer *et al.*, 1991), which can be computed as follows:

$$R = R_o - \frac{a_1 . \xi_S}{a_2 + \xi_S} \tag{3-13}$$

in which, R_o refers to the exponential transition elastic-plastic of steel fibre; however, a_1 and a_2 are referred to the first and second isotropic hardening parameters of the steel fibre. The values of the parameters $R_o, a_1,$ and a_2 are taken respectively as equal to 20, 18.5, and 0.15 as obtained from the experimental results achieved by Seckin (1981). Similar values were obtained by Filippou *et al.* (1983). Moreover, the parameter ξ_S in Eq. (3-13) is represented the variance between the maximum and initial values of the strains in loading or unloading paths.

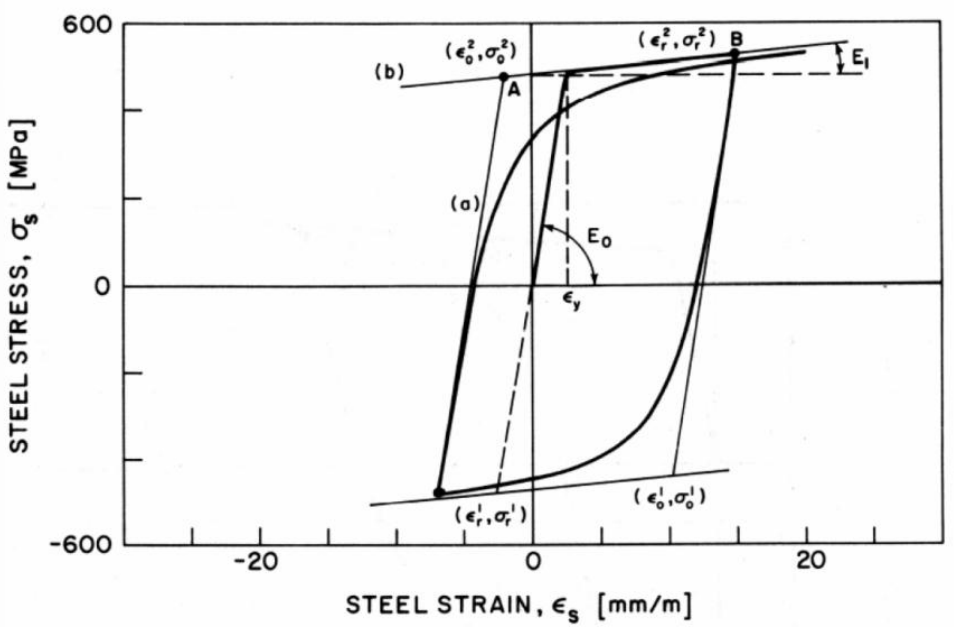

Figure 3.4 Stress-strain relationship of the steel reinforcement model (Menegotto and Pinto, 1973).

3.3 Generation of Earthquake Records

The appropriate selection of the base motion records as an input is one of the principle concerns in the dynamic analysis of the systems. The earthquake records should be chosen so as to be compatible with ground type where the structure is constructed (Iervolino *et al.*, 2008, 2009). In most of the current seismic codes provisions, e.g. EC8 (2004), a set of earthquake records is to be selected for the purposes of the analysis and design of the structures. These two purposes may require base motions data that often not available to the engineers. Moreover, it would be difficult to achieve a good fitting with a coded response spectrum (RS) of the selected base motions, if a suitable tool does not exist (Iervolino *et al.*, 2008, 2009). For analysis and design purposes, it is usually preferred to use a spectrum fitting accelerogram, which can be either natural or artificial earthquake database. On the other hand, natural records are known as the best choice to simulate the seismic effect for the structural evaluation. Therefore, considerable efforts have been made to provide and improve tools for aided code-based earthquake database generation (Naeim *et al.*, 2004).

Based on the provisions of the EC8 (2004), elastic response spectra of either Type 1 or Type 2 are considered to introduce the seismic effect. The latter type of RS should be used for the design and analysis purposes if the influence of the base motion has a magnitude of surface wave (Ms) less than 5.5, otherwise Type 1 should be adopted. In general, elastic RS shapes of Type 1 and Type 2 have a functional shapes based on the peak ground acceleration and ground type. For earthquakes having a value of Ms larger than 5.5, the elastic RS shapes $S_e(T)$ for the two horizontal orthogonal accelerograms can be calculated according to EC8 (2004) as follows:

$$
\begin{aligned}
S_e(T) &= a_g \cdot S \cdot \left[1 + \frac{T}{TB} \cdot (\eta \cdot 2.5 - 1)\right] && for\ 0 \le T \le TB \\
S_e(T) &= a_g \cdot S \cdot \eta \cdot 2.5 && for\ TB \le T \le TC \\
S_e(T) &= a_g \cdot S \cdot \eta \cdot 2.5 \left[\frac{TC}{T}\right] && for\ TC \le T \le TD \\
S_e(T) &= a_g . S \cdot \eta \cdot 2.5 \left[\frac{TC.TD}{T^2}\right] && for\ TD \le T \le 4s
\end{aligned}
\tag{3-14}
$$

where T is the vibration period of a linear SDOF system and a_g is the design value of the ground acceleration for ground type A and its value to be determined according to the national provisions. The terms TB and TC are, respectively, represented the lower and upper periods of the constant horizontal zone of the spectral shape (see Figure 3.5); however, TD is the value, which indicates the start point of the constant displacement limit of the spectrum. Furthermore, the parameter S is the soil factor and η is a factor that takes into account the correction due to a damping ratio. As per EC8 (2004) provision, the value of η is equal to 1.0 for the damping ratio of 5%. The recommended values of the parameters; S, TB, TC, and TD are given in Table 3.1 (EC8, 2004).

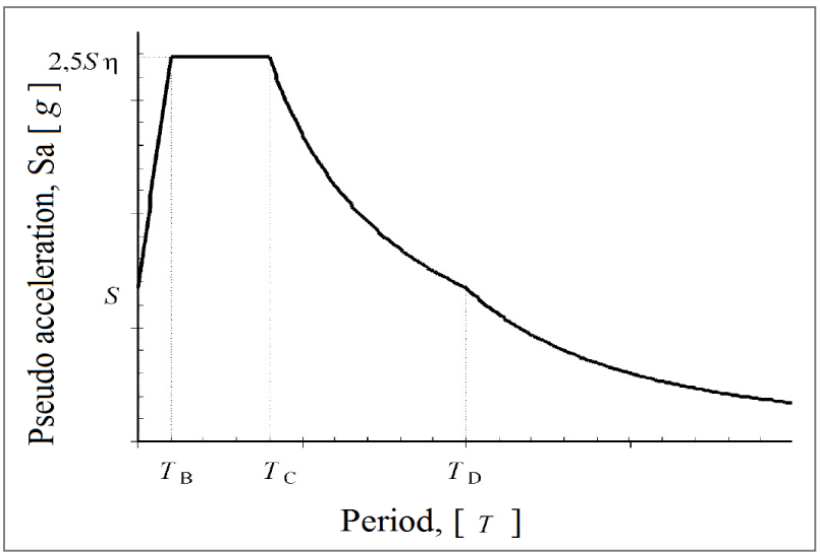

Figure 3.5 Shape of the elastic response spectrum according to the EC8 (2004).

Table 3.1 Description and parameter values of different ground types; namely A, B, C, D, and E for the EC8 (2004) Type 1 response spectrum.

Ground type	Description of stratigraphic profile	Elastic RS parameters			
		S	TB [s]	TC [s]	TD [s]
A	*"Rock or other rock-like geological formation, including at most 5 m of weaker material at the surface"*	1.00	0.15	0.40	2.00
B	*"Deposits of very dense sand, gravel, or very stiff clay, at least several tens of metres in thickness, characterised by a gradual increase of mechanical properties with depth"*	1.20	0.15	0.50	2.00
C	*"Deep deposits of dense or medium dense sand, gravel or stiff clay with thickness from several tens to many hundreds of metres"*	1.15	0.20	0.60	2.00
D	*"Deposits of loose-to-medium cohesionless soil (with or without some soft cohesive layers), or of predominantly soft-to-firm cohesive soil"*	1.35	0.20	0.80	2.00
E	*"A soil profile consisting of a surface alluvium layer and thickness varying between about 5 m and 20 m, underlain by stiffer material"*	1.40	0.15	0.50	2.00

For the seismic structural evaluation, EC8 (2004) allows the use of accelerograms that can be selected from neutral earthquakes, or artificially generated base motion records. To fulfil the provisions of EC8 in regards to the selection of the accelerograms that match with Type 1 or Type 2 elastic RS, the following criteria should be achieved (EC8, 2004; Iervolino *et al.*, 2008, 2009):

1. a minimum of 3 base motions should be adopted;
2. the average value of the spectral acceleration that estimates from the individual base motions at zero period should not be lower than the value of $a_g.S$ for ground under consideration, where *S* is the factor of the soil as given in Table 3.1;
3. in the limit of the vibration periods in the range of ($0.2T_1$ - $2T_1$), value of the average spectral acceleration that computes from the set of the base motion records with a 5% damping ratio, should be lower than 10% as a tolerance of that value given in the

coded elastic RS. The period T_1 represents the first fundamental vibration period of the P-structure.

According to the EC8 (2004) provisions (see clause 4.3.3.5.2-1), the seismic influence of the vertical accelerograms of the earthquakes should be considered only for structures designed as base isolation systems and for those structures designed as special cases. Some of these cases are: structures with horizontal structural elements that have a span equal to or greater than 20 m; cantilever members larger than 5 m and structures with pre-stressed members. Furthermore, the vertical seismic influence should be taken into account when the value of the design vertical acceleration (av_g) is larger than 0.25 g on ground type A. In the current research, the effect of the vertical accelerations has not been taken into account.

One of the main criteria for selecting the type of ground of each group of the considered P-structures in this research is herein explained. The experimental investigation by Negro *et al.* (2004) and the numerical study by Rozman and Fajfar (2009), on which parts of this research are based, adopted the elastic spectra of the longitudinal and transverse components of the natural records. These accelerograms are compatible with the EC8 (2004) Type 1 elastic spectrum for ground type C. Hence, for comparison purposes, the majority of the considered buildings were assumed to be constructed on ground type C (deep deposits of dense or medium-dense sand, gravel or stiff clay). However, several cases (i.e. 16 cases of P-structures) were assumed to be constructed on ground types A, B, D, and E, to investigate the effect of ground type on the seismic response of NSCs and to confirm that the conclusions drawn in the current research are not limited only to ground type C.

In addition, in order to increase confidence in the results of the estimation of the seismic behaviours of the NSCs during the nonlinear dynamic analyses, various sets consisting of 70 of either natural or artificial seismic records consistent with the elastic RS for ground types A, B, C, D, and E of EC8 (2004) were used in this research. The natural records as described later in Tables 3.2 to 3.5, were extracted from the ESD using the computer code REXEL Ver. 3.5 (beta) (Iervolino *et al.*, 2010a). Whereas, the artificial records as illustrated later in Figure 3.11, were generated by the use of SIMQKE code (SIMQKE, 1976; Gelfi, 2007).

In the following, explanations on the adopted earthquake records for the nonlinear dynamic analyses of each group of the considered P-structures. Strategy that used for choice the type of the records (i.e. source of the earthquakes (natural or artificial) and ground type) was based on the aforementioned criteria.

The natural earthquake records were used to investigate the seismic behaviour of NSCs integrated on different cases of buildings presented in the current research. It can be summarised as follows: The first group of buildings designed for ground type C (i.e. 4 cases of P-structures physically tested and/or previously modelled by Negro *et al.* (2004) and/or by Rozman and Fajfar (2009)) and the third group of buildings (16 cases of P-structures) designed for ground types A, B, and D of EC8 (2004). These two groups of buildings were presented in Chapter 5. Furthermore, the natural accelerograms were adopted for the cases of NSCs attached to eight P-structures having different eccentricity ratios and designed for ground type C as presented in Chapter 6.

However, artificial accelerograms were employed to evaluate the seismic response of the NSCs attached to the second group of buildings (5 cases of P-structures) designed for ground type C and for those NSCs mounted on P-structures in the third group of buildings designed only on ground type E as introduced in Chapter 5. Moreover, the artificial records were used for the cases of NSCs mounted on the P-structures having thirty cases of vertical mass irregularities as described in Chapter 7. Artificial accelerograms compatible with the EC8 (2004) Type 1 elastic RS for ground type E were selected instead of the natural earthquake records due to the shortage of natural records for this type of ground (i.e. "*soil profile consisting of a surface alluvium layer"* EC8, 2004) in the ESD (Iervolino *et al.*, 2008, 2010a).

The following sections describe the main features of the selected two computer codes; namely REXEL and SIMQKE. Furthermore, the substantial characteristics of the extracted natural and generated artificial records that were used in the dynamic analyses of the selected cases of P-S systems in this research are presented.

3.3.1 Extraction of the Natural Records

REXEL code (Iervolino *et al.*, 2010a, 2010b, 2010c) was used to extract the natural records based on EC8 (2004) provisions. This code can be operated using a MATHWORKS-MATLAB graphic user interface and a FORTRAN engine. Currently, the databases that are implemented in REXEL software are the European Strong-motion Database (ESD) and the Italian Accelerometric Archive (ITACA), as well as the records with "*Selected Input Motions for displacement-Base Assessment and Design* – SIMBAD". All data records that are included

in the REXEL code fulfilling the "free-field" state and they created by moment magnitude of accelerograms (Ms) greater than 4.0, as shown in Figure 3.6.

It can be seen from Figure 3.6 that the majority of the earthquake data, which recorded on ground types A, B, C, and D have values of the moment magnitudes larger than 5.5. However, for those records on ground type E, the values of the moment magnitudes are in the rage between 4.0 and 5.0.

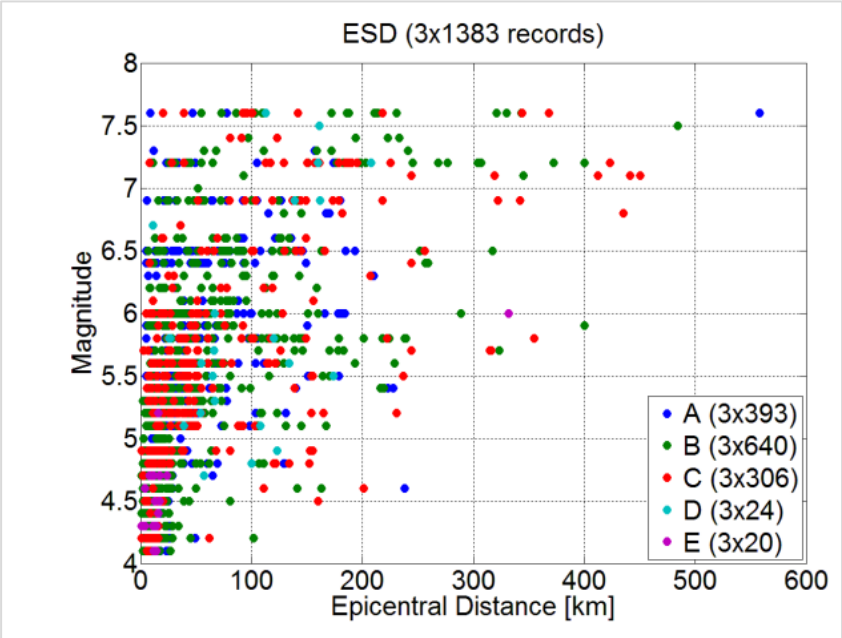

Figure 3.6 Relationship between the moment magnitude and distance distribution of the ESD records featured in the REXEL code (Iervolino *et al.*, 2010b).

Four sets of natural accelerograms have been extracted from the ESD by the use of REXEL code (Iervolino *et al.*, 2010a). Each of these sets consisting of 14 accelerograms (seven records in each of the X and Y directions) that match with the EC8 (2004) Type 1 elastic RS and for four types of ground; namely A, B, C, and D, with a 5% damping ratio. A minimum value of the surface wave magnitude equal to 6.0 was chosen as an input for the

selection of the databases. However, due to geological condition and shortage of the natural records on ground type E (see Figure 3.6) in the database of the ESD (Iervolino *et al.*, 2008, 2009, 2010a), seven artificial accelerograms matching with the EC8 (2004) Type 1 elastic RS for ground type E were generated, as described later in Section 3.3.2. A tolerance ratio of 10% was adopted for the lower and upper limits of tolerance, so that the mean values of the pseudo-accelerations (PSAs) of the resulted records fit with the coded RS within these two limits of tolerance.

Tables 3.2 to 3.5 summarise the main characteristics of the selected natural records that were extracted using the REXEL code. The mean response spectrum of the natural records selected using REXEL was not quite compatible with the EC8 (2004) Type 1 spectrum for ground types A, B, C, and D. The selected natural records were therefore modified using the computer software SeismoMatch Ver. 2.1 (Seismosoft, 2009) without increasing the number of motion cycles, as the case is for artificial records.

Table 3.2 Characteristics of the natural ground motion records compatible with ground type A of EC8 (2004) extracted from the ESD.

Code	Earthquake Name	Station ID	Date	Ms	PGA-X [m/s^2]	PGA-Y [m/s^2]
000055	Friuli	ST20	06/05/1976	6.5	3.499	3.097
000234	Montenegro (aftershock)	ST68	24/05/1979	6.2	0.667	0.754
000287	Campano Lucano	ST93	23/11/1980	6.9	1.363	1.776
000410	Golbasi	ST161	05/05/1986	6.0	0.383	0.538
004674	South Iceland	ST2486	17/06/2000	6.5	3.118	3.311
006335	South Iceland (aftershock)	ST2557	21/06/2000	6.4	1.248	1.132
007142	Bingol	ST539	01/05/2003	6.3	5.051	2.918
Mean				6.4	2.190	1.932

Table 3.3 Characteristics of the natural ground motion records compatible with ground type B of EC8 (2004) extracted from the ESD.

Code	Earthquake Name	Station ID	Date	Ms	PGA-X [m/s^2]	PGA-Y [m/s^2]
000147	Friuli (aftershock)	ST28	15/09/1976	6.0	1.384	2.319
000202	Montenegro	ST70	15/04/1979	6.9	0.411	0.572
000232	Montenegro (aftershock)	ST77	24/05/1979	6.2	0.560	0.543
000291	Campano Lucano	ST276	23/11/1980	6.9	1.526	1.725
001711	Ano Liosia	ST1255	07/09/1999	6.0	0.855	0.760
001713	Ano Liosia	ST1257	07/09/1999	6.0	1.087	0.839
004673	South Iceland	ST2482	17/06/2000	6.5	2.038	4.678
Mean				6.35	1.123	1.634

Table 3.4 Characteristics of the natural ground motion records compatible with ground type C of EC8 (2004) extracted from the ESD.

Code	Earthquake Name	Station ID	Date	Ms	PGA-X [m/s^2]	PGA-Y [m/s^2]
000133	Friuli (aftershock)	ST33	15/09/1976	6.0	1.069	0.932
000333	Alkion	ST121	24/02/1981	6.6	2.257	3.036
000334	Alkion	ST122	24/02/1981	6.6	2.838	1.671
000335	Alkion	ST121	25/02/1981	6.3	1.144	1.176
000600	Umbria Marche	ST223	26/09/1997	6.0	1.685	1.041
000879	Dinar	ST271	01/10/1995	6.4	2.674	3.131
001726	Adana	ST549	27/06/1998	6.3	2.158	2.644
Mean				6.3	1.975	1.947

Table 3.5 Characteristics of the natural ground motion records compatible with ground type D of EC8 (2004) extracted from the ESD.

Code	Earthquake Name	Station ID	Date	Ms	PGA-X [m/s^2]	PGA-Y [m/s^2]
000074	Gazli	ST27	17/05/1976	6.7	6.038	7.065
000155	Bucharest	ST39	04/03/1977	7.5	1.976	1.690
000204	Montenegro	ST72	15/04/1979	6.9	0.533	0.599
000472	Vrancea	ST39	30/05/1990	6.9	0.373	0.527
000614	Umbria Marche	ST229	26/09/1997	6.0	0.168	0.185
001249	Izmit	ST767	17/08/1999	7.6	2.580	1.721
003717	Duzce 1	ST767	12/11/1999	7.2	0.376	0.247
Mean				6.97	1.721	1.719

As shown in Figures 3.7 to 3.10, the mean pseudo-accelerations of the modified natural ground motions in the X and Y directions good match with the EC8 (2004) Type 1 elastic RS of each type of the adopted ground types and for the damping ratio equal to 5%.

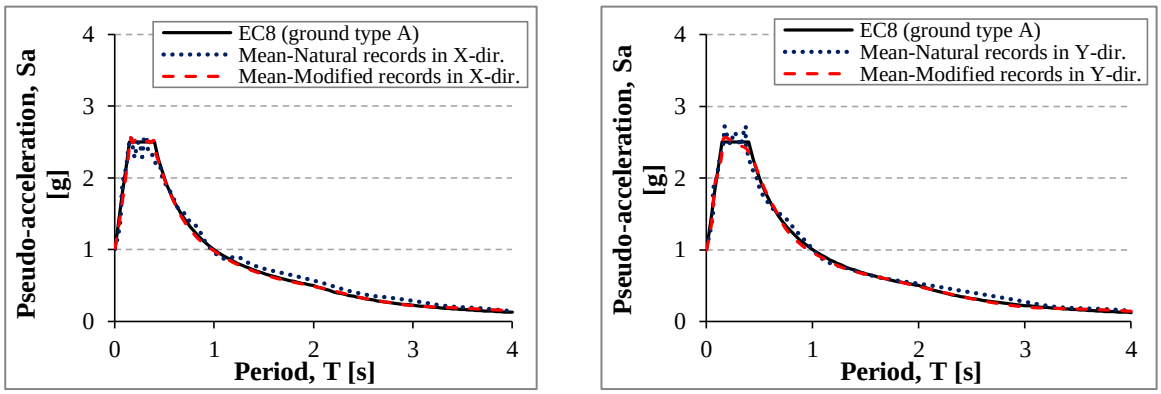

(a) (b)

Figure 3.7 Response spectra of the selected natural and modified ground motions of those matching with the EC8 (2004) Type 1 elastic RS for ground type A in the (a) X-direction and (b) Y-direction.

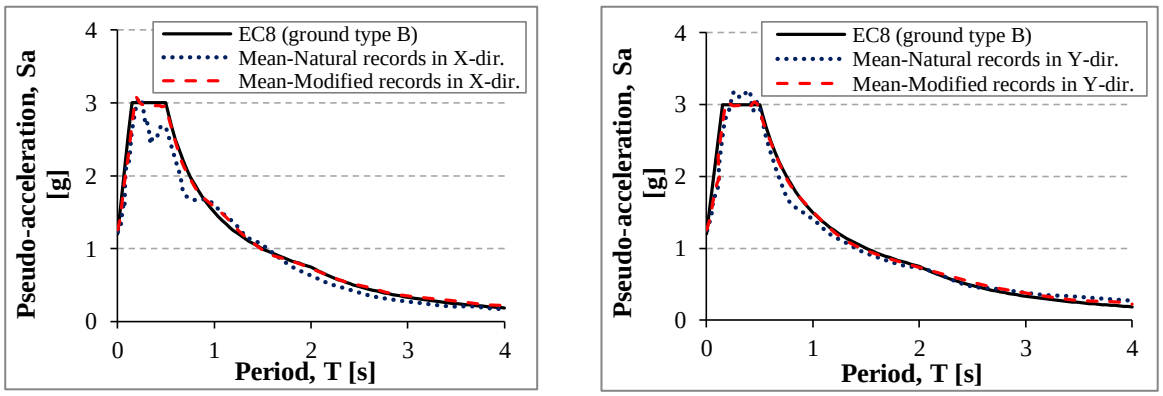

(a) (b)

Figure 3.8 Response spectra of the selected natural and modified ground motions of those matching with the EC8 (2004) Type 1 elastic RS for ground type B in the (a) X-direction and (b) Y-direction.

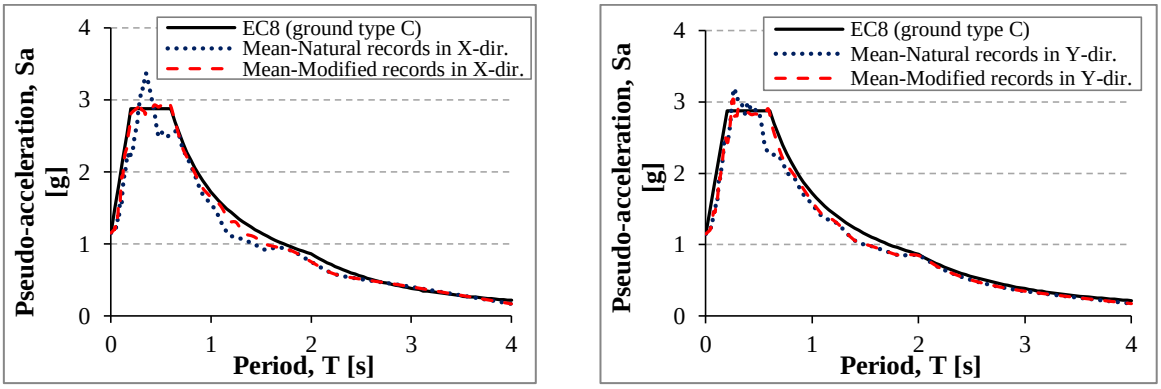

(a) (b)

Figure 3.9 Response spectra of the selected natural and modified ground motions of those matching with the EC8 (2004) Type 1 elastic RS for ground type C in the (a) X-direction and (b) Y-direction.

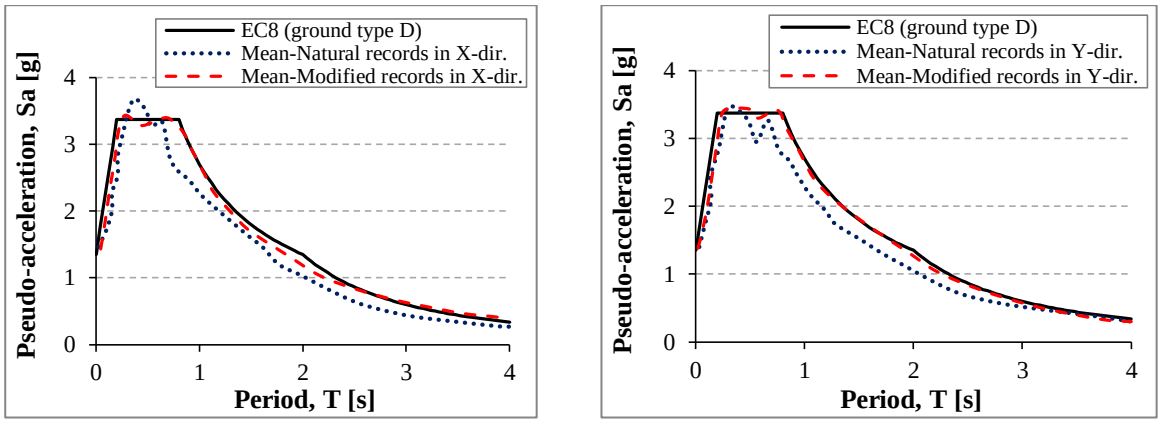

(a) (b)

Figure 3.10 Response spectra of the selected natural and modified ground motions of those matching with the EC8 (2004) Type 1 elastic RS for ground type D in the (a) X-direction and (b) Y-direction.

3.3.2 Generation of the Artificial Records

In the last two decades, different computer codes have been used to generate the artificial base motion records. PSEQGN code (Ruiz and Penzien, 1969) is one of the first programs operating in a DOS system that was used for the generation of random artificial motion records with reference to acceleration, velocity, or displacement. In 1976, SIMQKE code

(SIMQKE, 1976; Gasparini and Vanmarcke, 1976) was developed for the same purpose. The generation procedure of artificial records using SIMQKE code is very similar to that used for PSEQGN code and is also similar to most of the other codes such as RASCAL (Silva and Lee, 1987) and RSCTH (Halldorsson *et al.*, 2002).

A spectral density method that is based on the theory of random vibration has been adopted in most codes for the artificial generation of the accelerograms (Newmark and Rosenblueth, 1971; Vanmarke, 1976). The generated records using a spectral density method are actually just a pure mathematical description of the spectrum characteristics that are compatible to the reference coded RS. The advantage of this approach is that it can obtain accelerograms completely, which are compatible with the coded elastic RS, but it generates an excessive number of strong motion cycles with a high-energy content.

In this research, SIMQKE code Ver. 2.7 (SIMQKE, 1976; Gelfi, 2007), was used to generate artificial base motion records. The applicability of this code to produce sets of fitting artificial accelerograms that can be employed in nonlinear time history analyses were assessed by Booth (1999), Nguyen (2006) and Waller (2010). Their results showed that SIMQKE code is efficiency enough to create earthquake records that in conformity with the requirements of the EC8 (2004) provisions.

SIMQKE code (SIMQKE, 1976; Gelfi, 2007) allows the generating artificially of a predetermined envelop shapes of accelerograms, which are statistically independent and refer to a specified spectrum response (Gasparini and Vanmarcke, 1976). This code generates a power function of density spectral response from the adapted spectrum, then, draws sinusoidal

signals that have random phase angles and amplitudes. SIMQKE code can be operated with both DOS and windows systems using the Visual FORTRAN Compilers.

According to EC8 (2004), the generated artificial records should match the adopted elastic RS that is given in EC8 and for viscous damping ratio of 5%. Furthermore, the durations of the artificial records should be larger than or equal to 10 seconds. In addition, a minimum of three artificial records should be adopted.

In this research, two sets of artificial records were generated using SIMQKE code (SIMQKE, 1976; Gelfi, 2007). Each of these sets is consisted of seven accelerograms that matched with Type 1 RS of EC8 (2004). The first set of the records was generated so as its seven response spectra matched with the EC8 (2004) Type 1 RS for ground type C, as shown in Figure 3.11(a). As explained in Section 3.3.1, the number of the natural records on ground type E is very limited in the database of the ESD, as well as these records have a moment magnitude (Ms) less than 5.5; hence, they do not satisfy the recommendations of EC8 (2004) for RS Type 1. Therefore, seven artificial records that matched with Type 1 RS for ground type E were also generated, as shown in Figure 3.11(b).

It can be observed from Figure 3.11 that the RS of the mean of the seven generated artificial records is very well-matched with the EC8 (2004) Type 1 elastic response spectra for the selected ground types and for a 5% damping ratio.

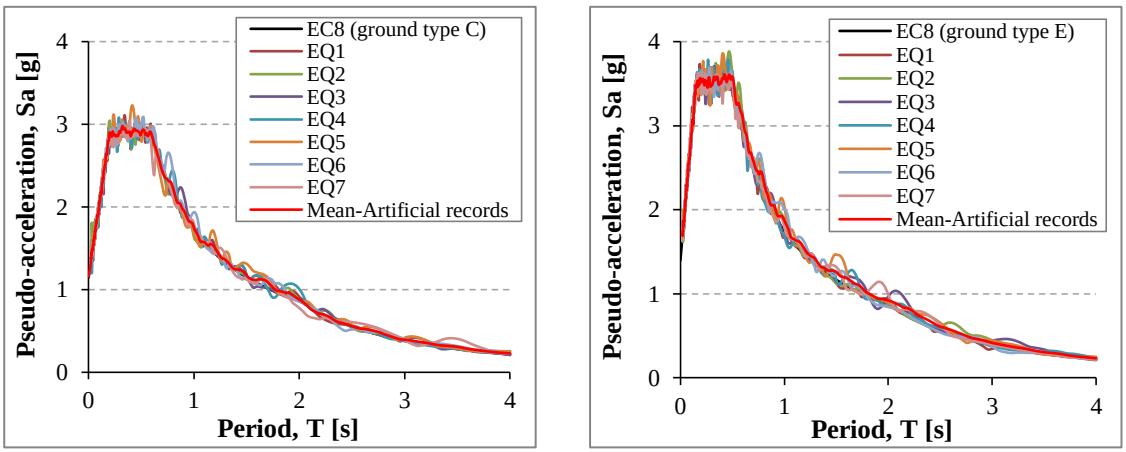

(a) (b)

Figure 3.11 Comparison between the response spectra of the generated artificial records with the EC8 (2004) Type 1 elastic RS with a 5% damping ratio for (a) ground type C and (b) ground type E.

3.4 Summary

As the current study deals with the case of non-structural components attached to various cases of simple or complex multi-storey primary structures designed for different amount and distribution of the steel reinforcements within their cross-sections; therefore, economic and accurate simulation of the primary structural elements during the nonlinear dynamic analyses of the primary-secondary systems was required. In this research, a distributed inelastic fibre beam-element that accurately can simulate the geometrical and mechanical properties of the concrete and steel reinforcement within the cross-section of the structural elements is selected. A perfect bond between the longitudinal steel bars and the concrete is assumed.

The nonlinear material constitutive models for the concrete and steel reinforcement, which adopted in the current research, were described in Chapter 3. The two well-known models of the concrete and steel, respectively namely, Mander *et al.* (1988) and Menegotto

and Pinto (1973) models are adopted to represent the non-linear behaviour of each material under the effect of dynamic loading. The great advantage of Mander *et al.* (1988) model is its significant ability to represent the effect of the shear reinforcements (i.e. confinement effectiveness) of the structural members on the global strength and ductility of the P-structures during earthquakes. However, simulation of various degrees of cyclic degradation of the inelastic relationship between the stresses and strains in reinforcing bars and considering for the effect of Bauschinger, are the main features of the constitutive model that proposed by Menegotto and Pinto (1973).

In Chapter 3, fifty-six natural earthquakes in the horizontal X and Y directions extracted using REXEL code and fourteen artificial records generated using SIMQKE code, were explained. The natural records were extracted from the European Strong-motion Database; however, the artificial records were generated with excessive number of strong motion cycles, which had higher energy content. All earthquake records were selected based on the EC8 (2004) criteria such as types of ground and the corresponding response spectrum of each ground. The resulted natural records using both the REXEL and SeismoMatch codes were found completely fitting with the elastic response spectra of EC8. Furthermore, the generated artificial records, which observed quite well-matched with the coded RS, demonstrated that the SIMQKE code was efficiency enough to produce such accelerograms.

CHAPTER FOUR: VALIDATION OF FINITE ELEMENT CODE FOR MODELLING OF REINFORCED CONCRETE IRREGULAR STRUCTURES AND NSCs

4.1 Introduction

In order to validate the finite element FE code used in this research and establish the reliability of the FE results, it was deemed necessary to base these results on a physically tested RC P-structure with significant torsional behaviour. The irregular three-storey RC P-structure "SPEAR" (Negro *et al.*, 2004) that exhibited significant torsional mode during the effect of bi-directional earthquakes was therefore selected for the validation of the FE code, as explained in detail in Section 4.2. However, verification of the modelling the NSCs using the FE approach by adopting both the modal and time-history analyses is illustrated in Section 4.3.

4.2 Verification of Modelling the P-structure

This section summarises the validation of the FE code, MIDAS Gen Ver. 3.1 (2013) that was adopted in this research for implementation dynamic analyses of irregular RC frame structures.

The building selected for the validation of the software is the SPEAR building (Negro *et al.*, 2004) because of its significant torsional behaviour. The SPEAR structure is an

asymmetric full-scale three-storey RC structure built and tested within a European research project at the Joint Research Centre-ELSA Laboratory in 2004. In the following sections, characteristics and modelling, and the dynamic FE analyses of the SPEAR structure, as well as the comparison between the FE results and the corresponding experimental data (Negro *et al.*, 2004; Fajfar *et al.*, 2006), are illustrated.

4.2.1 Characteristics and Modelling of the SPEAR Structure

The SPEAR building was designed according to the concrete design code employed in Greece between 1954 and 1995 (i.e. designed due to gravity load only, without specific provisions for seismic resistance). Detailed information on this structure is available in (Negro *et al.*, 2004; Rozman and Fajfar, 2009). The building is asymmetric in the plan in the horizontal directions (X and Y), as shown in Figure 4.1(a). This asymmetrical characteristic in the plan, made the centre of mass of the structure to be different from the centre of rigidity by values of eccentricity in the X and Y directions (e_x and e_y) equal to 1.3 m and 1.0 m respectively. The typical floor height is 3.0 metres (m) from top to top of the slab; however, the thickness of the slab is 150 mm, as shown in Figure 4.1(b).

The characteristic values of the permanent floor load and the variable action were taken as 0.5 kN/m^2 and 2.0 kN/m^2 respectively. The diameters of the longitudinal and transverse steel reinforcements of the columns were composed of 12 mm bars and 8 mm stirrups respectively. Clear concrete cover equal to 15 mm was adopted for the structural members. The dimensions of the square columns (i.e. C1-C5 and C7-C9) were 250 mm × 250 mm. However, the dimensions of the rectangular column i.e. C6, of 750 mm × 250 mm were

selected (see Figures 4.2(a) and 4.2(b)). In addition, Figure 4.2(c) shows a typical cross-section of the beams. Longitudinal steel reinforcement detail in a typical beam along the columns C5, C1, and C2 of the SPEAR building is shown in Figure 4.3.

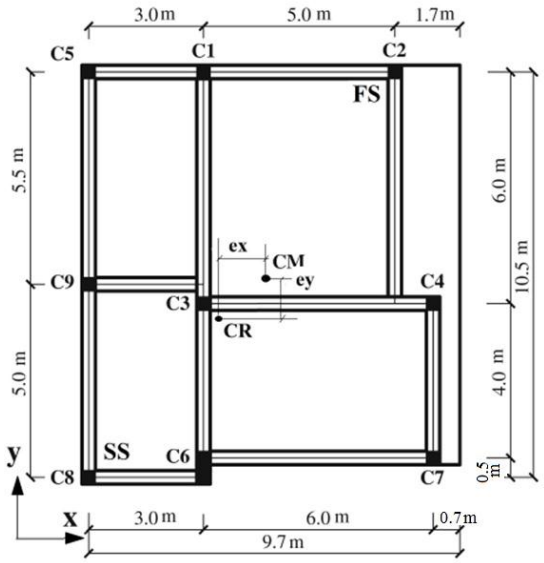

(a)

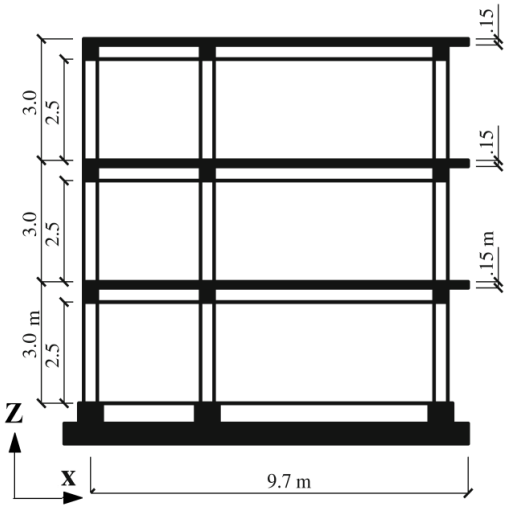

(b)

Figure 4.1 The SPEAR structure (a) plan and (b) elevation (Rozman and Fajfar, 2009) - all dimensions are in metres.

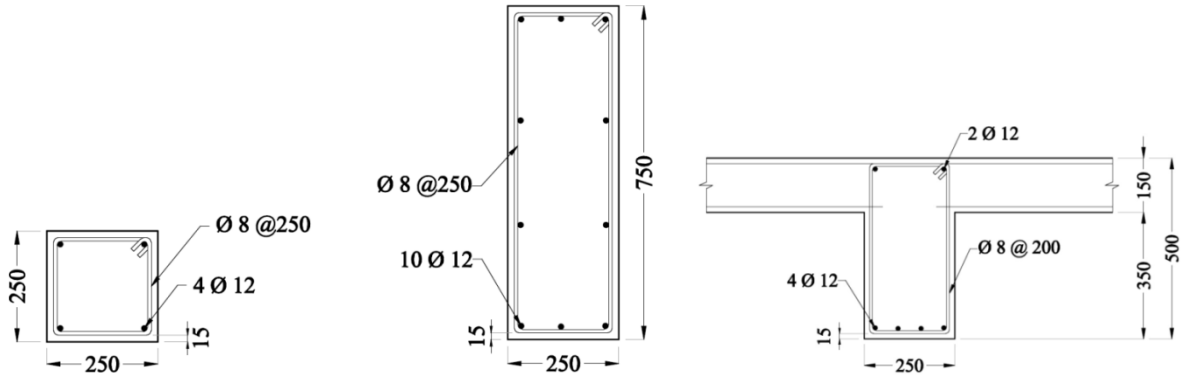

(a) (b) (c)

Figure 4.2 Details of the typical cross-sections of the SPEAR structure (a) square column, (b) rectangular column, and (c) beam (all dimensions are in millimetres).

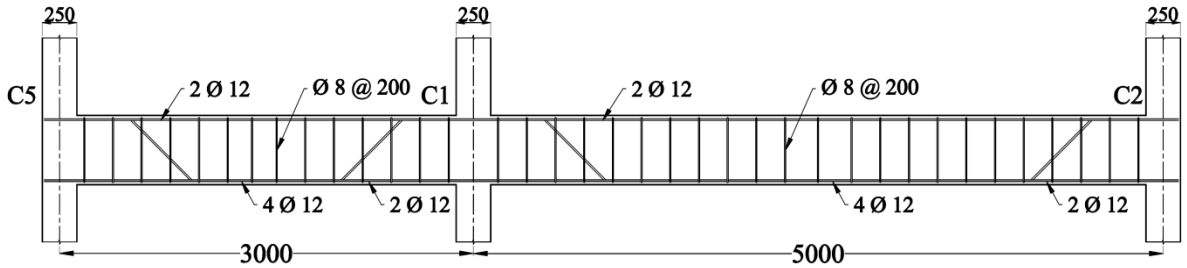

(b)

Figure 4.3 Typical longitudinal steel reinforcements of a beam along the columns C5, C1, and C2 (all dimensions are in millimetres).

Concrete class C25/30 and steel reinforcement with an average tensile strength of 459 MPa for both the longitudinal and transverse reinforcements were used (Rozman and Fajfar 2009). The structural elements (i.e. beams and columns) are simulated using a beam-element model with a distributed inelastic fibre elements as described in Chapter 3 (see Section 3.2). Centrelines of the structural elements were used for modelling the beams and columns of the structure. Most of the columns lie at points of intersections between two or more beams. However, for modelling the rectangular column C6 (see Figure 4.1(a)), the midpoint of a small beam was selected as a location of this column, as detailed in Figure 4.4. Each member

is subdivided into small fibre elements as shown in Figure 4.5, to effectively capture the expected inelasticity behaviour within each section.

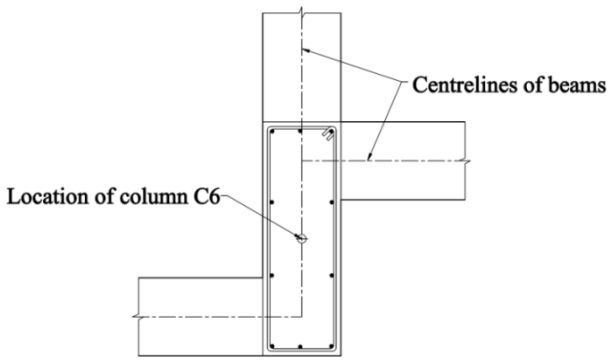

Figure 4.4 Modelling of the column C6 in the SPEAR structure.

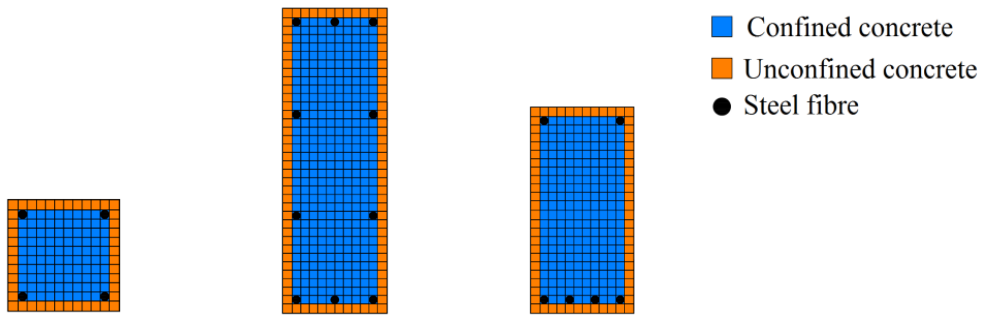

Figure 4.5 Fibre element modelling of the (a) square column, (b) rectangular column, and (c) beam of the SPEAR structure using MIDAS Gen code (2013).

In fibre element modelling, the integration method of the nonlinear relation between the stresses and strains of each fibre part was used to evaluate the total stress-strain relationship within the cross-section of a member. The concrete is modelled by employing a uniaxial constant confinement concrete model that was proposed by Mander *et al.* (1988). Longitudinal steel reinforcement has accounted by using a uniaxial steel model that developed by Menegotto and Pinto (1973). The input parameters required to define the adopted concrete model are the cylinder compressive strength (taken as 25 MPa) and the unconfined concrete

peak strain, which taken as 0.002 (Richart *et al.*, 1928). The concrete elastic modulus, tensile strength and tensile strain are automatically computed by the FE code (MIDAS Gen, 2013). However, the input parameters required to describe the adopted steel model are the yield strength (taken as 459 MPa), initial elastic modulus (taken as 206 GPa), and strain hardening ratio (taken as 0.005 for ordinary steel bars). Three constants (R_o, a_1, and a_2) required to control the transition from the elastic to the plastic branch of the steel constitutive model. The recommended values of these constants for ordinary steel bars are 20 for R_o, 18.5 for a_1, and 0.15 for a_2 (Menegotto and Pinto, 1973; Seckin, 1981; Filippou *et al.*, 1983).

An implicit Newmark method (Newmark, 1959) was used to numerically integrate the equations of motion of the system by adopting the direct integration approach. Constant average acceleration approach that supposes the acceleration of the system is kept constant during the time increment was adopted. Values of Newmark's time integration parameters γ and β were taken respectively as 0.5 and 0.25, so the solution of the dynamic equations becomes unconditionally stable and without introducing additional artificial damping (Newmark, 1959). During a time step, the parameter γ controls the amount of the artificial damping; however, β controls the variation in the acceleration. In addition, a very small value of stiffness proportional damping equal to 0.017 with zero value of mass proportional damping were adopted during the dynamic nonlinear analyses of the system. These two values of the proportional damping result a value of damping ratio for the system equal to 5% and do not cause additional external forces that can be effected the system during earthquakes (Wilson, 1998). To achieve the convergence of the solution for the nonlinear analysis, Newton-Raphson iterative approach was adopted.

4.2.2 Earthquake Accelerograms

The ground motion record Herceg-Novi 1979, which was used in the experimental study by Negro *et al.* (2004) is selected in the dynamic analyses. The two orthogonal components of the horizontal accelerations of Herceg-Novi record were extracted and from the European Strong-motion Database, and then scaled so as their PGAs equal to the value of 1.0, as shown in Figure 4.6.

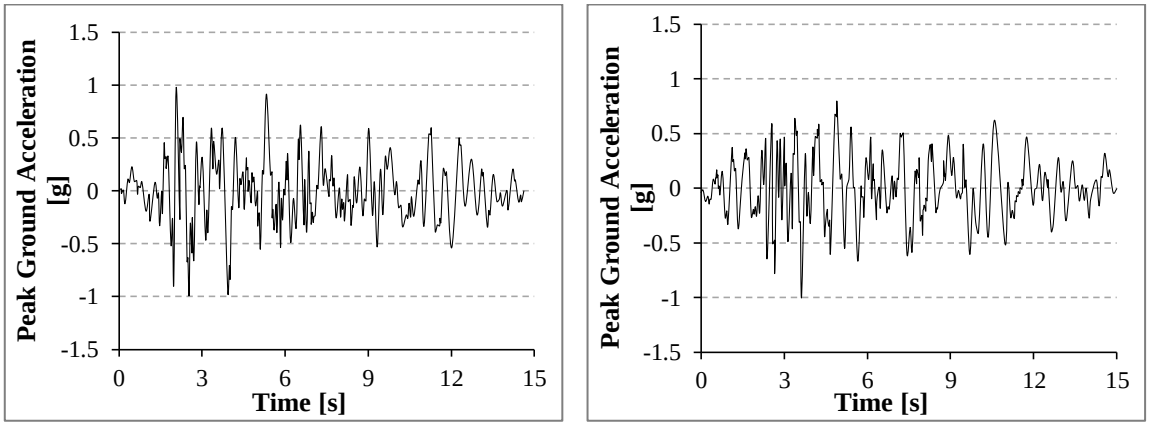

(a) (b)

Figure 4.6 Herceg-Novi earthquake records with a PGA equal to 1.0 g for accelerograms in (a) longitudinal-X and (b) transverse-Y (ESD).

The accelerogram records presented in Figure 4.6 were modified in such a way that their pseudo-accelerations were completely compatible with the EC8 (2004) Type 1 elastic RS for ground type C, as shown in Figure 4.7. The modification process of the Herceg-Novi records was implemented using the computer software, SeismoMatch Ver. 2.1 (Seismosoft, 2009) without changing the records characteristics (i.e. without increasing the number of motion cycles). Thereafter, the modified records were scaled to the values of PGAs equal to 0.15 g and 0.20 g, at the same values that were used in the experimental study (Negro *et al.*, 2004).

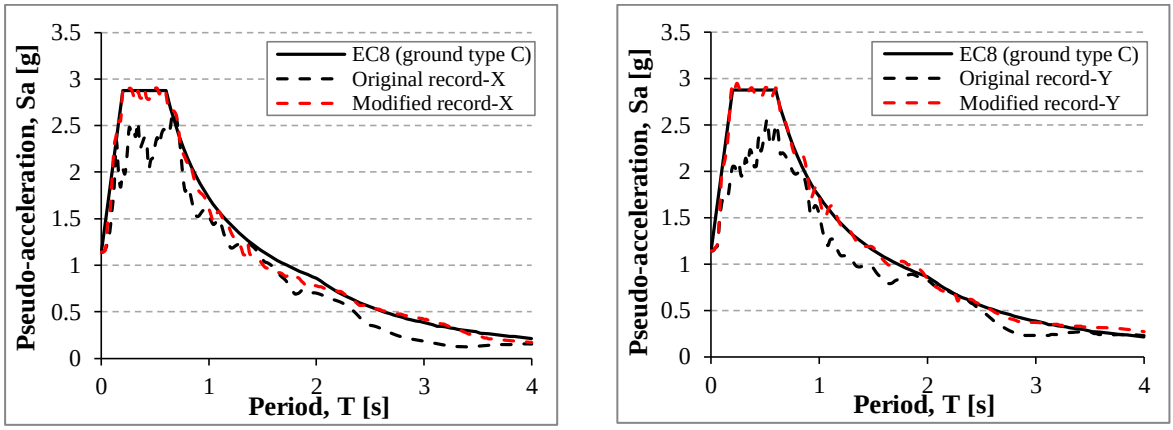

Figure 4.7 Original and modified response spectra of Herceg-Novi earthquake records with a PGA equal to 1.0 g for accelerograms in (a) longitudinal-X and (b) transverse-Y.

4.2.3 Dynamic Analysis of SPEAR Structure

During testing, the building was subjected to the Herceg-Novi records, which were scaled to the PGA values of 0.15 g and 0.20 g. Only minor cracks concentrating at the top of the columns and in the beams connected to Column C6 (see Figure 4.1(a)) occurred when the building was subjected to the PGA of 0.15 g. When the building was subjected to PGA of 0.20 g, the columns, especially those on the second floor, experienced higher damage levels. Some damage was also detected in the beams and floor slabs (Negro *et al.*, 2004). Hence, it can be concluded that the structure underwent inelastic behaviour. During finite element dynamic analyses, the SPEAR building is subjected first to gravity actions to simulate the existing real condition of the structure, then, nonlinear time-history analyses were performed on the stressed building by considering the base motions acting in the X and Y directions. The FE model for the SPEAR structure was also subjected to the Herceg-Novi records scaled to the PGA values of 0.15 g and 0.20 g.

The comparison between the numerical and experimental results (Negro *et al.*, 2004; Fajfar *et al.*, 2006) includes the top floor displacements in the X and Y directions at the CM (see Figure 4.1(a)) and the top floor rotations. Furthermore, the results of the base shears in the X and Y directions, as well as the base moments about the Z direction, were also used in the comparison. As a result of the accurate modelling of the SPEAR building using the FE computer code MIDAS Gen (2013), quite a good comparison was achieved between the FE and the corresponding experimental results presented in the studies by Negro *et al.* (2004) and Fajfar *et al.* (2006), as shown in Figures 4.8 and 4.9. The predicted behaviour was representative of the inelastic behaviour of the structure. MIDAS Gen code was able to model the composite cross-sections accurately; such as the correct location and the amount of the longitudinal steel reinforcements and the exact value of the concrete cover which amounted to 15 mm; as well as consideration of the effect of the shear reinforcements along each member of the SPEAR structure. During the test process, the SPEAR structure showed a nonlinear response at the PGA equal to 0.15 g; the minor damage had significant impact on the structure response to the PGA equal to 0.20 g, which itself led to heavy damage. This effect was taken into account in the current validation during the nonlinear dynamic analyses, by using the sequential loading option which is available in MIDAS Gen code (2013).

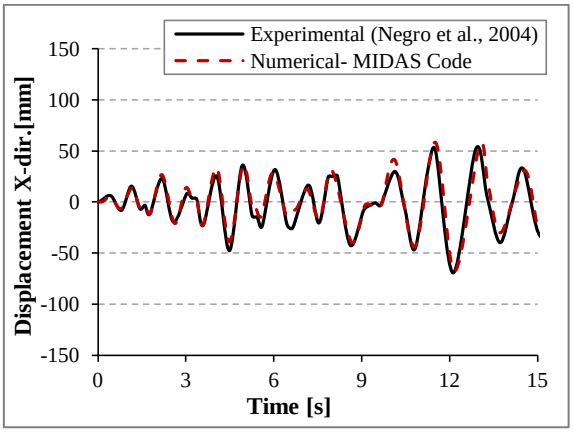

(a) displacement in the X-direction (*PGA*=0.15 g)

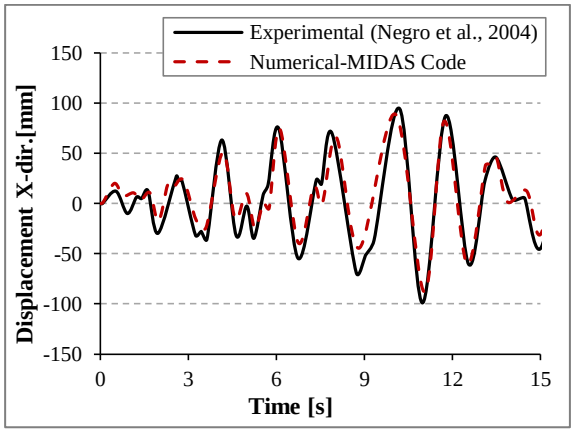

(b) displacement in the X-direction (*PGA*=0.20 g)

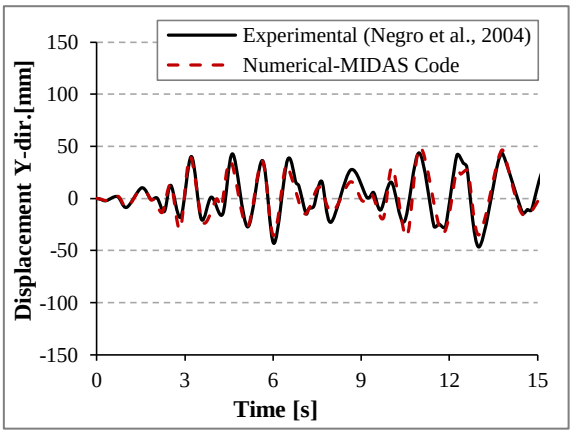

(c) displacement in the Y-direction (*PGA*=0.15 g)

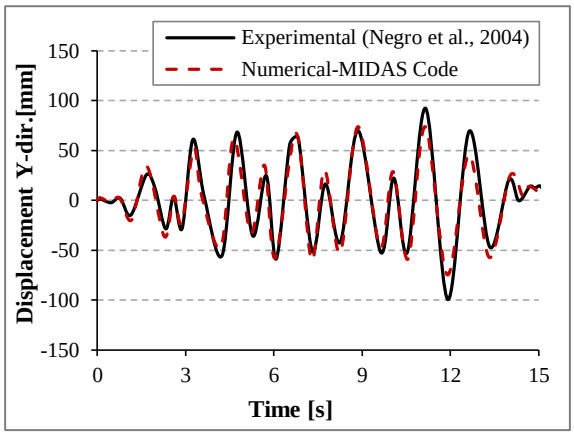

(d) displacement in the Y-direction (*PGA*=0.20 g)

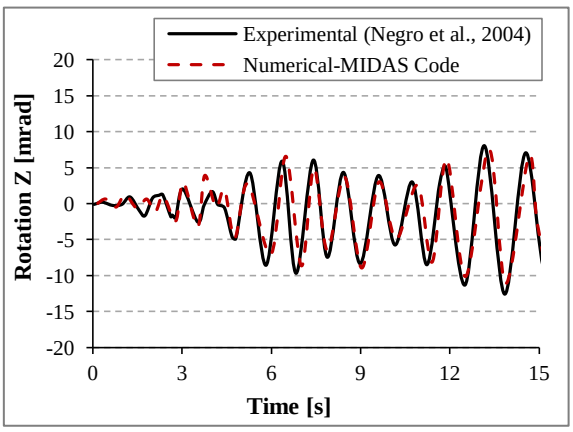

(e) rotation about the Z-direction (*PGA*=0.15 g)

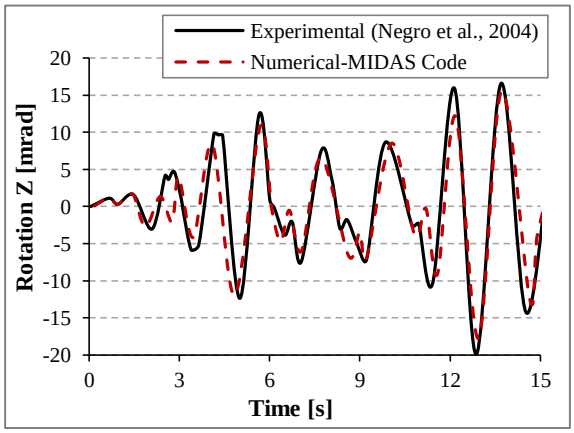

(f) rotation about the Z-direction (*PGA*=0.20 g)

Figure 4.8 Comparison between the experimental and numerical results of the top displacements and rotations at centre of mass (CM) for SPEAR building.

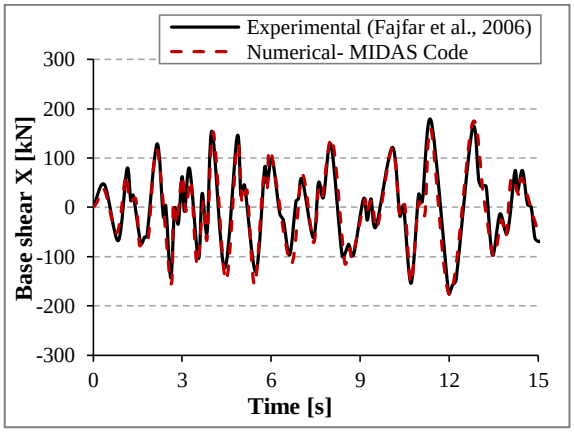

(a) base shear in the X-direction (*PGA*=0.15 g)

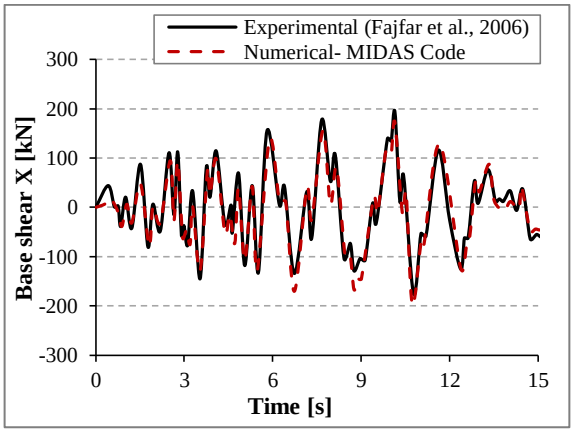

(b) base shear in the X-direction (*PGA*=0.20 g)

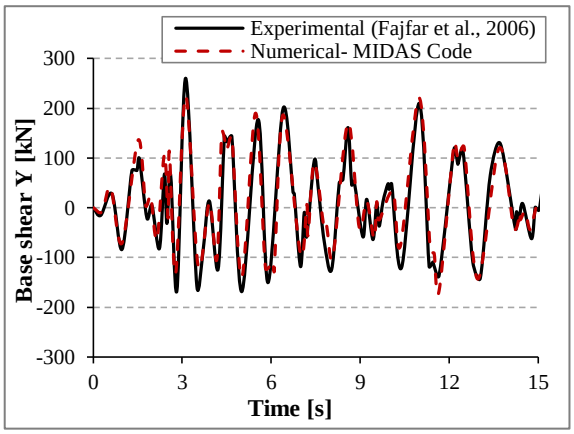

(c) base shear in the Y-direction (*PGA*=0.15 g)

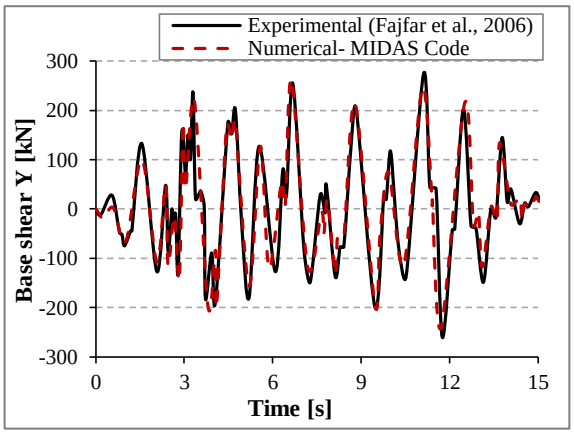

(d) base shear in the Y-direction (*PGA*=0.20 g)

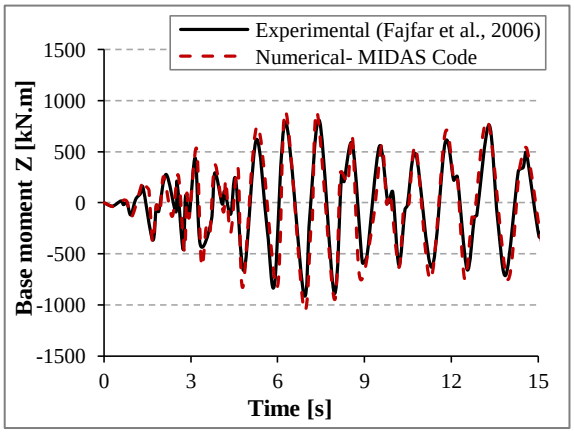

(e) base moment about the Z-direction (*PGA*=0.15 g)

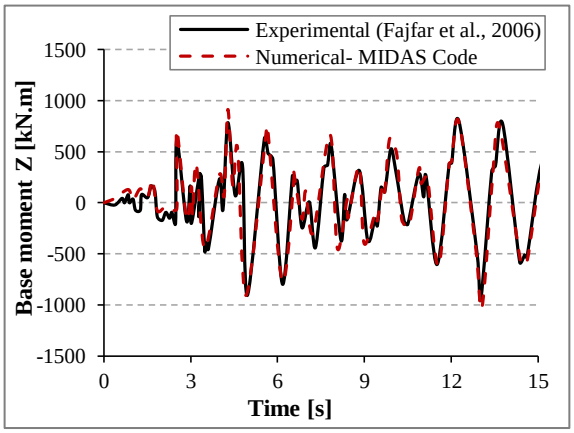

(f) base moment about the Z-direction (*PGA*=0.20 g)

Figure 4.9 Comparison between the experimental and numerical results of the base shears and moments for SPEAR building.

4.3 Verification of Modelling the NSCs

The following sections summarise the validation of the FE code, MIDAS Gen Ver. 3.1 (2013) for the modelling of the NSCs. The modelling and characteristics, and then the modal and time-history analyses of the NSCs are explained.

4.3.1 Modelling and Characteristics of the NSCs

As explained in Chapter 1 (see Section 1.4), the NSCs considered in this research are lightweight acceleration-sensitive mechanical, electrical, or medical equipment - such as those found in industrial, commercial, or medical buildings. Normally only the fundamental mode of such NSCs is of importance therefore they can be modelled as cantilevers fixed at their bases. Single-degree-of-freedom (SDOF) mechanical oscillators are commonly used to model such NSCs (Sackman and Kelly, 1979; Yang and Huang, 1993, 1998; Agrawal and Datta, 1997, 1998; Agrawal, 1999; Mohammed, *et al.*, 2008; Chudhuri and Villaverde, 2008; Opropeza *et al.*, 2010). This modelling approach was adopted in this research. Each cantilever has a 152×152×51 mm^3 lumped steel mass weighing about 9.25 kg. The arms of the cantilevers were modelled as circular sections, 40 mm in diameter. The circular cross-section was favoured because it has the same lateral stiffness in any horizontal direction.

Seven values of periods of NSCs were used to verify the modelling of the NSCs as a finite element SDOF. As given in Table 4.1, the adopted values of the NSCs periods are equal to 0.0 s, 0.25 s, 0.5 s, 0.75 s, 1.0 s, 1.5 s, and 2.0 s. The value of the period of NSC equal to

$T_C \approx 0$ s represents the rigid NSC (BSSC, 2003). Table 4.1 also gives the corresponding values of both the lengths (L_a) and the lateral stiffness (K_a) of the circular cantilever arms.

Table 4.1 Characteristics of the considered periods of NSCs used in the current verification.

NSC Period [s]	$T_C \approx 0$	T_C=0.25	T_C=0.50	T_C=0.75	T_C=1.0	T_C=1.5	T_C=2.0
$L_{a,}$ [m]	0.001	1.03	1.64	2.15	2.6	3.41	4.13
$K_{a,}$ [N/m]	6.41×10^{12}	5863.9	1452.7	644.7	364.6	161.6	90.9

4.3.2 Modal and Time-history Analyses of NSCs

To verify the values of both the lengths and stiffness of the arms of each NSC corresponding to its period which reported in Table 4.1, eigenvalue analyses were performed to evaluate the first mode of the considered NSCs. Figure 4.10 shows the FE results of the vibration periods of the NSCs. This figure demonstrates that the resulting values of the natural periods as presented in the legends of each NSC were found to be matching well with those presented in Table 4.1.

Thereafter, linear time-history analyses were carried out to achieve additional verification for modelling the NSC as cantilever with a mass at the top using a FE analysis. The horizontal X direction of Herceg-Novi earthquake as displayed in Figure 4.6(a), was selected as a ground motion input with a value of PGA equal to 1.0 g.

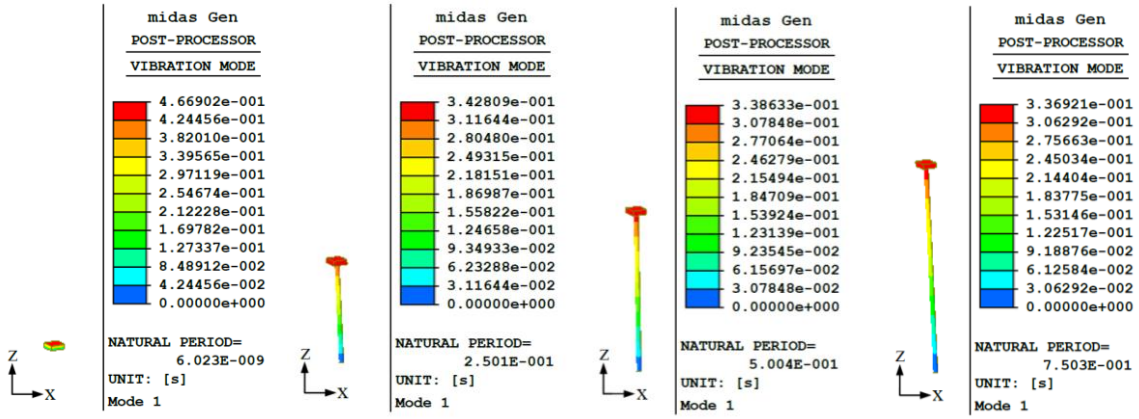

(a) (b) (c) (d)

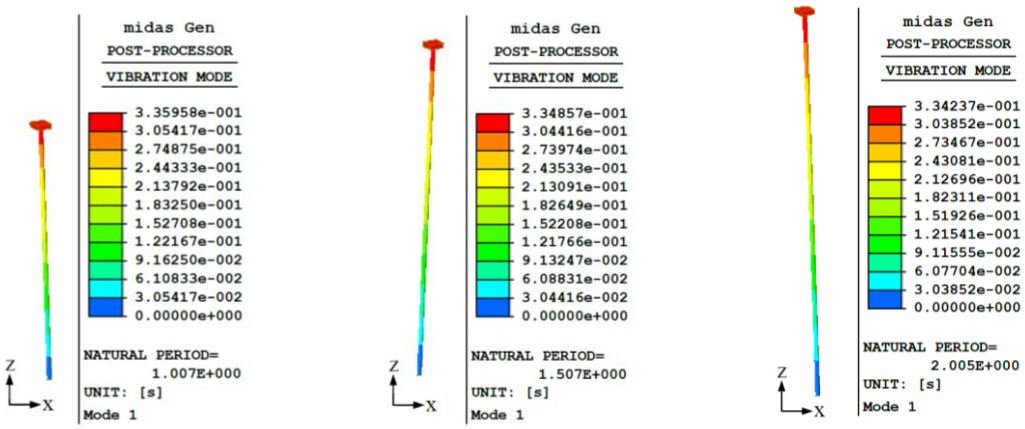

(e) (f) (g)

Figure 4.10 First mode shapes of NSCs having periods equal to (a) $T_C \approx 0$ s, (b) $T_C = 0.25$ s, (c) $T_C = 0.5$ s, (d) $T_C = 0.75$ s, (e) $T_C = 1.0$ s, (f) $T_C = 1.5$ s, and (g) $T_C = 2.0$ s.

The numerical results of PCA at the top of each NSC, which resulted from linear time-history analyses were compared with those values were resulted from the elastic pseudo-acceleration (PSA) of the selected earthquake record, as shown in Figure 4.11. Damping ratio of 5% was assumed for both the NSCs and the PSA of the Herceg-Novi earthquake record.

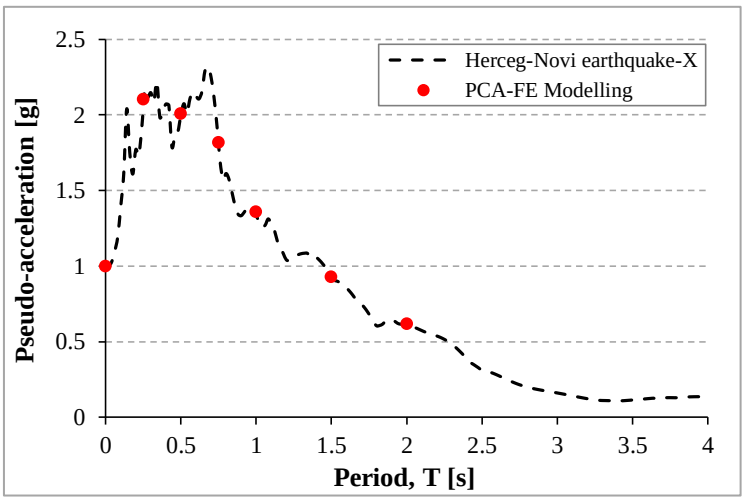

Figure 4.11 Comparison between the numerical results of peak components accelerations PCA and the actual values of the pseudo-accelerations of the Herceg-Novi earthquake-X at damping ratio of 5%.

It can be observed from Figure 4.11 that the FE results of the NSCs have shown a good agreement with the corresponding PSA values of the selected base motion. The resulting value of PCA for each NSC was found equal to the value of the PSA of the base motion record at period, T equal to the NSC vibration period. Furthermore, it can be seen from Figure 4.11 that the value of PCA for the rigid NSCs (i.e. $T_C \approx 0$ s) is equal to the value of PGA of the selected base motion (i.e. PGA = 1.0 g). Therefore, it can be observed that the dynamic responses of the NSCs integrated directly on ground were generally a function of the characteristics of the earthquake ground motions such as their PSAs and frequency content values. These results agree with the recommendations that are included in most of the current codes for the design of the rigid NSCs such as EC8 (2004), when a value of acceleration amplification factor equal to 1.0 is assumed for those rigid NSCs attached to ground level of a building.

4.4 Summary

Chapter 4 presented the validation of modelling both the primary and secondary systems using a finite element approach. The irregular three-storey RC frame "SPEAR" structure was selected to validate the modelling of the fibre elements and the nonlinear constitutive relationships of both the concrete and steel materials.

The comparison between the numerical results of the displacements and rotations values at the top floor, as well as the results of the base shears and base moments in the Z direction with the corresponding experimental results have shown a quite well agreement. Furthermore, verification of modelling the NSCs as a cantilever fixed at their bases and a mass at the top using a finite element method was implemented. It was observed that the numerical results of PCAs at the top of each NSC resulted from linear time-history analyses were well-matched with the elastic pseudo-acceleration response of the selected earthquake record.

It can be concluded from the results presented in Chapter 4 that the fibre beam-element and the nonlinear material constitutive models, which were implemented in the FE computer code MIDAS Gen (2013) were precisely modelled on the P-structure. Furthermore, the FE approach for modelling the NSCs as SDOFs were also precisely expressed their characteristics. Therefore, the same characteristics of the materials modelling of the concrete and steel reinforcement, as well as the modelling of the NSCs that was adopted in Chapter 4, were also used in the nonlinear dynamic analyses of the P-S systems presented in Chapters 5, 6, and 7.

CHAPTER FIVE: SEISMIC RESPONSE OF NSCs MOUNTED ON IRREGULAR REINFORCED CONCRETE STRUCTURES HAVING DIFFERENT DESIGN CHARACTERISTICS

5.1 Introduction

This chapter investigates the seismic response of lightweight acceleration-sensitive NSCs mounted on irregular multi-storey, two-way RC P-structures having different design characteristics. The aim of this chapter is to study the influence of: the NSC to the P-structure vibration period ratio, peak ground acceleration, the NSC to the P-structure height ratio, ground types, and the P-structure torsional behaviour on the seismic response of the NSCs. Furthermore, a comparison of the predictions of the nonlinear dynamic FE analyses with those of EC8 (2004) seismic design provisions for the NSCs is studied in this chapter.

Three groups of buildings consisting of 25 irregular RC frames in total were selected as the P-structures in Chapter 5. The characteristics of these buildings are explained in detail in Sections 5.2.1, 5.2.2, and 5.2.3. The first and second groups of buildings were designed on ground type C. However, to investigate the effect of ground type on the seismic behaviour of NSCs, the third group of buildings was designed on four different types of ground (namely ground types A, B, D, and E as defined in EC8).

Dynamic responses of the NSCs having different values of periods and attached to the first and second groups of buildings are presented in Section 5.6. However, those responses of the NSCs having only natural periods equal to the first vibration period of the P-structures of the third group of buildings are presented in Section 5.7. Sets of 70 natural and artificial

earthquake records were used to evaluate the seismic response of the NSCs in this chapter. The results presented in Sections 5.6, 5.7, and 5.8 are based on averages of 3066 nonlinear dynamic FE analyses of the P-S systems under the effect of bi-directional earthquakes.

5.2 Characteristics and Modelling of the RC P-structures

In order to establish the credibility of the finite element results under the effect of torsion, it is required to base the numerical investigation on physically tested and/or previously modelled irregular RC P-structures. The irregular three-storey RC P-structures "SPEAR (henceforward referred to as "Test")" (Negro *et al.*, 2004), "Test 0.15", "Test 0.25", and "EC8 M" (Rozman and Fajfar, 2009) were therefore selected as P-structures and their plan layout is used as the basic plan layout for the studied cases in this chapter. Additional five variants of buildings; namely: "EC8 M5", "EC8 M7", "EC8 M10", "EC8 M13", and "EC8 M15"; were designed by the researcher according to the EC8 (2004) seismic provisions. These buildings can provide a range of parameters (i.e. vibration periods, total heights, and torsional responses), which may be used to study the dynamic behaviours of NSCs attached to the RC P-structures with significant torsional behaviours. Except for the Test building, all the above-mentioned P-structures were designed on ground type C according to the EC8 (2004) provisions. In order to investigate the influence of different types of ground on the dynamic response of the NSCs, the buildings "EC8 M3", "EC8 M5", "EC8 M10", and "EC8 M15"; were designed on ground types A, B, D, and E according to the EC8 (2004) provisions. Figure 5.1 shows the plan of the three groups of buildings where the eccentricities between their centres of mass (CM) and centres of rigidity (CR) are in two directions. The terms SS and FS presented in Figure 5.1 refer respectively to the stiff and flexible sides of the P-structures. The typical height of the floor is 3 m, as explained previously in Chapter 4 (see Figure 4.1(b)). The effect of different

cases consisting of 25 irregular RC P-structures on the dynamic behaviour of NSCs is investigated in this chapter.

The adopted RC P-structures can be divided into three groups. The first group includes four irregular RC P-structures (Test, Test 0.15, Test 0.25, and EC8 M) with similar total height (9 m) but different design characteristics, as detailed in Section 5.2.1. The second group includes five irregular RC P-structures (EC8 M5, EC8 M7, EC8 M10, EC8 M13, and EC8 M15) with similar design characteristics but different total heights (15 m, 21 m, 30 m, 39 m, and 45 m), as detailed in Section 5.2.2. However, the third group of buildings includes RC P-structures (EC8 M3, EC8 M5, EC8 M10, and EC8 M15) designed on four ground types A, B, D, and E; therefore, the third group of buildings consists of 16 irregular RC P-structures, as detailed in Section 5.2.3. This strategy represented the most straightforward approach to consider the irregular RC P-structures with different vibration periods, heights, torsional behaviours, and ground types.

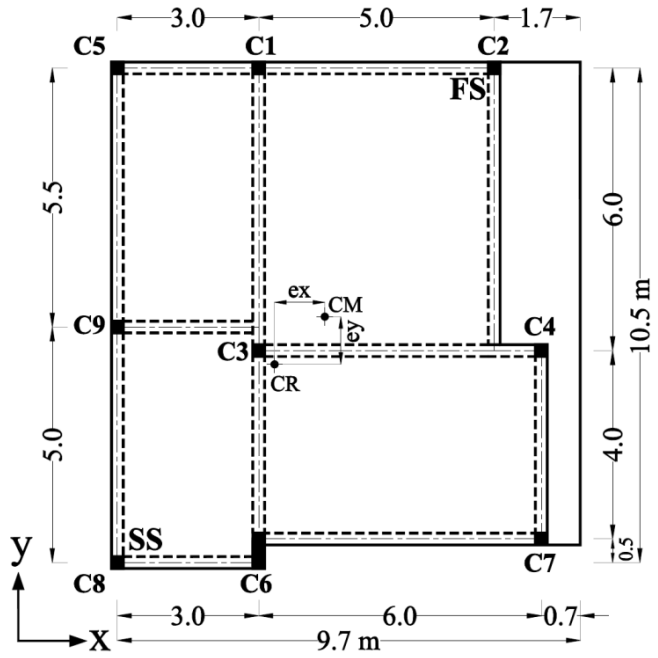

Figure 5.1 Plan of the three groups of P-structures considered in Chapter 5 (all dimensions are in metres).

5.2.1 General Description of the First Group of Buildings

The first group of buildings includes four irregular three-storey RC P-structures Test, Test 0.15, Test 0.25, and EC8 M, which have the same plan layout (see Figure 5.1) and number of storeys, but different cross-sectional dimensions and steel reinforcement in the beams and columns. The rationale adopted for the selection of the RC P-structures in this group of building is clearly explained in Section 5.2. A value of 2.0 kN/m^2 was taken into account for the variable action of the considered structures in the first group. Table 5.1 details the characteristics of this group of buildings.

Table 5.1 Description and design characteristics of the first group of buildings.

Building	Description and design characteristics	Eccentricity [m]	
		e_x	e_y
Test	SPEAR Structure (Negro *et al*., 2004) designed to gravity loads only (permanent load of 0.5 kN/m^2 was used). Thickness of the concrete cover equal to 15 mm was used.	1.30	1.00
Test 0.15	Had the same vertical load, plan layout, number of storeys and cross-sectional dimensions as Test building. Designed using the EC8 (2004) spectrum Type 1 for ground type C (design ground acceleration on type A ground, a_g= 0.15 g, behaviour factor (q) = 3.45, S = 1.15, design ground acceleration on type C ground = 0.173 g). A value of 30 mm was adopted for the thickness of the concrete cover.	1.30	1.00
Test 0.25	Had the same vertical load, plan layout, number of storeys and cross-sectional dimensions as Test building. Designed using the EC8 (2004) spectrum for ground type C (a_g = 0.25 g, q = 3.45, S = 1.15, design ground acceleration on type C ground = 0.29 g). A value of 30 mm was adopted for the thickness of the concrete cover.	1.30	1.00
EC8 M	Had the same plan layout and number of storeys as Test building. Permanent load of 2.7 kN/m^2 was used. The cross-sectional dimensions of the beams and columns were increased in order to meet the EC8 (2004) Ductility Class Medium (DCM) requirements. Designed using the EC8 (2004) spectrum for ground type C (a_g= 0.25 g, q = 3.45, S = 1.15, design ground acceleration on type C ground = 0.29 g). A value of 30 mm was used for the thickness of the concrete cover.	0.99	0.73

Building Test (Negro *et al.,* 2004) was designed without seismic criteria. The characteristic value of the permanent floor load was taken as 0.5 kN/m^2. Its cross-section and steel reinforcement details are given in Appendix A (see Section A3, Table A3-1). More details on the steel reinforcement of Test building "SPEAR structure" can be found in Chapter 4 (see Figures 4.3 and 4.4).

Buildings Test 0.15 and Test 0.25 had the same vertical load, plan layout, number of storeys and cross-sectional dimensions as Test building. They were designed using the EC8 (2004) Type 1 elastic spectrum for ground type C. Building Test 0.15 was designed for a value of design ground acceleration a_g of 0.15 g for ground type A. However, Test 0.25 building was designed for an a_g value of 0.25 g. Considering the soil factor of 1.15 for ground type C, the design ground accelerations on type C ground for Test 0.15 and Test 0.25 were 0.173 g and 0.29 g respectively. The amounts of the steel reinforcements used in Test 0.15 and Test 0.25 were higher than those amounts used in Test building (see Table A3-1, Figures A3-1 and A3-2 in Appendix A). However, the beams and columns cross-sectional dimensions of Test 0.15 and Test 0.25 did not fully meet the EC8 (2004) requirements. The values of the ratio between the resistance moments of the columns to the corresponding moments of the beams (i.e. the over-strength factor (γ_{Rd})) for Test 0.15 and Test 0.25 were 0.40 and 0.65 respectively. Hence, Test 0.15 and Test 0.25 did not fulfil the EC8 (2004) global and local ductility requirements (Rozman and Fajfar, 2009). Nonetheless, Test 0.15 and Test 0.25 were considered in this chapter for two reasons. Firstly, they are representative of building practice before the adoption of modern seismic codes (Rozman and Fajfar, 2009). Secondly, as their seismic capacities were higher than the basic model, i.e. Test building, they provided the

opportunity to study the effect of P-structure seismic capacity on the seismic response of NSCs.

EC8 M had the same plan layout and number of storeys as Test building. It was designed using the Type 1 elastic spectrum of EC8 (2004) for ground type C. EC8 M was designed for an a_g value of 0.25 g on ground type A. Considering the soil factor of 1.15 for ground type C, the design ground acceleration on type C ground for EC8 M was 0.29 g. The characteristic value of the permanent floor load was taken as 2.7 kN/m^2 instead of 0.5 kN/m^2. The cross-sectional dimensions and the amount of the steel reinforcements were increased in the case of EC8 M - compared to Test, Test 0.15, and Test 0.25 (see Tables A3-1 and A3-2, as well as Figure A3-3 in Appendix A) - in order to meet the DCM requirements of EC8 (2004). EC8 M had a γ_{Rd} value of 1.30 and fulfilled all EC8 (2004) requirements (Rozman and Fajfar 2009). Concrete class C25/30 and steel reinforcement Grade 400 were used in all buildings except Test, which had steel yield strength of 459 MPa (Rozman and Fajfar, 2009). Further information can be found in Negro *et al.* (2004) for Test building and in Rozman and Fajfar (2009) for buildings Test 0.15, Test 0.25, and EC8 M.

5.2.2 General Description of the Second Group of Buildings

The second group of buildings consists of the five irregular RC P-structures EC8 M5, EC8 M7, EC8 M10, EC8 M13, and EC8 M15, which have the same plan layout and storey height as the first group of buildings but differ in the total height, beams and columns cross-sectional dimensions and steel reinforcement details. In order to represent low- and medium-rise RC P-structures, buildings heights in the range of 15 m to 45 m were considered, as shown in Figure 5.2.

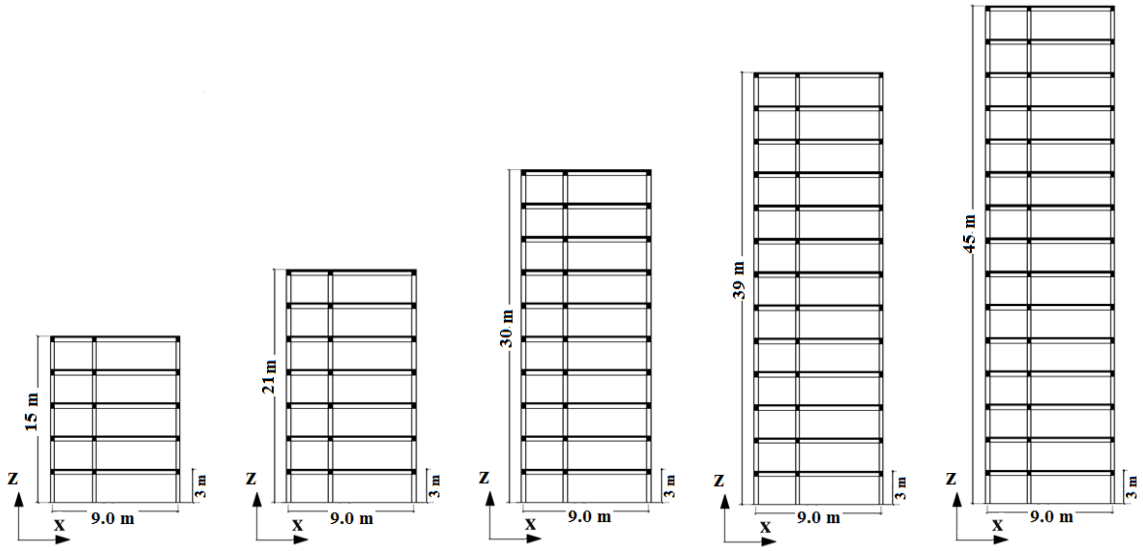

(a) (b) (c) (d) (e)

Figure 5.2 Elevation of the second group of the buildings (a) EC8 M5, (b) EC8 M7, (c) EC8 M10, EC8 M13, and (e) EC8 M15 (all dimensions are in metres).

The buildings are labelled as "EC8 M#"; the term "EC8 M" refers to buildings designed as per EC8 for medium ductility; whereas, the symbol "#" indicates the number of storeys (i.e. # = 5, 7, 10, 13, or 15). The Test buildings, on which parts of this investigation are based, employed the elastic spectra of the longitudinal and transverse accelerogram components which are consistent with the EC8 (2004) Type 1 elastic RS for ground type C. Hence, for comparison purposes, all buildings in the second group assumed to be constructed on ground type C. The characteristics of this type of ground were detailed in Chapter 3 (see Section 3.3 - Table 3.1)

The design of the RC P-structures of the second group in terms the imposed loads, member resistance, and seismic resistance was in accordance with the design provisions of EC1 (2002), EC2 (2004), and EC8 (2004) respectively. All P-structures were designed for Ductility Class M (DCM); therefore, the primary magnitude of the behaviour factor q_o equal to $3.\alpha_u/\alpha_1$, was used. The term α_u/α_1 is used to account for the influence of the flexural

resistance and formulation of the plastic hinges in the structural members. The value of α_u/α_1 is 1.3, for multi-storey, multi-bay frames (EC8, 2004). Furthermore, for P-systems which are not symmetrical in their plan (i.e. torsional structures), the suggested value of α_u/α_1 that can be adopted is equal to the average of 1.0 and of the value of α_u/α_1 (EC8, 2004). Consequently, the final value of the behaviour factor q is 3.45 which used in the design of the second group of irregular buildings to consider the inelastic deformation.

Value of design ground acceleration a_g equal to 0.25 g on ground type A was adopted. Considering the soil factor of 1.15 for ground type C, subsequently the value of the design ground acceleration on type C ground, can be estimated as 0.29 g. To fulfil the strong column/weak beam capacity design rule according to the EC8, the value of γ_{Rd} equal to 1.3 was adopted. The P-structures of the second group satisfied the EC8 (2004) DCM requirements, which necessitate the use of concrete of a class higher than C16/20 and Class B or C high ductility steel reinforcement in the main structural members. Concrete Class C25/30 and steel reinforcement Class C S500 were therefore used in the design of the structural elements.

Variable-live load in terms of uniformly distributed load amount to 2.0 kN/m^2 was used; however, a value of 2.7 kN/m^2 (excluding slab self-weight) was adopted for the permanent action. The resulting member dimensions and the amounts of longitudinal steel, as well as the shear and joint reinforcements of the second group of buildings were given in Appendix A (see Table A3-3). Furthermore, shown in Figure A3-4 (see Appendix A) is a sample explanation of the steel reinforcements of the beams and columns, as well as the

beam-column joint connection of the first floor of the EC8 M5 building, as given in the first row of Table A3-3.

5.2.3 General Description of the Third Group of Buildings

The third group of buildings includes of four RC P-structures (EC8 M3, EC8 M5, EC8 M10, and EC8 M15). These buildings have the same plan layout and storey height as the second group of buildings but differ in the type of ground assumed for construction. The heights of these buildings are in the range of 9 m to 45 m. The buildings are labelled as "EC8 M#". The term "EC8 M" refers to buildings designed as per EC8 (2004) Ductility Class M (DCM). The symbol "#" indicates the number of storeys (i.e. # = 3, 5, 10, or 15). Four types of ground; namely A, B, D, and E as defined in EC8 (2004); were adopted. Therefore, a total of 16 RC P-structures were considered. Elastic response spectra consistent with EC8 (2004) Type 1 RS for the above-mentioned ground types were used in the design. Explanation the criteria for the selecting of these types of ground can be found in Chapter 3 (see Section 3.3).

The design of the third group of buildings satisfied the provisions of EC1 (2002), EC2 (2004), and EC8 (2004). It can be summarised as follows: DCM with value of the behaviour factor (q) equal to 3.45; design ground acceleration (a_g) on Type A ground equal to 0.25 g; concrete class C25/30 for beams and columns and steel class C S500 for steel reinforcement. The characteristic values used for the floor loads were 2.7 kN/m^2 and 2.0 kN/m^2 for permanent and variable actions respectively. Considering the soil factors of 1.0, 1.2, 1.35, and 1.4 for ground types A, B, D, and E respectively, the design ground accelerations on these types of ground were equal to 0.25 g, 0.30 g, 0.34 g, and 0.35 g, respectively as shown in

Table 5.2. Shown in Figure 5.3 are the adopted design acceleration spectra according to the EC8 (2004) for ground types A, B, D, and E with a value of q equal to 3.45. Design acceleration spectrum for ground type C is also presented in Figure 5.3 for only comparison purposes with the other four spectra.

Table 5.2 Design acceleration values of the third group of buildings for ground types A, B, D, and E.

Building	Ground type	Design acceleration on Type A ground, a_g [g]	Soil factor, S	Design Acceleration on a specific ground type [g]
EC8 M3; EC8 M5; EC8 M10; EC8 M15	A	0.25	1.00	0.25
	B		1.20	0.30
	D		1.35	0.34
	E		1.40	0.35

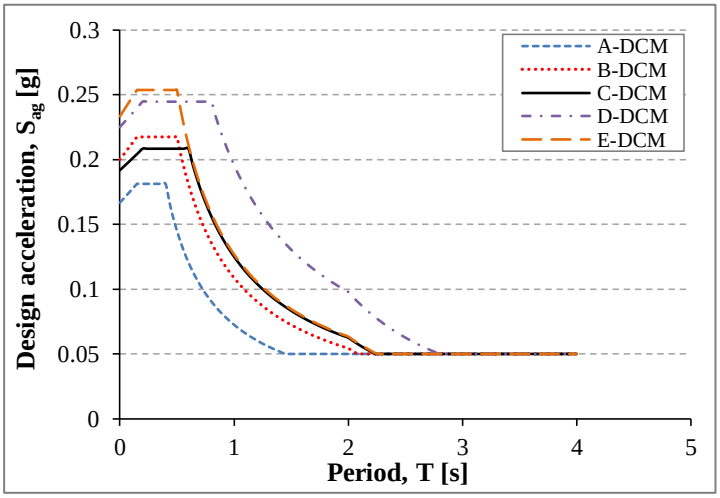

Figure 5.3 Design acceleration spectra according to EC8 (2004) for ground types A, B, C, D, and E with a value of the behaviour factor (q) equal to 3.45.

The resulting member dimensions and the amount of longitudinal, shear steel and joint reinforcements of the RC buildings designed for ground types A, B, D, and E can be found in Tables A3-4, A3-5, A3-6, and A3-7 in Appendix A, respectively.

The results of the cross-sections and the amounts of the steel reinforcements of the buildings in the third group, as presented in Appendix A (see Tables A3-3 to A3-7), can be compared with those results of the corresponding buildings in the first and second groups, which were designed on ground type C. For building EC8 M3 designed on ground types A and B, it seems that it has values of the cross-sections and steel reinforcements smaller than those of the corresponding building when it was designed on ground C (i.e. building termed as EC8 M of the first group). However, EC8 M3 has larger cross-section characteristics when it is designed on ground types D and E. Comparable results were obtained for buildings EC8 M5, EC8 M10, and EC8 M15.

Nevertheless, the characteristics of the buildings EC8 M5, EC8 M10, and EC8 M15 designed on ground type E were observed equal to those buildings of ground type C. The main reason for the resulting characteristics as described above is the effect of the values of the fundamental vibration periods of the P-structures as presented later in Section 5.3 (see Table 5.3). For instance, the EC8 M5 building had a fundamental period equal to a value of 0.66 s when it was designed on ground type C (i.e. building termed as EC8 M5 included in the second group of buildings, see Table 5.3). According to this value of the period, the design acceleration S_{ag} value was found approximately equal to 0.19 g when the building was assumed to be designed on both ground types of C and E (see Figure 5.3). Comparable results were obtained for the buildings EC8 M10 and EC8 M15 when their vibration periods on both ground types C and E are equal to 1.17 s and 1.39 s respectively (as given in Table 5.3).

5.2.4 Modelling of the RC P-structures of the Three Groups

Based on the results of the validation of the FE computer code MIDAS Gen Ver. 3.1 (2013) that were presented in Chapter 4 (see Section 4.2), it was concluded that the adopted distributed inelastic beam-element and the nonlinear material constitutive models can accurately describe the P-structure with torsional behaviour. Therefore, the same beam-element and the material models were also used during the nonlinear analyses of the studied cases of the P-S systems in this chapter. The input parameters of each the concrete and steel fibres during the dynamic nonlinear analyses can be summarised as follows: the concrete and steel models that were proposed by Mander *et al.* (1988) and Menegotto and Pinto (1973) respectively were used. A concrete compressive strength and unconfined concrete peak strain were taken as 25 MPa and 0.002 respectively. The yield strength of the steel reinforcement was taken as those reported in Sections 5.2.1, 5.2.2, and 5.2.3. For ordinary steel bars, the initial elastic modulus and the strain-hardening ratio were taken as 206 GPa and 0.005 respectively. The recommended values of (R_o, a_1, and a_2) for ordinary steel bars are 20 for R_o, 18.5 for a_1, and 0.15 for a_2 (Menegotto and Pinto, 1973; Seckin, 1981; Filippou *et al.*,1983). Further details on the modelling characteristics of the concrete and steel fibres can be found in Chapter 3 (see Section 3.2).

Newmark method (Newmark, 1959) was used in the dynamic analyses of the P-S systems to integrate the equations of motion with employing full Newton-Raphson iterations until convergence was reached. Average constant acceleration approach was used with Newmark's time integration parameters, γ and β, equal to 0.5 and 0.25 (Newmark, 1959) respectively. A damping ratio of 5% (Paz, 1994) is adopted for the P-structures.

5.3 Modal (Eigenvalue) Analysis of the RC P-structures of the three groups

Eigenvalue analyses were performed to calculate the vibration periods of the three groups of buildings as described in Sections 5.2.1, 5.2.2, and 5.2.3. These analyses are essential for the selection of the NSCs with natural frequencies match with the vibration periods of the P-structures.

The vibration periods of the first six modes (transitional modes in the X and Y directions and torsional modes) of the studied buildings of the three groups of buildings are presented in Table 5.3.

Table 5.3 Fundamental vibration periods of the studied three groups of buildings.

Group	Building	Ground type	Vibration periods [s]					
			T_1	T_2	T_3	T_4	T_5	T_6
First	Test	--	0.823	0.735	0.652	0.339	0.301	0.246
	Test 0.15, Test 0.25	C	0.823	0.735	0.652	0.339	0.301	0.246
	EC8 M	C	0.550	0.522	0.421	0.171	0.152	0.130
Second	EC8 M5	C	0.660	0.640	0.510	0.210	0.200	0.160
	EC8 M7	C	0.840	0.830	0.660	0.270	0.260	0.210
	EC8 M10	C	1.170	1.150	0.920	0.380	0.370	0.280
	EC8 M13	C	1.290	1.260	1.020	0.430	0.420	0.310
	EC8 M15	C	1.390	1.310	1.120	0.440	0.430	0.320
Third	EC8 M3	A	0.620	0.588	0.475	0.193	0.171	0.147
		B	0.590	0.560	0.452	0.183	0.163	0.139
		D	0.470	0.446	0.360	0.146	0.130	0.111
		E	0.520	0.494	0.398	0.162	0.144	0.123
	EC8 M5	A	0.750	0.727	0.580	0.239	0.227	0.182
		B	0.710	0.688	0.549	0.226	0.215	0.172
		D	0.610	0.592	0.471	0.194	0.185	0.148
		E	0.660	0.640	0.510	0.210	0.200	0.160
	EC8 M10	A	1.250	1.229	0.983	0.406	0.395	0.299
		B	1.220	1.199	0.959	0.396	0.386	0.292
		D	1.080	1.062	0.849	0.351	0.342	0.258
		E	1.170	1.150	0.920	0.380	0.370	0.280
	EC8 M15	A	1.500	1.414	1.209	0.475	0.464	0.345
		B	1.450	1.367	1.168	0.459	0.449	0.334
		D	1.280	1.206	1.031	0.405	0.396	0.295
		E	1.390	1.310	1.120	0.440	0.430	0.320

It can be seen that, as a result of similar cross-section dimensions of the columns and beams of the buildings Test, Test 0.15, and Test 0.25 designed on ground type C (see Table A3-1 in Appendix A), the values of the vibration periods of these buildings were also found similar. However, for P-structures that have similar heights in the second and third groups of buildings, the values of the vibration periods of these buildings were varied on different types of ground as a result of different cross-section dimensions of the columns and beams of the P-structures designed on different ground types (see Table A3-3 to A3-7 in Appendix A).

5.4 Non-structural Components: Characteristics and Modelling

Finite element approach was used to simulate the NSCs in this chapter. More details of the modelling and characteristics of the NSCs that adopting in the analyses can be found in Chapter 4 (see Section 4.3.1). Full dynamic interaction was considered between the NSCs and P-structures.

Based on the recommendations of Graves and Morante (2006), a linear viscous damping ratio (ξ_c) of 3% was used for the NSCs. These recommendations are based on review of codes provisions such as NRC (1973) and ASCE (2005). Near-resonance response is most critical for the P-S systems under the effect of base motions. Therefore, vibration periods of the NSCs match the fundamental periods of the three groups of buildings were adopted. The NSCs attached to the first and second groups of buildings with vibration periods as reported in Table 5.4 were considered in the dynamic analyses. It should be noted that the first three vibration periods (T_1, T_2, and T_3) reported in Table 5.4 for the NSCs attached to the first group of the buildings (Test, Test 0.15, Test 0.25, and EC8 M) are approximately equal to the first three vibration periods of these P-structures (see Table 5.3). The first (T_1) and second

(T_2) vibration periods of the second group of buildings were approximately equal (see Table 5.3). Hence, NSCs with vibration periods match with the second vibration periods of buildings from the second group (EC8 M5, EC8 M10, and EC8 M15), were not considered. In order to investigate the influence of the NSC to P-structure vibration period ratio of the first and second groups of buildings, additional NSCs vibration periods were considered as presented in Section 5.6.1.

Table 5.4 Vibration periods of the NSCs attached to the first and second groups of buildings.

Building	Natural periods of the NSCs [s]		
	T_1	T_2	T_3
Test, Test 0.15, Test 0.25	0.82	0.73	0.65
EC8 M	0.55	0.52	0.42
EC8 M5	0.66	-	0.51
EC8 M7	0.84	-	0.66
EC8 M10	1.17	-	0.92
EC8 M13	1.29	-	1.02
EC8 M15	1.39	-	1.12

In regards to NSCs, the arms of the cantilevers were modelled with appropriate lengths and stiffness to match the vibration periods of the P-structures in the first and second groups of buildings. The lengths (L_a) and lateral stiffness (K_a) values of the circular cantilever arms are given in Table 5.5. These values were chosen in such a way that the NSC vibration periods (T_C) match one of the first three vibration periods (T_1, T_2, or T_3) of the P-structures.

For NSCs attached to the third group of buildings, periods of NSCs equal only to the first period T_1 of the P-structures were adopted, as reported in Table 5.6. This table also shows the characteristic values (i.e. the lengths and lateral stiffness of the cantilever arms) of the NSCs integrated on the third group of buildings.

Table 5.5 Characteristics of the NSCs attached to the first and second groups of buildings.

Building	Characteristics of arms of NSCs					
	NSCs with $T_C = T_1$		NSCs with $T_C = T_2$		NSCs with $T_C = T_3$	
	L_a [m]	K_a [N/m]	L_a [m]	K_a [N/m]	L_a [m]	K_a [N/m]
Test, Test 0.15, Test 0.25	2.29	533.6	2.12	672.5	1.96	851.0
EC8 M	1.75	1195.6	1.69	1327.5	1.46	2058.9
EC8 M5	1.24	840.2	-	-	1.05	1383.8
EC8 M7	1.46	514.7	-	-	1.24	840.2
EC8 M10	1.82	265.7	-	-	1.55	430.2
EC8 M13	1.94	219.4	-	-	1.66	350.2
EC8 M15	2.04	188.7	-	-	1.77	288.9

Table 5.6 Characteristics of the NSCs attached to the third group of buildings.

Building	Ground type	Natural periods of the NSCs [s]	Characteristics of arms of NSCs	
		T_1	L_a [m]	K_a [N/m]
EC8 M3	A	0.62	1.19	950.6
	B	0.59	1.15	1053.3
	D	0.47	0.99	1650.9
	E	0.52	1.06	1345.0
EC8 M5	A	0.75	1.35	651.1
	B	0.71	1.31	712.6
	D	0.61	1.18	975.0
	E	0.66	1.24	840.2
EC8 M10	A	1.25	1.90	233.6
	B	1.22	1.87	245.0
	D	1.08	1.73	309.4
	E	1.17	1.82	265.7
EC8 M15	A	1.50	2.15	161.2
	B	1.45	2.10	173.0
	D	1.28	1.93	222.8
	E	1.39	2.04	188.7

It should also be noted that the seismic response of the rigid NSCs (i.e. $T_C \approx 0$ s) was also investigated in this chapter. For rigid NSCs, the values of their peak components accelerations (PCAs) should be equal to the values of PGA when they attached to ground levels of a building as explained in Chapter 4 (see Section 4.3.2). However, for rigid NSCs attached to the floors of the building, the values of PCAs should be equal to the values of the

peak floors accelerations (PFAs) at the point of the attachment with the NSCs. Therefore, in this chapter, the values of the PFA_{xy} were used to represent the values of the accelerations for rigid NSCs.

5.5 Nonlinear Static Analyses of the RC P-structures

Nonlinear static (push-over) analyses were carried out for the three groups of buildings to calculate their elastic and maximum seismic capacities. Values of the base shear and the top displacements of the P-structures in the critical direction (i.e. the most critical direction, characterised by the lowest strength and highest demand, is the positive X direction) were recorded. The top displacement values at near collapse (NC) were modified by considering the torsional effect using the extension of the N2 procedure (Fajfar, 2002; Fajfar *et al.*, 2005a, 2005b; Kreslin and Fajfar, 2010; Stefano and Pintucchi, 2010). The extension of the N2 method is described in details in Appendix A (see Section A1).

Figure 5.4 displays the values of the normalised top displacements obtained from push-over and elastic dynamic analyses, as well as the correction factors of the first group of buildings. The normalised top floors displacements were calculated using the ratio between the top floors displacements at the flexible sides and the corresponding displacements at the centres of mass at the top floors (see Figure 5.1). It seems from Figure 5.4 that the push-over analysis gives values of the normalised displacements approximately in the range between 1.02 and 1.03 for the buildings in the first group; whereas, the elastic dynamic analyses provided values of the normalised displacements equal to 1.32, 1.29, 1.27, and 1.16 for the buildings Test, Test 0.15, Test 0.25, and EC8 M, respectively. Therefore, values of the torsion

correction factors were obtained by dividing all these values of the normalised displacements obtained from the elastic dynamic analyses by those corresponding values obtained from the push-over analyses. Accordingly, the values of the correction factors due to the effect of the torsion were found as 1.28, 1.25, 1.23, and 1.14 corresponding to the aforementioned buildings. Moreover, Figure 5.5 shows the corrected values of the top displacements at NC of the first group of buildings due to the torsional effect.

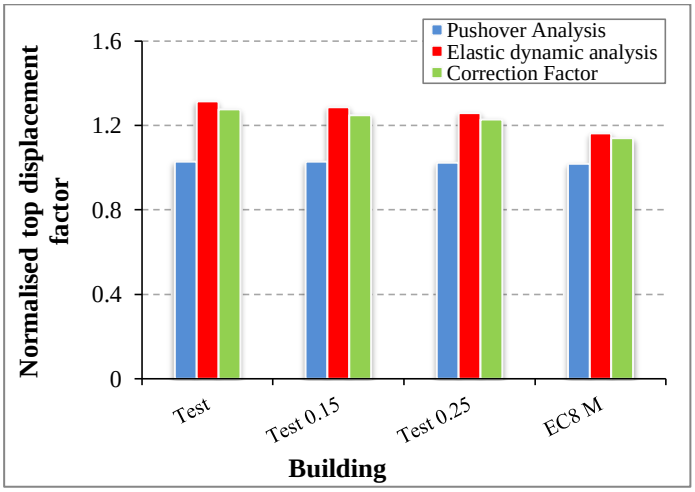

Figure 5.4 Push-over and elastic dynamic analyses results: normalised top displacement factors of the first group of buildings.

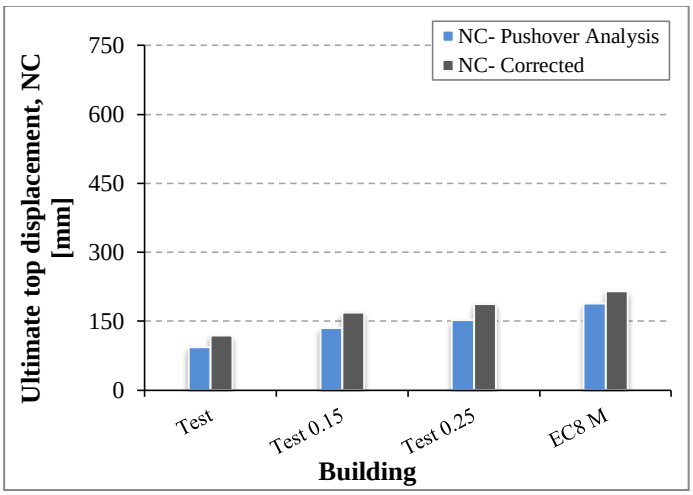

Figure 5.5 Push-over analyses results: corrected top displacements values due to torsional effect of the first group of buildings.

In Figure 5.5, the values of the top floors displacements at NC, which were obtained from the push-over analyses, were correct due to the effect of the torsion by multiplying these values of displacements by the corresponding correction factors as reported above. Consequently, the corrected values of the displacements at the top floors were 119 mm, 168 mm, 187 mm, and 215 mm for Test, Test 0.15, Test 0.25, and EC8 M buildings respectively.

The same procedures that were used in the first group of buildings for the determination of the correction factors of the top displacements at NC due to the torsional effect were also adopted for the second and third groups of buildings. Figure 5.6 displays the values of the normalised top displacements and the correction factors obtained from push-over and elastic dynamic analyses of the second group of buildings. The values of the correction factors were 1.277, 1.251, 1.23, and 1.14 for the buildings EC8 M5, EC8 M7, EC8 M10, EC8 M13, and EC8 M15, respectively. However, Figure 5.7 shows the corrected values of the top displacements at NC of the second group of buildings due to the torsional effect. These values were 315 mm, 385 mm, 481 mm, 521 mm, and 552 mm, respectively for the above-mentioned buildings.

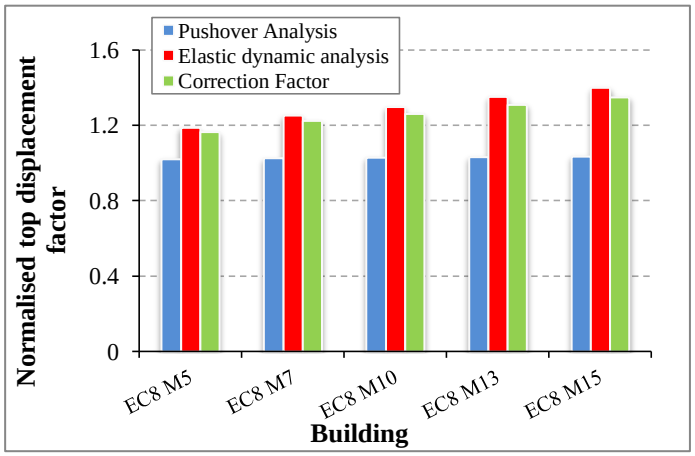

Figure 5.6 Push-over and elastic dynamic analyses results: normalised top displacement factors of the second group of buildings.

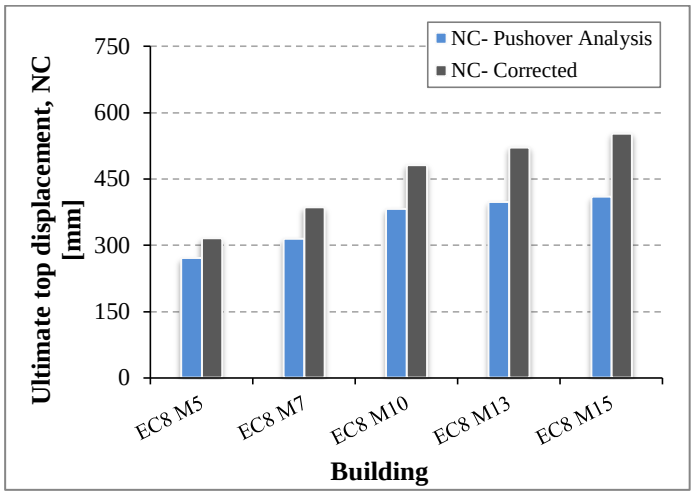

Figure 5.7 Push-over analyses results: corrected top displacements values due to torsional effect of the second group of buildings.

Shown in Figure 5.8 are the values of the normalised top displacement factors evaluated from push-over and elastic dynamic analyses, as well as the values of the correction factor of the third group of buildings. Moreover, Figure 5.9 displays the corrected values of the top displacements at NC of this group of buildings due to the effect of torsion. The corrected values of the top floors displacements were 150 mm, 185 mm, 200 mm, and 186 mm for the EC8 M3 building when it was designed on ground types A, B, D, and E, respectively. However, for EC8 M5 building, these values of the corrected top displacements were 205 mm, 260 mm, 400 mm, and 315 mm, respectively for the above mentioned ground types. Values of 310 mm, 390 mm, 660 mm, and 418 mm were observed for the corrected top displacements of the EC8 M10 building and values of 340 mm, 450 mm, 711 mm, and 552 mm were found for the top displacements of the EC8 M15 building when they were also designed for ground types A, B, D, and E, respectively.

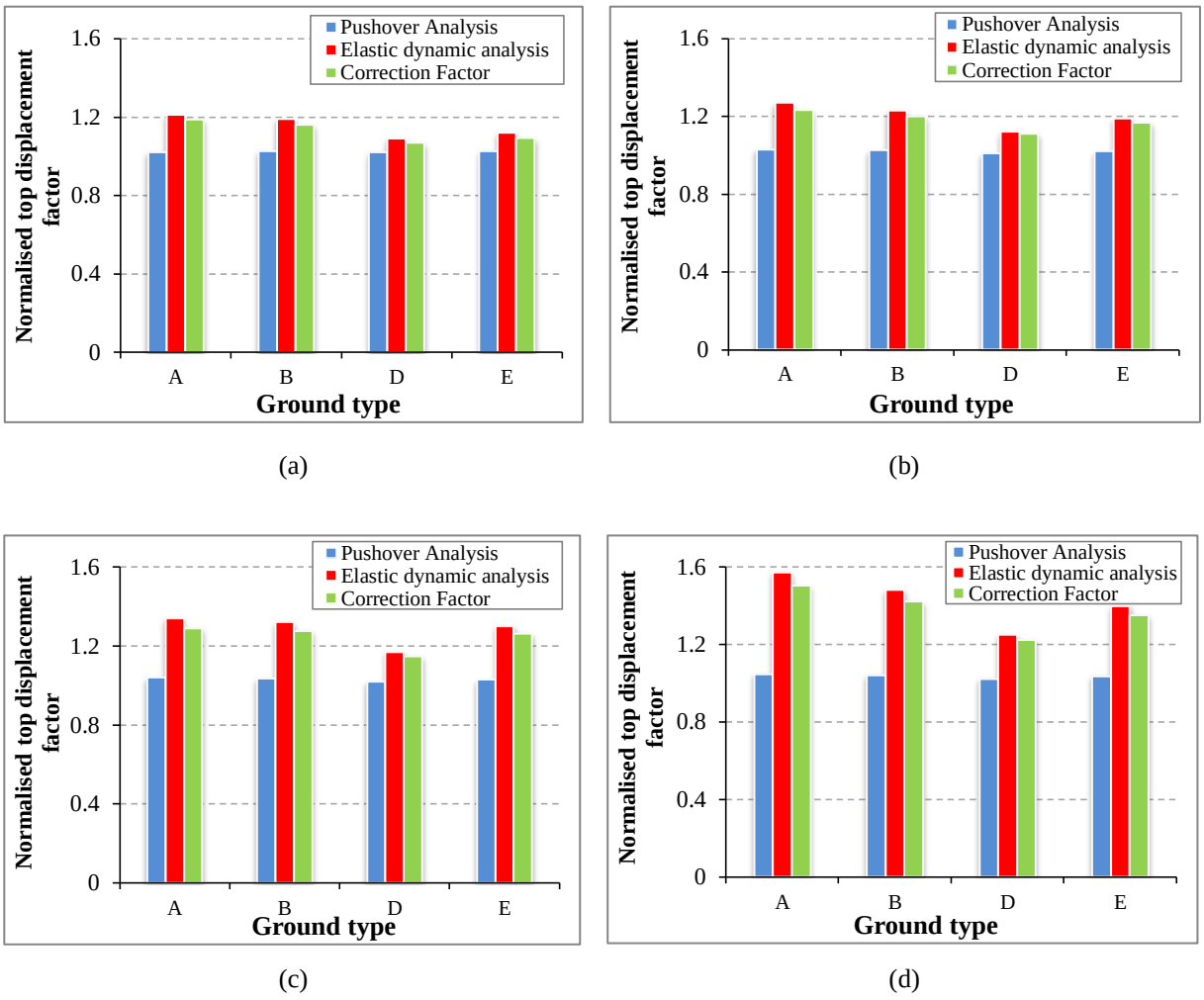

Figure 5.8 Push-over and elastic dynamic analyses results: normalised top displacement factors of the third group of buildings (a) EC8 M3, (b) EC8 M5, (c) EC8 M10, and (d) EC8 M15.

By adopting the corrected values of the top displacements as explained in Figures 5.5, 5.7, and 5.9, the elastic and maximum seismic capacities of the P-structures were computed according to the expressions of Annex B of EC8 (2004). These expressions are presented in details in Appendix A (see Section A2).

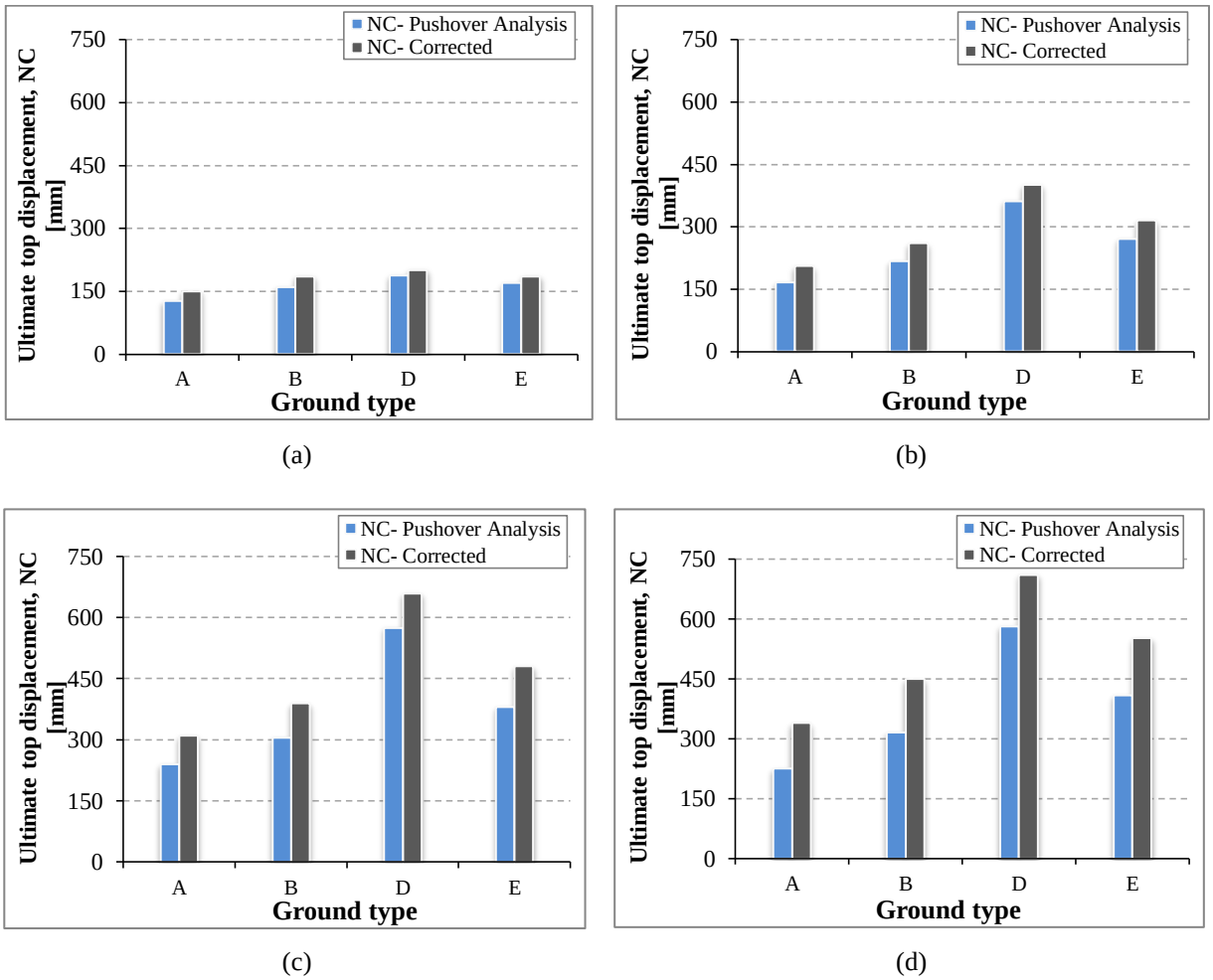

Figure 5.9 Push-over analyses results: corrected top displacements values due to torsional effect of the third group of buildings (a) EC8 M3, (b) EC8 M5, (c) EC8 M10, and (d) EC8 M15.

Figures 5.10(a) and 5.10(b) show the capacity curves of the first and second groups of buildings respectively. The values of the ultimate displacements (i.e. near collapse NC deformations) presented in these curves are corrected based on the values of the torsional correction factors, as explained in Figures 5.5 and 5.7.

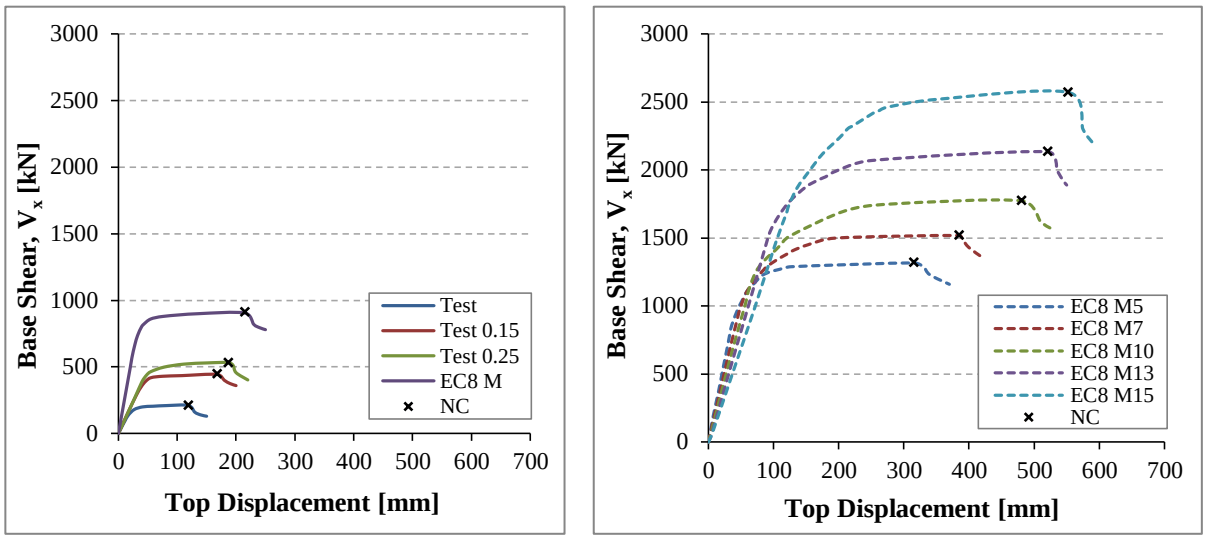

(a) (b)

Figure 5.10 Capacity curves of the (a) first group and (b) second group of buildings.

For each considered building of the P-structures, Tables 5.7 and 5.8 detail the characteristics of the idealised elastic-perfect plastic force-displacement relationship. According to Annex B of EC8 (2004), the initial stiffness of the idealized system is determined in such a way that the areas under the actual and idealized force-displacement curves are equal (see Figure A2-1 in Appendix A). The idealised force-displacement curves were used to calculate the elastic and maximum seismic capacities of the buildings. For each building, the characteristics detailed in Tables 5.7 and 5.8 are: the maximum seismic capacity; weight (W); effective mass (m^*); transformation constant (Γ); base shear (F_y); equivalent to near collapse displacement (d_m); actual deformation energy (E_m); yield displacement (d_y); effective period of the idealised equivalent SDOF system (T^*); elastic acceleration response (S_{ae}) at T^*; acceleration at the yield point (S_{ay}); and target displacement of the multi-degree of freedom system (d_t). It can be seen from Tables 5.7 and 5.8 that the maximum seismic capacity for each building is given by a value of PGA corresponds to a value of d_m/d_t approximately equal to 1.0.

Table 5.7 Maximum seismic capacities and characteristics of the idealised force-displacement relationship of the first and second groups of buildings.

Building	Ground Type	Max. seismic capacity [g]	W [kN]	m^* [kg].10^3	Γ	F_y [kN]	d_m [m]	E_m [kN.m]	d_y [m]	T^* [s]	S_{ae} [g]	S_{ay} [g]	d_t [m]
Test	--	0.26	1935.0	135.0	1.26	211.0	0.119	21.4	0.0347	0.94	0.43	0.12	0.118
Test 0.15	C	0.46	1935.0	141.0	1.24	444.0	0.168	63.6	0.0494	0.79	0.87	0.25	0.166
Test 0.25	C	0.51	1935.0	141.0	1.24	583.0	0.187	88.1	0.0717	0.83	0.89	0.33	0.188
EC8 M	C	0.76	2850.0	192.0	1.28	905.0	0.215	175.5	0.0722	0.59	1.89	0.37	0.213
EC8 M5	C	0.74	4536.6	308.1	1.36	1317.4	0.315	365.6	0.075	0.83	1.33	0.32	0.312
EC8 M7	C	0.69	6659.0	428.4	1.40	1519.4	0.385	509.0	0.100	1.05	0.97	0.26	0.376
EC8 M10	C	0.63	9993.9	628.0	1.43	1773.6	0.481	724.5	0.145	1.42	0.66	0.20	0.475
EC8 M13	C	0.58	14699.3	875.3	1.44	2134.3	0.521	930.6	0.170	1.66	0.52	0.17	0.511
EC8 M15	C	0.58	18515.6	1083.3	1.45	2571.6	0.552	1188.1	0.180	1.73	0.51	0.17	0.545

Table 5.8 Maximum seismic capacities and characteristics of the idealised force-displacement relationship of third group of buildings.

Building	Ground Type	Max. seismic capacity [g]	W [kN]	m^* [kg].10^3	Γ	F_y [kN]	d_m [m]	E_m [kN.m]	d_y [m]	T^* [s]	S_{ae} [g]	S_{ay} [g]	d_t [m]
EC8 M3	A	0.69	2686.6	181.6	1.28	601.0	0.150	105.3	0.038	0.67	1.04	0.26	0.147
	B	0.72	2799.4	189.3	1.28	750.0	0.185	143.1	0.040	0.63	1.43	0.31	0.184
	D	0.83	3116.4	210.7	1.28	1200.6	0.200	180.6	0.043	0.54	2.08	0.45	0.194
	E	0.79	3031.2	204.9	1.28	1105.7	0.186	159.8	0.044	0.56	1.80	0.42	0.183
EC8 M5	A	0.64	4108.7	284.4	1.36	850.0	0.205	189.1	0.067	0.94	0.68	0.22	0.201
	B	0.68	4393.0	303.9	1.36	1050.0	0.260	277.5	0.070	0.89	0.95	0.26	0.257
	D	0.78	5066.0	350.7	1.36	1850.0	0.400	542.1	0.079	0.77	1.96	0.40	0.393
	E	0.74	4536.6	308.1	1.36	1317.4	0.315	365.6	0.075	0.83	1.33	0.32	0.312
EC8 M10	A	0.57	8687.7	556.8	1.43	1006.5	0.310	353.1	0.108	1.52	0.37	0.13	0.304
	B	0.59	9289.9	595.4	1.43	1402.3	0.390	516.0	0.130	1.48	0.50	0.17	0.390
	D	0.70	11042.3	707.7	1.43	2600.0	0.660	1174.8	0.160	1.31	1.06	0.26	0.650
	E	0.63	9993.9	628.0	1.43	1773.6	0.481	724.5	0.145	1.42	0.66	0.20	0.475
EC8 M15	A	0.50	14965.7	892.4	1.45	1561.0	0.340	492.6	0.155	1.87	0.27	0.12	0.340
	B	0.54	15949.2	951.1	1.45	2003.1	0.450	784.2	0.174	1.80	0.38	0.15	0.440
	D	0.64	20625.0	1229.7	1.45	3420.0	0.711	2122.1	0.179	1.59	0.75	0.20	0.687
	E	0.58	18515.6	1083.3	1.45	2571.6	0.552	1188.1	0.180	1.73	0.51	0.17	0.545

According to Annex B of EC8 (2004), a building can be considered within the elastic range if its ductility factor (μ) is within the range of 0 to 1.0. Hence, the elastic seismic capacity may be defined as the PGA value corresponding to the value of μ equal to 1.0.

Tables 5.9 and 5.10 give the values of the elastic seismic capacities of the considered P-structures together with the values of the spectral accelerations, S_{ae} and S_{ay}.

Table 5.9 Elastic seismic capacities of the first and second groups of buildings.

Building	Ground type	Elastic seismic capacity [g]	S_{ae} [g]	S_{ay} [g]
Test	--	0.070	0.124	0.12
Test 0.15	C	0.100	0.256	0.25
Test 0.25	C	0.120	0.335	0.33
EC8 M	C	0.135	0.375	0.37
EC8 M5	C	0.160	0.33	0.32
EC8 M7	C	0.160	0.26	0.26
EC8 M10	C	0.160	0.20	0.20
EC8 M13	C	0.170	0.18	0.17
EC8 M15	C	0.170	0.17	0.17

Table 5.10 Elastic seismic capacities of the third group of buildings.

Building	Ground type	Elastic seismic capacity [g]	S_{ae} [g]	S_{ay} [g]
EC8 M3	A	0.120	0.257	0.26
	B	0.131	0.310	0.31
	D	0.149	0.464	0.45
	E	0.143	0.420	0.42
EC8 M5	A	0.142	0.220	0.22
	B	0.156	0.260	0.26
	D	0.179	0.412	0.40
	E	0.160	0.320	0.32
EC8 M10	A	0.135	0.129	0.13
	B	0.150	0.172	0.17
	D	0.178	0.278	0.26
	E	0.160	0.198	0.20
EC8 M15	A	0.148	0.120	0.12
	B	0.168	0.149	0.15
	D	0.192	0.204	0.20
	E	0.170	0.173	0.17

The values of the elastic and maximum seismic capacities of the P-structures were used together with other values of the PGA to study the seismic behaviour of the NSCs, as detailed in Sections 5.6 and 5.7.

5.6 Dynamic Response of NSCs Attached to the First and Second Groups of Buildings

As explained in Sections 5.2.1 and 5.2.2, the buildings in the first and second groups were designed on ground type C. Therefore, natural and artificial records that match with the EC8 (2004) Type 1 elastic spectrum for ground type C were used to investigate the behaviours of the NSCs. The natural records were adopted in the dynamic analyses of the P-S systems of the first group of buildings; however the artificial records were used for the NSCs attached to the second group of buildings. Further details information on the adopted base motion records can be found in Chapter 3 (see Section 3.3). The results presented in the following sections are based on averages of the selected natural or artificial record earthquakes. Maximum values of standard deviations equal to 0.015 g and 0.011 g were observed when the NSCs accelerations evaluated under the effect of seven pairs of the natural and artificial records respectively.

Due to the three-dimensional nature of the P-structures considered in this chapter, there were found two different values of the accelerations in the horizontal X and Y directions at each floor of the buildings during earthquakes. Therefore, the values of the peak floor accelerations (PFA_{xy}) and the peak component accelerations (PCA_{xy}) were calculated as the square root of the sum of the squares (SQRSS) of (PFA_x and PFA_y) and (PCA_x and PCA_y) respectively. In the following sections, reference will be made to the elastic and maximum seismic capacities for a given P-structure of the first and second groups of buildings as given in Tables 5.9 and 5.7 respectively.

5.6.1 Effect of the NSC to P-structure Vibration Period Ratio

The NSC to P-structure vibration period ratio is one of the main parameters that affect the response of the NSCs. The importance of this parameter stems from the fact that the NSCs resonate when their natural periods match the vibration periods of the P-structures (Igusa and Der Kiureghian, 1985; Yang and Huang, 1993). Shown in Figure 5.11 is the relationship between peak component acceleration and NSC to P-structure vibration period ratio (T_C/T_1) for the NSCs mounted on the flexible sides (FS - see Figure 5.1) of the top floors of the first group of buildings.

Figure 5.11(a) shows the results at the elastic seismic capacity (0.07 g, 0.10 g, 0.12 g, and 0.135 g) whereas Figure 5.11(b) shows the results at the maximum seismic capacity (0.26 g, 0.46 g, 0.51 g, and 0.76 g) for Test, Test 0.15, Test 0.25, and EC8 M, respectively. Figure 5.11 exhibits three zones of dynamic response. In Zone 1, NSCs accelerations increase gradually with the increase in T_C/T_1 from 0.0 to 0.68. In Zone 2, a sharp increase in NSCs accelerations occurs between T_C/T_1 values of 0.765 and 1.0. This was to be expected since the NSCs resonate when their vibration periods match the third and first vibration periods of the P-structures at T_C/T_1 values of 0.765 and 1.0 respectively. Zone 3 is marked by a sudden drop in NSCs accelerations at T_C/T_1 values greater than 1.0.

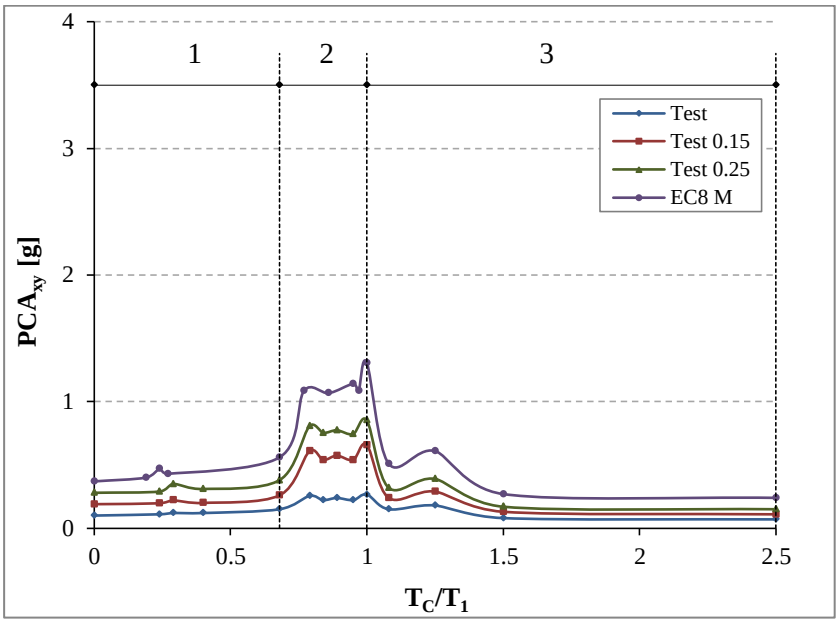

(a)

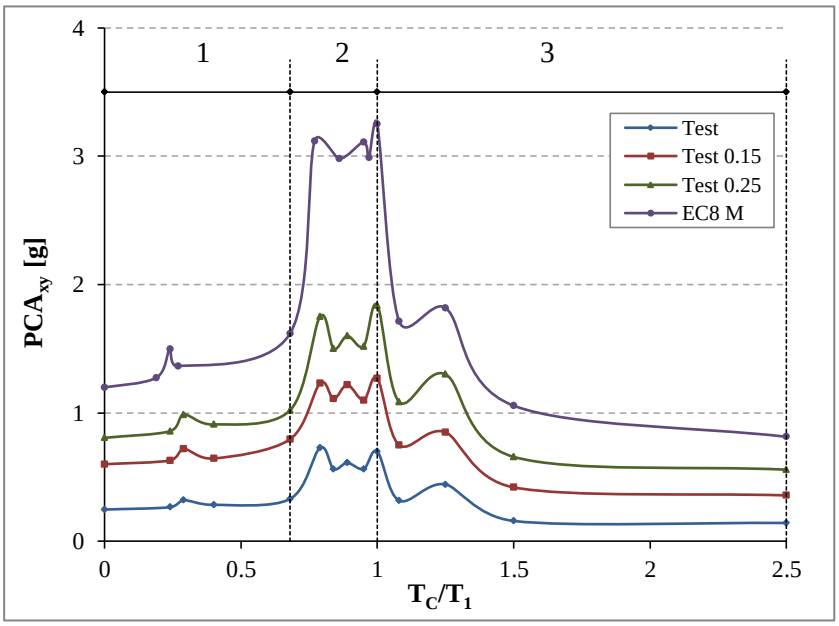

(b)

Figure 5.11 Variations of peak component acceleration (PCA_{xy}) vs. NSC to P-structure vibration period ratio (T_C/T_1) for the NSCs mounted on the flexible sides of the top floors of the first group of buildings at the PGA values corresponding to (a) the elastic seismic capacities and (b) the maximum seismic capacities.

For $T_C = T_1$, the NSCs accelerations at the maximum seismic capacities as presented in Figure 5.11(b) were on average 125% higher than the corresponding values at the elastic seismic capacities of the buildings as shown in Figure 5.11(a). For a given T_C/T_1 value, the NSCs attached to EC8 M experienced the highest acceleration. This may be explained by the fact that this building had the highest elastic (0.135 g) and maximum (0.76 g) seismic capacities and hence was subjected to higher PGA values. On the other hand, the NSCs attached to Test building experienced the lowest accelerations as this building had the least elastic (0.07 g) and maximum (0.26 g) seismic capacities.

Figure 5.12 shows the variation of NSCs accelerations with T_C/T_1 for the NSCs attached to the flexible sides of the top floors of EC8 M5, EC8 M10, and EC8 M15. It can be seen from Figure 5.12 that the NSCs attached to buildings from the second group had the same three-zone dynamic response experienced by the NSCs attached to the first group of buildings. Furthermore, for $T_C = T_1$, the NSCs accelerations at the maximum seismic capacities were on average 107% higher than the corresponding values at the elastic seismic capacities of the buildings.

Unlike the NSCs mounted on the first group of buildings, the NSCs attached to EC8 M5, EC8 M10, and EC8 M15 had approximately the same response at a given T_C/T_1 value. The second group of buildings had approximately the same elastic seismic capacities (0.16 g – 0.17 g, see Table 5.9) hence there was no change in the NSCs response at this PGA value.

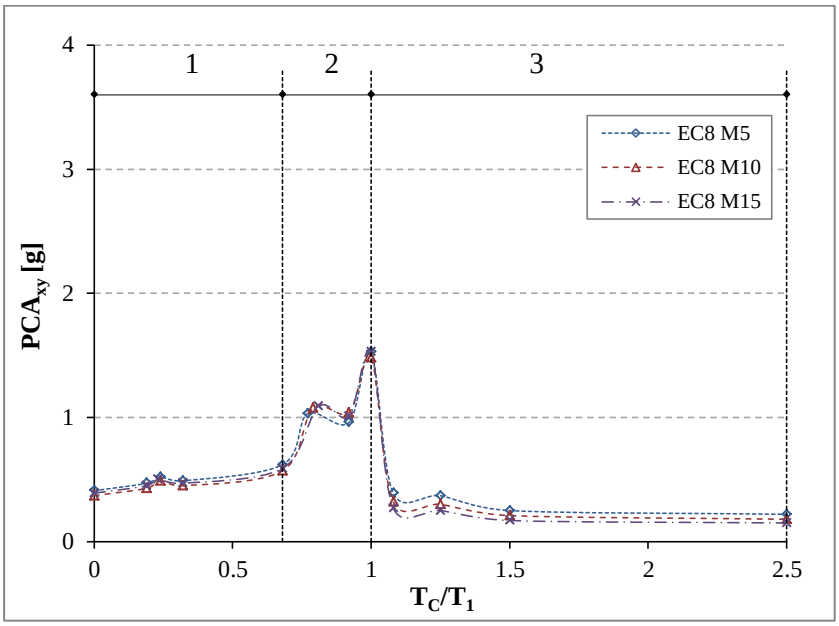

(a)

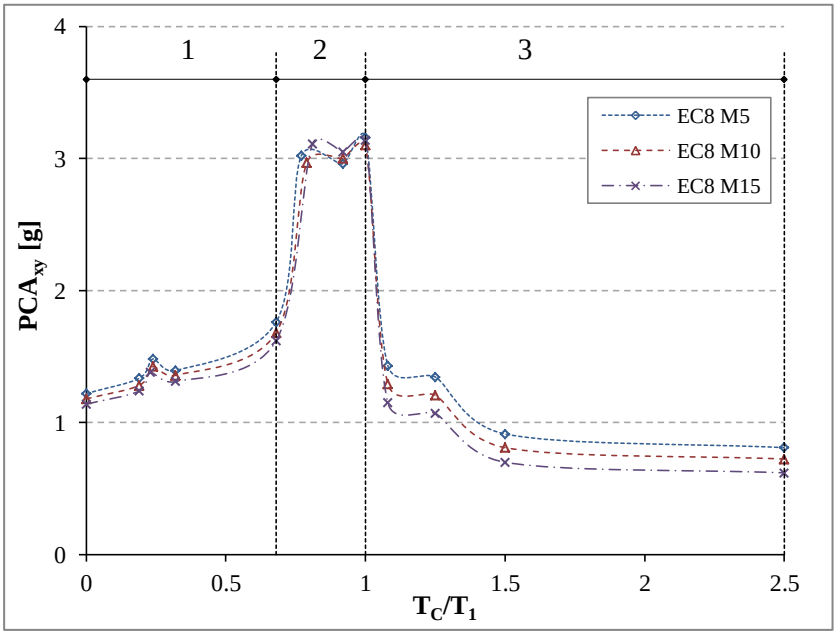

(b)

Figure 5.12 Variations of peak component acceleration (PCA_{xy}) vs. NSC to P-structure vibration period ratio (T_C/T_1) for the NSCs mounted on the flexible sides of the top floors of the second group of buildings; EC8 M5, EC8 M10, and EC8 M15 at the PGA values corresponding to (a) the elastic seismic capacities and (b) the maximum seismic capacities.

The maximum seismic capacities of the buildings EC8 M5, EC8 M10, and EC8 M15 were inversely proportional to their heights (see Table 5.7). This suggests that, for a given T_C/T_1 value, the NSCs attached to EC8 M15 (subjected to 0.58 g) and EC8 M10 (subjected to 0.63 g) should have lower acceleration values than the NSCs attached to EC8 M5 (subjected to 0.74 g). However, Figure 5.12(b) shows clearly that the NSCs attached to the flexible sides of EC8 M5, EC8 M10, and EC8 M15 had comparable response at the maximum seismic capacities of these P-structures. This result suggests that EC8 M15 and EC8 M10 had stronger torsional behaviour than EC8 M5. Consequently, the response of the NSCs attached to EC8 M15 was more affected by the torsional behaviour than the response of the NSCs attached to EC8 M10 and EC8 M5. Eventually, this resulted in the comparable response shown in Figure 5.12(b). This result will be further investigated in Section 5.6.4.

5.6.2 Effect of Peak Ground Acceleration

The effect of the peak ground acceleration (PGA) on the seismic behaviour of the NSCs was investigated by considering PGA values in the range of 0.05 g to the maximum seismic capacity of each building as given in Table 5.7. Values of the PCA_{xy} were obtained to investigate the effect of the intensity values of the base motions on the dynamic response of the NSCs attached to the two groups of buildings. Figures 5.13 and 5.14 display the variation of PCA_{xy} with PGA for the NSCs with vibration periods T_C equal to T_1 and mounted on the flexible sides and centres of rigidity of the top floors of the first and second groups of buildings respectively.

For a given P-structure in Figures 5.13 and 5.14, the NSCs accelerations vary approximately linearly with base excitation up to the PGA value corresponding to the elastic seismic capacity of the P-structure. At higher PGA values, damage reduces the global stiffness of the P-structures and consequently changes its dynamic characteristics. This, in turn, reduces the rate of increase of the P-structure and NSCs accelerations and results in a nonlinear relationship between NSCs accelerations and PGA.

Figures 5.13(a) and 5.13(b) show that, for a given PGA value, the NSCs attached to EC8 M, which was designed according to EC8 (2004), had higher acceleration values than the corresponding NSCs attached to Test, Test 0.15, and Test 0.25; which were not in full compliance with EC8 (2004) provisions (see Section 5.2.1). Due to its relatively high stiffness, EC8 M had a lower fundamental vibration period (0.55 s) compared to the other three buildings which had a fundamental vibration period of 0.823 s. Conversely, the NSCs attached to Test, which was the least stiff building, experienced the lowest accelerations. Of note is that the NSCs attached to the flexible sides had accelerations that were on average 42% higher than the accelerations of the NSCs attached to the centres of rigidity.

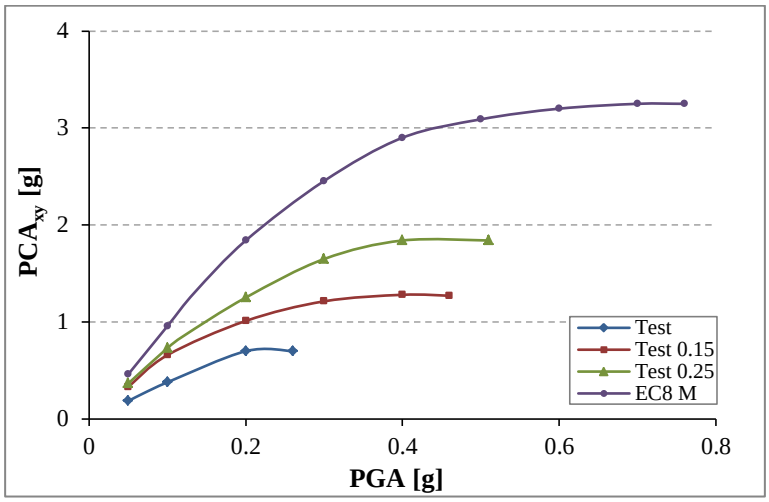

(a)

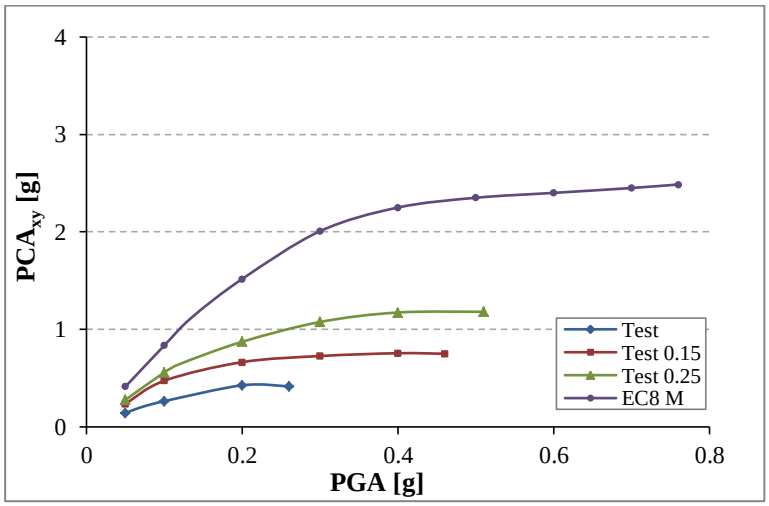

(b)

Figure 5.13 Variations of peak component acceleration (PCA_{xy}) vs. peak ground acceleration (PGA) for the NSCs with $T_C = T_1$ and attached to the top floors of the first group of buildings at (a) flexible sides and (b) centres of rigidity.

Figure 5.14(a) shows that the NSCs attached to the flexible sides of the second group of buildings had approximately the same acceleration response. However, Figure 5.14(b) shows that the NSCs attached to the centres of rigidity of the second group of buildings had accelerations that were inversely proportional to the heights of the P-structures. The main factor that has effected on this trend is the fundamental vibration periods of the P-structures which were increased with the increase of the height of the building (see Table 5.3). This fact

is recognised in most of elastic response spectra of different types of ground as defined in EC8 (2004). For values of fundamental periods that are larger than the upper periods of the constant horizontal zone of the spectral shape (see Figure 3.5), the higher the period of T, the lower the value of pseudo acceleration will be produced.

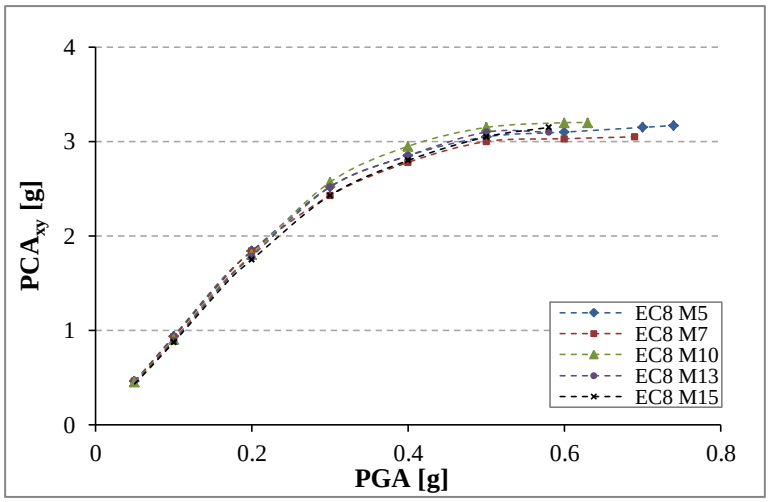

(a)

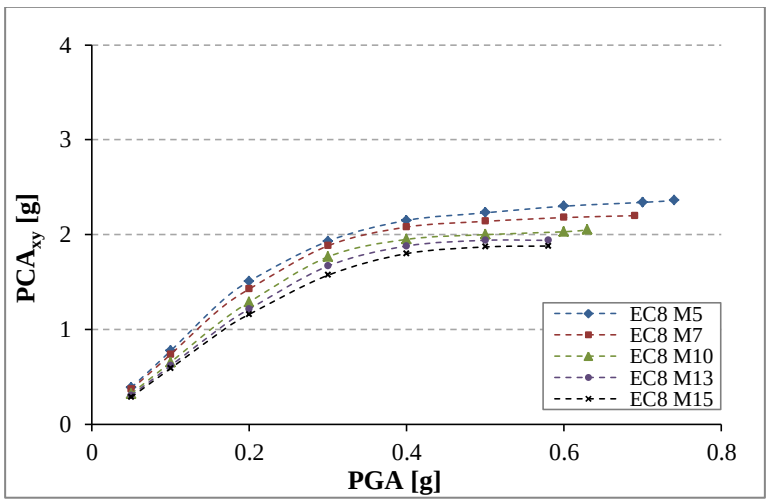

(b)

Figure 5.14 Variations of peak component acceleration (PCA_{xy}) vs. peak ground acceleration (PGA) for the NSCs with $T_C = T_1$ and attached to the top floors of the second group of buildings at (a) flexible sides and (b) centres of rigidity.

It can be concluded from Figure 5.14(b) that the NSCs were not affected by the torsional behaviour when they were attached to the floors at the centres of rigidity regions.

However, as a result that the values of the floor rotational displacements of buildings EC8 M15, EC8 M10 and EC8 M13 are larger than those of EC8 M7 and EC8 M5 (These results will be discussed in Section 5.6.4); therefore, the values of the PCA_{xy} were found approximately equal. This trend could be an opposite to that found when the NSCs attached to the centre of rigidity regions. Once more, this result also suggests that the NSCs attached to the flexible sides of taller buildings were more affected by the torsional behaviour than those attached to the flexible sides of shorter buildings.

The component acceleration amplification factor (A_p^a), defined in this research as PCA_{xy}/PGA, accounts for the dynamic amplification in the acceleration response of NSCs. During the elastic response of the P-structures (i.e. PGA values equal to or less than the elastic seismic capacities), values of A_p^a should be constant. However, Figures 5.15 and 5.16 show that the maximum values of the acceleration amplification factor occur at the PGA values corresponding to the elastic seismic capacities of the P-structures which are indicated by the vertical lines (see Table 5.9). Nonetheless, for all considered NSCs, the maximum difference in A_p^a values within the elastic range of the P-structures was less than 5.5%. This result suggests that the flexibility of the NSCs (flexible NSCs with $T_C = T_1$) could have a slight effect on their amplifications under different values of PGAs. At elastic range, the higher the intensity of PGA, the higher the acceleration amplification factor will be. In other words, the vibration of flexible NSCs may more amplify under higher PGA when they attached to elastic P-structures. Beyond the elastic limit, the change in the dynamic characteristics of the P-structures reduces the resonance effect experienced by the NSCs. Hence, the maximum values of the acceleration amplification factor occur at the elastic seismic capacities of the P-structures. This trend could be similar to that found in most of

previous studies (Lin and Mahin, 1985; Sewell et al., 1986; Singh et al., 1993; Rodriguez et al., 2002; Medina et al., 2006; Chaudhuri and Villaverde, 2008; Mohammed et al., 2008) presented in the literature review section where the amplification responses decreased immediately beyond the elastic range of the P-systems.

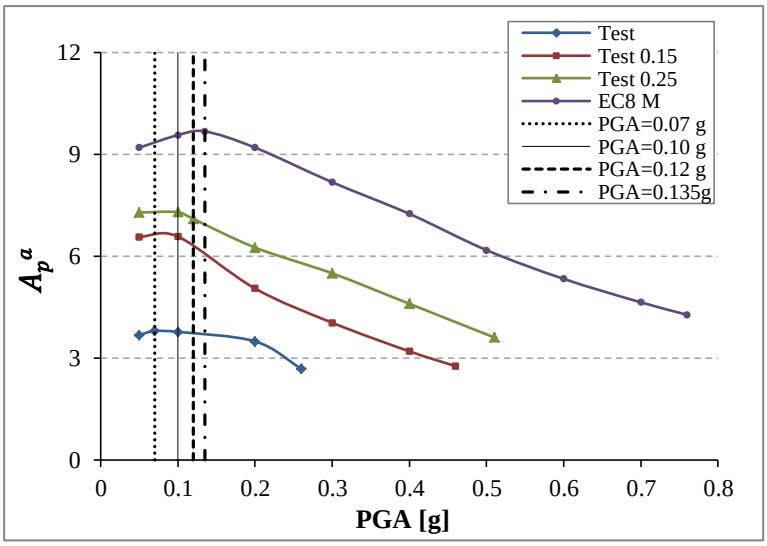

(a)

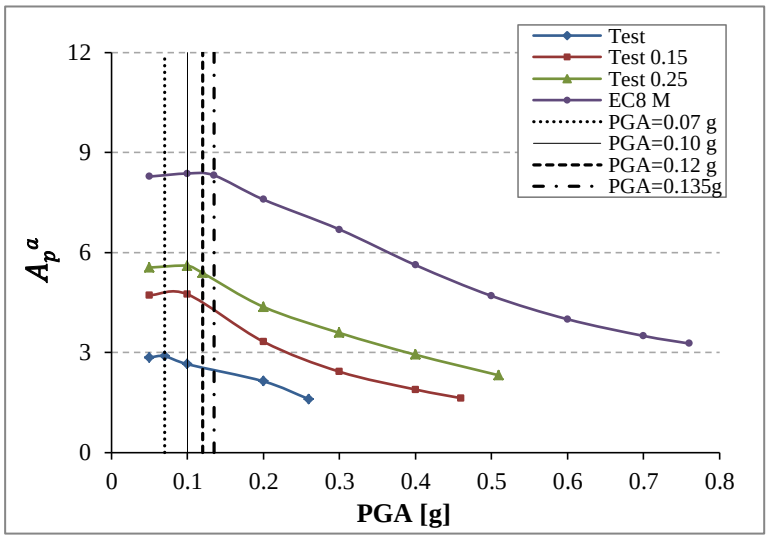

(b)

Figure 5.15 Variations of component acceleration amplification factor (A_p^a) vs. peak ground acceleration (PGA) for the NSCs with $T_C = T_1$ and attached to the top floors of the first group of buildings at (a) flexible sides and (b) centres of rigidity. (The vertical lines refer to the PGA values corresponding to the elastic seismic capacities of the 1st group of buildings).

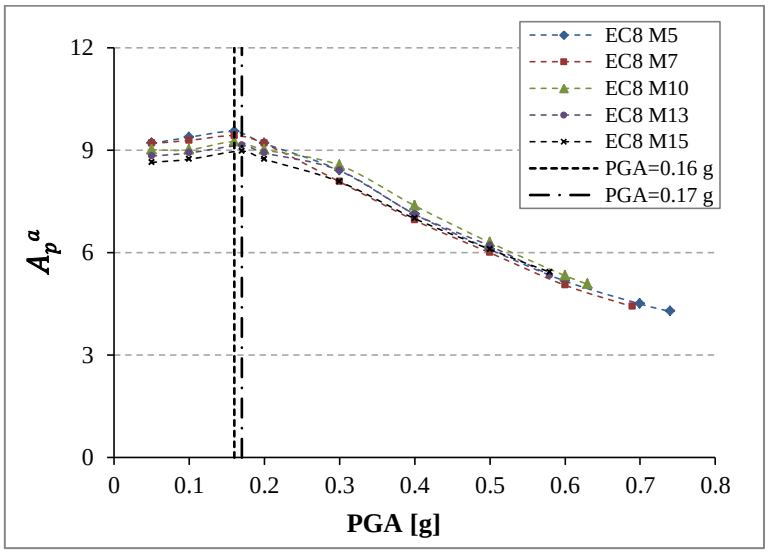

(a)

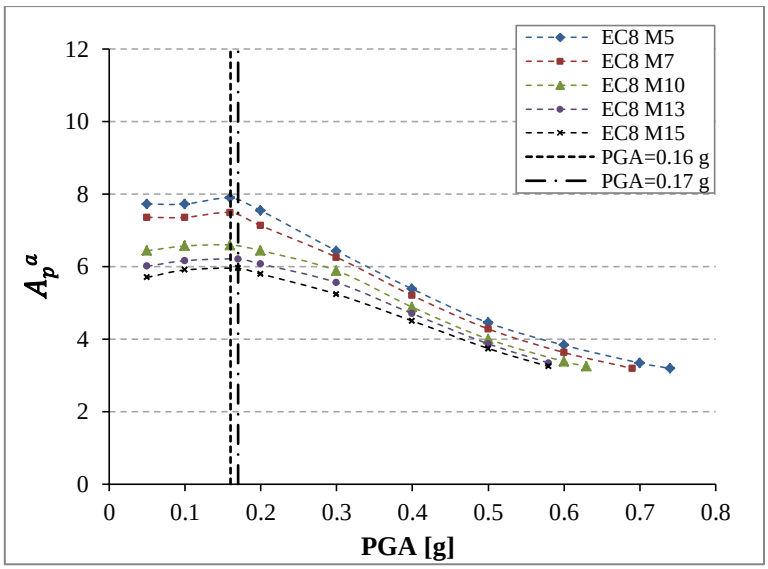

(b)

Figure 5.16 Variations of component acceleration amplification factor (A_p^a) vs. peak ground acceleration (PGA) for the NSCs with $T_C = T_1$ and attached to the top floors of the second group of buildings at (a) flexible sides and (b) centres of rigidity. (The vertical lines refer to the PGA values corresponding to the elastic seismic capacities of the 2nd group of buildings).

5.6.3 Effect of NSC to P-structure Height Ratio

Shown in Figure 5.17 is the relationship between NSC to P-structure height ratio (z_c/H) and peak component acceleration for the NSCs with $T_C = T_1$. The height ratio refers to the height (z_c) at which the NSC is located relative to the height of the building (H). The NSCs were attached at varying heights to the flexible sides (FS) and centres of rigidity (CRs) of the P-structures designed according to EC8 (2004), i.e. EC8 M, EC8 M5, EC8 M7, EC8 M10, EC8 M 13, and EC8 M15. In each case, two PGA values corresponding to the elastic and maximum seismic capacities of each building were considered. The legend used in Figure 5.37(a) applies to the remaining curves in Figure 5.17.

The FE predictions suggest that the relationship between z_c/H and PCA_{xy} is linear in the case of EC8 M which had the least height (9 m) and fundamental vibration period (0.55 s). With the increase in the P-structures heights and fundamental vibration periods, the curves become piecewise-linear and then nonlinear. For a given building and a given PGA value, there are two curves showing the variations of z_c/H versus PCA_{xy} for the NSCs attached to the FS and CR of the building. It can be noted form Figure 5.17 that the acceleration values for the NSCs attached to the flexible sides were higher than the corresponding values for the NSCs were attached to the centres of rigidity. Furthermore, the component acceleration values at the maximum seismic capacities were observed higher than the corresponding values at the elastic seismic capacities of the P-structures. These observations apply to all the NSCs considered in this chapter regardless of their z_c/H value or the P-structure height. For a given building, the NSCs attached to the top floor of the building, i.e. when z_c/H =1.0, experienced the maximum accelerations regardless of the PGA value. This trend matches the EC8 (2004) design guidelines which will be detailed in Section 5.8.

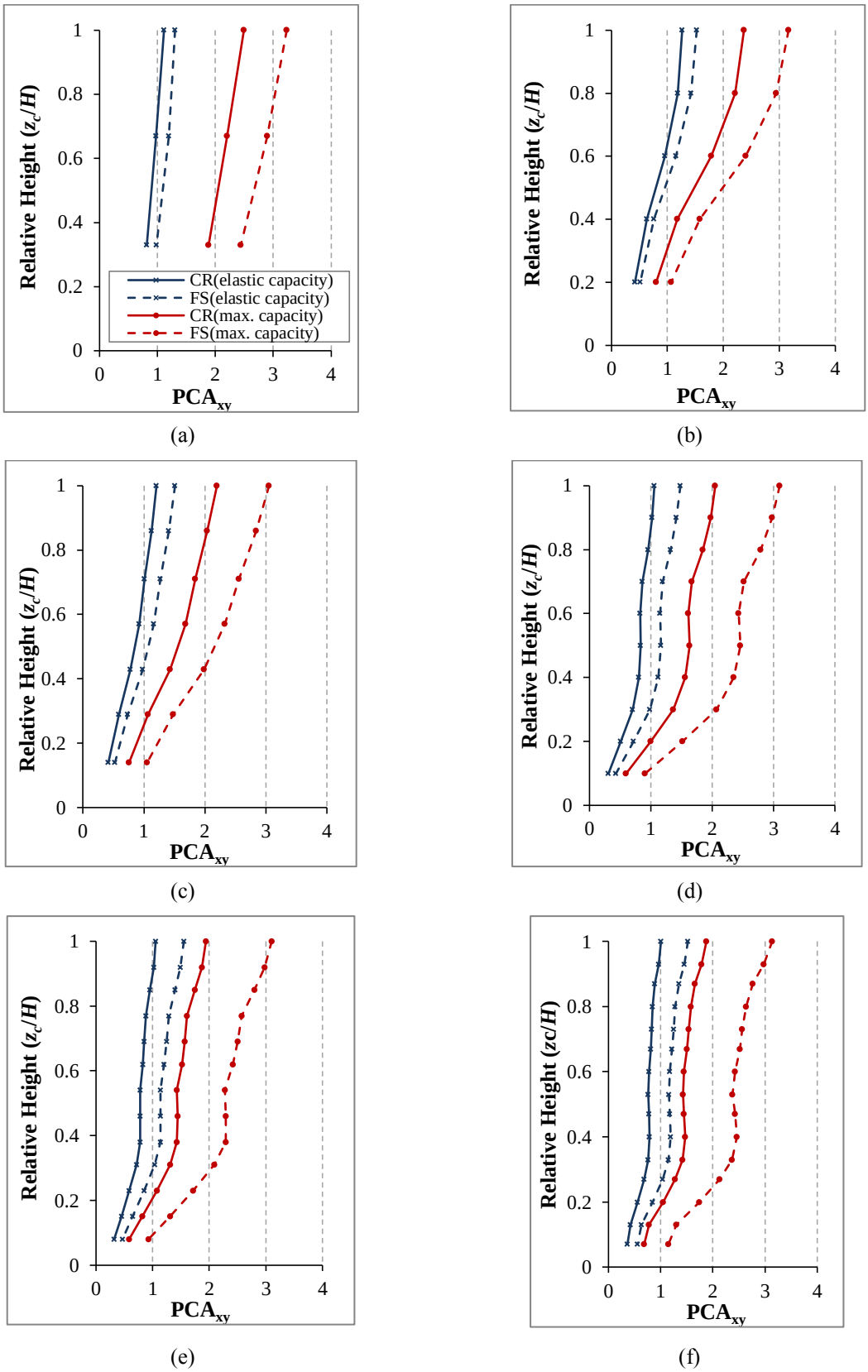

Figure 5.17 Variations of NSC to P-structure height ratio (z_c/H) vs. peak component acceleration (PCA_{xy}) for the NSCs with $T_C = T_1$ and attached to the buildings: (a) EC8 M, (b) EC8 M5, (c) EC8 M7, (d) EC8 M10, (e) EC8 M13, and (f) EC8 M15.

The results in Figure 5.17 also show that the NSCs accelerations are inversely proportional to the heights of the P-structures when the NSCs attached to the centres of rigidity of the P-structures. The main factor that has effected on this trend is the fundamental vibration periods of the P-structures which increased with the increase in their heights.

5.6.4 Effect of the Torsional Behaviour of the P-structures

During earthquakes, the accelerations recorded at the centre of rigidity (CR) of a P-structure are due to transitional modes only of the P-structures. Recorded values of the accelerations at the flexible side (FS) of a building give accelerations due to lateral modes and any torsional modes (Hart and DiJulio, 1974; Hart *et al.*, 1975). Therefore, the torsional amplification factor (F_T) for NSCs accelerations may be defined as the ratio of the peak component acceleration at the flexible side ($PCA_{xy,FS}$) to the corresponding value at the centre of rigidity ($PCA_{xy,CR}$), i.e. ($F_T = PCA_{xy,FS}/PCA_{xy,CR}$).

For the NSCs with vibration periods T_C equal T_1 and attached to the top floors of the first and second groups of buildings, Figures 5.18 and 5.19 show the variations of F_T and top floor rotation (θ) of the P-structures with PGA. The values of PGA considered were in the range of 0.05 g to the maximum seismic capacity of each building.

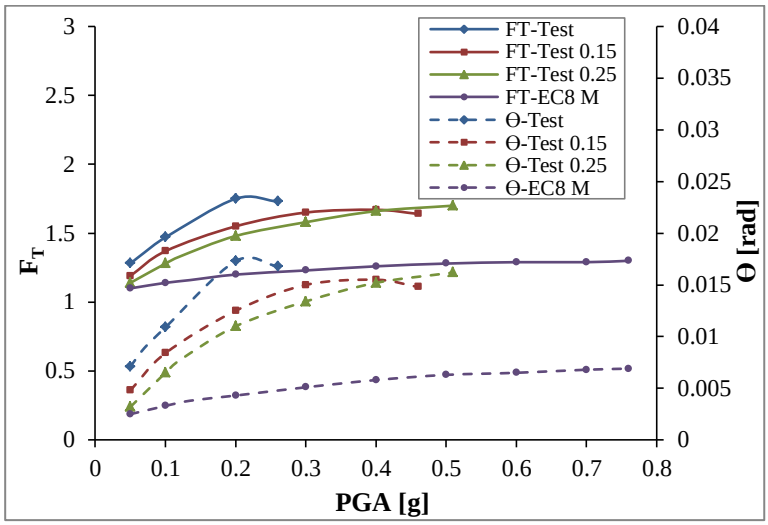

Figure 5.18 Variations of top floor rotation (θ) of the first group of buildings and torsional amplification factor (F_T) for the NSCs with $T_C = T_1$ vs. peak ground acceleration (PGA).

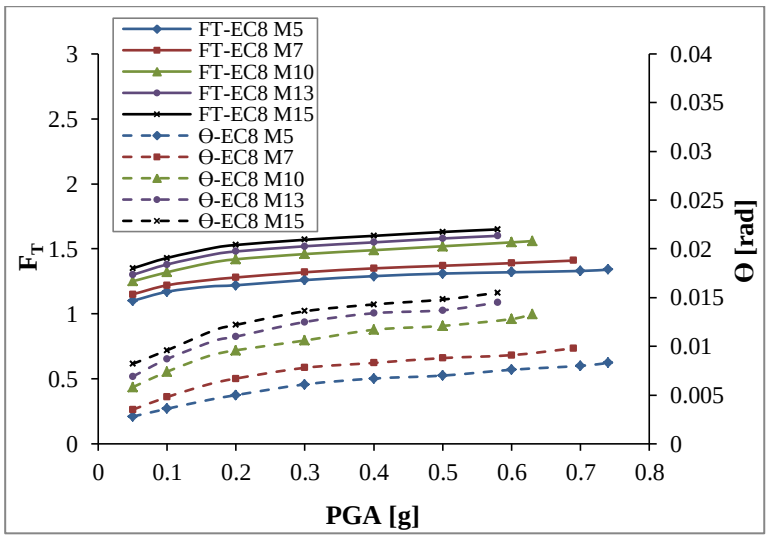

Figure 5.19 Variations of top floor rotation (θ) of the second group of buildings and torsional amplification factor (F_T) for the NSCs with $T_C = T_1$ vs. peak ground acceleration (PGA).

For the first group of buildings, Figure 5.18 shows that due to high flexibility of Test building, experienced the highest top floor rotation of 0.0173 rad and consequently had the most significant torsional behaviour. The torsional amplification factor for the NSCs attached to the flexible side of the top floor of Test was 1.75. The NSCs attached to the flexible sides of the top floors of Test 0.15 and Test 0.25 had F_T values of 1.67 and 1.70 respectively. These

approximately equal F_T values may be explained by the fact that the Test 0.15 and Test 0.25 had comparable top floors rotations (0.0155 rad and 0.0162 rad respectively) and consequently similar torsional behaviour. EC8 M had the least top floor rotation of 0.0069 rad and the NSCs attached to the flexible side of this building had the least torsional amplification factor of 1.30.

For the second group of buildings, Figure 5.19 shows that, at a given PGA, the torsional amplification factors and top floors rotations increased with the increase in total height of the P-structure. This result further clarifies why the NSCs with $T_C = T_1$ and attached to the FS of the top floors of EC8 M5, EC8 M10, and EC8 M15 had comparable acceleration values at the maximum seismic capacity of each building in spite of the different seismic capacities of the buildings (see Figure 5.12(b)). The maximum seismic capacities of EC8 M5, EC8 M10, and EC8 M15 were 0.76 g, 0.63 g, and 0.58 g, respectively. The NSCs with $T_C = T_1$ and attached to the top floors of these buildings had F_T values of 1.34, 1.56, and 1.65, respectively. It can be seen that EC8 M10 and EC8 M15 had higher torsional amplification factors than EC8 M5. This, in turn, resulted in the comparable NSCs accelerations at the different maximum seismic capacities of these buildings (see Figure 5.12(b)).

For a given P-structure, Figures 5.18 and 5.19 suggest that there is a strong correlation between F_T and θ. Figure 5.20 shows that the relationship between F_T and θ may be expressed as follows:

$$F_T = 43.3\,\theta + 1.0 \qquad (5\text{-}1)$$

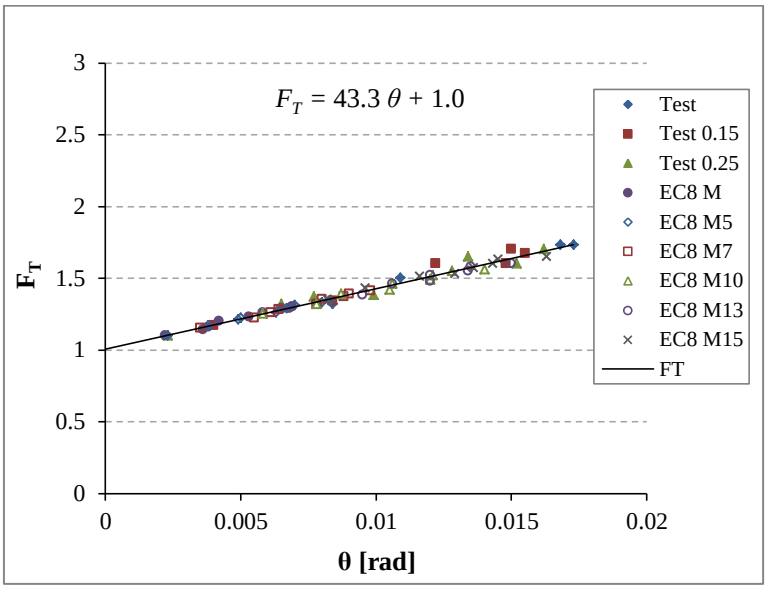

Figure 5.20 Relationship between the torsional amplification factor (F_T) for the NSCs with T_C equal to T_1 and top floor rotation (θ) of the first and second groups of buildings.

Equation (5-1) is valid for both regular and irregular P-structures. For a regular P-structure that does not experience floors rotations during earthquakes, Eq. (5-1) predicts a torsional amplification factor of 1.0. F_T becomes greater than 1.0 when the P-structure exhibits torsional behaviour. It can be concluded that the increase in θ, which is a measure of the torsional behaviour of the P-structure, results in a corresponding increase in F_T and consequently increases the accelerations of the NSCs attached to the flexible side of the P-structure. In addition, Eq. (5-1) is only valid for NSCs having periods equal to the first vibration period (T_1) of the considered RC P-structures designed on ground type C. To assess the applicability of Eq. (5-1) for those NSCs attached to P-structures designed on other types of ground, further cases of P-structures designed on ground types A, B, D, and E as defined in EC8 (2004) should be investigated. In Section 5.7, sixteen irregular RC frames in total were selected as the P-structures to investigate the effect of ground types on the seismic response of NSCs.

Linear time-history analyses were performed for the first and second groups of buildings to evaluate the values of the top floors rotations. Comparisons are made in Figures 5.21 and 5.22, between the values of the top floors rotations resulted from the linear analyses with the corresponding values computed from the nonlinear dynamic analyses that were presented in Figures 5.18 and 5.19 for the first and second groups of buildings respectively.

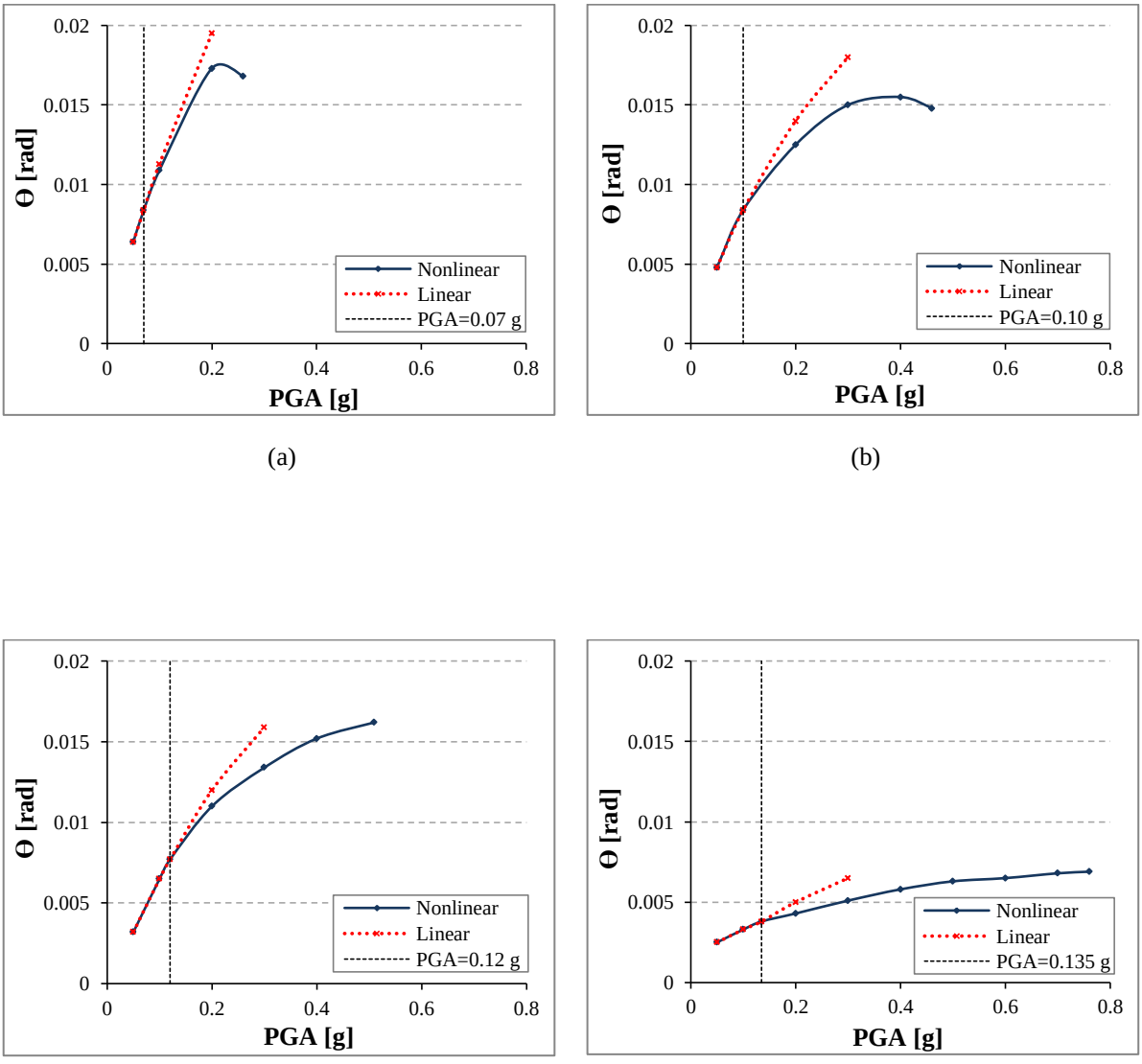

Figure 5.21 Linear and nonlinear time-history analyses results: variations of top floor rotation (θ) vs. peak ground accelerations (PGA) of the first group of buildings: (a) Test, (b) Test 0.15, (c) Test 0.25, and (d) EC8 M.

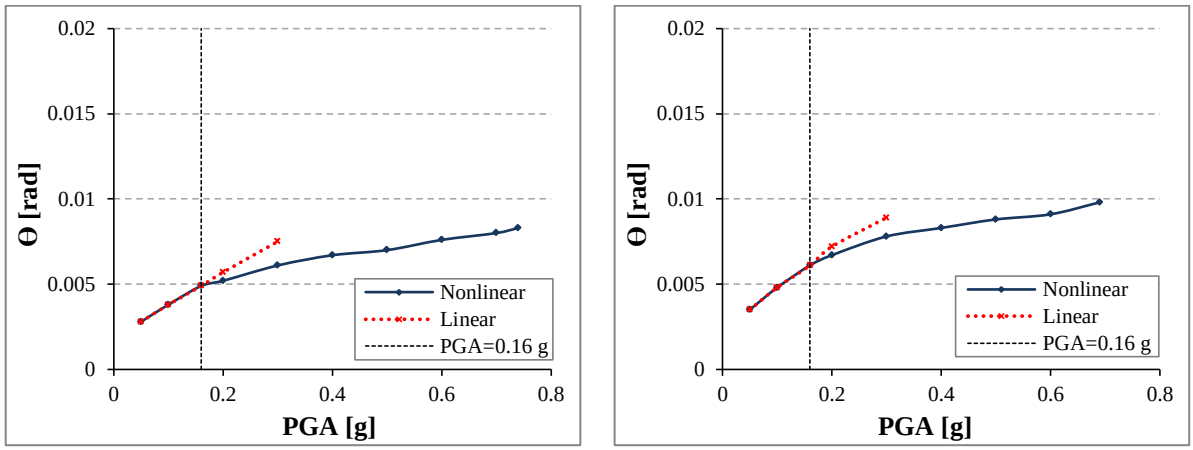

(a)

(b)

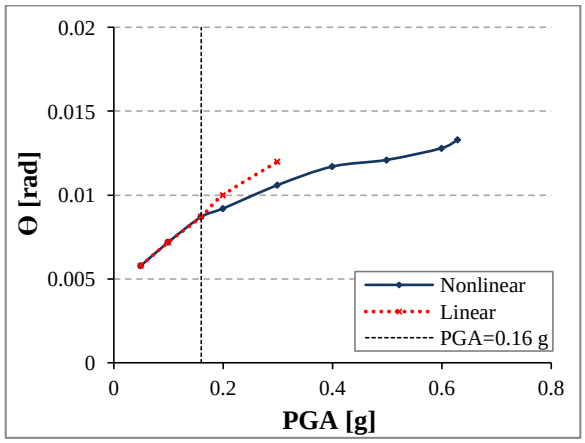

(c)

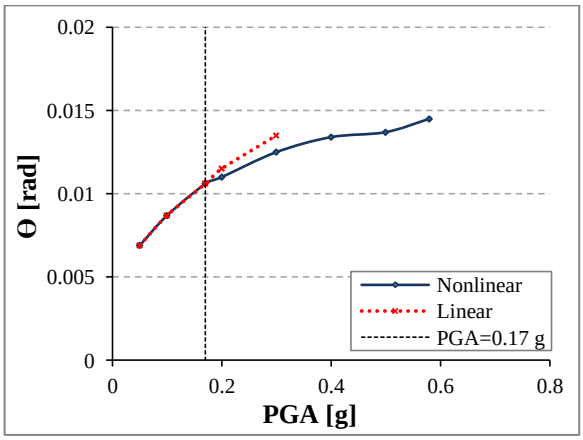

(d)

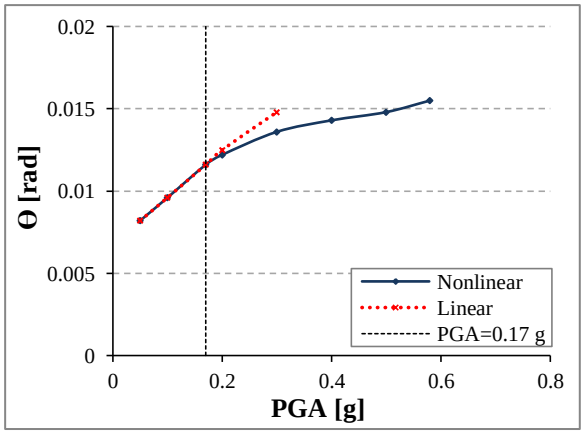

(e)

Figure 5.22 Linear and nonlinear time-history analyses results: variations of top floor rotation (θ) vs. peak ground accelerations (PGA) of the second group of buildings: (a) EC8 M5, (b) EC8 M7, (c) EC8 M10, (d) EC8 M13, and (e) EC8 M15.

It can be seen from the results of the comparisons in Figures 5.21 and 5.22 that the values of the top floors rotations derived from both the linear and nonlinear analyses were found identical when the values of PGA are equal or less than the elastic seismic capacity of each case of building (see Table 5.9). However, when the values of the PGA were larger than the elastic seismic capacity, the values of the top floors rotations resulted from the linear analyses were observed larger than those values of the rotations were recorded due to the nonlinear analyses. Consequently, values of the top floors rotations at PGA values corresponding to the elastic seismic capacities (i.e. PGA that gives a value of $\mu = 1.0$, see Table 5.9) can be evaluated directly from the linear time-history analysis.

5.7 Dynamic Response of NSCs Attached to the Third Group of Buildings

This section studies the effect of ground type (namely ground types A, B, D, and E as defined in EC8 (2004)) on the seismic response of lightweight acceleration-sensitive NSCs integrated on irregular multi-storey RC structures. The third group of buildings that consists of 16 RC P-structures, as described in Section 5.2.3, was adopted. Three sets of natural earthquakes consisting of 42 records compatible with the EC8 (2004) Type 1 elastic RS for ground types A, B, and D were used. However, for ground type E, seven artificial accelerograms were employed. More details on the selected accelerograms can be found in Chapter 3 (see Sections 3.3.1 and 3.3.2 for natural and artificial accelerograms respectively). The results presented in this section are based on the average of the selected earthquake records. Maximum values of standard deviations equal to 0.017 g and 0.012 g were found when the NSCs accelerations are evaluated under the effect of seven pairs of the natural and artificial records respectively.

Nonlinear dynamic FE analyses of the P-S systems were performed under the effect of PGA values in the range between a value of 0.05 g and the maximum seismic capacity of each building as given in Table 5.8. Shown in Figure 5.23 is the variations of PCA_{xy} with PGA for the NSCs with vibration periods T_C equal to T_1 (see Table 5.6) and attached to the flexible sides (FS - see Figure 5.1) of the top floors of the third group of buildings designed on different types of ground.

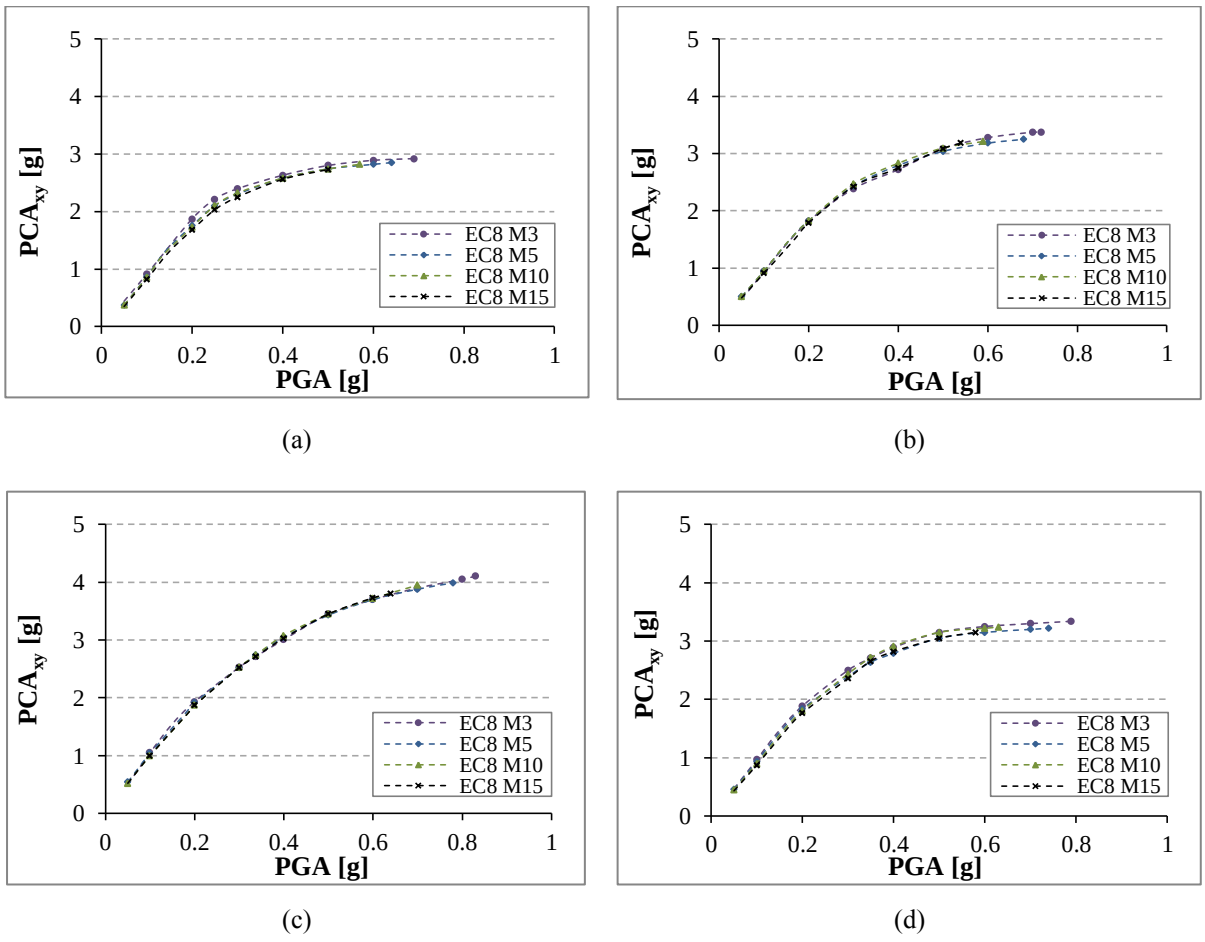

Figure 5.23 Variations of peak component acceleration (PCA_{xy}) vs. peak ground acceleration (PGA) for the NSCs having periods equal to T_1 and attached to the flexible sides of the top floors of the third group of buildings designed on ground types: (a) A, (b) B, (c) D, and (d) E.

Due to the increase in the fundamental vibration period of the P-structures with the increase in their heights (see Table 5.3), the response of the NSCs should be reduced.

However, Figure 5.23 shows that the NSCs attached to the FS of buildings EC8 M3, EC8 M5, EC8 M10, and EC8 M15 had approximately the same acceleration response when these P-structures were designed for construction on a given type of ground. It seems from this result that the NSCs attached to the flexible side of the P-structures have been affected by the torsional behaviours of the buildings in addition to the lateral accelerations. The NSCs attached to the flexible side of taller buildings were more significantly affected by the torsional behaviour than those attached to the flexible side of shorter buildings as torsional rotation increases significantly with the increase of the building height. This trend is explained later in Figure 5.26 where the values of the torsional amplification factors (F_T) were found higher for NSCs attached to the taller buildings than for those mounted on shorter buildings. Therefore, these results give additional confirmation on the outcome presented in Section 5.6.1, when the results suggested that the NSCs integrated on the flexible sides of taller RC structures designed on ground type C were more influenced by the rotational response than those mounted on the flexible sides of shorter RC structures designed also for construction on ground type C.

Moreover, due to the increase in the fundamental vibration periods of the P-structures in the third group with the increase in their heights (see Table 5.3), the acceleration response of NSCs attached to the centres of rigidity (CR - see Figure 5.1) of the top floors reduced with the increase in height of the P-structures as shown in Figure 5.24. Once more, these results suggest that the NSCs attached to the centres of rigidity were not affected by the torsional behaviour of the P-structures.

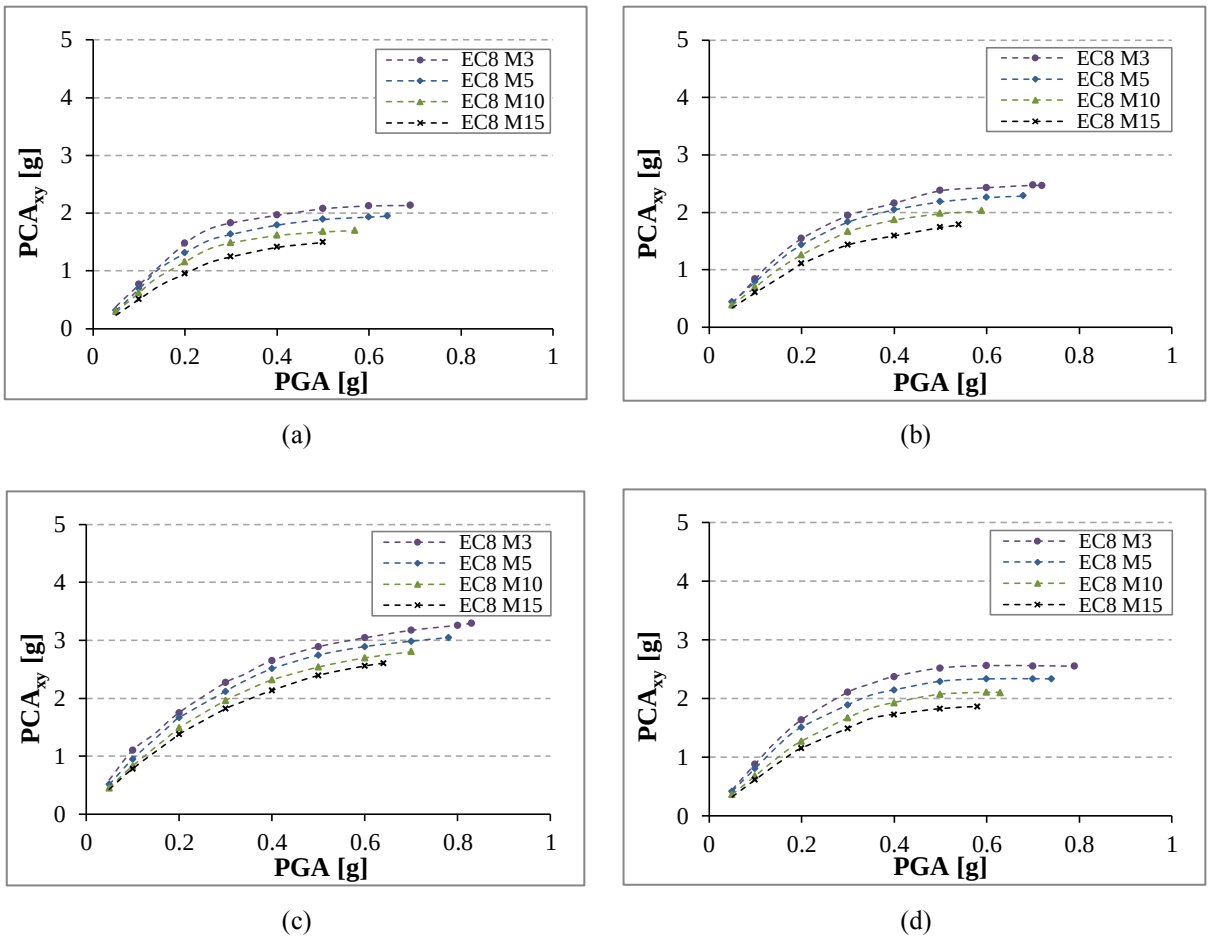

Figure 5.24 Variations of peak component acceleration (PCA_{xy}) vs. peak ground acceleration (PGA) for the NSCs having periods equal to T_1 and attached to the centres of rigidity of the top floors of the third group of buildings designed on ground types: (a) A, (b) B, (c) D, and (d) E.

To explain the effect of ground type on NSCs accelerations, Figure 5.25 shows the variations of PCA_{xy} versus PGA for those NSCs attached to the FS and CR of the top floor of EC8 M15 building designed on different ground types. It can be seen from Figure 5.25 that the minimum and maximum values of PCA_{xy} were found for the NSCs attached to the buildings designed on ground types A and D respectively. This result can be related to the maximum seismic capacities of the P-structures (see Table 5.8) especially when the NSCs attached to the centres of rigidity. For a given P-structure designed on different ground types, the higher the value of the maximum seismic capacity (i.e. the stiffer P-structure), the higher the NSCs acceleration.

Under the effect of the PGA values corresponding to the maximum seismic capacities of the P-structures (as given in Table 5.8), NSCs acceleration values equal to 2.73 g and 3.8 g were observed for the NSCs attached to the FS of the buildings designed on ground types A and D respectively. However, these two values were found respectively equal to 1.5 g and 2.6 g for the NSCs attached to CRs of the top floor of EC8 M15 building as shown in Figure 5.25(b). Comparable results were obtained for the NSCs attached to EC8 M3, EC8 M5, and EC8 M10. In general, the values of PCA_{xy} at the flexible sides of the P-structures designed on ground type D were higher than the corresponding values on ground types A, B, and E.

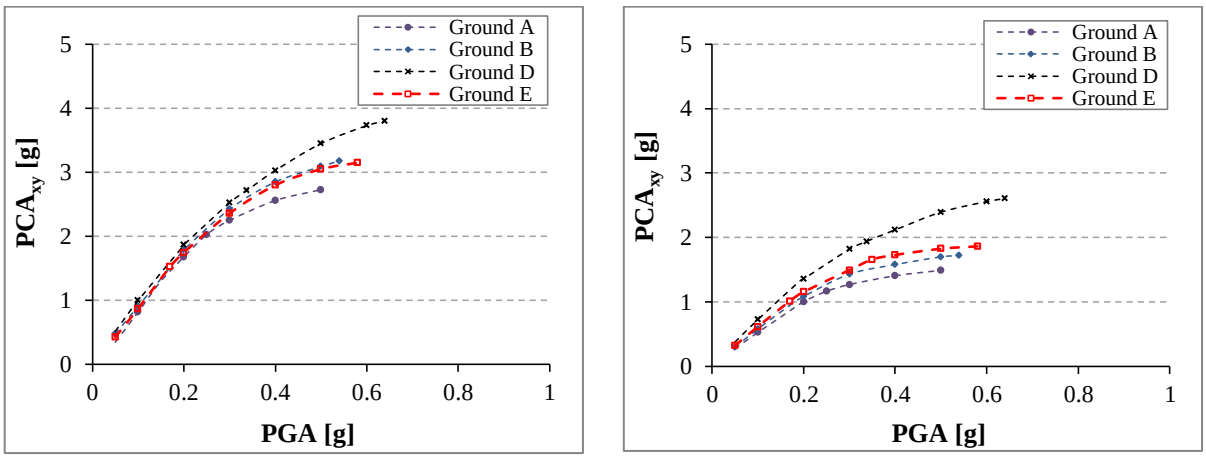

(a) (b)

Figure 5.25 Variations of peak component acceleration (PCA_{xy}) vs. peak ground acceleration (PGA) for the NSCs having a period equal to T_1 and attached to the EC8 M15 building designed on different types of ground: (a) flexible side and (b) centre of rigidity.

The torsional amplification factor (F_T) for NSCs was defined in Section 5.6.4 as the ratio of the peak component acceleration at the flexible side ($PCA_{xy,FS}$) to the corresponding value at the centre of rigidity ($PCA_{xy,CR}$), i.e. ($F_T = PCA_{xy,FS}/PCA_{xy,CR}$). For the NSCs with periods equal to T_1 and attached to the top floors of the third group of buildings, Figure 5.26 shows the variations of F_T and the top floors rotations θ with the values of the PGA. It can be

seen from Figures 5.26(a) to 5.26(d) that, for buildings designed on different types of ground, both the values of the torsional amplification factor of the NSCs and top floor rotation of the P-structures increased with the increase in the values of PGA.

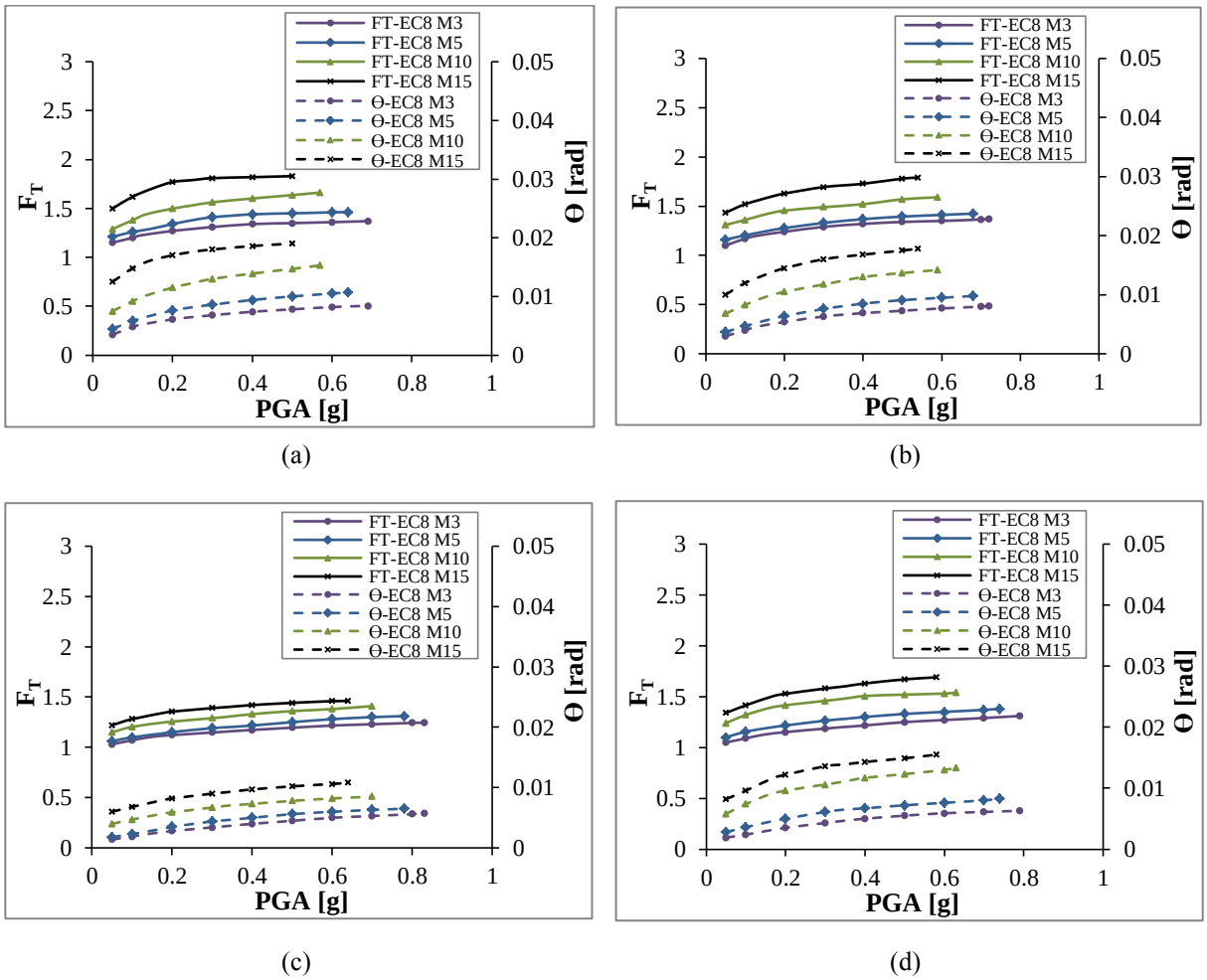

Figure 5.26 Variations of F_T and θ with PGA for the NSCs with $T_C = T_1$ and attached to the top floors of the third group of buildings designed on ground types: (a) A, (b) B, (c) D, and (d) E.

Moreover, it can be observed from Figure 5.26 that at a given value of PGA, the values of F_T and θ increased with the increase in total height of the P-structures. These findings further verify the conclusions of the results presented in Section 5.6.4, when the torsional amplification factors of NSCs and the top floor rotations were increased with the increase in total height of the RC buildings designed on ground type C. In addition, it can be

seen that the NSCs with $T_C = T_1$ and attached to the flexible side of the top floor of EC8 M15 designed on ground type A had a maximum value of F_T equal to 1.83, which was produced due to the maximum value of the top floor rotation of 0.019 rad as shown in Figure 5.26(a). The minimum value of F_T was 1.25 for the NSCs attached to the flexible side of EC8 M3 designed on ground type D which had a minimum value of θ equal to 0.0057 rad as displayed in Figure 5.26(c).

For a given P-structure, Figures 5.26(a) to 5.26(d) suggest that there is also a strong correlation between F_T and θ. Figures 5.27(a), 5.27(b), 5.27(c), and 5.27(d) show that the relationship between F_T and θ may be expressed as given in Eqs. (5-2), (5-3), (5-4), and (5-5) when the NSCs are attached to P-structures designed on grounds types A, B, D, and E, respectively.

$$F_T = 43.66\,\theta + 1.0 \tag{5-2}$$

$$F_T = 43.01\,\theta + 1.0 \tag{5-3}$$

$$F_T = 45.27\,\theta + 1.0 \tag{5-4}$$

$$F_T = 43.50\,\theta + 1.0 \tag{5-5}$$

Equations (5-2) to (5-5) also predict a value of F_T equal to 1.0 when the NSCs attached to non-torsional P-structure. To generalise the relation between the values of the torsional amplification factors for NSCs with $T_C = T_1$ and the top floors rotations of the P-structures that were designed on different types of ground such as A, B, C, D, and E, Figure 5.28 shows the results presented in Section 5.6.4 for the NSCs attached to the P-structures designed on ground type C (see Figure 5.20), together with those results given in Figure 5.27. The generalised relationship (i.e. the average values) between F_T and θ for all types of ground can be expressed as follows:

$$F_T = 43.13\,\theta + 1.0 \qquad (5\text{-}6)$$

Equation (5-6) is valid for acceleration-sensitive NSCs that are resonant with the first vibration period of studied RC P-structures designed on ground types A, B, C, D, and E as described in EC8 (2004). To assess the applicability range of Eq. (5-6), further cases of P-structures with different plan layouts should be investigated. Therefore, two additional groups of buildings consisting of 39 irregular RC frames in total were selected as the P-structures in Chapters 6 and 7.

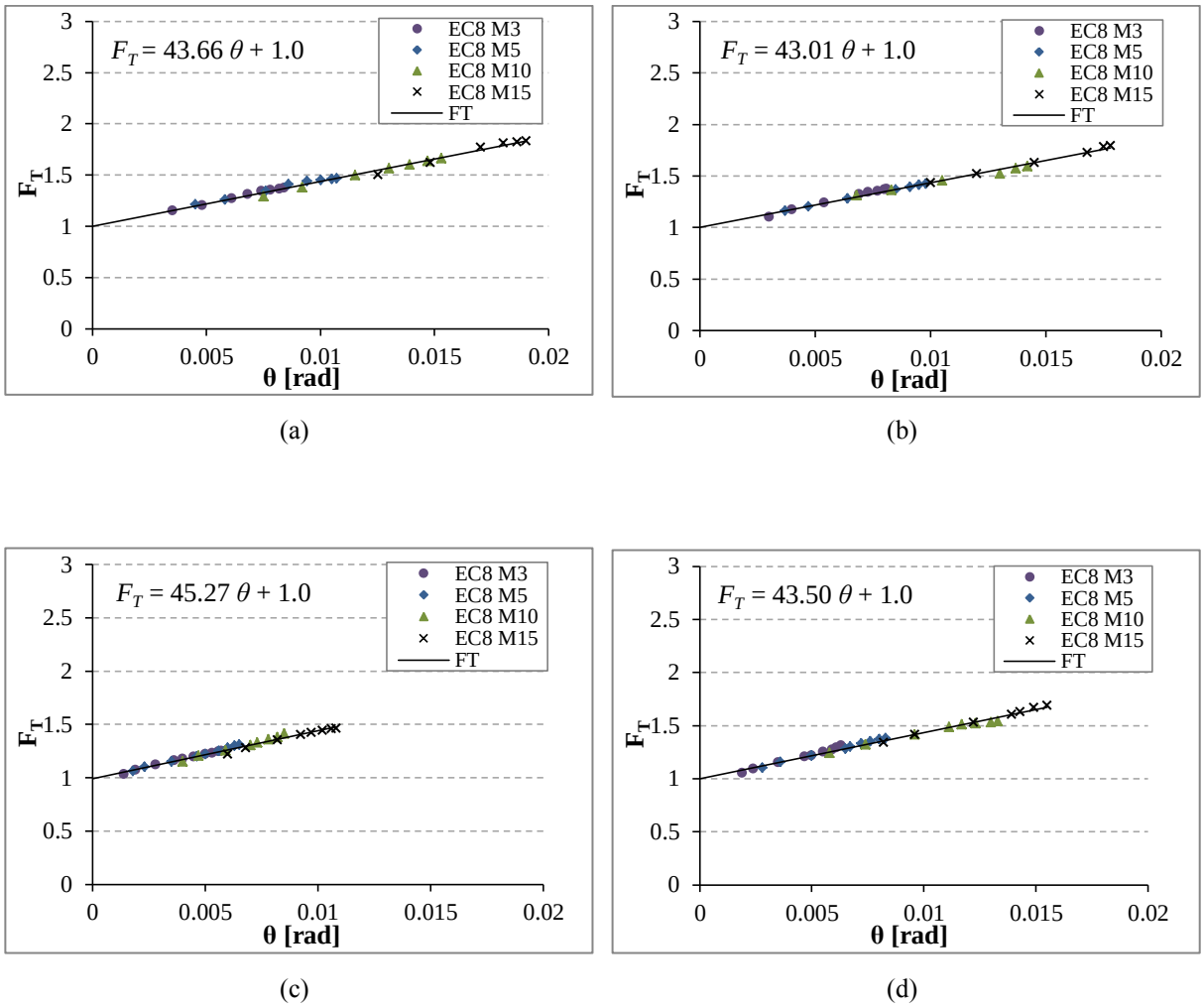

Figure 5.27 Relationship between the torsional amplification factor (F_T) for the NSCs with $T_C = T_1$ and top floor rotation (θ) of the third group of buildings designed on ground types: (a) A, (b) B, (c) D, and (d) E.

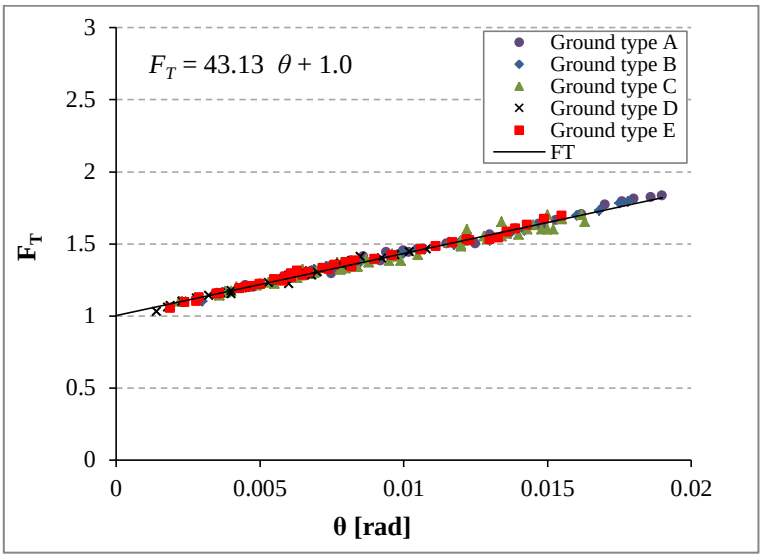

Figure 5.28 Relationship between the torsional amplification factor (F_T) for the NSCs with $T_C = T_1$ and top floor rotation (θ) of the first, second and third groups of buildings designed in full compliance with the EC8 provisions for ground types A, B, C, D, and E.

5.8 Comparison between FE Results and EC8 Recommendations

As explained in Chapter 1 (see Section 1.4), multiplying S_a, as given by Eq. (1-1), by the acceleration of gravity (g) yields the EC8 (2004) prediction for the design acceleration of NSCs. This approach was used to predict the accelerations of the NSCs attached to the considered P-structures. Damping ratio of 3% (Graves and Morante, 2006) was adopted for the NSCs in all cases of the comparisons presented in the following sections.

5.8.1 NSCs Attached to the First and Second Groups of Buildings

For NSCs attached to the first group of buildings: Test 0.15, Test 0.25, and EC8 M, comparisons are made between the numerical results of the NSCs accelerations and the

recommendations of EC8 (2004) (i.e. the predictions of Eq. (1-1)). The results of the comparisons are shown in Figures 5.29 to 5.31.

Building Test 0.15 was designed for an a_g value of 0.15 g on ground type A. Considering the soil factor of 1.15 for ground type C. Hence, the term αS in Eq. (1-1) was taken as 0.173. However, the buildings Test 0.25 and EC8 M of the first group were designed for an a_g value of 0.25 g on ground type A. Considering the soil factor of 1.15 for ground type C. Consequently, the term αS in Eq. (1-1) was taken as 0.29. In the comparison, two values of PGA were used; the first PGA is the value of the design acceleration of the P-structures (i.e. PGA = 0.173 g for Test 0.15 and PGA = 0.29 g for Test 0.25 and EC8 M building). However, the second value of PGA is the maximum seismic capacity of the above-mentioned buildings, as given in Table 5.7.

It can be seen from Figures 5.29 and 5.30 that, for the buildings Test 0.15 and Test 0.25, the recommendations of EC8 (2004) well-predicted the seismic response of the NSCs at PGA values corresponding to the design ground accelerations. Whereas, at PGA values corresponding to the maximum seismic capacities of Test 0.15 and Test 0.25 buildings (i.e. 0.46 g and 0.51 g respectively), the predictions of EC8 underestimated the NSCs accelerations with periods equal to T_1 by about 25% and 14% when the NSCs attached to the Test 0.15 and Test 0.25 buildings respectively.

However, the predictions of the EC8 (2004) provisions underestimated the seismic response of the NSCs with $T_C = T_1$ when they attached to the EC8 M building by about 33.6%

and 51.4% of the numerical corresponding results at values of the PGA equal to the design value (0.29 g) and maximum seismic capacity (0.76 g) respectively, as shown in Figure 5.31.

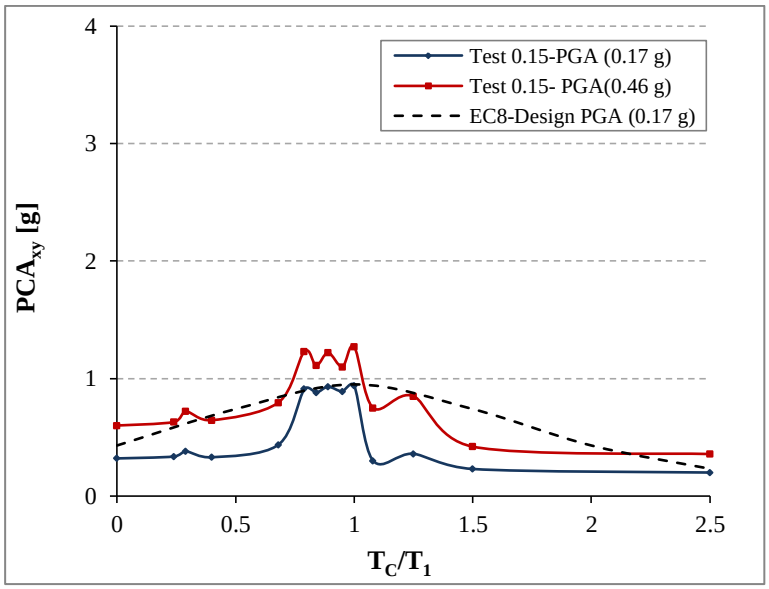

Figure 5.29 Variations of peak component acceleration (PCA_{xy}) vs. NSC to P-structure vibration period ratio (T_C/T_1) for the NSCs mounted on the flexible side of the top floor of Test 0.15 building at the PGA values corresponding to the design value and the maximum seismic capacity of the Test 0.15 building.

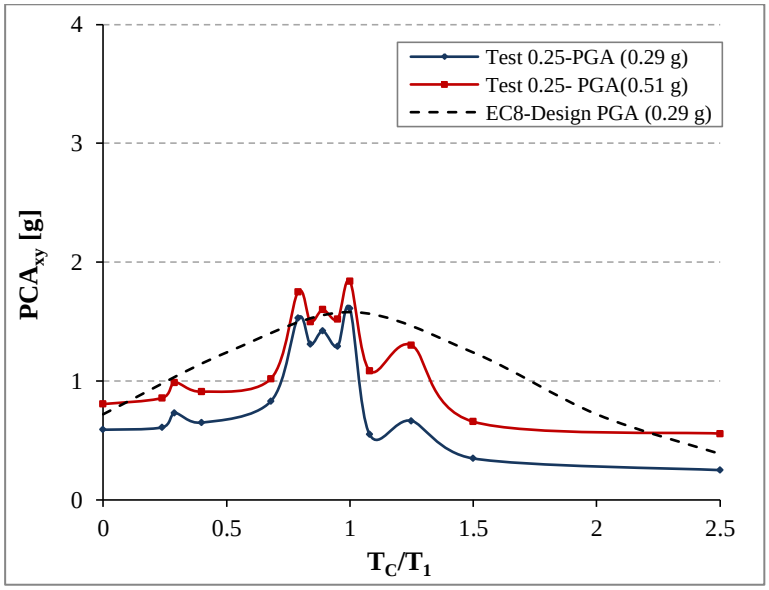

Figure 5.30 Variations of peak component acceleration (PCA_{xy}) vs. NSC to P-structure vibration period ratio (T_C/T_1) for the NSCs mounted on the flexible side of the top floor of Test 0.25 building at the PGA values corresponding to the design value and the maximum seismic capacity of the Test 0.25 building.

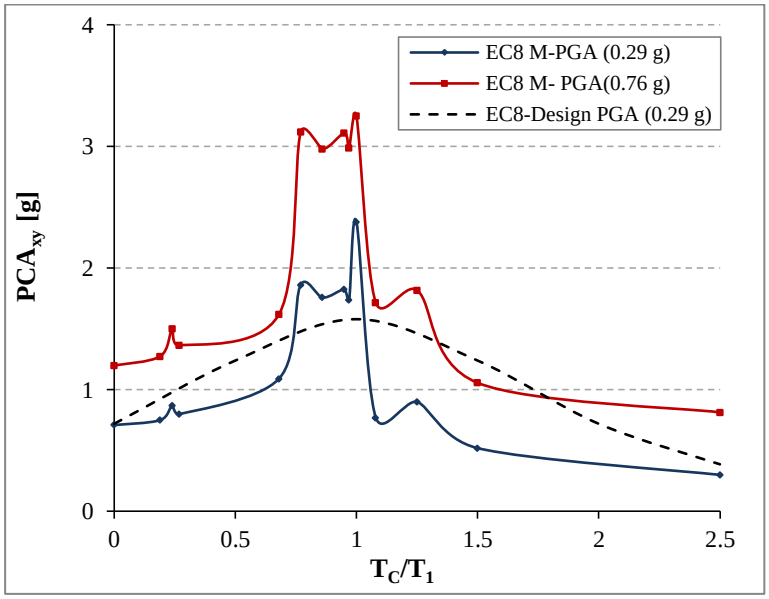

Figure 5.31 Variations of peak component acceleration (PCA_{xy}) vs. NSC to P-structure vibration period ratio (T_C/T_1) for the NSCs mounted on the flexible side of the top floor of EC8 M building at the PGA values corresponding to the design value and the maximum seismic capacity of the EC8 M building.

Predictions of the NSCs accelerations were investigated for those having periods equal to T_1, T_3, and the rigid NSCs attached at varying heights to the second group of the buildings i.e. EC8 M5, EC8 M7, EC8 M10, EC8 M13, and EC8 M15. These structures were designed for an a_g value of 0.25 g. Considering the soil factor of 1.15 for ground type C; hence, the term αS in Eq. (1-1) was taken as 0.29.

Figures 5.32 to 5.34 compare the average values of the peak component accelerations obtained from the FE analyses (i.e. average of the effect of the adopted artificial base motion records) with the corresponding values estimated by the recommendations of EC8 (2004) for NSCs with periods equal to T_1, T_3, and $T_C \approx 0$ s.

As shown in Figure 5.32, EC8 (2004) predicts a linear relationship between NSC to P-structure height ratio (z_c/H) and peak component acceleration (PCA_{xy}). For the NSCs with $T_C = T_1$ and attached to ground levels of the P-structures ($z_c/H = 0$), EC8 (2004) predicts an acceleration of 0.725 g. For the NSCs attached to the top floors of the P-structures ($z_c/H = 1.0$), EC8 (2004) predicts an acceleration of 1.58 g. These predictions apply to all the NSCs attached to the second group of buildings regardless of the torsional behaviour of the P-structures. The FE results clearly demonstrated that the NSCs accelerations increase with the increase in the floors rotations due to torsion. Figure 5.32 shows that the recommendations of EC8 (2004) reasonably predicted the component accelerations at the centres of rigidity (CRs) with a mean predicted-to-numerical ratio of 0.94 and a standard deviation of 0.18. On the other hand, the EC8 (2004) predictions for the component accelerations at the flexible sides (FS) were alarmingly underestimated with a mean predicted-to-numerical ratio of 0.67 and a standard deviation of 0.13. It is worthwhile noting that, for the NSCs with $T_C = T_1$, the EC8 (2004) also underestimated the NSCs accelerations at the top floors of the second group of buildings on average by about 50% when the P-S systems subjected to the base motions with PGA values corresponding to the maximum seismic capacities of the P-structures. The predictions of EC8 can be compared with those values of PCA_{xy} at the maximum seismic capacities of the second group of buildings, as presented in Figure 5.17. The comparison results give an impression that the NSCs will not be functional when they are affected by earthquakes with PGA either equal or more than the design value of irregular P-structure.

In Figure 5.33, comparisons are made between the numerical results and the predictions of EC8 (2004) for those NSCs having a period equal to T_3 and attached to the FS and CRs of the second group of buildings under the effect of the PGA value corresponding to

the design value (0.29 g). It can be seen from Figure 5.33 that on average, the EC8 overestimates the seismic response of the NSCs mounted at CRs of the top floors by about 16% with respect to the FE results. However, it was found that the EC8 predictions underestimated the NSCs accelerations when they were attached to the floors at the flexible sides. At the top floors of the second group of buildings, the EC8 underestimated the dynamic response of the NSCs resulted from the FE analyses by minimum and maximum percentage values equal to 12% and 21% respectively.

It can be seen from Figure 5.34 that the majority values of PCA_{xy} for rigid NSCs ($T_C \approx 0$ s) attached to the CRs of the floors along the heights of the second group of buildings were found within the range of the predictions of EC8 (2004). However, the values of PCA_{xy} for NSCs attached to the flexible sides at the lower third of the buildings that have 10, 13, and 15-storey were exceeded the EC8 predictions. On average, the EC8 underestimated the dynamic response of the NSCs attached to such locations by about 14.5%.

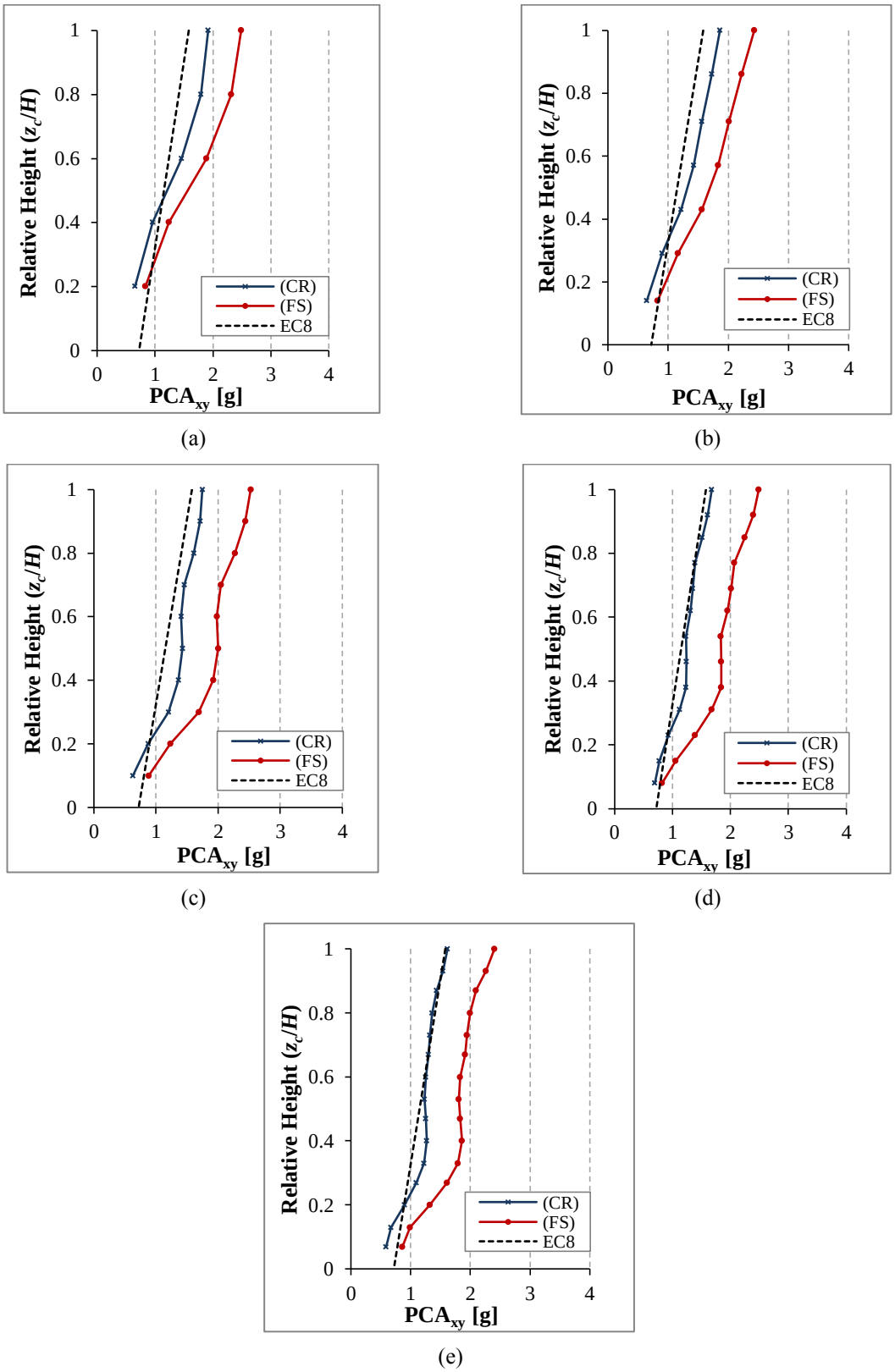

Figure 5.32 Comparison between FE and EC8 acceleration predictions for the NSCs with $T_C = T_1$ and attached to the flexible sides (FS) and centres of rigidity (CRs) at the PGA value corresponding to the design ground acceleration of each building of the second group: (a) EC8 M5, (b) EC8 M7, (c) EC8 M10, (d) EC8 M13, and (e) EC8 M15.

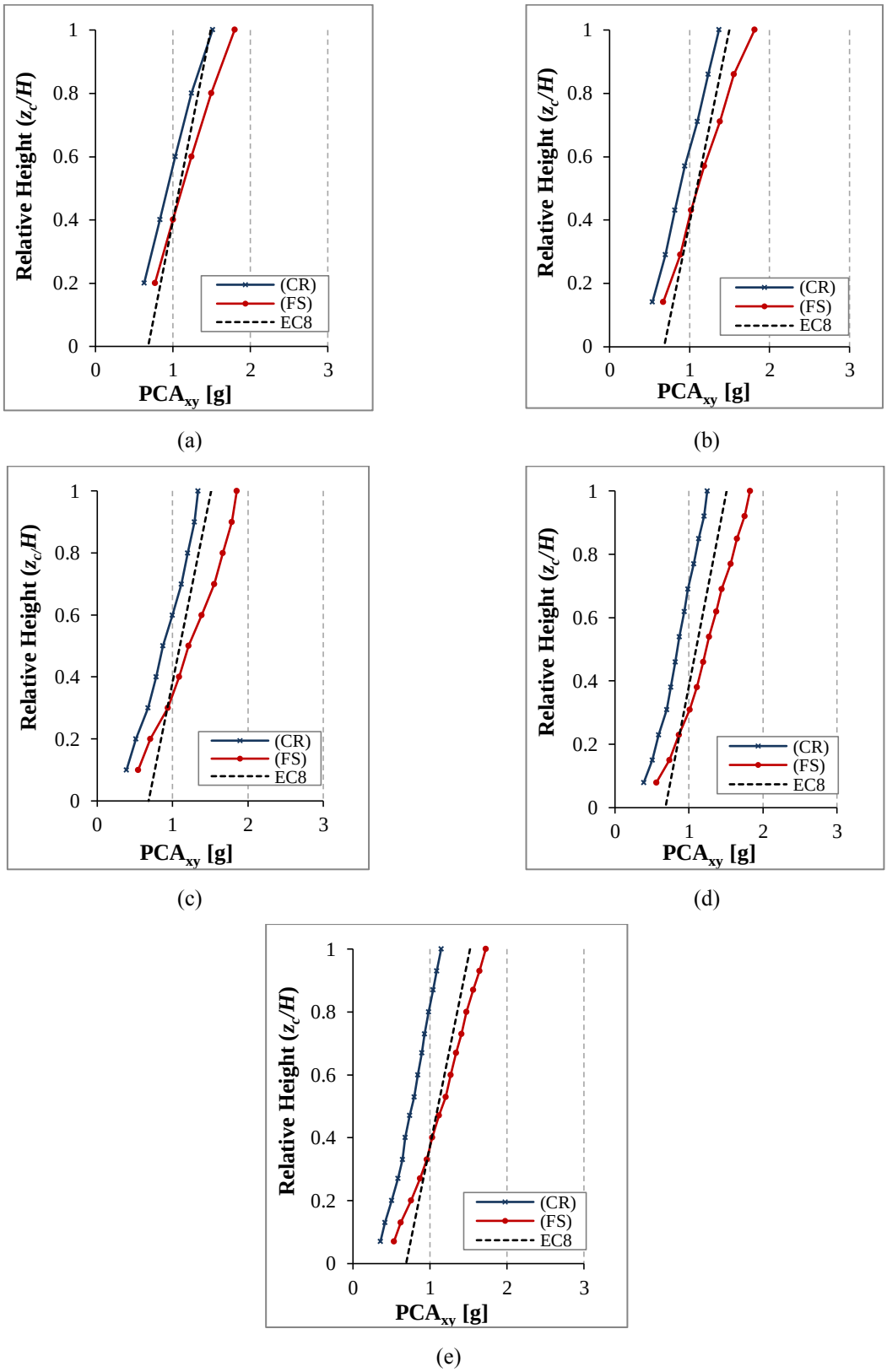

Figure 5.33 Comparison between FE and EC8 acceleration predictions for the NSCs with $T_C = T_3$ and attached to the flexible sides (FS) and centres of rigidity (CRs) at the PGA value corresponding to the design ground acceleration of each building of the second group: (a) EC8 M5, (b) EC8 M7, (c) EC8 M10, (d) EC8 M13, and (e) EC8 M15.

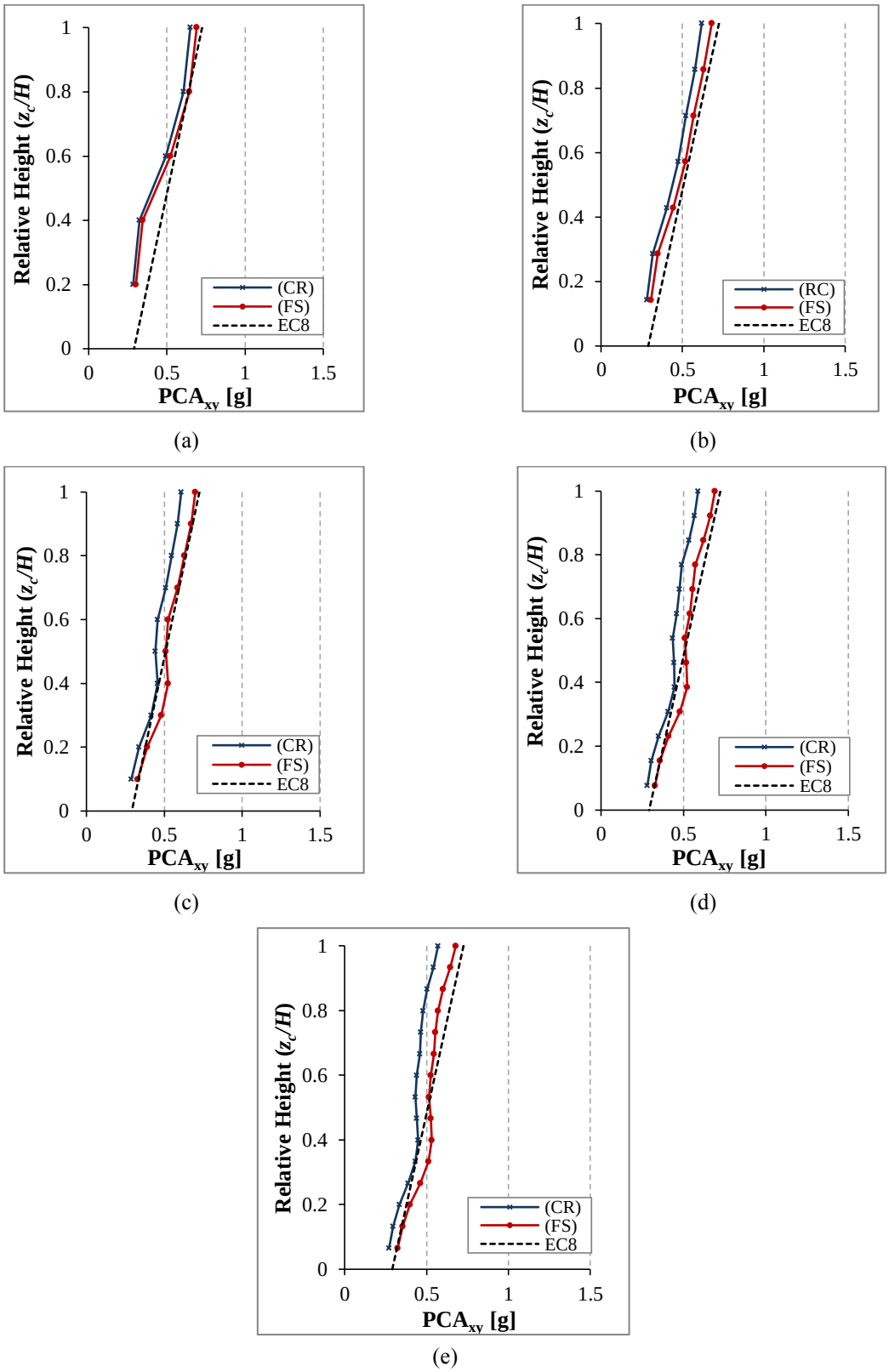

Figure 5.34 Comparison between FE and EC8 acceleration predictions for the rigid NSCs ($T_C \approx 0$ s) and attached to the flexible sides (FS) and centres of rigidity (CRs) at the PGA value corresponding to the design ground acceleration of each building of the second group: (a) EC8 M5, (b) EC8 M7, (c) EC8 M10, (d) EC8 M13, and (e) EC8 M15.

To sum up, the comparison results between the predictions of EC8 (2004) and the numerical results of the current investigation, values of PCA_{xy} that were recorded at the flexible sides and the centres of rigidity of the top floors of the first and second groups of buildings are drawn in Figures 5.35(a) to 5.35(c). These values of PCA_{xy} were recorded under the effect of PGA values corresponding to the design ground accelerations of the P-structures (i.e. a_g equal to 0.173 g for Test 0.15 building and 0.29 g for Test 0.25, EC8 M, EC8 M5, EC8 M7, EC8 M10, EC8 M13, and EC8 M15).

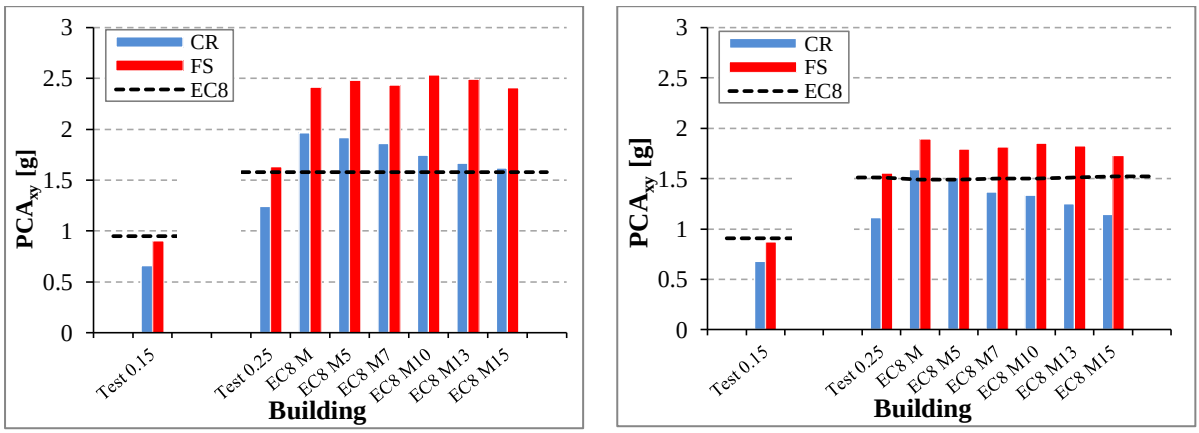

(a) (b)

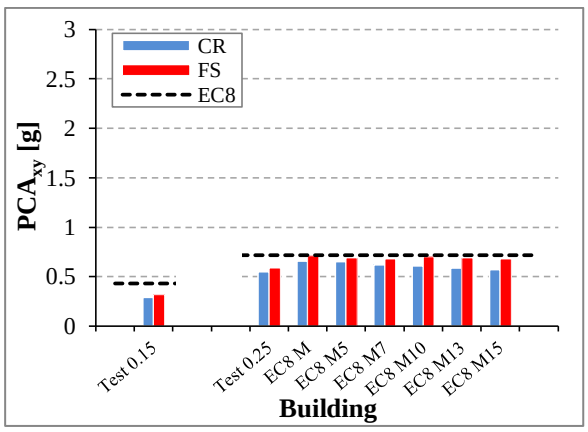

(c)

Figure 5.35 Comparison between FE and EC8 acceleration predictions for the NSCs attached to the centres of rigidity (CRs) and the flexible sides (FS) of the top floors of the first and second groups of buildings, for the NSCs having periods equal to (a) $T_C = T_1$, (b) $T_C = T_3$, and (c) $T_C \approx 0$ s.

It can be seen from Figures 5.35(a) and 5.35(b), EC8 provides underestimate (unconservative) predictions for NSCs periods equal to the T_1 and T_3 attached to the FS of the top floors of the studied buildings. Furthermore, the majority of PCA_{xy} values for NSCs having a period equal to T_3 attached to the CRs were found within the range of the EC8 predictions as shown in Figure 5.35(b). On the other hand, in general, for rigid NSCs attached to the FS and CRs of the top floors, the values PCA_{xy} were observed within the predictions of the EC8 provisions, as shown in Figure 5.35(c).

5.8.2 NSCs Attached to the Third Group of Buildings

In this section, comparisons are made between the predictions of EC8 and the numerical results of the NSCs attached to the third group of buildings designed on different types of ground. All buildings were designed for an a_g value of 0.25 g on ground type A. Considering the soil factors of 1.0, 1.2, 1.35, and 1.4 for ground types A, B, D, and E respectively, the design ground accelerations on these types of ground were 0.25 g, 0.30 g, 0.34 g, and 0.35 g, respectively, (see Table 5.2). Hence, the term αS in Eq. (1-1) was taken as 0.25, 030, 0.34, and 0.35 for NSCs attached to the P-structures designed on ground types as presented above respectively. Therefore, for comparison purposes between the FE results and the predictions of EC8 (2004), the adopted earthquake records were scaled in such a way that their PGAs were equal to the above-mentioned values of the term αS (i.e. values of design ground accelerations).

Values of PCA at roof level equal to 1.375 g, 1.65 g, 1.87 g, and 1.925 g are predicted by the EC8 provisions for the NSCs having a period equal to T_1 and attached to P-structures

designed on ground types A, B, D, and E, respectively. Finite element results of PCA_{xy} recorded at the flexible and centre of rigidity regions of the top floors of the considered buildings for those NSCs having a period equal to T_1 are shown in Figure 5.36. It can be observed from Figure 5.36 that, in general, EC8 underestimates the NSCs accelerations at the design ground accelerations values of the P-structures. EC8 (2004) underestimated the NSCs accelerations on average by about 34.8%, 32.1%, 31.5%, and 28.2% when they were attached to the flexible sides of the top floors of the buildings designed on ground types A, B, D, and E, respectively. However, these percentages of the underestimations increased to the values of 51.4%, 49.3%, 52.8%, and 40.5% when the P-S systems subjected to the base motions that had PGA values corresponding to the maximum seismic capacities of the P-structures (see Table 5.8). The above results were derived from the comparisons between the predictions of EC8 and those values of PCA_{xy} resulted due to the effect of PGA values corresponding to the maximum seismic capacities of the third group of buildings as presented in Figure 5.23. Once again, these results give a conclusion that the NSCs which are housed inside such as irregular structures would lose their functionality when they are subjected to earthquakes having value of PGA more than the design value of the P-structure.

Only few cases of the numerical results were comparable to the predictions of EC8, especially for those NSCs attached to the centres of rigidity of the top floors of buildings EC8 M10 and EC8 M15. It is worthwhile to note that the values of PCA_{xy} for the NSCs attached to the buildings at their centres of rigidity decreased with the increase in the total height of the buildings due to the increase in the fundamental vibration periods of the P-structures. On the other hand, due to the torsional effect, the accelerations are approximately equal for the NSCs attached to the flexible sides the top floors regardless of the building height. Therefore, it can

conclude that the ratio between the values of PCA_{xy} at the flexible sides and the corresponding values at the centre of rigidity increases with the increase of the buildings heights.

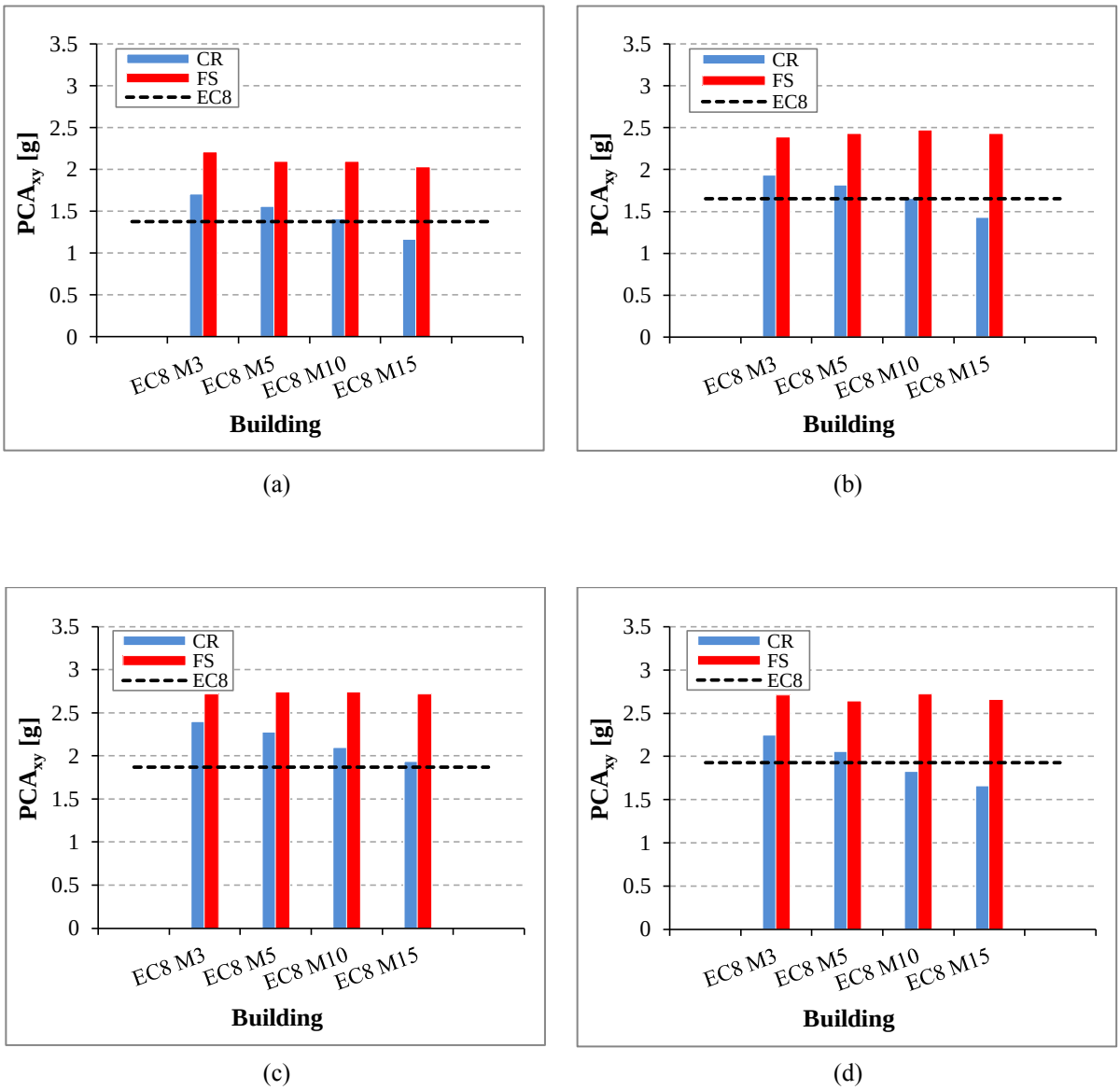

Figure 5.36 Comparison between FE and EC8 acceleration predictions for the accelerations of the NSCs having periods equal to T_1 and attached to the flexible sides (FS) and centres of rigidity (CRs) of the top floors of the third group of buildings designed on ground types (a) A, (b) B, (c) D, and (d) E.

5.9 Summary

Chapter 5 presented an investigation of the seismic response of NSCs mounted on irregular RC P-structures that had different design characteristics. The influences of NSC to P-structure vibration period ratio, peak ground acceleration, NSCs to P-structure height ratio, ground type, and P-structure torsional behaviour on the seismic response of the NSCs were studied. The results showed that the NSCs had different dynamic behaviours when they attached to the buildings having similar values of the fundamental periods, but differ in their design characteristics. Furthermore, the amount and distribution of the steel reinforcements within the cross-sections of the considered cases of irregular RC buildings have a considerable effect on the NSCs accelerations. The maximum dynamic response of NSCs was found when they attached to the buildings that had high amounts of steel reinforcements, especially when the buildings underwent in the nonlinear range. For the case of the NSCs with 3% damping ratio and attached to the buildings designed due to the gravity load only or those buildings designed to fulfil only the steel requirements of EC8, the NSCs accelerations at the PGA corresponding to the maximum seismic capacities of the P-structures were found on average 125% higher than those values of accelerations when the NSCs subjected to earthquakes with PGA values corresponding to the elastic seismic capacities. However, this percentage was observed on average 107% when the NSCs mounted on P-structures designed to fulfil both the cross-sections and steel reinforcement requirements of the structural members according to the EC8 seismic provisions. In addition, the results showed that for the NSCs with vibration periods T_C equal to the first fundamental periods T_1 of the P-structures and damping ratio of 3%, the NSCs accelerations at the flexible sides of the P-structures had accelerations that were on average 42% higher than the accelerations of the NSCs were attached to the

centres of rigidity.

It was observed from the results that the torsional amplification factor F_T of NSCs increased with the increase in height of the buildings. This trend seems to be affected by the floor rotation values of the P-structures which increased with the increase of the building height. In addition, the minimum and maximum values of peak component accelerations were found for the NSCs attached to the buildings designed on ground types A and D respectively. This result suggests that the maximum seismic capacity of a P-structure could have a significant effect on the seismic behaviour of the NSCs especially for those attached to centres of rigidity of the P-structure.

The numerical results were compared with the predictions of EC8 at values of peak ground accelerations corresponding to the design acceleration values of the adopted P-structures. One of the more significant findings raised during the comparison between the numerical results and the recommendations of the EC8 is that, due to the effect of the floors rotations along the heights of the irregular buildings, the accelerations of the NSCs located at the flexible sides and have periods equal to the fundamental vibration periods of the P-structures underestimated by the EC8 provisions. For the NSCs with vibration periods T_C equal to T_1 and damping ratio of 3%, the predictions of EC8 (2004) provision underestimated the NSCs accelerations on average by about 32.5% at PGA values corresponding to the design ground acceleration values of the P-structures when the NSCs attached to the flexible sides of the top floors of the P-structures designed in full compliance with the seismic provisions of EC8 (2004) and for different ground types.

Therefore, it is recommended that the effect of other parameters such as eccentricity ratio and vertical mass irregularity of the P-structures on the seismic response of the NSCs should further investigate to develop a general relationship between the amplification in the NSCs accelerations and the rotational behaviour of the P-structures. These two parameters are the subject of the next chapters in this research.

CHAPTER SIX: SEISMIC RESPONSE OF NSCs ATTACHED TO REINFORCED CONCRETE STRUCTURES WITH DIFFERENT ECCENTRICITY RATIOS

6.1 Introduction

As presented in Chapter 5 that during earthquakes, the seismic response of NSCs attached to the floors of irregular RC P-structures can be amplified by the torsional behaviour of the P-structures. In irregular P-structures, the inertia forces act at the centre of mass (CM) whereas the resisting forces of the structural elements act at the centre of rigidity (CR). Attributable to these two non-coincident forces, floor rotations that vary with time produce torsional modes in addition to the translational modes (Chandler, 1986; Chandler and Hutchinson, 1986).

As the static eccentricity, defined as the eccentricity between the CM and CR, is the main cause of the coupling between the translational and torsional modes of irregular P-structures (De la Llera and Chopra, 1994a, 1994b; Chopra and De la Llera, 1996), it is important to study its effect on the seismic response of NSCs attached to the floors of such P-structures. A careful evaluation of the literature presented in Chapter 2 (see Section 2.3) suggests that further research is needed to clarify the effect of P-structure eccentricity ratio on the seismic response of NSCs.

Of note is that the seismic response of NSCs attached directly to the ground depends on the characteristics of the ground motion such as its frequency content. However, the

behaviour of NSCs attached to the floors of an irregular RC P-structure depends on the torsional behaviour of the P-structure among other factors such as the NSC to P-structure vibration period ratio, peak ground acceleration (PGA), and the heights of the NSCs relative to that of the P-structure.

The main objective of this chapter is to calculate the influence of different values of the eccentricity ratios of the P-structures on the seismic response of NSCs having different values of damping ratios. Eight cases of one-bay three-storey RC frames were chosen as the P-structures. In the following sections, the characteristics and modelling of the P-structures and NSCs considered in this chapter are detailed. Effects of different parameters were also investigated such as the effect of NSC to P-structure vibration period ratio, peak ground acceleration, P-structure eccentricity ratio, and NSC damping ratio on the NSCs acceleration response. This chapter also evaluates the accuracy of EC 8 (2004) design provisions for NSCs by comparing the average numerical results with EC8 predictions.

The results presented in Sections 6.5 and 6.6 are based on averages of 2128 nonlinear dynamic FE analyses of NSCs attached to the floors of RC P-structures with different eccentricity ratios under the effect of natural bi-directional earthquakes. General Description and Modelling of the P-structures.

6.2 General Description and Modelling of the P-structures

Eight variants of a single-bay three-storey RC structure with different eccentricity ratios were selected as P-structures. The eccentricity ratio was varied by changing the sizes of the corner

columns of the P-structures. This specific configuration was chosen as it represented the most straightforward approach to investigating the effect of P-structure eccentricity ratio on the seismic response of NSCs. Shown in Figures 6.1(a) and 6.1(b) are the plan and elevation of the P-structures respectively. The P-structures, for simplicity, had a 5.5 m centre-to-centre single span in both the X and Y directions (see Figure 6.1(a)) and square column cross-sections.

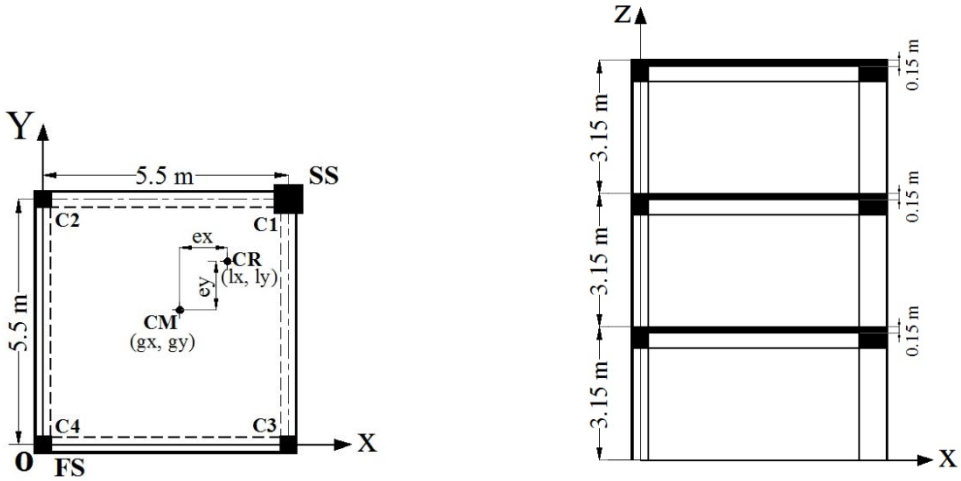

(a) (b)

Figure 6.1 One-bay three-storey RC P-structure (a) plan and (b) elevation.

Tables 6.1 and 6.2 detail the characteristics of the RC P-structures. A regular symmetrical RC structure with eccentricity ratio (R_{ex}=R_{ey}) equal to 0.0 and has 500 mm × 500 mm column cross-sections was designed as a reference structure. For the remaining seven variants of the reference structure, the static eccentricity was varied by changing the cross-sectional dimensions of the corner columns. The column cross-sections were designed in such a way that the total lateral elastic stiffness in the horizontal directions (X and Y) was constant for each structure (see Table 6.1). For each P-structure, the CM coordinates (g_x,g_y) and the CR coordinates (l_x,l_y) reported in Table 6.1 are measured from Point O at the lower left corner of Figure 6.1(a). Furthermore, for each P-structure in Table 6.1, the values of the floor

elasticity radius (r_x=r_y) and floor eccentricity ratio (R_{ex}=R_{ey}) were evaluated based on the values of the storey lateral (K_x=K_y) and torsional (K_R) elastic stiffness by the use of the formulae expressed as follows:

$$r_x = \sqrt{\frac{K_R}{\sum K_y}} \quad \text{or} \quad r_y = \sqrt{\frac{K_R}{\sum K_x}} \tag{6-1}$$

and,

$$R_{ex} = \frac{e_y}{r_x} \quad \text{or} \quad R_{ey} = \frac{e_x}{r_y} \tag{6-2}$$

where, e_x and e_y are, respectively, the eccentricities in the X and Y directions of the P-structures.

Table 6.1 Eccentricity and stiffness details of one-bay three-storey RC P-structures.

Building	CM coordinates (g_x,g_y), [m]	CR coordinates (l_x,l_y), [m]	Eccentricity (e_x=e_y), [m]	Storey lateral stiffness (K_x=K_y), [kN/m]	Storey torsional stiffness (K_R), [kN.m/rad]	Floor elasticity radius (r_x=r_y), [m]	Floor eccentricity ratio (R_{ex}=R_{ey})
Reference	(2.75,2.75)	(2.75,2.75)	0.00	291435	4407957	3.89	0.000
Modified 1	(2.85,2.85)	(2.95,2.95)	0.10	291435	4385210	3.88	0.026
Modified 2	(2.95,2.95)	(3.18,3.18)	0.23	291435	4302459	3.84	0.060
Modified 3	(3.07,3.07)	(3.44,3.44)	0.37	291435	4133195	3.77	0.098
Modified 4	(3.21,3.21)	(3.73,3.73)	0.52	291435	3843441	3.63	0.143
Modified 5	(3.37,3.37)	(4.07,4.07)	0.70	291435	3390371	3.41	0.205
Modified 6	(3.58,3.58)	(4.45,4.45)	0.87	291435	2720631	3.06	0.284
Modified 7	(3.88,3.88)	(4.88,4.88)	1.00	291435	2104515	2.69	0.372

The considered P-structures in this chapter were designed according to the provisions of EC1 (2002), EC2 (2004), and EC8 (2004). In the design of irregular buildings, it is very important to select an appropriate layout and cross-sections of the columns that result in a difference between the centre of mass and the centre of rigidity as minimal as possible. Based on the design provisions of EC8 (2004), values of the elastic eccentricity (e) in both horizontal directions and the torsional radius (r) at each floor of the P-structure should be within the limitations of two conditions. Lateral-torsional response condition states that the

value of the eccentricity (e) should be equal or less than the value of (0.3 r). However, the torsional rigidity condition states that the value of torsional radius (r) should be equal or larger than the value of (ls). The term (ls) refers to *"radius of gyration of the floor mass in plan that can be estimated as a square root of the ratio of the polar moment of inertia of the total floor mass in plan with respect to the centre of mass of the floor mass*" (EC8, 2004). Furthermore, the criteria of assessment the regularity in plan according to the manual for the seismic design of structures according to EC8 (IStructE, 2010), it is considered that the building is irregular if the ratio between the eccentricity value (e) and the corresponding side length, L of the building is greater than 0.1. The information provided in Table 6.2 can be used to examine the regularity criteria of the selected P-structures. The adopted values of the eccentricity (e) and the elasticity radius (r) of each building in Table 6.2 can be found in Table 6.2. It can be seen from Table 6.2, that the buildings termed as Reference, Modified 1, Modified 2, Modified 3, and Modified 4 are satisfied the EC8 provision for regularity; whereas, the buildings termed as Modified 5, Modified 6, and Modified 7 are classified as irregular in plan P-structures where the value of e/L is larger than 0.1. Therefore, in the design process of the considered buildings in this chapter, the maximum value of the behaviour factors q were selected according to the irregularity cases for each building.

Table 6.2 Regularity criteria of one-bay three-storey RC P-structures.

Building	L [m]	l_s [m]	$r \geq l_s$	$\frac{e}{L}$	$\frac{e}{L} > 0.1$	Irregularity in plan
Reference	6.0	2.45	Yes	0.000	No	Regular
Modified 1	6.0	2.45	Yes	0.017	No	Regular
Modified 2	6.0	2.45	Yes	0.038	No	Regular
Modified 3	6.0	2.45	Yes	0.062	No	Regular
Modified 4	6.0	2.45	Yes	0.087	No	Regular
Modified 5	6.0	2.45	Yes	0.117	Yes	Irregular
Modified 6	6.0	2.45	Yes	0.145	Yes	Irregular
Modified 7	6.0	2.45	Yes	0.167	Yes	Irregular

The RC P-structures were designed using the EC8 (2004) Type 1 elastic spectrum for ground type C. Explanation the criteria for the selecting of this type of ground can be found in Chapter 3 (see Section 3.3). The design ground acceleration on type A ground (a_g) was taken as 0.15 g. Considering the soil factor of 1.15 for ground type C, the design ground acceleration on type C ground was 0.173 g. All P-structures were designed as a DCM; therefore, the primary magnitude of the behaviour factor equal to $3.\alpha_u/\alpha_1$, was used. The value of α_u/α_1 is 1.2, for regular multi-storey, one-bay frames (EC8, 2004). However, for irregular multi-storey frames, the adopted value of α_u/α_1 is equal to the average of 1.0 and of the value of α_u/α_1. Consequently, the final value of the behaviour factor q equal to 3.6 was used in the design of the cases of buildings: Reference, Modified 1, Modified 2, Modified 3, and Modified 4 (see Table 6.2). However, a value of 3.3 was adopted in the design of the buildings: Modified 5, Modified 6, and Modified 7.

To fulfil the strong column/weak beam criterion, the over-strength factor (γ_{Rd}) was taken as 1.30 for all P-structures. Concrete Class C25/30 and steel reinforcement Class C S500 were used in the design of the structural elements. The characteristic values of the floor loads were taken as 2.5 kN/m^2 and 2.0 kN/m^2 for permanent (excluding slab self-weight) and variable actions respectively. The total permanent action acting on the columns at each floor level was kept constant. Table A4-1 in Appendix A reports the resulting columns cross-sections and amount of the steel reinforcements of the considered case of the RC P-structures. However, cross-section dimensions and steel reinforcements for beams equal to (345 mm × 500 mm) and (7Ø18 mm) were obtained respectively for all the designed RC buildings.

For each designed building under consideration, details of the longitudinal and transverse steel reinforcements of the columns cross-sections are shown in Appendix A (see Figures A4-1 to A4-8). Furthermore, Figure A4-9 in Appendix A explains the details of a typical cross-section of the beam-column joint connection at the first floor of the reference case of building.

Modal analyses were carried out to determine the vibration periods of the RC P-structures experienced different values of eccentricity ratios. The values of the first six fundamental periods of the RC P-structures are reported in Table 6.3. It can be seen from this table, that the vibration periods for the transitional modes (i.e. T_1, T_2, T_4, and T_5) of the P-structures are equal. This is attributable to the fact that the global lateral stiffness of the P-structures was constant (see Table 6.1). On the other hand, the vibration periods for the torsional modes (i.e. T_3 and T_6) increase gradually with the increase in eccentricity ratios (see Tables 6.1 and 6.3).

Table 6.3 Fundamental vibration periods of one-bay three-storey RC P-structures.

Building	Vibration periods [s]					
	T_1	T_2	T_3	T_4	T_5	T_6
Reference	0.385	0.379	0.261	0.108	0.105	0.076
Modified 1	0.385	0.379	0.261	0.108	0.105	0.077
Modified 2	0.385	0.379	0.262	0.108	0.105	0.077
Modified 3	0.385	0.379	0.263	0.108	0.105	0.077
Modified 4	0.385	0.379	0.264	0.108	0.105	0.078
Modified 5	0.385	0.379	0.267	0.108	0.105	0.079
Modified 6	0.385	0.379	0.271	0.108	0.105	0.079
Modified 7	0.385	0.379	0.275	0.108	0.105	0.080

6.3 Characteristics of Non-structural Components

The NSCs were modelled as a finite element SDOF with varying lengths to match their periods to the fundamental vibration periods of the P-structures (see Chapter 4 - Section 4.3.1). Full dynamic interaction was considered between the NSCs and the P-structures. A value of linear viscous damping ratio (ξ_c) equal to 3% (Graves and Morante, 2006) is adopted for the NSCs. To investigate the effect of NSC damping ratio on the amplification or de-amplification in NSCs acceleration response, additional values of ξ_c equal to 0.01%, 0.2%, 0.5%, 1%, 2%, 4%, and 5% were also considered for parametric study, as explained later in Section 6.5.4.

As was previously mentioned that eigenvalue analyses of the P-structures are essential for the selection of the periods of NSC; therefore, frequencies of NSCs match the first six fundamental periods were adopted in the analyses. Furthermore, to study the seismic response of NSCs with long vibration periods, T_C values of $2T_1$ and $4T_1$ are also considered in this chapter. In addition, the dynamic behaviours of the rigid NSCs (i.e. $T_C \approx 0$ s) were also reported in some cases by adopting the values of the peak floors accelerations (PFA_{xy}) at the point of the attachment with the NSCs. The length (L_a) and lateral stiffness (K_a) values of the circular cantilever arms of the NSCs are given in Table 6.4.

Table 6.4 Characteristics of the NSCs attached to one-bay three-storey RC P-structures.

NSC Period, [s]	$T_C=T_1$	$T_C=T_2$	$T_C=T_3$	$T_C=T_4$	$T_C=T_5$	$T_C=T_6$	$T_C=2T_1$	$T_C=4T_1$
	0.385	0.379	0.261	0.108	0.105	0.076	0.770	1.540
L_a, [m]	1.38	1.36	1.06	0.59	0.58	0.47	2.19	2.19
K_a, [N/m]	2438.2	2547.3	5380	31199.5	32841.2	61717.7	610.1	152.5

6.4 Nonlinear Static Analyses of the P-structures

As will be detailed in Section 6.5, PGA values ranging from 0.05 g to the maximum seismic capacity of each P-structure, including the PGA values corresponding to their elastic seismic capacities, were used to investigate the seismic response of the NSCs. Nonlinear static analyses were therefore carried out to evaluate the elastic and maximum seismic capacities of the RC P-structures. The displacement values at near collapse (NC) obtained from the nonlinear static analyses were corrected by considering the torsional effect using the extension of the N2 procedure (Fajfar *et al.*, 2005b). Further details on the extended N2 procedure can be found in Appendix A (see Section A1).

Shown in Figure 6.2(a) are the values of the normalised top floors displacements evaluated from the push-over and elastic dynamic analyses of the studied cases of buildings. This figure also shows the torsional correction factors of the top displacements at NC. It can be seen from Figure 6.2(a), that the minimum and maximum correction factors of 1.005 and 1.423 resulted due to the effect of torsion were observed for the cases of the buildings termed as the Reference and Modified 7 P-structures respectively (i.e. P-structures with values of eccentricity ratios equal to 0.0 and 0.372 respectively). Furthermore, Figure 6.2(b) displays the values of the top displacements at NC obtained from push-over analyses together with the corrected values of the top displacements of the studied cases. The corrected ultimate top displacement values were found in the range between 154 mm and 176 mm for the P-structures with values of eccentricity ratios equal to 0.0 and 0.372 respectively.

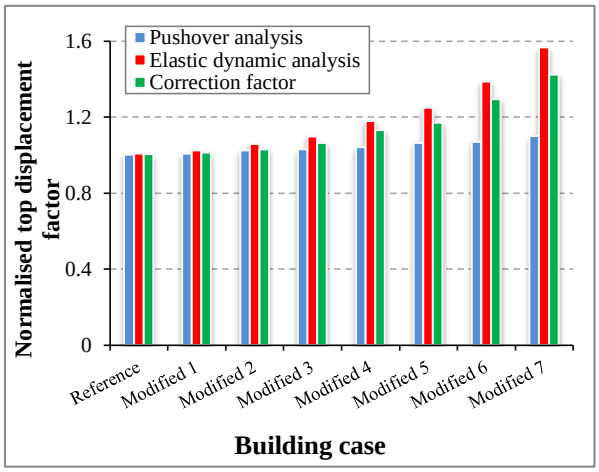

(a)

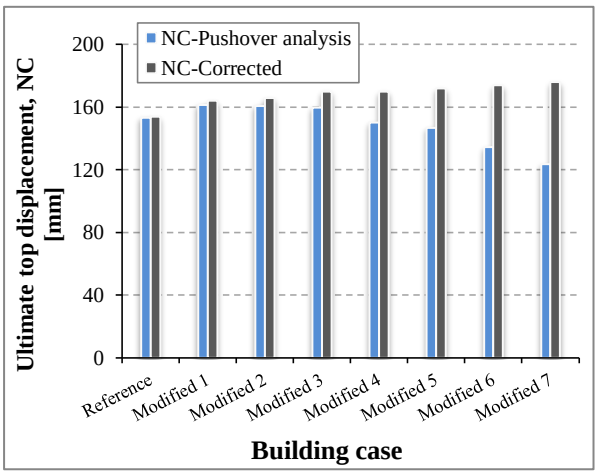

(b)

Figure 6.2 Push-over and elastic dynamic analyses results: (a) normalised top displacement factor and (b) corrected top displacements values at near collapse (NC) of one-bay three storey RC P-structures.

For each P-structure, Table 6.5 details the characteristics of the idealised elastic-perfectly plastic force-displacement relationship determined according to Annex B of EC8 (2004). It can be seen from Table 6.5 that the maximum seismic capacity of each P-structure is given by the PGA value corresponding to a value of (d_m/d_t) approximately equal to 1.0, where d_m and d_t stand for the displacement at ultimate strength and target displacement of the multi-degree of freedom (MDOF) system respectively.

For each case of building, Table 6.6 gives the values of the elastic seismic capacity (i.e. PGA value corresponding to the value of μ equal to 1.0) together with the values of the spectral accelerations, S_{ae} and S_{ay}. The elastic seismic capacities values were either 0.14 g or 0.15 g. Once more, it can be noted from Tables 6.5 and 6.6 that due to the method used for the selection of the dimensions of the corner columns, the produced values of the elastic or maximum seismic capacities were found approximately equal for all the studied cases. The values of the PGA corresponding to the elastic and maximum seismic capacities of the P-

structures are used in Section 6.5 to interpret the numerical results and compare them with EC8 (2004) predictions.

Table 6.5 Maximum seismic capacities and characteristics of the idealised force-displacement relationship of one-bay three-storey RC P-structures.

Building case	Maximum seismic capacity [g]	W [kN]	m^* [kg].10^3	Γ	F_y [kN]	d_m [m]	E_m [kN.m]	d_y [m]	T^* [s]	S_{ae} [g]	S_{ay} [g]	μ	d_t [m]
Reference	0.57	1632	115.0	1.27	528.9	0.154	75.5	0.023	0.44	1.44	0.37	3.91	0.149
Modified 1	0.57	1632	115.0	1.27	508.2	0.164	77.3	0.023	0.45	1.44	0.35	4.06	0.159
Modified 2	0.56	1632	115.0	1.27	506.4	0.166	77.9	0.025	0.47	1.41	0.35	3.99	0.166
Modified 3	0.55	1632	115.0	1.27	504.0	0.170	79.2	0.026	0.48	1.39	0.35	3.96	0.170
Modified 4	0.55	1632	115.0	1.27	502.5	0.170	79.0	0.026	0.48	1.39	0.35	3.96	0.170
Modified 5	0.55	1632	115.0	1.27	519.7	0.172	82.4	0.027	0.49	1.39	0.36	3.82	0.170
Modified 6	0.54	1632	115.0	1.27	519.2	0.174	83.0	0.028	0.49	1.35	0.36	3.74	0.174
Modified 7	0.54	1632	115.0	1.27	519.5	0.176	84.0	0.028	0.49	1.35	0.36	3.73	0.171

Table 6.6 Elastic seismic capacities of one-bay three-storey RC P-structures.

Building case	Elastic seismic capacity [g]	S_{ae} [g]	S_{ay} [g]
Reference	0.15	0.37	0.37
Modified 1	0.14	0.36	0.35
Modified 2	0.14	0.36	0.35
Modified 3	0.14	0.36	0.35
Modified 4	0.14	0.36	0.35
Modified 5	0.15	0.37	0.36
Modified 6	0.15	0.37	0.36
Modified 7	0.15	0.37	0.36

6.5 Dynamic Analyses of the Primary-secondary Systems

In this chapter, in order to evaluate the seismic response of NSCs during the nonlinear dynamic analyses, a set consisting of natural base motion records was used. This set consisted of seven pairs of natural earthquakes, all of which are matching the EC8 (2004) Type 1 elastic RS for ground type C. The main characteristics of these seven pairs of natural records can be found in Chapter 3 (see Table 3.4). The results presented hereinafter are based on averages of the NSCs acceleration response to the natural earthquake records. Maximum value of standard deviation equal to 0.014 g was found when the values of peak components accelerations calculated under the effect of seven pairs of natural records. Due to the 3D nature of the P-structures considered in this chapter, there are two peak component acceleration (PCA) values in the horizontal X and Y directions, i.e. PCA_x and PCA_y respectively. The resultant peak component acceleration (PCA_{xy}) is calculated as the square root of the sum of the squares of PCA_x and PCA_y.

In the following sections, reference will be made to the elastic and maximum seismic capacities of a given P-structure as given in Tables 6.6 and 6.5 respectively. The results that will be presented in Sections 6.5.1, 6.5.2, and 6.5.3 are for NSCs with a damping ratio of 3% (based on Graves and Morante (2006)). However, Section 6.5.4 identifies the effect of different values of NSC damping ratio on the seismic behaviour of NSCs.

6.5.1 Effect of NSC to P-structure Vibration Period Ratio

The effect of NSC to P-structure vibration period ratio (T_C/T_1) on the acceleration response of the NSCs was investigated by considering different values of T_C/T_1. For NSCs attached to the flexible sides (FS) (see Figure 6.1(a)) of the top floors of the RC P-structures, Figure 6.3(a) shows the variations of PCA_{xy} with T_C/T_1 at the PGA values corresponding to the elastic seismic capacities (either 0.14 g or 0.15 g, as given in Table 6.6) of the P-structures. However, Figure 6.3(b) presents the corresponding variations at the PGA values corresponding to the maximum seismic capacities of the P-structures (as given in Table 6.5).

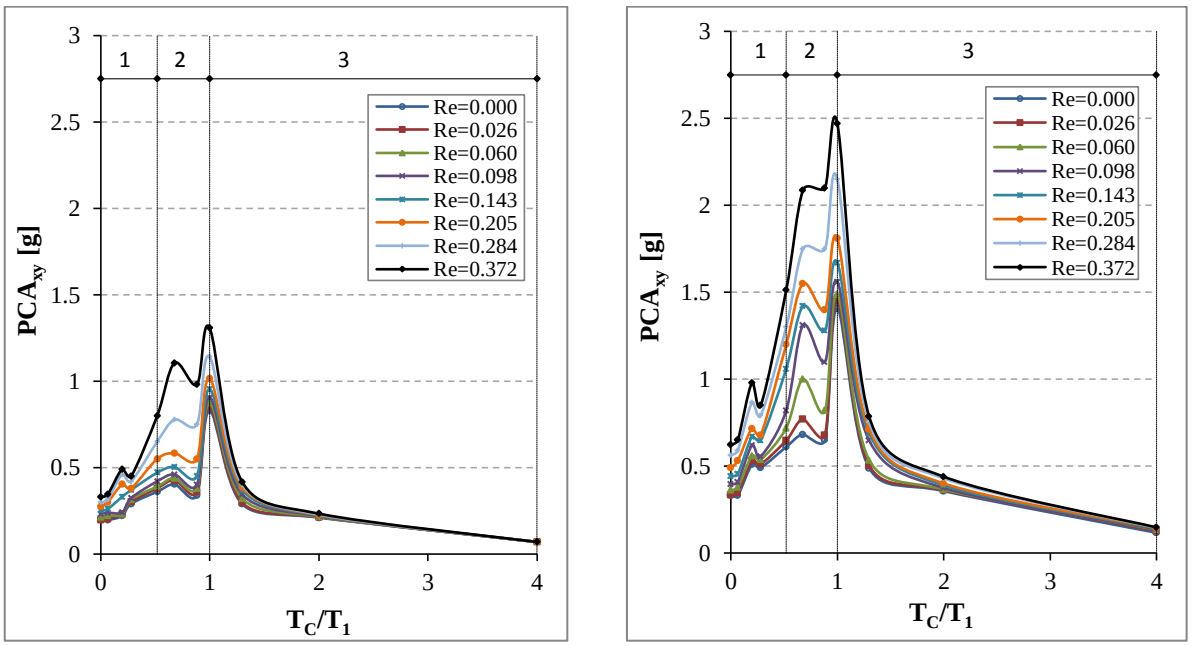

(a) (b)

Figure 6.3 Variations of the peak component acceleration (PCA_{xy}) vs. NSC to P-structure vibration period ratio (T_C/T_1) for the NSCs attached to the flexible sides of the top floors of one-bay three-storey RC P-structures with different eccentricity ratios (R_e) at the PGA values corresponding to (a) the elastic seismic capacities and (b) the maximum seismic capacities.

Similar to the numerical results that were presented in Chapter 5 (see Section 5.6.1), Figures 6.3(a) and 6.3(b) show that the NSCs exhibit three zones of seismic response depending on the value of T_C/T_1. In Zone 1, NSCs accelerations increase gradually with the increase in T_C/T_1 values from 0 to 0.52. In Zone 2, the acceleration response of the NSCs increases sharply when their vibration periods match one of the first three vibration periods of the P-structures. A sharp reduction in the acceleration response of the NSCs occurs in Zone 3 for T_C/T_1 values greater than 1.0 (i.e. long periods of NSCs).

It can be seen from Figure 6.3(a) that, for $T_C = T_1$, the NSCs acceleration response increases significantly with the increase in the P-structure eccentricity ratios. For the reference P-structure (i.e. plan-regular P-structure without eccentricity), the value of PCA_{xy} was 0.83 g. However, the value of PCA_{xy} was 1.31 g (i.e. 57.8% higher) for the P-structure with eccentricity ratio of 0.372.

Figure 6.3(b) shows similar trends to those depicted in Figure 6.3(a). At the PGA values corresponding to the maximum seismic capacities of the P-structures (Figure 6.3(b)), the NSCs with $T_C = T_1$ had accelerations that were on average 77% higher than the corresponding accelerations at the elastic seismic capacities of the P-structures.

6.5.2 Effect of Peak Ground Acceleration

Different PGA values, ranging from 0.05 g to the PGA value corresponding to the maximum seismic capacity of each P-structures (see Table 6.5), were used to investigate the seismic response of the NSCs. Figure 6.4 shows the variations of PCA_{xy} with PGA for the NSCs with

$T_C = T_1$ and attached to the FS and CRs (see Figure 6.1(a)) of the top floors of the P-structures. It can be seen from Figure 6.4 that, for all considered eccentricity ratios, the FE models correctly predicted that the NSCs accelerations must vary linearly with base excitation up to the PGA values corresponding to the elastic seismic capacities of the P-structures (i.e. either 0.14 g or 0.15 g). The increase in PGA values results in a corresponding increase in the P-structures floor accelerations which, in turn, increase the NSCs accelerations. At higher PGA values, damage changes the dynamic characteristics of the P-structures and results in a non-linear relationship between NSCs accelerations and PGA. Due to torsional effects, PCA_{xy} values for the NSCs attached to the FS were higher than the corresponding values for the NSCs attached to the CRs.

Furthermore, Figure 6.4(a) shows that the acceleration response of the NSCs attached to the FS increases with the increase in eccentricity ratios of the P-structures. At the PGA values corresponding to the elastic seismic capacities of the P-structures (i.e. either 0.14 g or 0.15 g), the NSCs attached to the FS of the P-structures with the eccentricity ratios of 0.026 and 0.372 had accelerations that were 2.7% and 57.9% higher respectively than the accelerations of the NSCs attached to the flexible side of the P-structure without eccentricity. At the PGA values corresponding to the maximum seismic capacities (see Table 6.5), the corresponding increases were 3.6% and 76.4% respectively.

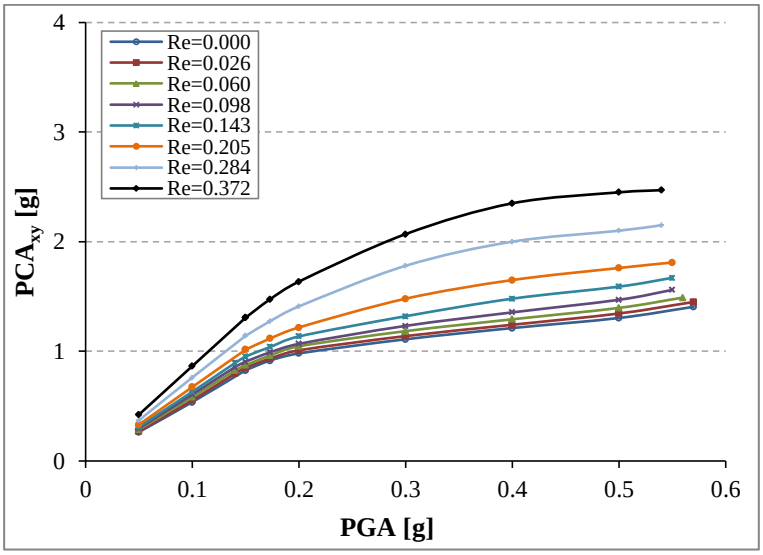

(a)

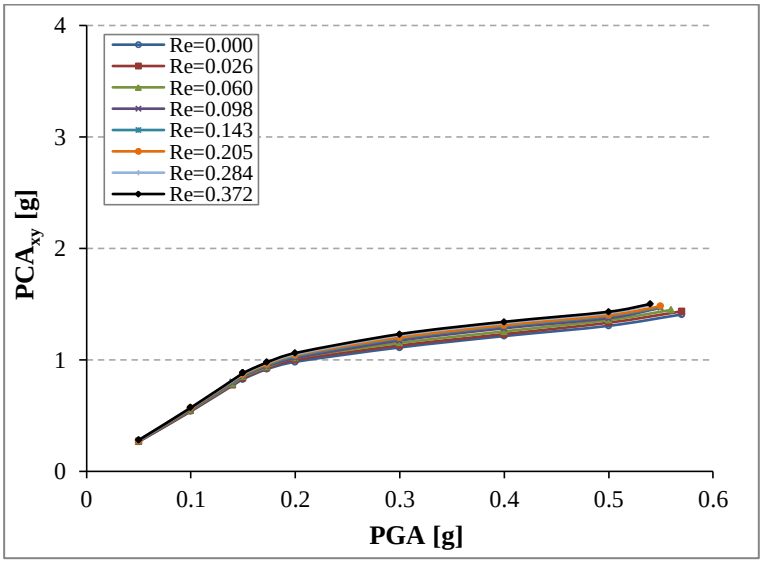

(b)

Figure 6.4 Variations of peak component acceleration (PCA_{xy}) vs. peak ground acceleration (PGA) for the NSCs with $T_C = T_1$ and attached to the top floors of one-bay three-storey RC P-structures at (a) flexible sides and (b) centres of rigidity.

On the other hand, Figure 6.4(b) shows that the eccentricity ratio does not significantly affect the acceleration response of the NSCs attached to the CRs of the P-structures. The NSCs accelerations at the PGA values corresponding to the elastic seismic capacities of the P-structures were approximately equal. At the PGA values corresponding to

the maximum seismic capacities, the NSCs attached to the P-structure with the highest eccentricity ratio (0.372) had accelerations that were 7% higher than the accelerations of the NSCs attached to the P-structure without eccentricity. The approximately equal accelerations at a given PGA value (Figure 6.4(b)) may be explained by the fact that the accelerations at the CRs are affected by the translational rather than the torsional characteristics of the P-structures. In this chapter, all P-structures had similar translational characteristics (see Tables 6.1 and 6.3). It should be noted that the comparison of the maximum values of PCA_{xy} (as shown in Figure 6.4(a)) with respect to the eccentricity ratio values is more explained later in Figure 6.7.

Figures 6.5(a) and 6.5(b) show the variations of acceleration amplification factor (A_p^a), defined in this research as PCA_{xy}/PGA, with base excitation for the NSCs with $T_C = T_1$ and attached to the FS and CRs of the top floors of the P-structures respectively. Figures 6.5(a) and 6.5(b) show that the maximum values of the acceleration amplification factor occur at the PGA values corresponding to the elastic seismic capacities of the P-structures (i.e. either 0.14 g or 0.15 g). Similar results were reported in Section 5.6.2 (see Figure 5.16) where argued that within the elastic range of the P-structures the NSCs accelerations vary approximately linearly with PGA. Beyond the elastic limit, the change in the dynamic characteristics of the P-structures reduces the resonance effect experienced by the NSCs. Hence, the maximum values of the acceleration amplification factor occur at the elastic seismic capacities of the P-structures.

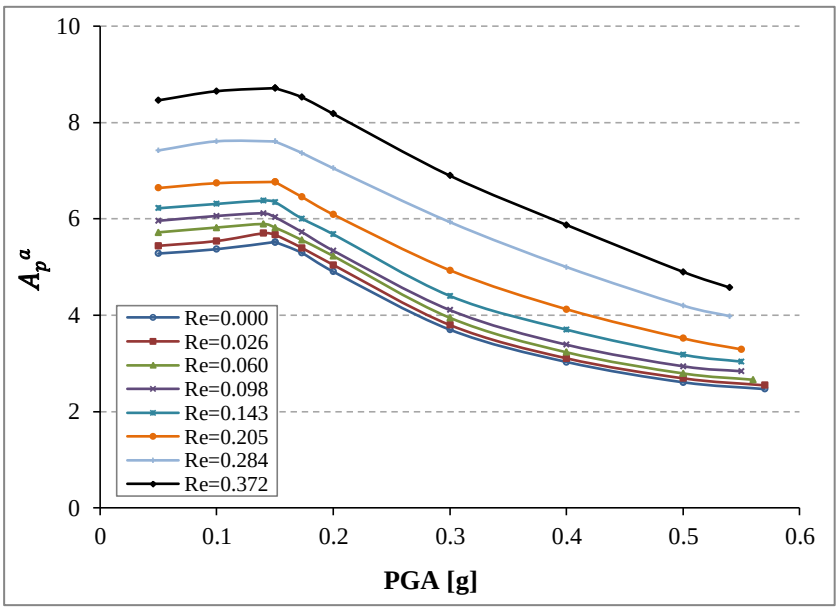

(a)

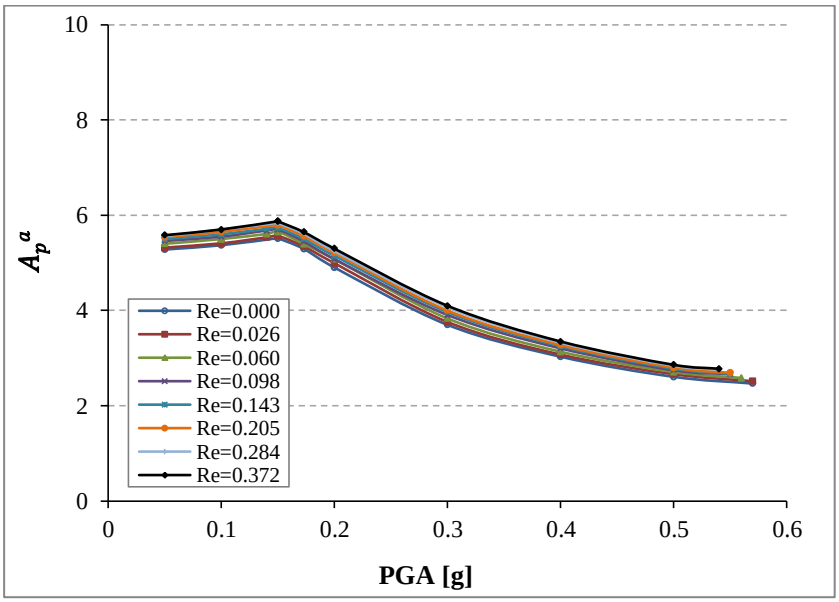

(b)

Figure 6.5 Variations of acceleration amplification factor (A_p^a) vs. peak ground acceleration (PGA) for the NSCs with $T_C = T_1$ and attached to the top floors of one-bay three-storey RC P-structures at (a) flexible sides and (b) centres of rigidity.

6.5.3 Effect of P-structures Eccentricity Ratio

This section reports on the effect of P-structure eccentricity ratio on the acceleration response of NSCs with damping ratio of 3%. Figure 6.6 presents the peak component accelerations for the NSCs with $T_C = T_1$ and attached along the 7.78 m long diagonal line between the stiff sides (SS) and FS of the top floors of the P-structures (see Figure 6.1(a)).

For a given P-structure in Figure 6.6, the NSCs located between the SS and the CRs had approximately equal accelerations. Beyond the CRs, the acceleration response increased with the increase in the relative distance from the SS. At the PGA values corresponding to the elastic and maximum seismic capacities, the values of PCA_{xy} were increased at a relative distance from the stiff side equal to 0.2 and 0.3 for the cases of the buildings having values of eccentricity ratio equal to 0.372 and 0.284 respectively, as shown in Figures 6.6(a) and 6.17(b). Whereas, the values of PCA_{xy} were increased at a relative distance equals to 0.4 for buildings that have eccentricity ratios equal to 0.06, 0.098, 0.143, and 0.205. While, in the case of the building with low value of eccentricity ratio of 0.026, the first increase was occurred at a relative distance equals to 0.5 (i.e. at the middle of the top floor). These results suggest that there is no de-amplification in the acceleration response of the NSCs attached to the SS. It can also be seen from Figure 6.6 that, at a given relative distance beyond the CRs, the acceleration response increases with the increase in the eccentricity ratio.

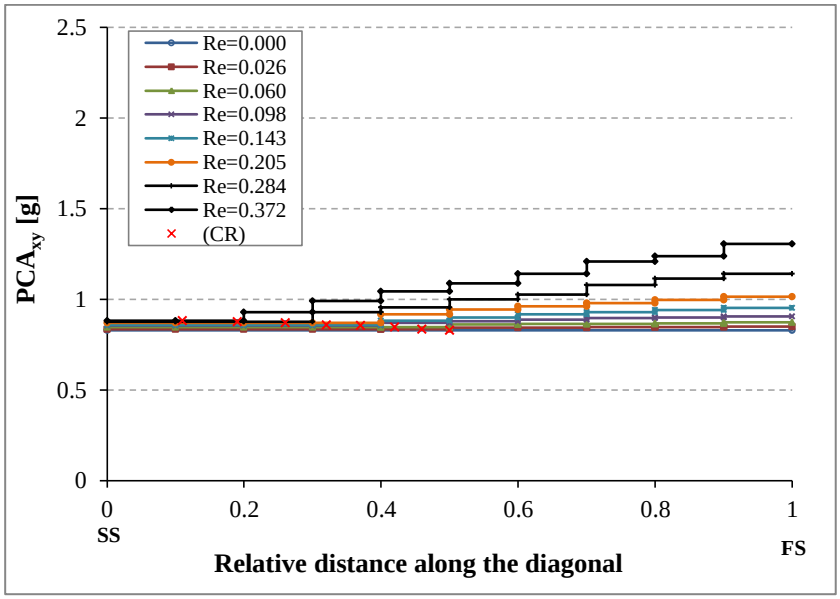

(a)

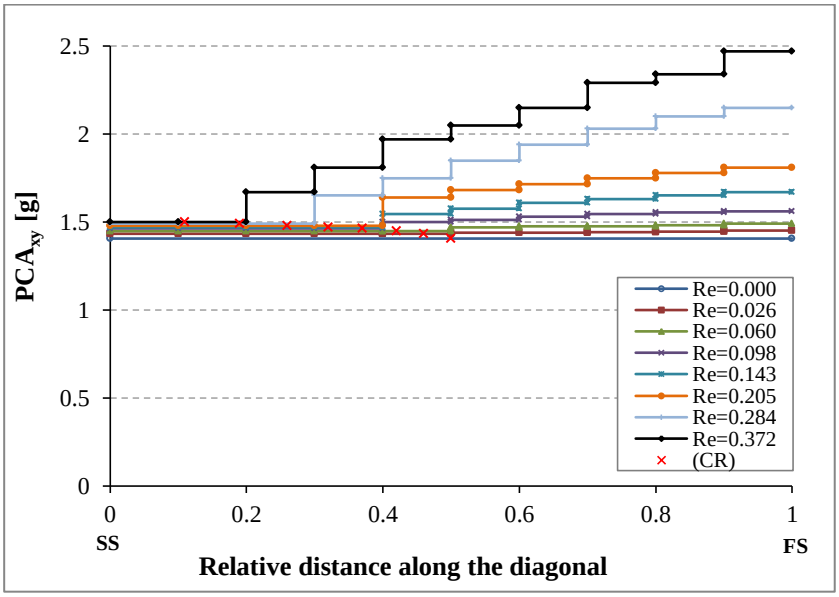

(b)

Figure 6.6 Peak component acceleration (PCA_{xy}) for the NSCs with $T_C = T_1$ and attached between the stiff sides and flexible sides of the top floors of one-bay three-storey RC P-structures at the PGA values corresponding to (a) the elastic seismic capacities and (b) the maximum seismic capacities.

In this research, the torsional amplification factor (F_T) is used to quantify the relationship between the NSCs accelerations and the torsional behaviour of the P-structures

caused by the eccentricity ratio. The torsional amplification factor for NSCs accelerations was defined in Chapter 5 (see Section 5.6.4) as the ratio of peak component acceleration at the flexible side ($PCA_{xy,FS}$) to the corresponding value at the centre of rigidity ($PCA_{xy,CR}$) i.e. ($F_T = PCA_{xy,FS}/PCA_{xy,CR}$).

Figure 6.7 shows the variations of top floor rotation (θ) with eccentricity ratio. This figure shows that, for a given PGA value, θ increases with the increase in the eccentricity ratio. The P-structure with the highest eccentricity ratio (0.372) experienced the highest top floor rotation (0.014 rad) at the PGA value corresponding to its maximum seismic capacity (0.54 g). Figure 6.8, which depicts the variations of F_T with eccentricity ratio, shows that the NSCs attached to the P-structure with the highest eccentricity ratio (0.372) had the highest torsional amplification factor (1.61). On the other hand, the P-structures with the eccentricity ratios of 0.0, 0.026, and 0.060 had the lowest top floor rotations (ranging from 0.00001 rad to 0.00083 rad) and lowest values of F_T (ranging from 1.0 to 1.04).

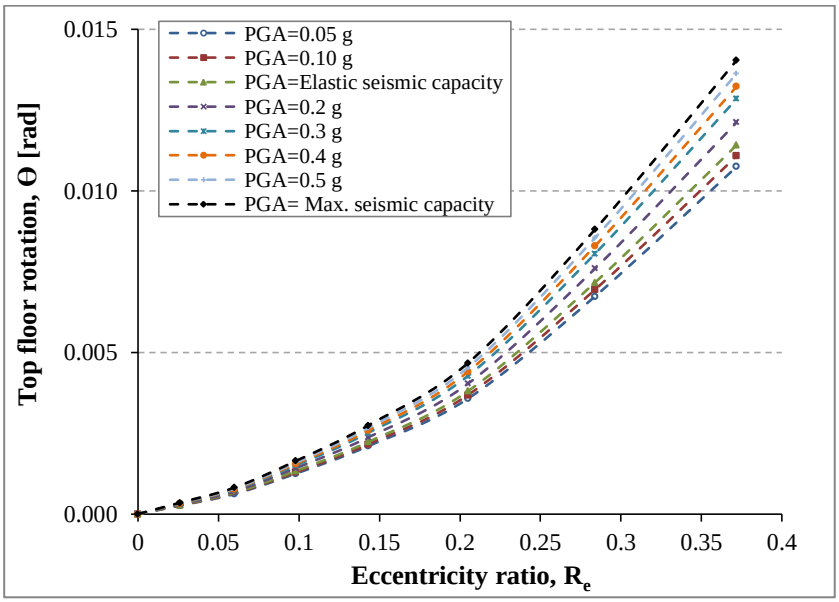

Figure 6.7 Variations of top floor rotation (θ) vs. eccentricity ratio of one-bay three-storey RC P-structures.

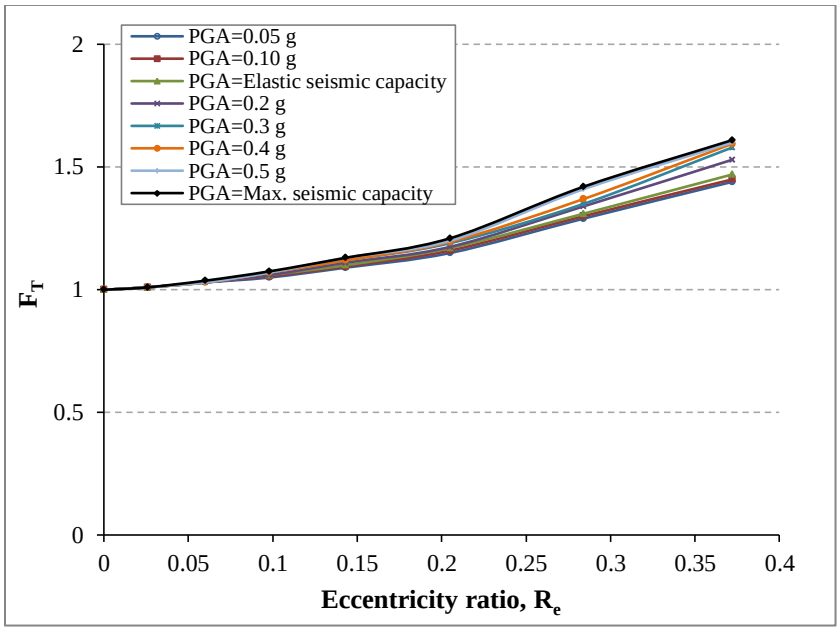

Figure 6.8 Variations of torsional amplification factor (F_T) for NSCs with $T_C = T_1$ vs. eccentricity ratio, for the NSCs attached to the top floors of one-bay three-storey RC P-structures.

Figures 6.7 and 6.8 suggest that there is a strong correlation between F_T and θ. Figure 6.9 shows that the relationship between F_T and θ may be expressed as follows:

$$F_T = 45.40\,\theta + 1.0 \tag{6-3}$$

Similar to Eq. (5-1) presented in Chapter 5, Eq. (6-3) is also valid for those P-structures with or without eccentricity. For a P-structure that does not experience torsional modes under the effect of seismic loading, Eq. (6-3) predicts a value of 1.0 for the torsional amplification factor (F_T). However, for a P-structure with torsional modes (i.e. P-structure with eccentricity), this equation predicts a value of F_T larger than 1.0. A maximum standard deviation of 0.026 was observed between Eq. (6-3) as presented above and the corresponding relationship that given in Eq. (5-1).

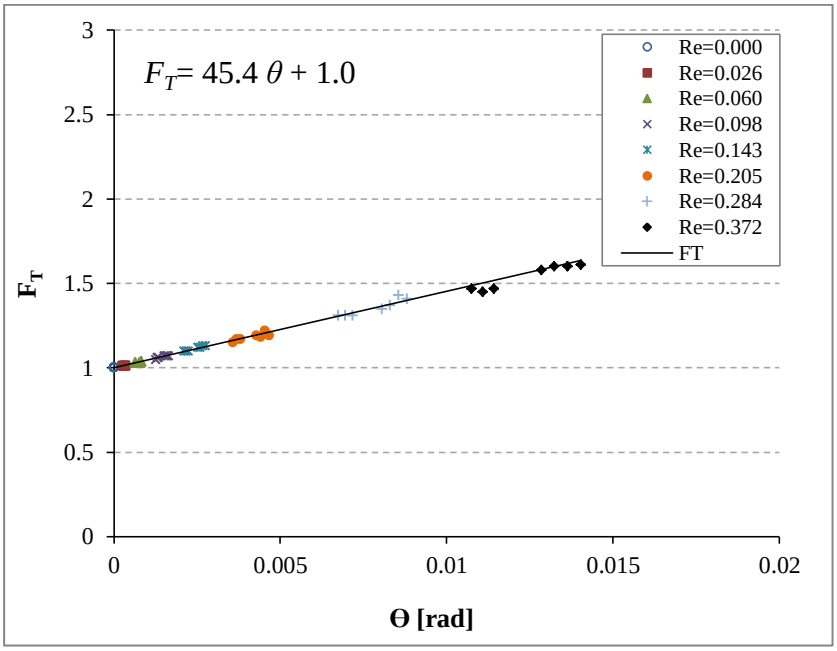

Figure 6.9 Relationship between the torsional amplification factor (F_T) for NSCs with periods equal to T_1 and top floor rotation (θ) of one-bay three-storey RC P-structures.

6.5.4 Effect of NSCs Damping Ratio

Evaluating the effect of NSC damping ratio is important to quantify the NSCs accelerations sensitivity during earthquakes. NSCs damping ratios in the range between 0.01% and 5% were considered in this section. These values were selected based on the premise that NSCs damping ratios are, in general, much less than P-structures damping ratios.

At the PGA values corresponding to the elastic seismic capacities (either 0.14 g or 0.15 g), Figures 6.10(a) and 6.10(b) show the variations of peak component accelerations with NSC damping ratio for the NSCs mounted on the flexible sides of the top floors of the P-structures with the lowest (0.026) and highest (0.372) eccentricity ratios respectively. It can be seen from Figure 6.10(a) that the NSCs with vibration periods tuned to the first three

vibration periods of the P-structures (i.e. T_1, T_2, and T_3) had higher accelerations than the NSCs tuned to the remaining vibration periods of the P-structures (i.e. T_4, T_5, and T_6).

The accelerations of the NSCs with $T_C = T_1$, T_2, or T_3 decreased with the increase in damping ratio from 0.01% to 3%. For the P-structures with the eccentricity ratios of 0.026 and 0.372, the NSCs accelerations decreased by about 40% and 48% respectively with the increase in damping ratio from 0.01% to 3%. The accelerations of the NSCs with $T_C = T_4$, T_5, or T_6 were less affected by the increase in damping ratio. The average percentage decrease in these NSCs accelerations ranged from 21% to 23% when the damping ratio was increased from 0.01% to 3%. At higher damping ratios (i.e. from 3% to 5%), the NSCs accelerations were not significantly affected by the increase in damping ratio.

At the PGA values corresponding to the maximum seismic capacities (either 0.57 g or 0.54 g), Figures 6.11(a) and 6.11(b) show the variations of peak component accelerations with NSC damping ratio for the NSCs mounted on the flexible sides of the top floors of the P-structures with the lowest (0.026) and highest (0.372) eccentricity ratios respectively.

Figure 6.11 features similar trends to those plotted in Figure 6.10. For the P-structures with the eccentricity ratios of 0.026 and 0.372, the accelerations of the NSCs with $T_C = T_1$, T_2, or T_3 decreased by about 41% and 50% respectively with the increase in damping ratio from 0.01% to 3%. The accelerations of the NSCs with $T_C = T_4$, T_5, or T_6 were less affected by the increase in damping ratio. The average percentage decrease in these NSCs accelerations ranged from 22% to 26% when the damping ratio was increased from 0.01% to 3%. At higher

damping ratios (i.e. from 3% to 5%), the NSCs accelerations were not significantly affected by the increase in damping ratio.

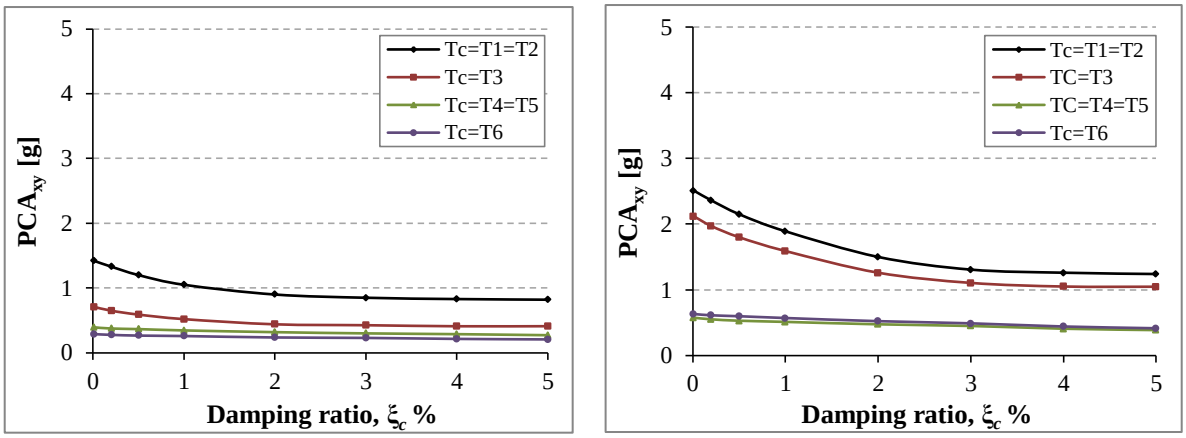

(a) (b)

Figure 6.10 Variations of peak component accelerations (PCA_{xy}) vs. NSC damping ratio (ξ_c) at the PGA values corresponding to the elastic seismic capacities of the P-structures with the eccentricity ratio of: (a) 0.026 and (b) 0.372.

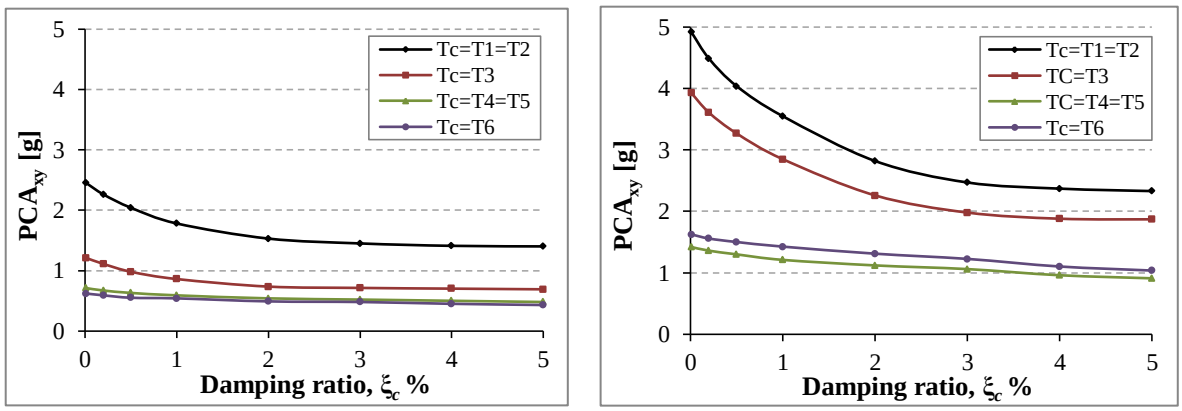

(a) (b)

Figure 6.11 Variations of peak component accelerations (PCA_{xy}) vs. NSC damping ratio (ξ_c) at the PGA values corresponding to the maximum seismic capacities of the P-structures with the eccentricity ratio of: (a) 0.026 and (b) 0.372.

To calculate the influence of torsion on the amplification in the accelerations of NSCs with low and high damping ratios of the NSC (i.e. ratio between the values of PCA_{xy} at value of ξ_c = 0.01% and the corresponding values at ξ_c = 3.0%), a relation is suggested between the

damping amplification factor (A_p^{ξ}) and the top floor rotation (θ). Figure 6.12 shows that the proposed relationship can be written as follows:

$$A_p^{\xi} = 32.0\,\theta + 1.65 \tag{6-4}$$

Equation (6-4) shows that the minimum value of A_p^{ξ} is 1.65 for the NSC attached to P-structure without eccentricity.

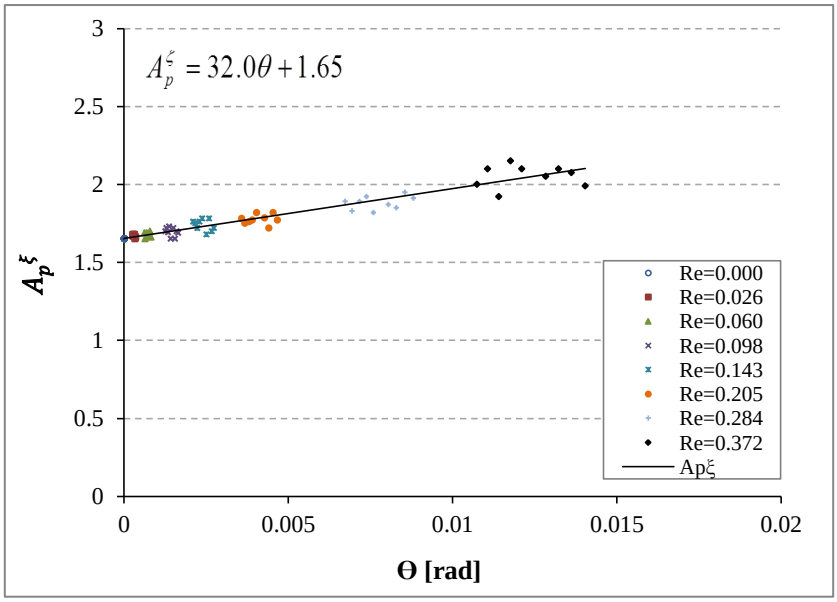

Figure 6.12 Relationship between the damping amplification factor (A_p^{ξ}) for NSCs with T_C equal to T_1 and top floor rotation (θ) of one-bay three-storey RC P-structures.

6.6 Comparison between the FE Results and EC8 Predictions

EC8 (2004) suggests the expression that given in Chapter 1 (see Eq. (1-1)) for the calculation of the seismic factor (S_a) applicable to secondary systems. The P-structures in this chapter (i.e. one-bay three storey RC buildings having different values of the eccentricity ratios) were designed for an a_g value of 0.15 g on ground type A. Considering the soil factor of 1.15 for

ground type C. In order to compare the predictions of Eq. (1-1) with the FE results, the term αS in Eq. (1-1) was taken as 0.173. Subsequently, the natural earthquake records, which adopted in this chapter were scaled using the PGA value of 0.173 g (i.e. the design ground acceleration on type C ground).

Shown in Figures 6.13, 6.14, and 6.15 are the comparisons between the predictions of Eq. (1-1) and the corresponding numerical values for different values of T_C/T_1 for the NSCs with damping ratio of 3% and attached to the CRs and FS of the first, second, and top floors of the P-structures respectively. Good agreement can be observed in Figures 6.13(a), 6.14(a), and 6.15(a) between the EC8 (2004) predictions and the numerical results for the accelerations of the NSCs with T_C equal to (T_1 or T_2) and attached to the CRs of the P-structures. For other values of T_C/T_1, EC8 (2004) provides conservative estimates for the accelerations of the NSCs attached to the CRs of the P-structures.

On the other hand, as can be seen in Figures 6.13(b) and 6.14(b), EC8 (2004) underestimates the accelerations of the NSCs with T_C equal to (T_1 or T_2) and attached to the FS of the first and second floors of the P-structures with eccentricity ratios higher than 0.098. For the NSCs with $T_C = T_1$ and attached to the FS of the P-structures with the eccentricity ratios of 0.143, 0.205, 0.284, and 0.372; EC8 (2004) underestimates the acceleration response of the NSCs attached to the first floors by about 2.9%, 10.6%, 21.7%, and 33% respectively and the acceleration response of the NSCs attached to the second floors by about 3.7%, 10.3%, 22%, and 33.3%, respectively.

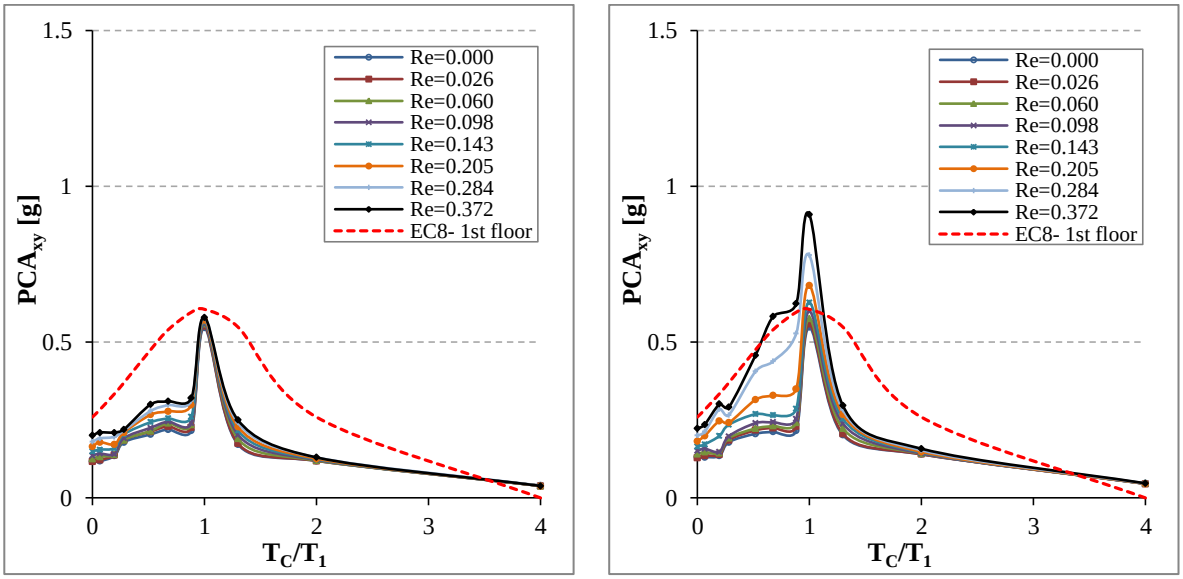

Figure 6.13 Comparison between FE and EC8 acceleration predictions for different values of T_C/T_1 for the NSCs attached to the first floors of different cases of one-bay three-storey RC P-structures at (a) centres of rigidity and (b) flexible sides.

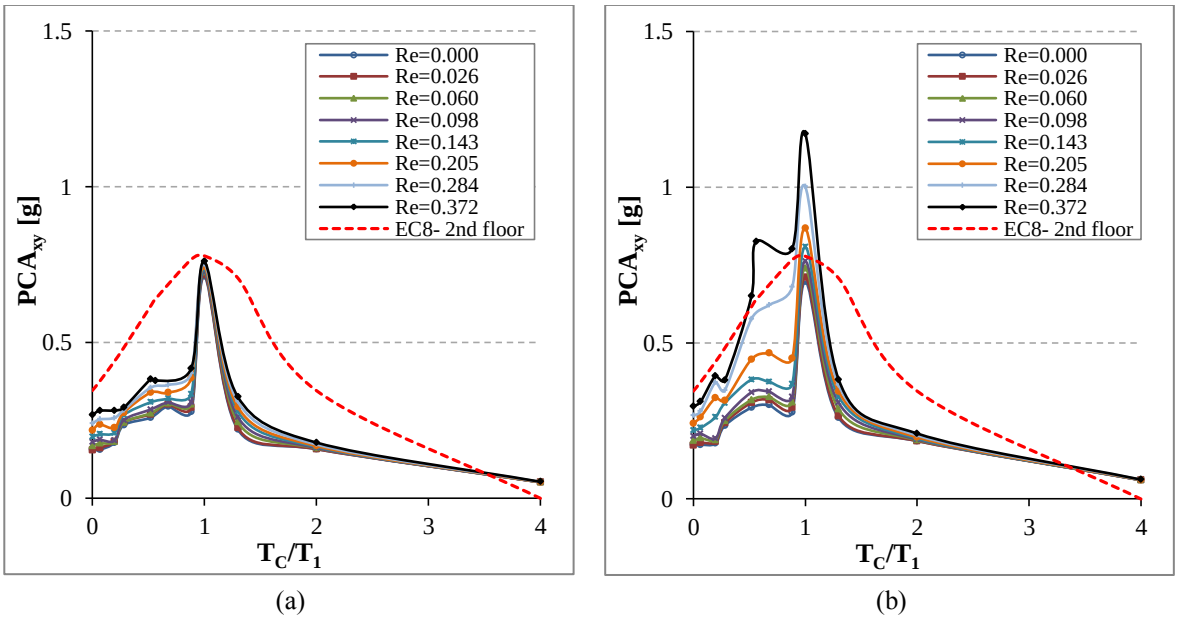

Figure 6.14 Comparison between FE and EC8 acceleration predictions for different values of T_C/T_1 for the NSCs attached to the second floors of different cases of one-bay three-storey RC P-structures (a) centres of rigidity and (b) flexible sides.

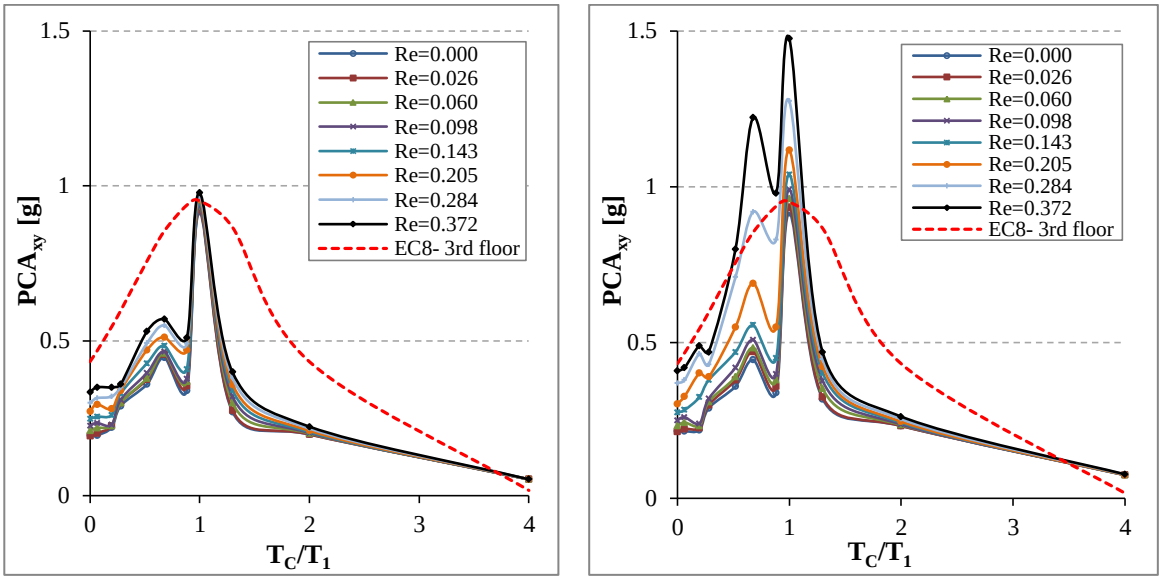

Figure 6.15 Comparison between FE and EC8 acceleration predictions for different values of T_C/T_1 for the NSCs attached to the top floors of different cases of one-bay three-storey RC P-structures at (a) centres of rigidity and (b) flexible sides.

Figure 6.15(b) shows that EC8 (2004) underestimates the NSCs accelerations by up to 35.6% for NSCs with T_C equal to (T_1 or T_2) and attached to the FS of the top floors of the P-structures with eccentricity ratios higher than 0.026. More explanation can be found in Figure 6.16(a), when the NSCs with periods equal to T_1 and T_2 and attached to the FS and CRs of the top floors of the P-structures having different values of eccentricity ratios. It seems from this figure that the NSCs accelerations predicted well by the EC8 recommendations when they attached to the CRs of all the considered cases of P-structures with different eccentricity ratios.

Furthermore, Figure 6.16(b) shows that the EC8 (2004) well-estimates the seismic response of the NSCs having a period equal to T_3 and attached to the top floor of the flexible side of P-structures having eccentricity ratios equal or less than 0.205; whereas beyond the latter value, the EC8 underestimates the NSCs accelerations. For NSCs which are resonant

with the torsional mode of the P-structures (i.e. $T_C = T_3$), the values of PCA_{xy} were increased dramatically for those NSCs attached to the buildings that have an eccentricity ratios more than 0.143. The values of PCA_{xy} were found equal to 0.56 g and 1.22 g at values of eccentricity ratios equal to 0.143 and 0.372 respectively. It can be seen from Figure 6.16(b) that the EC8 (2004) underestimates the NSCs accelerations by about 7.6% and 30.4% for the NSCs with $T_C = T_3$ and attached to the P-structures with the eccentricity ratios of 0.284 and 0.372 respectively.

Figures 6.16(c) and 6.16(d) shows that, for short periods of NSCs (i.e. $T_C = T_4$, T_5, and T_6), the EC8 (2004) recommendations good predict the seismic response when the NSCs attached to the P-structures having eccentricity ratios larger than 0.205. However, the EC8 overestimates the NSCs accelerations on average by about 104% for those NSCs mounted on the FS and CRs of the top floors of RC buildings with eccentricity ratios equal or less than 0.205. This result suggests that any modification on the EC8 equation for the design of such as NSCs (i.e. NSCs with short periods or those are close to rigid equipment), should ensure it does not cause any increase in the accelerations at these range of periods.

On the other hand, for those NSCs having periods equal to $T_C = 4T_1$ (i.e. very long NSCs period) and attached to both the centres of rigidity and the flexible sides of the top floor of the P-structures, the predictions of EC8 (2004) are unconservative for the values of the component accelerations as shown in Figures 6.13 to 6.15. This fact is recognised in the manual for design of buildings according to EC8 (IStructE, 2010), when it is stated that the EC8 (2004) equation for the seismic design of NSCs may unconservative the responses for very long period of NSCs. Therefore, it is recommended that the value of (T_C/T_1) in the

expression of the EC8 (i.e. Eq. (1-1), as presented in Chapter 1), should be limited to a maximum value of 2.0 for design purposes of the NSCs.

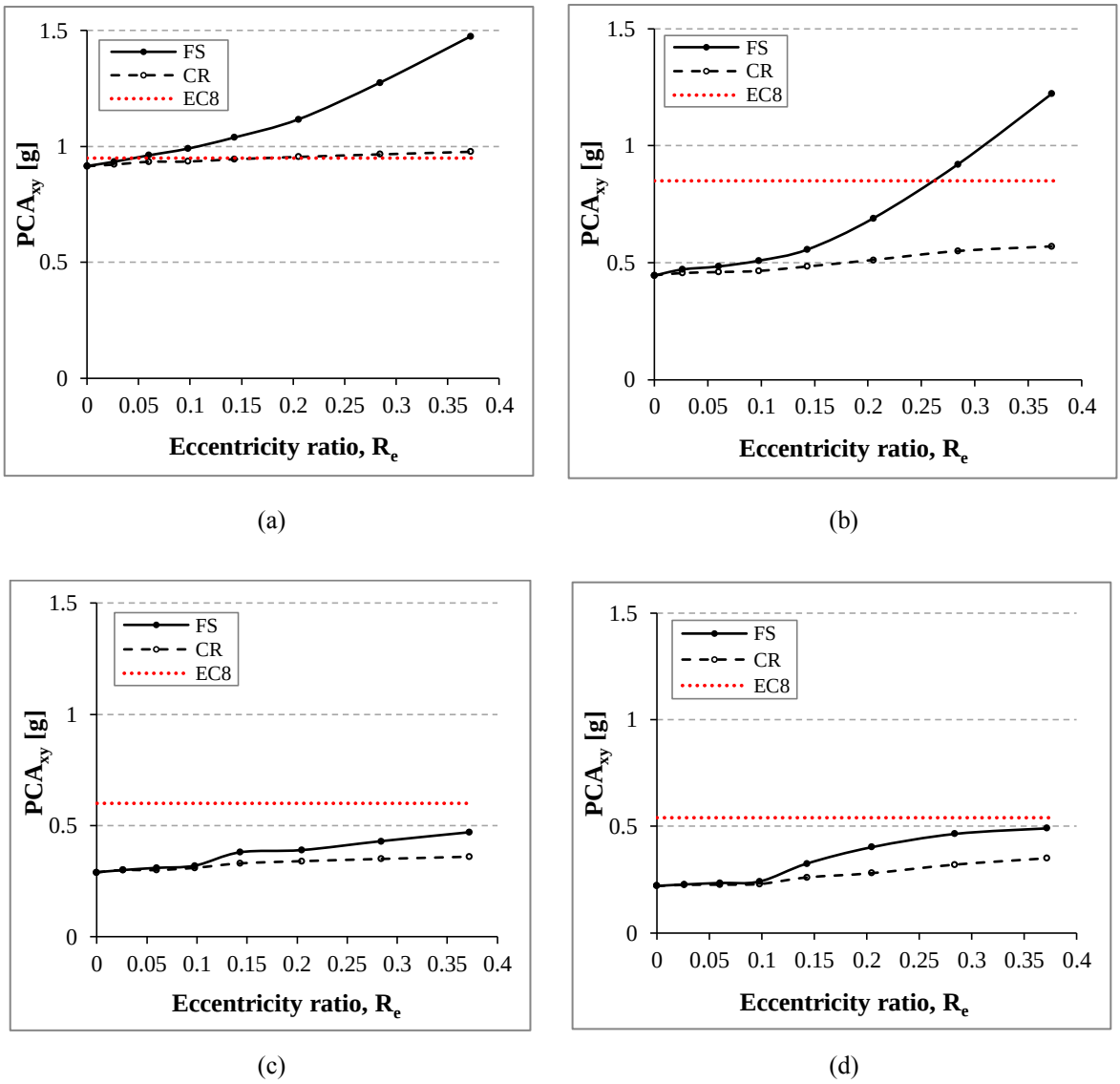

Figure 6.16 Comparison between FE and EC8 acceleration predictions for the NSCs attached to the FS and CRs of the top floors of different cases of one-bay three-storey RC P-structures, for NSCs having periods equal to (a) T_1 and T_2, (b) T_3, (c) T_4 and T_5, and (d) T_6.

It is worth to note from the results presented in Section 6.5.1 (see Figure 6.3(b)) that, the predictions of EC8 (2004) provide a large underestimation of PCA_{xy}. This is for the NSCs with periods equal to T_1 attached to the flexible sides of the top floors of the P-structures

under the effect of base motions with PGA values corresponding to the maximum seismic capacities of the P-structures. EC8 underestimated the NSCs accelerations by about 32.3% and 61.5% when the NSCs attached to the regular structure without eccentricity and the P-structure with the highest (0.372) eccentricity ratio respectively. Therefore, it seems that the NSCs attached to such as these locations, they would suffer from the damage under the effect of earthquakes with PGA either corresponding or more than the design value of the P-structures.

6.7 Summary

In Chapter 6, seismic responses of NSCs integrated on the flexible sides and centres of rigidity of eight cases of RC P-structures with different eccentricity ratios were studied. The selected buildings were designed according to the seismic provisions of EC8 (2004) for the Ductility Class Medium and by considering the plan regularity criteria. Dynamic analyses of the P-S systems were performed to investigate the variations of the NSCs accelerations with different parameters such as different values of peak ground accelerations, ratio of natural periods of NSCs and the vibration periods of the P-structures, eccentricity ratios of the P-structures, and different values of damping ratios of NSCs. It can be concluded from the foregoing results that the seismic responses of NSCs were affected by the behaviours of the P-structures due to a full dynamic interaction with the primary structures. It was observed that the higher the value of eccentricity ratio of the P-structure, the higher the acceleration value that affected the NSCs.

A relationship between the amplification in the values of peak components accelerations due to the effect of eccentricity ratios in terms of the top floors rotations is suggested. The torsional amplification factor F_T of NSCs, was found equal to 1.0 when the NSC attached to P-structure without eccentricity (i.e. non-torsional structure). Furthermore, a relationship is proposed to evaluate the influence of torsion on the amplification in acceleration of NSCs due to the ratio between high and low damping values for NSCs having vibration periods T_C equal to the first fundamental periods T_1 of the P-structures. The minimum value of the damping amplification factor A_p^{ξ} of NSC due to a reduction in the damping ratio from 3% to 0.01% is 1.65 when the NSC attached to the regular P-structure with eccentricity ratio equal to 0.0.

The findings of the comparison between the numerical results and the corresponding predictions determined by the EC8 provision showed that the latter provisions underestimated the accelerations of the NSCs integrated on different floor levels of the flexible sides of the RC buildings that were experienced torsional behaviour during earthquakes. The most values of the periods that were influenced by the torsional modes of the P-structure were those matched with the first three fundamental vibration periods of the P-structures. For NSCs (T_C = T_1 and 3% damping ratio) attached to the flexible side of the top floors of the RC P-structure that had a high value of eccentricity ratio (0.372), the predictions of the EC8 (2004) underestimated the NSCs accelerations up to the value of 35.5% at the PGA value corresponding to the design ground acceleration of the P-structure.

CHAPTER SEVEN: INFLUENCE OF PLAN AND VERTICAL MASS IRREGULARITIES OF REINFORCED CONCRETE STRUCTURES ON THE SEISMIC RESPONSE OF NSCs

7.1 Introduction

As explained in Chapter 1 (see Section 1.2) that in modern structures, vertical mass irregularities and plan asymmetry are two features which would cause significant disadvantages in seismic zones. In such structures, strong torsional effects induced by moderate and strong base motions are usually responsible for the damage of the main structural elements (Chandler and Hutchinson, 1986). Hence, maintaining the symmetry and regularity of buildings in seismic zones is an important design rule. Yet, vertical mass irregularity is usually unavoidable in large buildings. For example, a discontinuity created due to the different use of one floor compared to the other floors in a structure such as a factory with heavy machineries, an educational institution with a library at lower floor level, parking floor, mechanical and electrical floor in a hospital, or floor with a swimming pool, etc. (Valmundsson and Nau, 1997; Sadashiva *et al*., 2009).

Structures, given the above reasons, can never achieve a perfectly regular state and hence will always have some sort of vertical irregularities according to the provisions of the existing codes (Sadashiva *et al*., 2009). For example, according to the provisions of EC8 (2004), a particular P-system is to be classified as being mass irregular in elevation, if the

total weight of the individual floor level does not remain constant (i.e. with abrupt variations) from the bottom to the top floors. On the other hand, FEMA-178 (BSSC, 1992) considers mass irregularities to exist when the actual mass of any floor level (consisting of both the partitions and the secondary systems masses in addition to the floor acting permanent actions) is larger than 150% of an adjacent floor.

Several studies (Hutchinson *et al.*, 1993; Valmundsson and Nau, 1997; Al Ali and Krawinkler, 1998; Choi, 2004; Chopra and Goel, 2004; Chintanapakdee and Chopra, 2004; Poncet and Tremblay, 2004; Tremblay and Poncet, 2005; Kalkan and Kunnath, 2006; Michalis *et al.*, 2006; Karavasilis *et al.*, 2008; Poonam *et al.*, 2012) investigated the behaviour of P-structures with vertical irregularity. Nonetheless, to date (to the best of the researcher knowledge), none of the available studies considered NSCs attached to P-structures with vertical mass irregularity. Furthermore, the P-structures considered in most of the aforementioned studies were modelled as 2D regular structures. As a result, most of the investigated behaviours were determined in terms of inter-storey drifts rather than rotational accelerations or rotational displacements responses. In addition, most of past investigations on P-structures with the influence of the vertical irregularity do not satisfy the convenience of the regularity parameters suggested in modern design provisions, e.g. EC8 (2004).

As irregularity of the P-structures along their heights, besides their plan irregularity, can be caused a costly damage during earthquakes, therefore, their combined effects on the attached NSCs are worthy of investigation under seismic loading. It may lead to unsafe design of the NSCs if the effects of both the vertical irregularity and torsion of the P-structures are

ignored. Therefore, this chapter presents nonlinear dynamic FE analyses of NSCs attached to the floors of plan asymmetric RC P-structure with different cases of vertical mass.

Thirty P-structures with different vertical mass irregularities, in addition to the reference P-structure, were suggested in this investigation. A plan asymmetric, multi-bay, twenty-storey RC building was chosen as a P-structure. Floor mass ratios of either 2 or 4 were adopted. These cases of mass irregularities were presented by increasing the mass value of one to three consecutive floors; whereas the masses of the other floors were kept constant. The evaluated numerical results are based on averages of seven artificial ground motion inputs in the two horizontal directions (X and Y). These artificial records were generated in such a way that their PSAs were completely compatible with the EC8 (2004) Type 1 elastic RS for ground type C, as presented in Chapter 3 (see Figure 3.11(a)).

The investigated behaviours were presented in terms of the ratio between the effect of the modified and reference cases. The main objectives of this chapter are:

- To investigate the effect of P-structure vertical mass irregularity on the seismic response of elastic lightweight acceleration-sensitive NSCs, and
- To compare the predictions of the nonlinear dynamic FE analyses with those of EC8 (2004) seismic design provisions for NSCs, and
- To propose expressions that can be used to evaluate the percentage of increase in the acceleration of NSCs due to the increase in the total masses of the floors along the heights of the buildings.

Average numerical results of 1561 nonlinear dynamic FE analyses of the P-S systems are presented in Sections 7.6, 7.7, and 7.8 for different cases of vertical mass irregularities and for three period values of NSCs equal to T_1, T_2, and T_3 of the P-structures, as well as $T_C \approx 0$ s (i.e. rigid NSCs).

7.2 Characteristics and Modelling of Irregular 20-storey RC P-structure

7.2.1 General Description of RC P-structure

Thirty one variants of a multi-bay, twenty-storey, asymmetric RC building with different vertical mass distributions were selected as P-structures in this chapter. The configuration of the P-structures was chosen as it represented one of the simplest forms of multi-bay, multi-storey, asymmetric structures that provide both transitional and torsional vibration modes during an earthquake. Figure 7.1(a) shows a three-dimensional schematic of adopted typical RC P-structure. The height of the first storey is equal to 5 m whereas the typical height of the upper 19 storeys is 4 m as shown in Figure 7.1(b). The areas of the first and fourth floors are about 2003 m^2 and 1373 m^2 respectively.

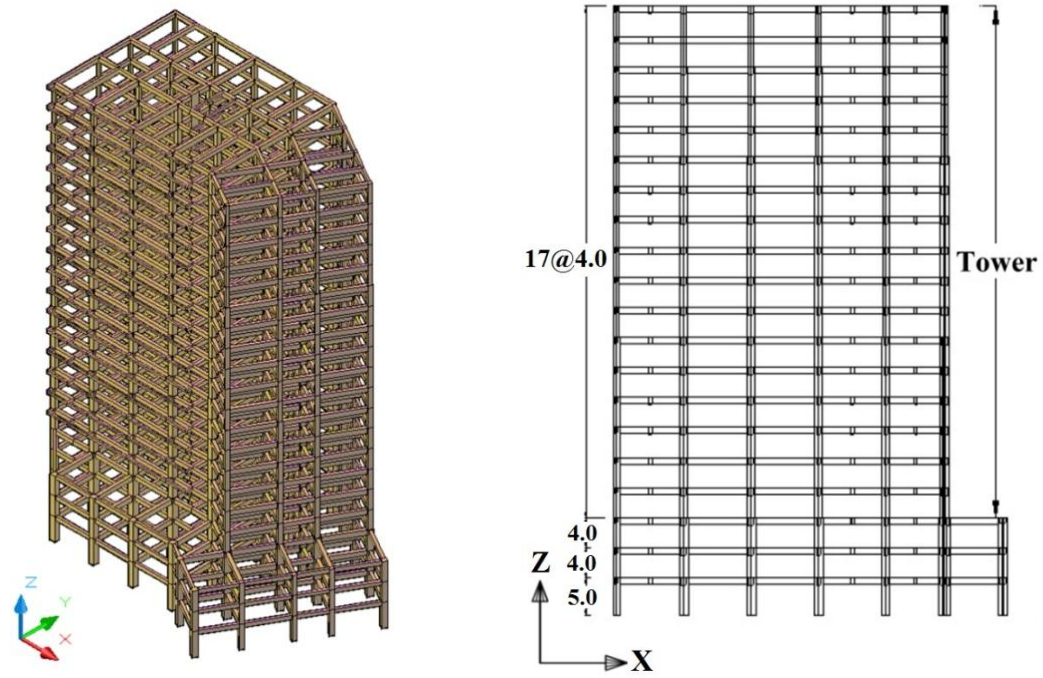

(a) (b)

Figure 7.1 A typical RC P-structure: (a) three-dimensional schematic and (b) elevation (all dimensions are in metres).

Shown in Figures 7.2 to 7.5 are the details of the columns, girders and beams. The centre of mass (CM) of the first three storeys moves away from the centre of rigidity (CR) by values of e_x and e_y equal to 0.70 m and 0.32 m respectively (i.e. eccentricity ratios equal to 0.0155 and 0.035 respectively). However, these two values are 1.08 m and 0.54 m (i.e. eccentricity ratios equal to 0.027 and 0.059 respectively) for the upper 17 storeys of the building. The term (FS) as presented in Figure 7.3 represents the flexible side of the P-structure. Its location was selected based on the results of the nonlinear dynamic analysis as explained later in Section 7.6 (see Figure 7.15).

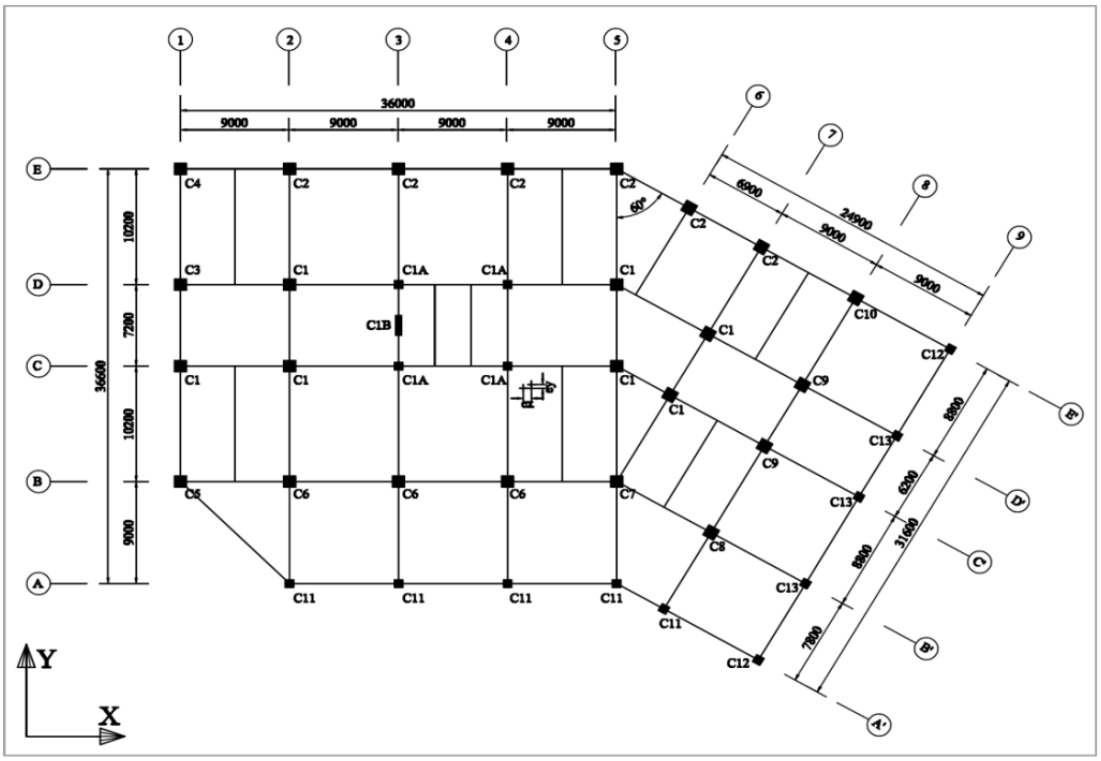

Figure 7.2 Plan layout of the columns for the first 3 storeys of irregular 20-storey, multi-bay RC building (all dimensions are in millimetres).

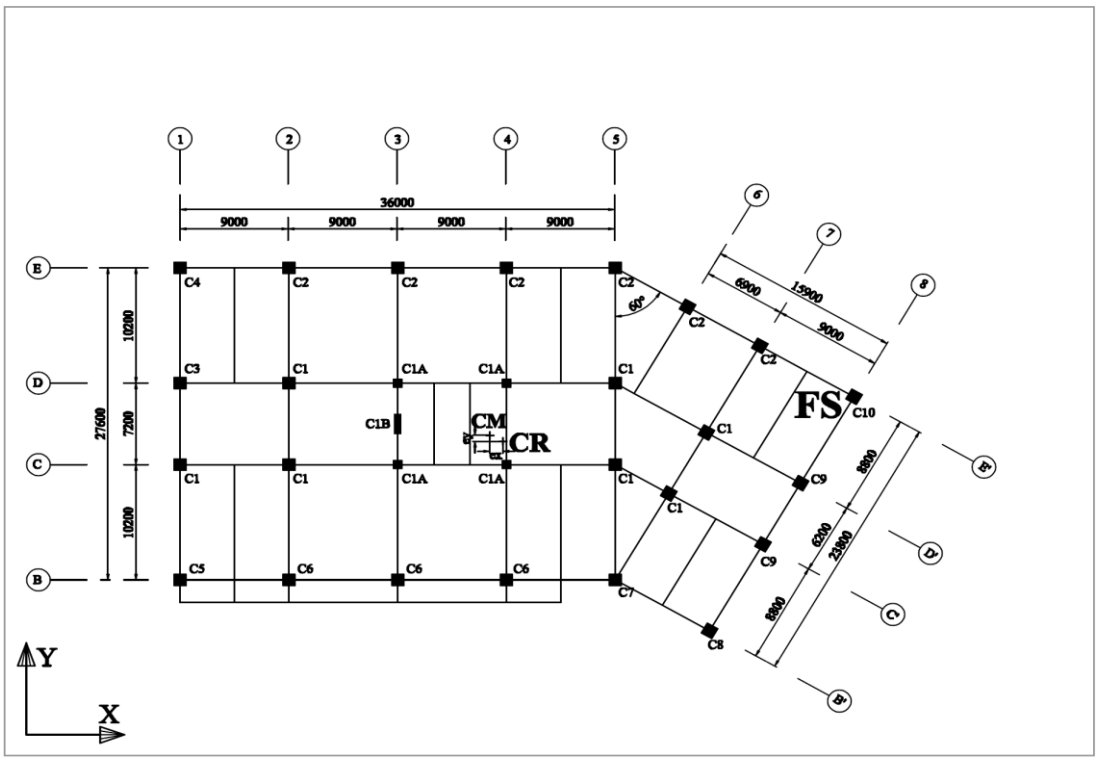

Figure 7.3 Plan layout of the columns for the upper 17 storeys of irregular 20-storey, multi-bay RC building (all dimensions are in millimetres).

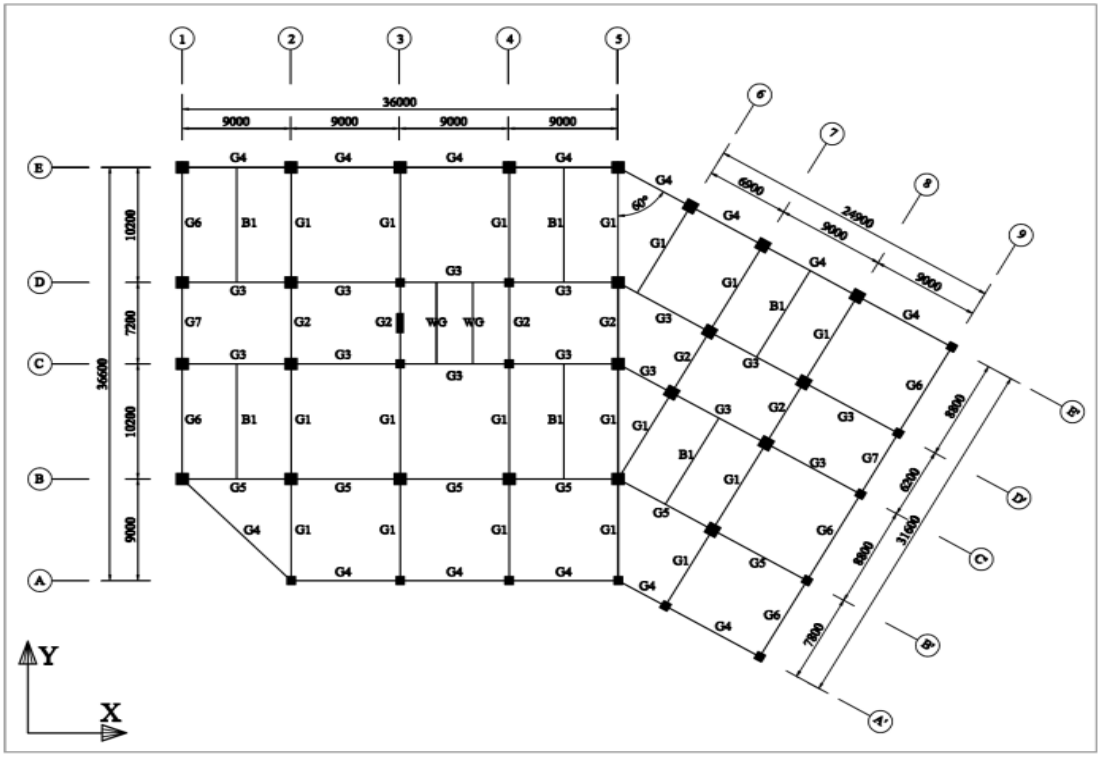

Figure 7.4 Plan layout of the girders and beams for the first 3 storeys of irregular 20-storey, multi-bay RC building (all dimensions are in millimetres).

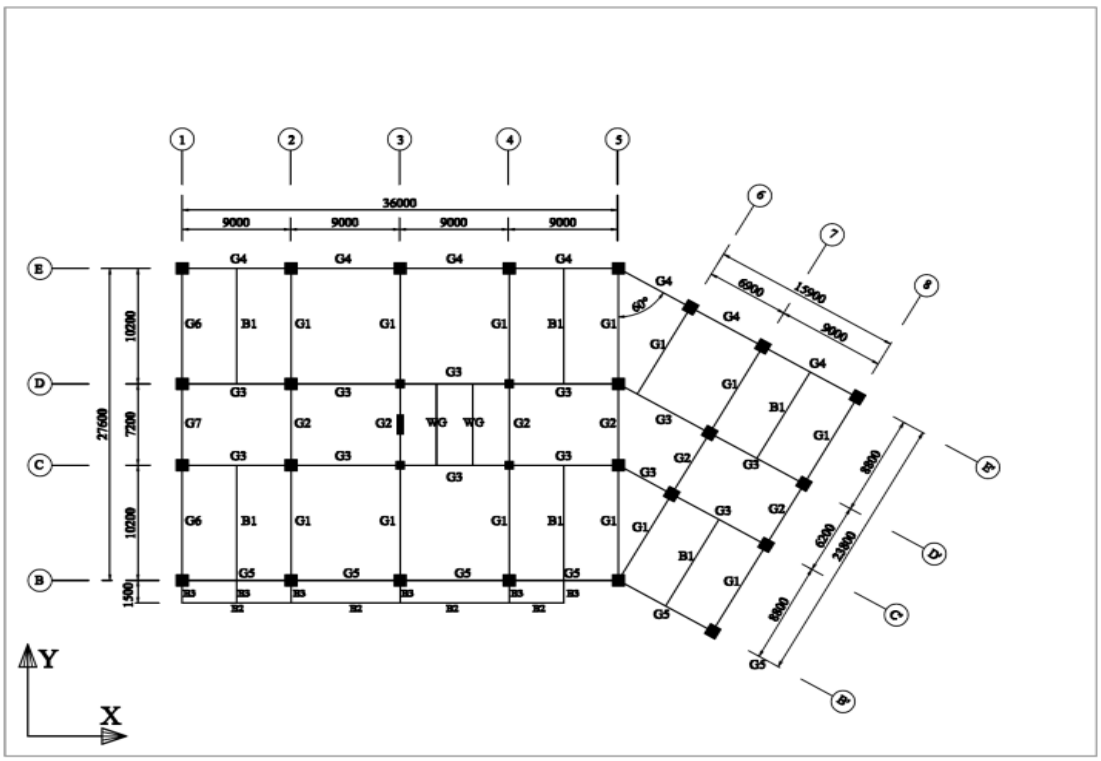

Figure 7.5 Plan layout of the girders and beams for the upper 17 storeys of irregular 20-storey, multi-bay RC building (all dimensions are in millimetres).

The RC P-structures were designed according to the provisions of EC1 (2002), EC2 (2004), and EC8 (2004). The characteristic values of the floor loads were taken as 2.5 kN/m^2 and 4.5 kN/m^2 for variable and permanent (excluding slab self-weight) actions respectively. The most important reason for choosing this value of permanent load is to ensure that no failure can be occurred in any floor along the building height when the mass ratio is equal to 4.0. The EC8 (2004) Type 1 elastic RS for ground type C was adopted. Explanation the criteria for the selecting of this type of ground can be found in Chapter 3 (see Section 3.3). The importance factor (γ_I) was taken as 1.2 (Importance Category III). The design reference peak ground acceleration (a_{gR}) on type A ground was taken as 0.25 g. Considering the soil factor of 1.15 for ground type C, the design ground acceleration on type C ground was 0.345 g. All P-structures satisfied the EC8 (2004) Ductility Class M (DCM) requirements. The basic value of the behaviour factor q_o equal to $3.\alpha_u/\alpha_1$ (EC8, 2004), was used. The value of α_u/α_1 is 1.3, for multi-storey, multi-bay frames. For asymmetrical P-structure, the value of α_u/α_1 can be evaluated as an average of 1.0 and ($\alpha_u/\alpha_1 = 1.3$). According to the EC8 (2004), buildings with irregularities along the height are penalised as the irregularities tend to induce concentration of ductility demands at some locations of the structures, as opposed to the more uniform spread of ductility demands in regular buildings. Therefore, EC8 (2004) provisions included a moderate reduction of 20 per cent in the behaviour factor for structures with this type of irregularity. Consequently, the final value of the behaviour factor q used in the design to consider the inelastic deformation can be calculated as 2.76.

Concrete Class C25/30 and steel reinforcement Class C S500 were therefore used in the design of the structural elements. To fulfil the strong column/weak beam criterion, the over-strength factor (γ_{Rd}) was taken as 1.30 for all P-structures. The resulting member

dimensions and amount of steel longitudinal and shear reinforcement are given in Appendix A (see Tables A5-1 and A5-2).

7.2.2 Vertical Mass Irregularities

In previous studies investigating the behaviour of the P-structures with vertical mass irregularities as reported in Section 7.1, different cases of mass distributions along the heights of the structures were considered. For example, in a study by Hutchinson *et al.* (1993) the mass of a heavy floor was chosen to be five times greater than the mass of a typical floor to represent an extreme case of vertical mass irregularity. Valmundsson and Nau (1997) adopted heavy – to – typical floor mass ratios ranging from 0.1 to 5.0 whereas Kalkan and Kunnath (2006), adopted a heavy – to – typical floor mass ratio of 2.0. In all above studies, the heavy floors were located in the lower, middle, or upper parts of the P-structures.

The vertical mass distributions adopted in the current chapter cover the majority of the cases studied in the above-mentioned research studies. Reference and thirty modified cases of vertical mass distributions were investigated. The reference case can be defined as a building with a regular floor mass ratio of 1.0 along its height. The modified cases are those buildings with floor mass ratios of either 2 or 4. The heavy floors were located in the lower, middle, upper, lower and upper, or middle and upper parts of the P-structures as depicted in Figures 7.6 to 7.10. The number of heavy floors at a given part of a building varied between 1 and 3. The designation T_C-L_m-ή-m_r is used to identify the NSCs integrated on the P-structures with vertical mass irregularity. T_C is the NSC vibration period (taken as 0 s (i.e. rigid) or equal to T_1, T_2, or T_3 for a given P-structure), L_m is the location of the mass irregularity along the height of the tower (i.e. bottom, middle, top, top and bottom, or top and middle of the

building), ṅ is the number of heavy floors (i.e. ṅ = 1, 2, or 3), and m_r is the floor mass ratio (i.e. m_r = 1, 2, or 4). Although some cases with mass irregularities of 4 times the reference building might not be realistic, they were studied in order to investigate the effects of extreme irregularity on the dynamic response of NSCs. Figures 7.6 to 7.10 illustrate the thirty cases of vertical mass distribution chosen in the current chapter.

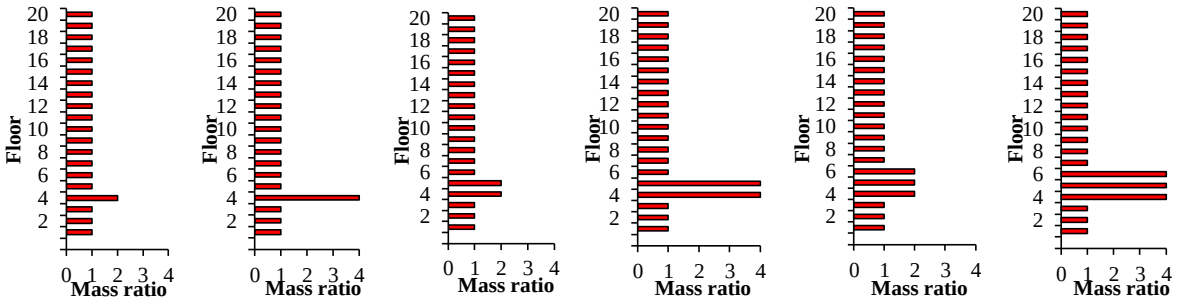

Figure 7.6 Mass irregularities at the bottom floors of the tower.

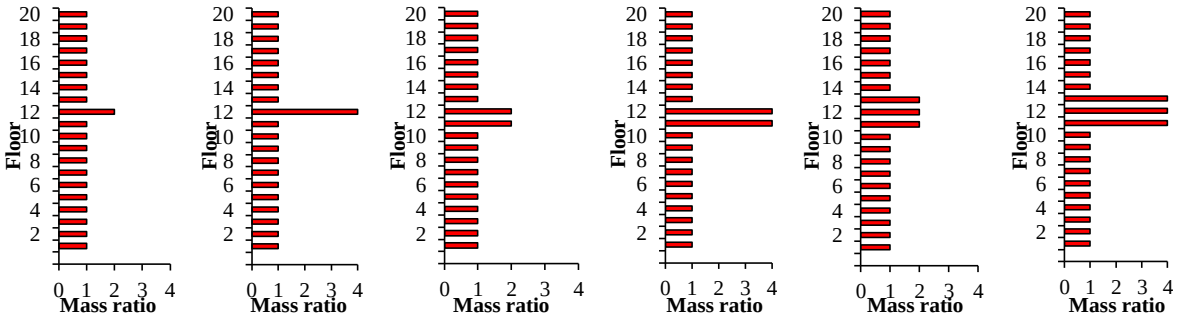

Figure 7.7 Mass irregularities at the middle floors of the tower.

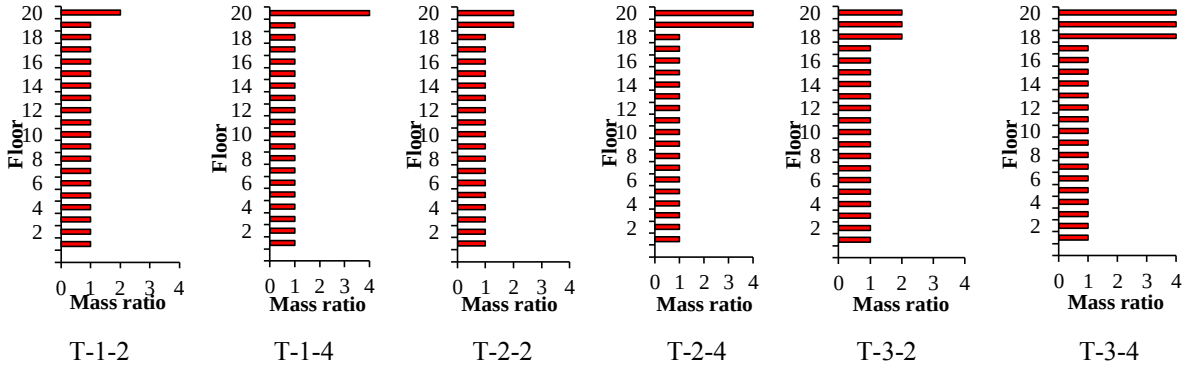

Figure 7.8 Mass irregularities at the top floors of the tower.

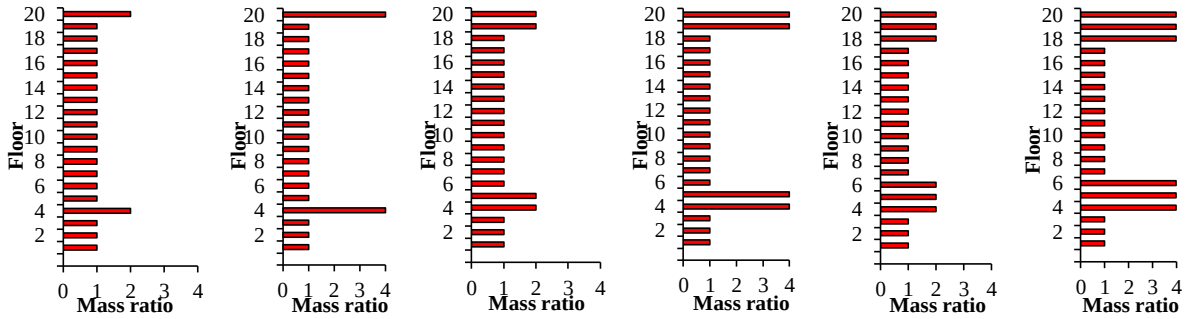

Figure 7.9 Combination of mass irregularities at the top and bottom floors of the tower.

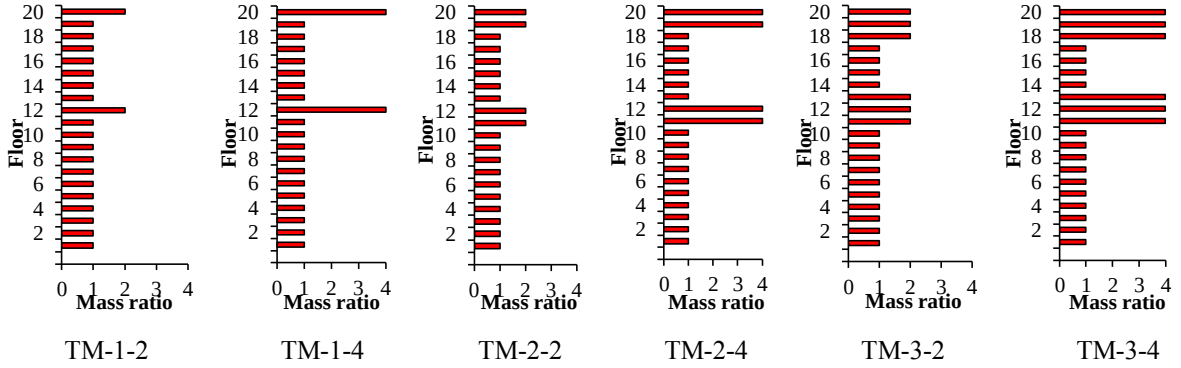

Figure 7.10 Combination of mass irregularities at the top and middle floors of the tower.

7.3 Modal Analyses of Irregular 20-storey RC P-structures

In order to calculate the vibration periods of the reference building (i.e. P-structure that has a vertical regular mass ratio equal to 1.0 along its height), modal analysis was carried out using MIDAS Gen code (2013). Shown in Table 7.1 are the first three vibration periods and modal direction factors of the reference case. It can be seen from Table 7.1 that in the 2nd and 3rd modes, the torsional and transitional-Y modes are the control modes. Shown in Figure 7.11 are the first mode shapes of six selected cases of mass irregularities, as explained in the

legend of this figure. It can be seen that the amplitudes of the modal shapes of all cases occurred at the top of the P-structures (i.e. value of z_c/H equal to 1.0).

Table 7.1 Vibration periods and modal direction factors for the reference P-structure.

Mode No.	Period [s]	Modal direction factor (%)			Control Mode
		Transition-X	Transition-Y	Rotation-Z	
1	2.13	95.25	0.26	4.48	Transition-X
2	1.87	1.88	67.01	31.10	Transition-Y + Rotation-Z
3	1.66	1.29	34.44	64.26	Rotation-Z + Transition-Y

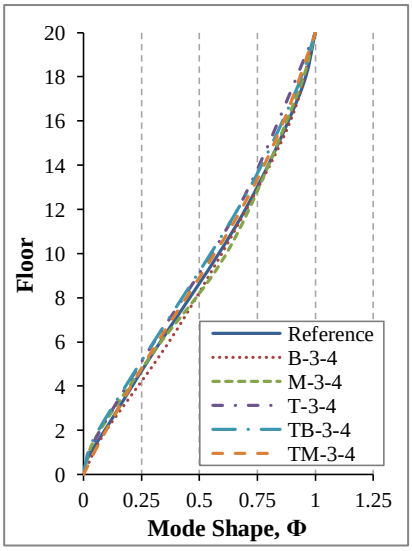

Figure 7.11 The first mode shapes of six cases of vertical mass irregularities.

Eigenvalue analyses were also carried out for the modified P-structures (i.e. the thirty cases of vertical mass irregularities, as described in Section 7.2.2). Variations of the first vibration period of the modified cases with respect to the reference case (i.e. T_1 Modified /T_1 Reference) are as shown in Figure 7.12. The term ṅ in this figure refers to the number of heavy floors (i.e. ṅ = 1, 2, or 3). It can be seen that due to an increase in the total mass of each modified P-structure, the first vibration period ratios of all modified P-structures increased in comparison with the reference case.

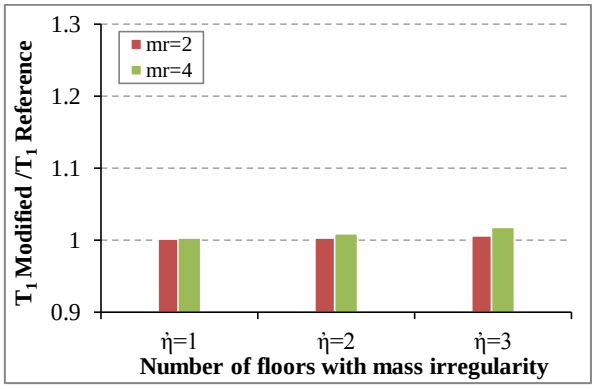

(a) L_m = bottom

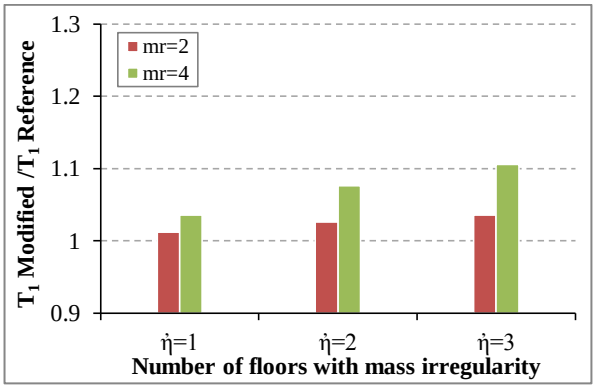

(b) L_m = middle

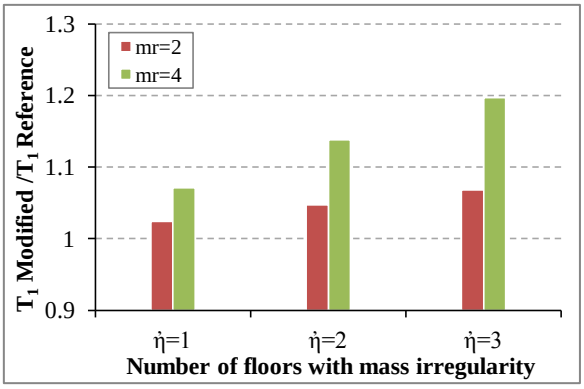

(c) L_m = top

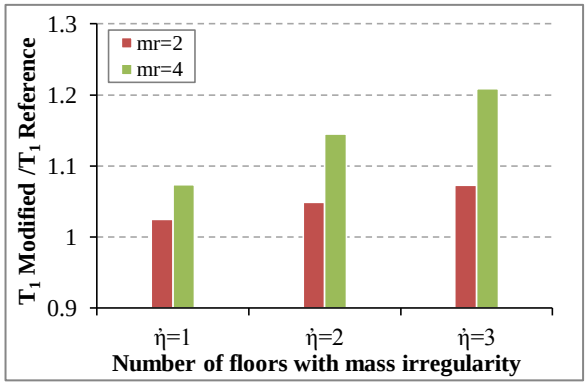

(d) L_m = top and bottom

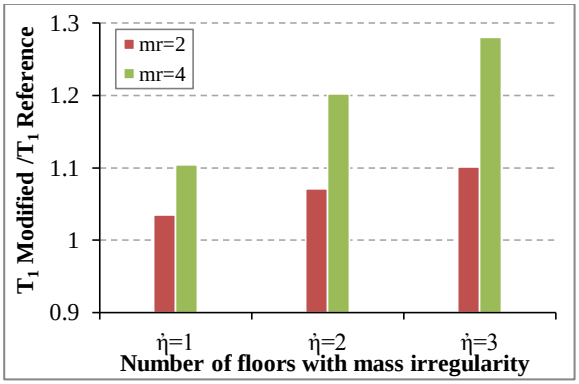

(e) L_m = top and middle

Figure 7.12 Values of (T_1 Modified /T_1 Reference) for the P-structures with location of mass irregularities (L_m) at the (a) bottom, (b) middle, (c) top, (d) top and bottom, and (e) top and middle of the tower.

Another trend that can be noted from Figure 7.12 is that, due to the amplitudes of the modal shapes of the upper floors being larger than those of the lower floors (see Figure 7.11),

the increase in the first vibration period ratios of the P-structures with mass irregularity at the higher floors is more than that of the P-structures with mass irregularity at the lower floors. For example, the buildings designated T-3-4, M-3-4, and B-3-4 where the mass irregularity was at the top, middle, and bottom floors respectively had T1 Modified /T1 Reference values of 1.20, 1.10, and 1.02, respectively. Similarly, the buildings designated TM-3-4 and TB-3-4 where the mass irregularity was at the top and middle floors, and top and bottom floors respectively had T1 Modified /T1 Reference values of 1.28 and 1.21 respectively (see Figures 7.12(d) and 7.12(e)).

7.4 Characteristics of Non-structural Components

The NSCs were modelled as vertical cantilevers with masses on the free ends as described in Chapter 4 (see Section 4.3.1). Damping ratio equal to 3% (Graves and Morante, 2006) was adopted for all cases of the NSCs. The NSCs were assumed to be directly attached to the floors (i.e. full dynamic interaction) of the P-structure. Vibration periods of NSCs as given in Table 7.2 were adopted in the dynamic analyses of the P-S systems presented in this chapter.

Table 7.2 also shows the characteristics of NSCs (i.e. the length (L_a) and stiffness (K_a) of their arms) for those NSCs with vibration periods equal to T_1, T_2, and T_3 of the P-structures. Similar to that adopted in Chapters 5 and 6, the values of the peak floors accelerations (PFA_{xy}) at the point of the attachment with the NSCs were used to express the accelerations of the rigid NSCs (i.e. $T_C \approx 0$ s) along the height of the P-structure.

Table 7.2 Characteristics of the NSCs attached to the P-structures with different vertical mass irregularities.

Building case	$T_C = T_1$			$T_C = T_2$			$T_C = T_3$		
	T [s]	L_a [m]	K_a [N/m]	T [s]	L_a [m]	K_a [N/m]	T [s]	L_a [m]	K_a [N/m]
Reference	2.13	2.71	80.49	1.87	2.49	103.76	1.66	2.30	131.66
B-1-2	2.13	2.71	80.49	1.88	2.50	102.52	1.69	2.33	126.64
B-1-4	2.14	2.72	79.60	1.89	2.51	101.30	1.71	2.35	123.44
B-2-2	2.14	2.72	79.60	1.89	2.51	101.31	1.71	2.35	123.44
B-2-4	2.15	2.73	78.73	1.90	2.52	100.10	1.72	2.35	123.44
B-3-2	2.14	2.72	79.60	1.89	2.51	101.31	1.71	2.35	123.44
B-3-4	2.17	2.75	77.03	1.92	2.53	98.92	1.72	2.35	123.44
M-1-2	2.16	2.74	77.87	1.91	2.52	100.10	1.73	2.36	121.87
M-1-4	2.21	2.78	74.56	1.95	2.56	95.48	1.75	2.38	118.83
M-2-2	2.19	2.77	75.37	1.93	2.54	97.76	1.74	2.37	120.34
M-2-4	2.29	2.85	69.20	2.00	2.60	91.14	1.80	2.43	111.64
M-3-2	2.21	2.78	74.56	1.95	2.56	95.48	1.75	2.38	118.83
M-3-4	2.35	2.90	65.68	2.14	2.72	79.60	1.85	2.47	106.30
T-1-2	2.18	2.76	76.19	1.92	2.53	98.92	1.75	2.38	118.64
T-1-4	2.28	2.84	69.93	2.00	2.60	91.14	1.82	2.44	110.27
T-2-2	2.23	2.80	72.97	1.97	2.58	93.28	1.80	2.43	111.64
T-2-4	2.42	2.96	61.77	2.12	2.71	80.49	1.95	2.56	95.48
T-3-2	2.27	2.83	70.68	2.01	2.61	90.10	1.83	2.45	108.93
T-3-4	2.55	3.06	55.91	2.29	2.85	69.20	2.05	2.65	86.08
TB-1-2	2.18	2.76	76.19	1.92	2.53	98.92	1.83	2.45	108.93
TB-1-4	2.29	2.85	69.20	2.03	2.63	88.06	1.91	2.52	100.10
TB-2-2	2.24	2.81	72.20	1.97	2.58	93.28	1.88	2.50	102.52
TB-2-4	2.44	2.97	61.15	2.15	2.73	78.73	2.02	2.62	89.07
TB-3-2	2.29	2.85	69.20	2.03	2.63	88.06	1.92	2.53	98.92
TB-3-4	2.57	3.08	45.83	2.34	2.89	66.37	2.15	2.73	78.73
TM-1-2	2.21	2.78	74.56	1.96	2.57	94.37	1.82	2.44	110.27
TM-1-4	2.35	2.90	65.68	2.07	2.66	85.11	1.93	2.54	97.76
TM-2-2	2.28	2.84	69.93	2.00	2.60	91.14	1.87	2.49	103.76
TM-2-4	2.56	3.07	55.36	2.25	2.82	71.43	2.10	2.69	82.30
TM-3-2	2.34	2.89	66.37	2.05	2.65	86.08	1.93	2.54	97.76
TM-3-4	2.73	3.20	48.89	2.50	3.02	58.16	2.23	2.80	72.97

7.5 Nonlinear Static Analyses of Irregular 20-storey RC P-structures

Nonlinear static (Push-over) analyses were carried out to evaluate the elastic and maximum seismic capacities of the reference and modified P-structures. The displacement values at near collapse (NC) that derived from the nonlinear static analyses were corrected by considering the torsional effect using the extension of the N2 procedure (Fajfar *et al.*, 2005b), as described in Section A1 of Appendix A.

Figure 7.13 shows the values of the normalised top floors displacements evaluated from push-over and elastic dynamic analyses of different cases of vertical mass irregularities. This figure also shows the torsional correction factors of the top displacements at NC. It can be seen from Figure 7.13, that the smallest and largest correction factors of 1.1 and 1.5 resulted due to the effect of the torsion, were observed for the cases of the P-structures termed as M-1-2 and TB-3-4 respectively. Furthermore, Figure 7.14 displays the values of the top displacements at NC obtained from push-over analyses together with the corrected values of the top displacements of the studied cases.

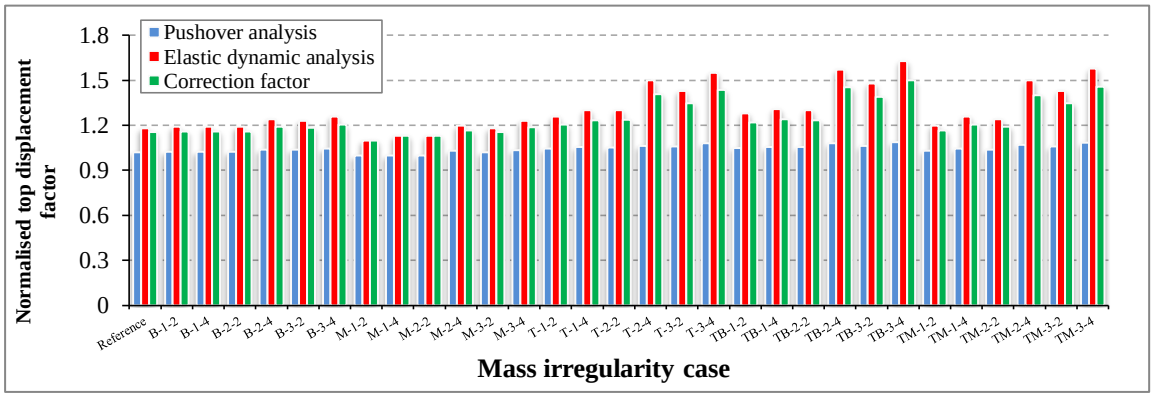

Figure 7.13 Push-over and elastic dynamic analyses results: normalised top displacement factors of different cases of vertical mass irregularities.

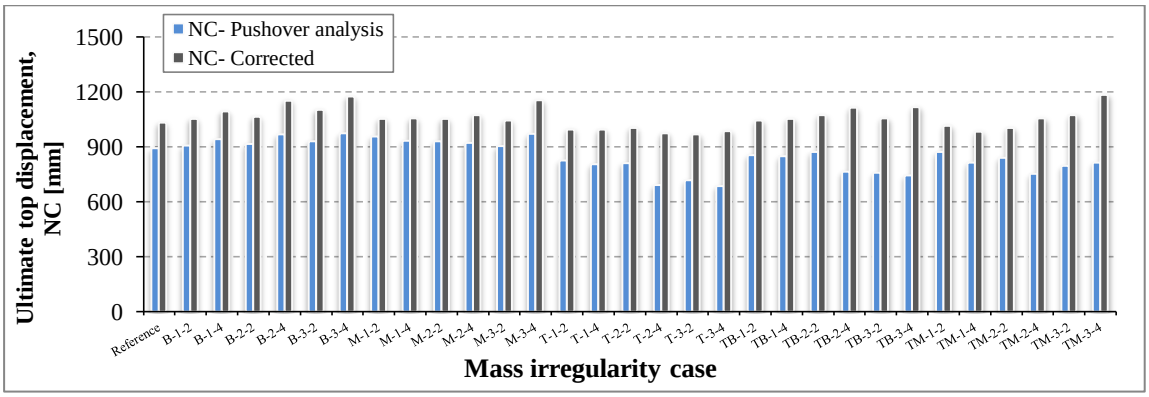

Figure 7.14 Push-over analyses results: corrected top displacements values due to torsional effect of different cases of vertical mass irregularities.

The corrected values of the top displacements as presented in Figure 7.14, which also given in Table 7.3 (see values of d_m) were used to evaluate the maximum seismic capacities of the P-structure with different cases of vertical mass irregularities. Table 7.3 shows the characteristics of the elastic-perfectly plastic of the strength-deformation curves, which were calculated according to the expressions of Annex B of EC8 (2004) as detailed in Appendix A (see Section A2).

Table 7.3 Maximum seismic capacities and characteristics of the idealised force-displacement relationships of the RC P-structure with different vertical mass irregularities.

Mass Case	Max. seismic capacity [g]	W [kN]	m^* [kg].10^3	Γ	F_y [kN]	d_m [m]	E_m [kN.m]	d_y [m]	T^* [s]	S_{ae} [g]	$de^*=d_t^*$ [m]	d_t [m]
Reference	0.65	337988.3	168.5	1.48	41436	1.03	33988.0	0.419	2.35	0.41	0.699	1.035
B-1-2	0.66	353834.1	171.7	1.50	43332	1.05	36176.6	0.430	2.35	0.42	0.713	1.069
B-1-4	0.67	385525.7	178.0	1.54	47109	1.09	40707.6	0.452	2.36	0.42	0.714	1.099
B-2-2	0.66	369679.9	175.6	1.52	45187	1.06	37934.7	0.441	2.36	0.41	0.703	1.068
B-2-4	0.67	433063.1	189.9	1.60	52614	1.15	48055.9	0.473	2.37	0.42	0.714	1.143
B-3-2	0.66	385525.7	180.4	1.54	46987	1.10	41325.5	0.441	2.36	0.41	0.694	1.069
B-3-4	0.66	480600.5	204.1	1.66	57874	1.17	53395.4	0.495	2.39	0.41	0.716	1.188
M-1-2	0.64	353834.1	178.0	1.49	42864	1.05	36017.1	0.419	2.38	0.39	0.686	1.022
M-1-4	0.63	385525.7	197.0	1.50	45620	1.05	38332.8	0.419	2.44	0.38	0.683	1.025
M-2-2	0.64	369679.9	186.7	1.50	44178	1.05	37121.2	0.419	2.41	0.39	0.698	1.047
M-2-4	0.62	433063.1	223.2	1.53	49320	1.07	42162.9	0.430	2.53	0.36	0.702	1.075
M-3-2	0.63	385525.7	197.0	1.50	45622	1.04	37878.3	0.419	2.43	0.39	0.698	1.047
M-3-4	0.64	480600.5	254.1	1.53	53277	1.15	49807.8	0.430	2.60	0.36	0.740	1.133
T-1-2	0.64	353834.1	184.3	1.42	42372	0.99	33289.1	0.409	2.41	0.39	0.700	0.994
T-1-4	0.64	385525.7	216.0	1.34	44120	0.99	34899.7	0.398	2.52	0.38	0.735	0.985
T-2-2	0.64	369679.9	199.4	1.38	43301	1.00	34684.7	0.398	2.46	0.39	0.706	0.975
T-2-4	0.63	433063.1	261.2	1.28	46672	0.97	36235.6	0.387	2.67	0.34	0.746	0.955
T-3-2	0.63	385525.7	213.6	1.36	44258	0.96	33681.1	0.398	2.51	0.37	0.709	0.964
T-3-4	0.62	480600.5	304.0	1.25	49231	0.98	38714.5	0.387	2.81	0.33	0.784	0.980
TB-1-2	0.66	369679.9	187.5	1.44	44221	1.04	36714.7	0.419	2.41	0.40	0.715	1.029
TB-1-4	0.66	433063.1	225.5	1.38	49428	1.05	41266.6	0.430	2.52	0.39	0.757	1.044
TB-2-2	0.66	401371.5	206.5	1.42	46893	1.07	40087.8	0.430	2.47	0.39	0.746	1.059
TB-2-4	0.67	528137.9	282.6	1.35	56572	1.11	50320.8	0.441	2.69	0.37	0.813	1.097
TB-3-2	0.65	433063.1	225.5	1.41	49478	1.05	41308.2	0.430	2.52	0.38	0.740	1.043
TB-3-4	0.64	623212.7	339.6	1.35	63169	1.11	55509.5	0.463	2.84	0.34	0.836	1.129
TM-1-2	0.64	369679.9	193.8	1.43	43769	1.01	35261.9	0.409	2.43	0.39	0.698	0.998
TM-1-4	0.62	433063.1	244.5	1.37	48100	0.98	37307.6	0.409	2.59	0.35	0.733	1.004
TM-2-2	0.63	401371.5	217.6	1.41	45948	1.00	36557.8	0.409	2.52	0.37	0.714	1.007
TM-2-4	0.62	528137.9	315.9	1.34	53878	1.05	45271.3	0.419	2.82	0.33	0.807	1.081
TM-3-2	0.65	433063.1	225.5	1.41	48235	1.07	40975.8	0.441	2.59	0.37	0.761	1.073
TM-3-4	0.64	623212.7	339.6	1.35	59679	1.18	55978.5	0.484	3.01	0.31	0.858	1.159

As shown in Table 7.3 that the maximum seismic capacities of the P-structures with different mass irregularities were found in the range between 0.62 g and 0.67 g, which correspond to d_m/d_t approximately equal to 1.0. For all the adopted cases, the values of PGA that correspond to the value of μ equal to 1.0 (i.e. values of elastic seismic capacities) were determined according to the results of nonlinear static analyses of the studied buildings and by using the expressions of Annex B of EC8 (2004). Table 7.4 gives the values of the elastic seismic capacities of the reference and modified cases.

Table 7.4 Elastic seismic capacities of the RC P-structure with different vertical mass irregularities.

Mass Case	Elastic seismic capacity [g]	S_{ae} [g]	S_{ay} [g]
Reference	0.213	0.162	0.163
B-1-2	0.216	0.164	0.165
B-1-4	0.222	0.167	0.169
B-2-2	0.218	0.166	0.166
B-2-4	0.224	0.169	0.170
B-3-2	0.218	0.165	0.166
B-3-4	0.219	0.168	0.168
M-1-2	0.210	0.158	0.159
M-1-4	0.205	0.151	0.151
M-2-2	0.208	0.154	0.155
M-2-4	0.199	0.142	0.142
M-3-2	0.205	0.151	0.151
M-3-4	0.209	0.134	0.134
T-1-2	0.213	0.159	0.159
T-1-4	0.210	0.149	0.150
T-2-2	0.211	0.154	0.154
T-2-4	0.204	0.137	0.137
T-3-2	0.208	0.149	0.149
T-3-4	0.199	0.126	0.127
TB-1-2	0.216	0.159	0.161
TB-1-4	0.219	0.154	0.156
TB-2-2	0.216	0.156	0.157
TB-2-4	0.218	0.145	0.145
TB-3-2	0.214	0.153	0.153
TB-3-4	0.214	0.134	0.135
TM-1-2	0.210	0.154	0.155
TM-1-4	0.203	0.140	0.141
TM-2-2	0.206	0.147	0.147
TM-2-4	0.196	0.124	0.125
TM-3-2	0.214	0.149	0.149
TM-3-4	0.214	0.127	0.128

The PGA values corresponding to the elastic and maximum seismic capacities of the P-structures were used to study the seismic behaviour of the NSCs as detailed in Section 7.6.

7.6 Dynamic Response of NSCs Attached to Irregular 20-storey RC P-structures

In this chapter, in order to evaluate the seismic response of NSCs, a set of seven artificial base motion records with duration of 30 seconds, was used in the nonlinear dynamic analyses. These records were generated the use of the computer code SIMQKE (SIMQKE, 1976; Gelfi, 2007). The EC8 (2004) Type 1 elastic response spectrum for ground type C together with a damping ratio of 5% were used as input to generate the seven accelerograms. More details about these artificial records can be found in Chapter 3 (see Section 3.3.2). A maximum value of standard deviation equal to 0.01 g was realised when the NSCs accelerations estimated under the effect of seven pairs of the adopted artificial records.

To study the effect of torsion that can be resulted from different cases of vertical mass irregularities, values of NSCs accelerations at the flexible side of a building should be recorded. In order to define the critical flexible region on the plan of the studied P-structure, a nonlinear dynamic analysis was implemented for the reference case of building under the effect of PGA value corresponding to the design value (0.345 g) of the P-structure. The values of the peak floors accelerations (PFA_{xy}) were estimated by using the method of square root of the sums of the squares (SQRSS) of accelerations in the X and Y directions. Figure 7.15 shows the contour lines of the floors accelerations resulted from the dynamic analysis of the reference case of building. A flexible side (FS) as specified in Figure 7.15(b) was recorded the maximum value of top floor acceleration (6.76 m/s^2); accordingly, this region was selected to accommodate the secondary systems, which investigated in this chapter. It can be

seen from Figure 7.15 that more than 25% of the total area of the top floor has been affected by high values of accelerations under the effect of earthquake with PGA value corresponding to the design ground acceleration of the P-structure. This percentage of the floor area may increase when the building is subjected to base motion with PGA values lager than the design value i.e. under severe earthquakes.

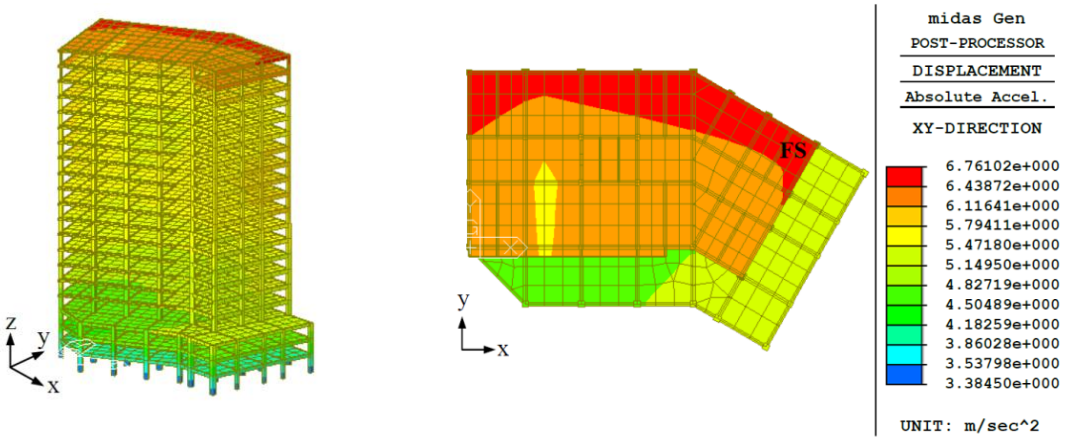

(a) (b)

Figure 7.15 Dynamic analysis results: floors acceleration contour lines of the reference case of irregular 20-storey RC P-structure (a) three-dimensional view and (b) top view.

Nonlinear dynamic analyses of the P-S systems were performed at PGA values ranging between 0.1 g and the maximum seismic capacities of the P-structures. For the NSCs with $T_C = T_1$-Reference and attached to the flexible side (FS) of the top floor of the reference structure (see Figures 7.3 and 7.15(b)), Figure 7.16 shows the variations of PCA_{xy} and A_p^a (the amplification factor for NSCs accelerations defined as $A_p^a = PCA_{xy}/PGA$) with PGA. Similar to the trend observed in previous chapters (see Figures 5.15, 5.16, and 6.5), Figure 7.16 shows that the acceleration amplification factor maximum value of 9.55 occurs at approximately the PGA value corresponding to the elastic seismic capacity (0.213 g) of the reference building. However, due to the effect of the nonlinearity behaviour of the P-structure, a reduction was

found in the values of the acceleration amplification factors under the effect of earthquakes with values of PGA larger than 0.213 g. For example, the acceleration amplification factors were 8.33 and 6.38 for the NSCs the NSCs with $T_C = T_1$-Reference and attached to the top floor under effect of PGA value equal to 0.4 g and 0.6 g respectively.

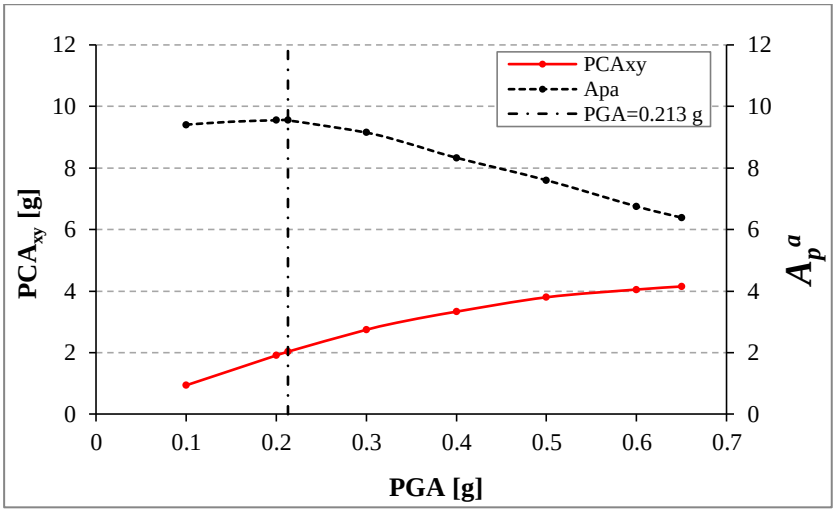

Figure 7.16 Variations of peak component acceleration (PCA_{xy}) and NSCs acceleration amplification factor (A_p^a) vs. peak ground acceleration (PGA) for the NSCs with $T_C = T_1$ and attached to the flexible side of the top floor of the reference building.

The acceleration response of rigid NSCs as well as that of NSCs with vibration periods matching the second or third vibration periods of the reference P-structure was studied at the PGA value of 0.213 g. Figure 7.17 compares the average values of PCA_{xy} for the aforementioned NSCs with the corresponding values for the NSCs with $T_C = T_1$-Reference. It can be seen from Figure 7.17 that the NSCs with $T_C \approx 0$ s and $T_C = T_1$-Reference had the minimum and maximum accelerations respectively. For rigid NSCs and NSCs with $T_C = T_3$-Reference, T_2-Reference and T_1-Reference, the predicted PCA_{xy} values at the top floor level were 0.39 g, 1.34 g, 1.64 g, and 2.03 g respectively. As would be expected, the accelerations of NSCs attached to the top floors were larger than the accelerations of those attached to the lower floors. This is attributable to the fact that the seismic load intensity

increases with increasing height of the P-structure. This point is recognised and implemented by the majority of current seismic design codes such as UBC (1997), IBC (2012), EC8 (2004), and ASCE (2010). For example, EC8 (2004) provisions suggest acceleration amplification factors of 5.5 and 2.5 for NSCs in resonance with the fundamental vibration period of the P-structure and attached at the top floor and ground floor levels respectively. Of note is that a comparable trend can be observed for the variation of floor rotation (θ) along the height of the reference P-structure. As can be seen in Figure 7.18, the values of floor rotation increased nonlinearly with increasing height of the P-structure, and the maximum value of floor rotation was predicted at the top floor level.

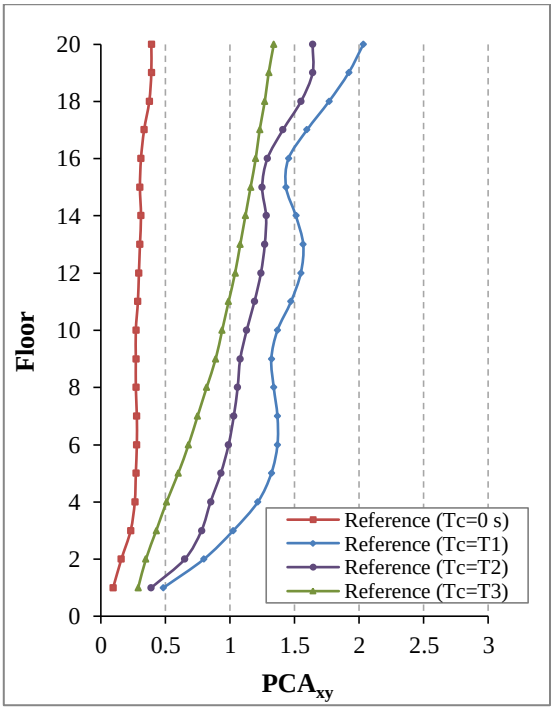

Figure 7.17 Variations of NSCs accelerations (PCA_{xy}) along the height of the reference P-structure at the PGA value of 0.213 g.

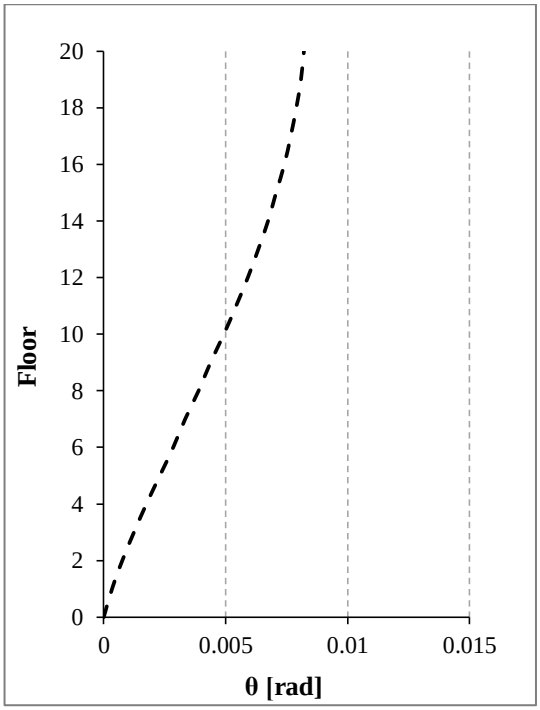

Figure 7.18 Variation of floor rotation (θ) along the height of the reference P-structure at the PGA value of 0.213 g.

Figures 7.19 to 7.23 compare the results of the normalised NSCs accelerations (PCA_{xy} Modified / PCA_{xy} Reference) for the NSCs with $T_C = T_1$, and normalised floor rotations (θ Modified / θ Reference). The NSCs accelerations and floor rotations were normalised by dividing a given result for one of the thirty cases of mass irregularity depicted in Figures 7.6 to 7.10 by the corresponding result for the reference case.

Figure 7.19(a) shows that, when the lower floors of the P-structures had higher masses (see Figure 7.6), the NSCs attached to these floors had the maximum acceleration ratios. The main reason for this trend is that the maximum floor rotation ratios occurred at the lower floors as shown in Figure 7.19 (b). For example, the maximum accelerations of T_1-B-1-2 and T_1-B-3-4 were 11.3% and 34.5% higher, respectively, than the corresponding accelerations of T_1-Reference as the floor rotations of the corresponding P-structures were 14.5% and 59% higher, respectively, than the corresponding floor rotation of the reference P-structure. The effect of floor rotation on NSCs accelerations is detailed in Section 7.7.

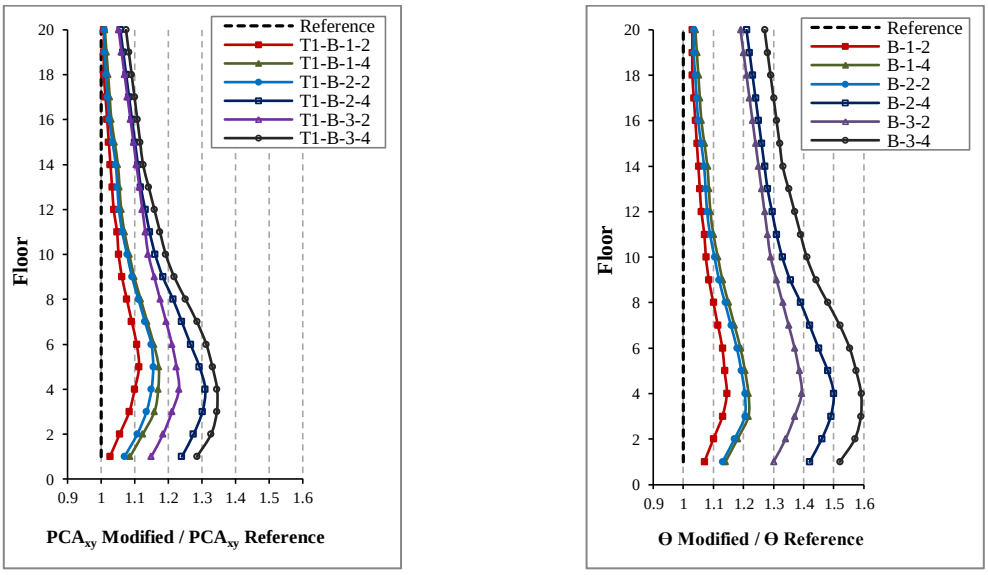

(a) (b)

Figure 7.19 Variations of (a) normalised NSCs accelerations and (b) normalised floor rotations along the heights of the P-structures with mass irregularity at their bottom floors.

Figure 7.20(a) shows that, when the middle floors of the P-structures had higher masses (see Figure 7.7), the accelerations of the NSCs were, in general, lower than the corresponding values for the NSCs mounted on the reference P-structure. This trend is clearly evident for T_1-M-1-2, T_1-M-1-4, T_1-M-2-2, T_1-M-2-4, and T_1-M-3-2. The only exception is the acceleration response of T_1-M-3-4 which was slightly higher than the corresponding response for T_1-Reference.

Figure 7.20(b) shows that, for cases M-1-2, M-1-4, and M-2-2, the top floor rotations were 23%, 15%, and 16% lower, respectively, than the corresponding value for the reference P-structure. Consequently, the accelerations of the NSCs attached to the top floors of the above-mentioned P-structures were 6%, 4%, and 4.5% lower, respectively, than the corresponding value for the NSCs mounted on the top floor of the reference P-structure.

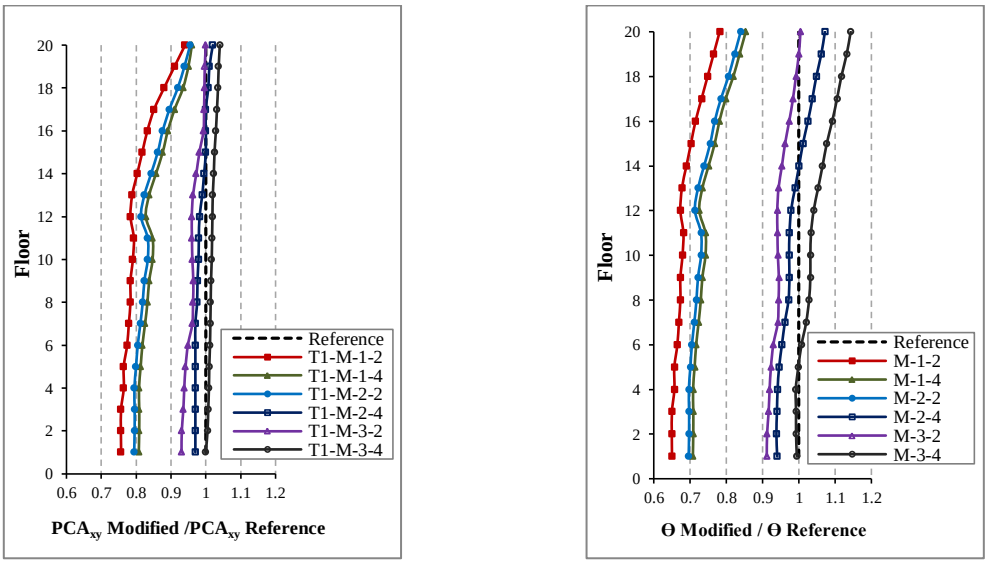

(a) (b)

Figure 7.20 Variations of (a) normalised NSCs accelerations and (b) normalised floor rotations along the heights of the P-structures with mass irregularity at their middle floors.

Figures 7.21(a) and 7.21(b) show, respectively, the variations of normalised NSCs accelerations and normalised floor rotations along the heights of the P-structures with mass irregularity at their top floors (see Figure 7.8). These cases of mass irregularity resulted in higher NSCs accelerations and floor rotations compared with the corresponding values for the reference case of mass irregularity, especially at the upper floors. The minimum and maximum percentage increases in normalised NSCs accelerations were 8% and 33%, respectively, for T_1-T-1-2 and T_1-T-3-4 respectively. The corresponding percentage increases in normalised floor rotations were 29% and 120% respectively.

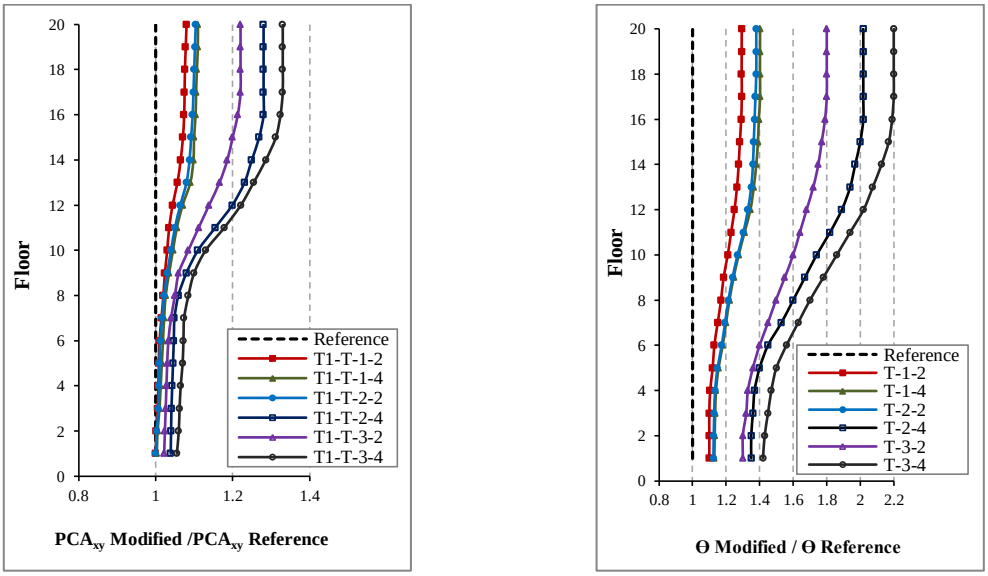

(a) (b)

Figure 7.21 Variations of (a) normalised NSCs accelerations and (b) normalised floor rotations along the heights of the P-structures with mass irregularity at their top floors.

The variations of normalised NSCs accelerations and normalised floor rotations along the heights of the P-structures with mass irregularity at their top and bottom floors are shown in Figures 7.22(a) and 7.22(b) respectively. Figure 7.22(a) shows that the maximum

normalised NSC acceleration is approximately 1.4 for T_1-TB-3-4. The corresponding normalised top floor rotation increased by a ratio of 2.47 as shown in Figure 7.22 (b).

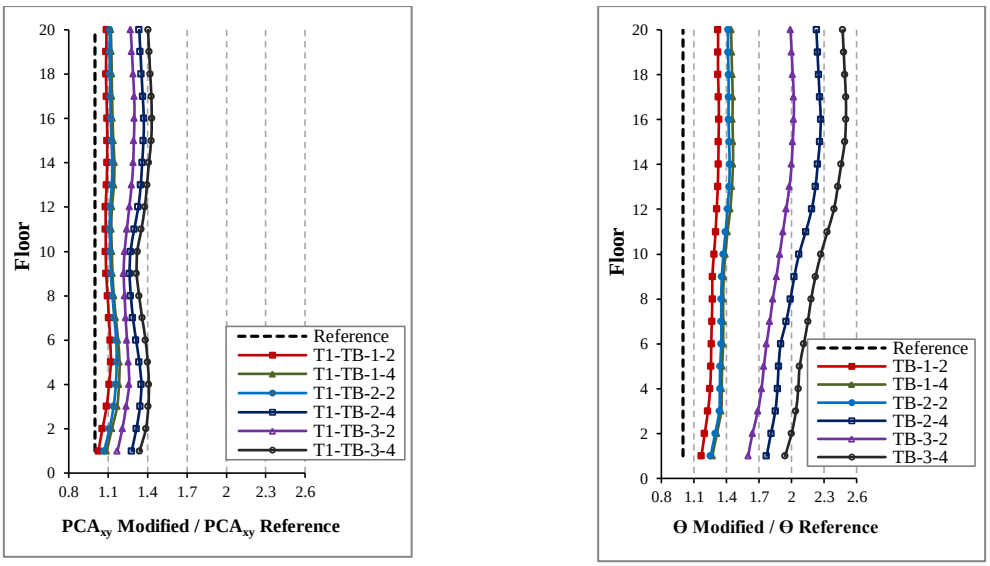

(a) (b)

Figure 7.22 Variations of (a) normalised NSCs accelerations and (b) normalised floor rotations along the heights of the P-structures with mass irregularity at their top and bottom floors.

For the P-structures with mass irregularity at their top and middle floors, Figure 7.23(a) shows that the accelerations of the NSCs attached to the upper floors were higher than the accelerations of the NSCs attached to the middle or lower floors. Moreover, the accelerations of T_1-TM-1-2, T_1-TM-1-4, and T_1-TM-2-2 were, in general, less than or approximately equal to the corresponding values for T_1-Reference. On the other hand, the accelerations of T_1-TM-2-4, T_1-TM-3-2, and T_1-TM-3-4 were, in general, higher than or approximately equal to the corresponding values for T_1-Reference. Comparable trends can be observed in Figure 7.23(b) for the normalised floor rotations.

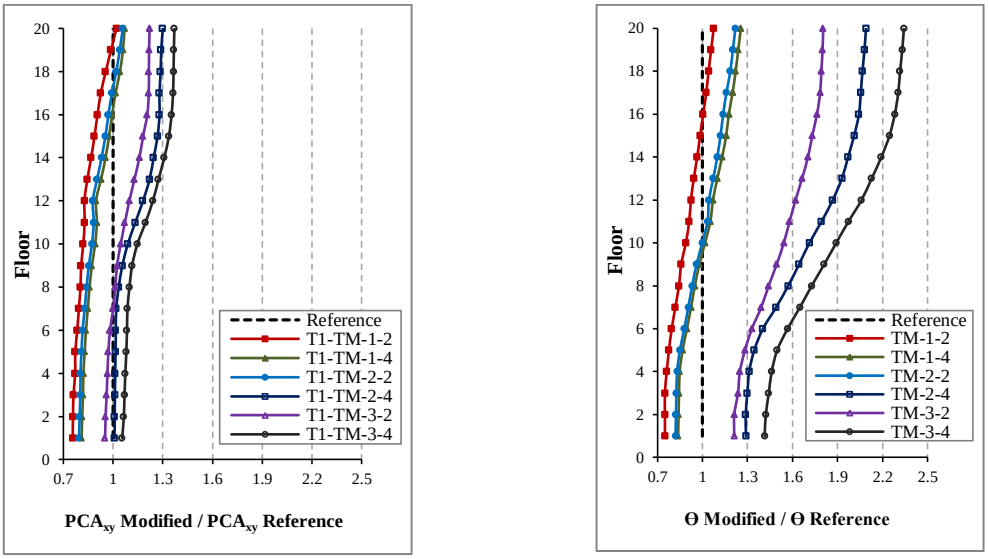

(a) (b)

Figure 7.23 Variations of (a) normalised NSCs accelerations and (b) normalised floor rotations along the heights of the P-structures with mass irregularity at their top and middle floors.

Except for the NSCs attached to the P-structures with mass irregularity at their middle or top and middle floors, the NSCs accelerations at the flexible sides of the modified P-structures were higher than the corresponding values at the flexible side of the reference P-structure. Furthermore, it can be concluded that the vertical mass irregularities B-3-4, T-3-4, TB-3-4, and TM-3-4 were critical as they resulted in NSCs accelerations that were 33% to 40% higher than the corresponding accelerations for the NSCs attached to the reference P-structure with uniform mass distribution.

Figure 7.24 summarises the numerical results (values of the top floors rotations and PCA_{xy} recorded at the roof level of the P-structure with different vertical mass irregularities) that were presented in Figures 7.19 to 7.23. It can be found from Figure 7.24 that there is a relation between the variation in the values of floors rotations and the values of PCA_{xy}. For instance, in the cases of masses termed as: T_1-M-1-2, T_1-M-1-4, and T_1-M-2-2, there were

found reductions in the percentage of PCA_{xy} with respect to the reference mass case due to the decreases in the percentage of the floors rotations of the irregular building cases: M-1-2, M-1-4, and M-2-2 respectively. For the above-mentioned irregular mass cases respectively, the percentage of decrease of the top floors rotations were found equal to 23%, 15%, and 16%. These also caused reduction in the values of PCA_{xy} with respect to the reference case by 6%, 4%, and 4.5%, respectively.

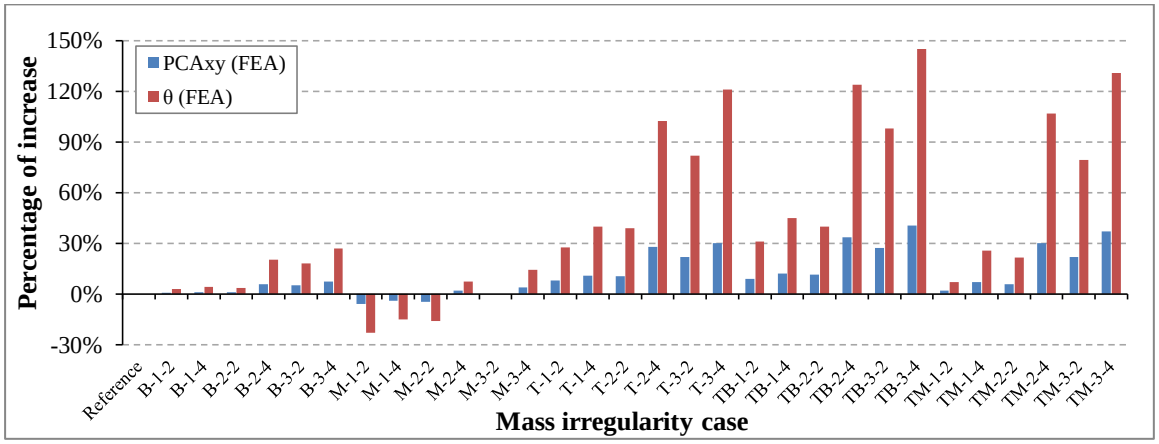

Figure 7.24 Percentage of variations in the values of the top floors rotations (θ) and the peak component accelerations (PCA_{xy}) with $T_C = T_1$ for different cases of vertical mass irregularities.

It can be concluded from Figure 7.24, that the critical mass cases are the modified buildings termed as B-3-4, M-3-4, T-3-4, TB-3-4, and TM-3-4 (i.e. the total mass ratio equal to 12 with mass irregularities located at the bottom, middle, top, top and bottom; and top and middle, respectively). The rotation values of the top floors of these critical cases increased by 27%, 14.2%, 121%, 145%, and 130%, respectively, with respect to the reference case. As a result, the PCA_{xy} values at the top floors increased by 7.4%, 4%, 30%, 40.4%, and 37%, respectively.

For the NSCs with $T_C = T_1$ and attached at the top floor level, analytical relationships were proposed (see Figure 7.25) between the percentage increase in NSCs accelerations, with respect to the corresponding values for T_1-Reference, and the increase in total mass ratio, Ḿ (i.e. Ḿ= $\dot{\eta}.m_r$).

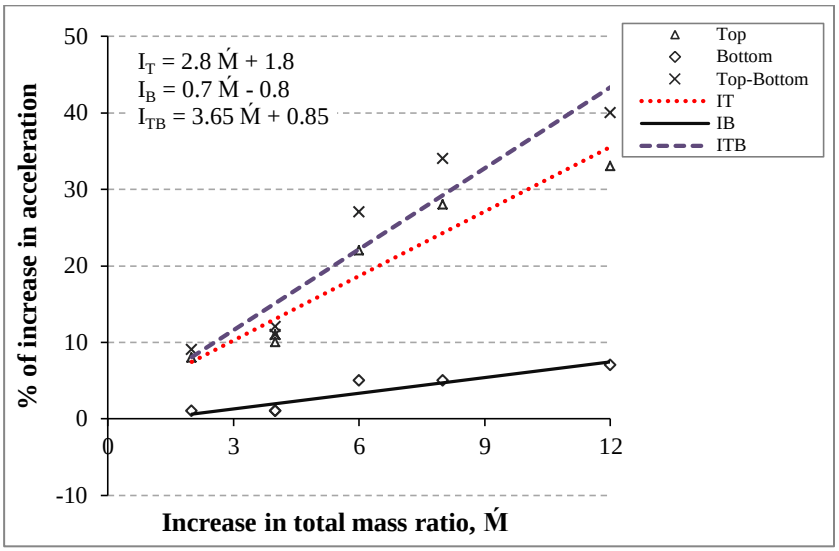

(a)

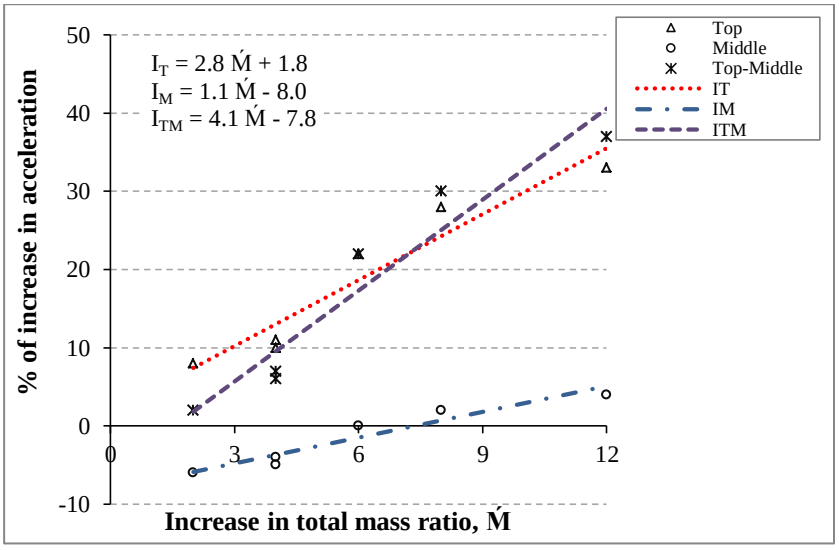

(b)

Figure 7.25 Relationships between the percentage increase in accelerations of the NSCs with $T_C = T_1$ and the increase in total mass ratio: (a) top and bottom floors and (b) top and middle floors.

The terms I_T, I_B, and I_{TB} in Figure 7.25(a) refer to the percentage increase in NSCs accelerations when the mass irregularity is at the top, bottom, or top and bottom floors respectively. Similarly, the terms I_M and I_{TM} in Figure 7.25(b) denote the percentage increase in NSCs accelerations when the mass irregularity is at the middle, or top and middle floors respectively. It can be seen from Figures 7.25(a) and 7.25(b) that, at the top floor level, the NSCs accelerations increase linearly with the increase in total mass. The maximum percentage increase in the accelerations of the NSCs with $T_C = T_1$ and attached at the top floor level was 44.65% for T_1-TB-3-4 (i.e. for the case of total mass ratio equal to 12).

The percentages of increase in the responses of NSCs having periods equal to T_2, T_3, and $T_C \approx 0$ s are also determined. A summary of the numerical results of these periods is presented in Figures 7.26, 7.27, and 7.28 respectively to the above-mentioned period values. It can be observed that in the case of all periods under consideration, the NSCs were behaved linearly amplifying in their responses due to the increase in the total mass ratios. In the case of the NSCs with periods equal to T_2, the maximum percentages of increase in the acceleration response as shown in Figures 7.26(a) and 7.26(b) were found equal to 40% and 37.7% for those NSCs termed as T_2-TB-3-4 and T_2-TM-3-4 respectively. While these maximum values were observed equal to 36.8% and 33.4% for the NSCs that had a period equal to T_3 for those labelled as T_3-TB-3-4 and T_3-TM-3-4 respectively, as shown in Figures 7.27(a) and 7.27(b). The lowest percentages of increase in the accelerations were observed for rigid NSCs (i.e. $T_C \approx 0$ s) which defined as T_0-TB-3-4 and T_0-TM-3-4, as displayed in Figures 7.28(a) and 7.28(b). The percentages were found equal to 30.7% and 28.2% respectively. By using the proposed equations that were reported in Figures 7.25 to 7.28 and re-written in Table 7.5, the percentage values of increase in the acceleration of NSCs attached to the top floor of the

modified cases can be obtained for values of total ratios of mass irregularities ranging between 2 and 12.

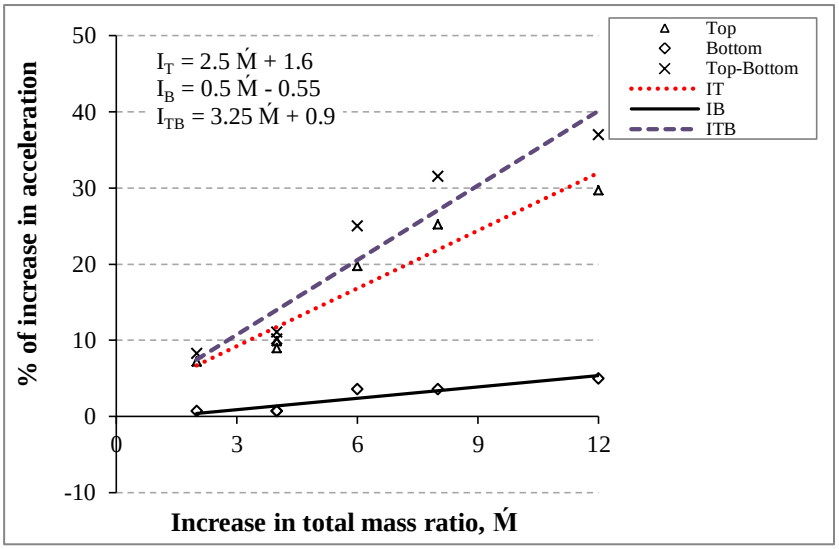

(a)

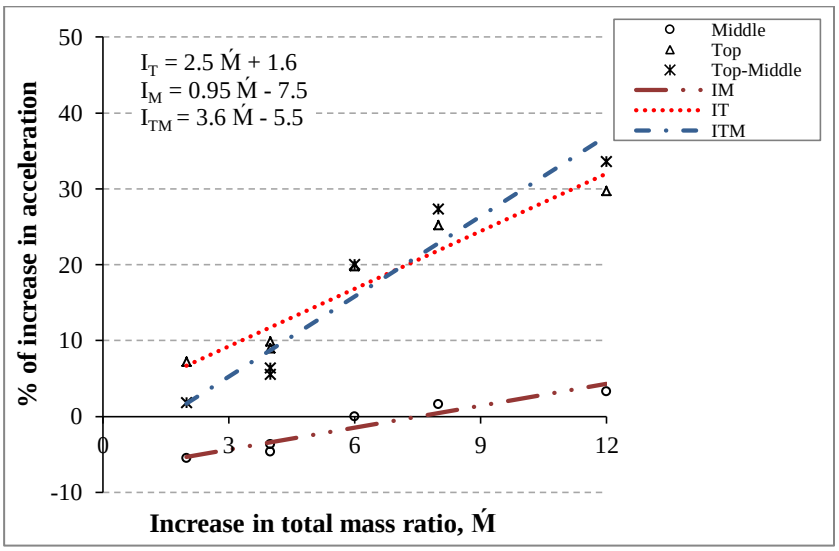

(b)

Figure 7.26 Relationships between the percentage increase in accelerations of the NSCs with $T_C = T_2$ and the increase in total mass ratio: (a) top and bottom floors and (b) top and middle floors.

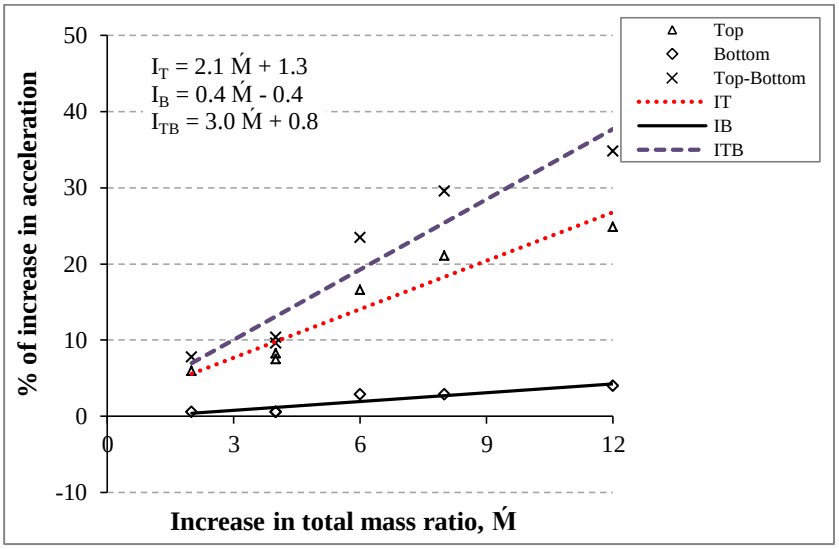

(a)

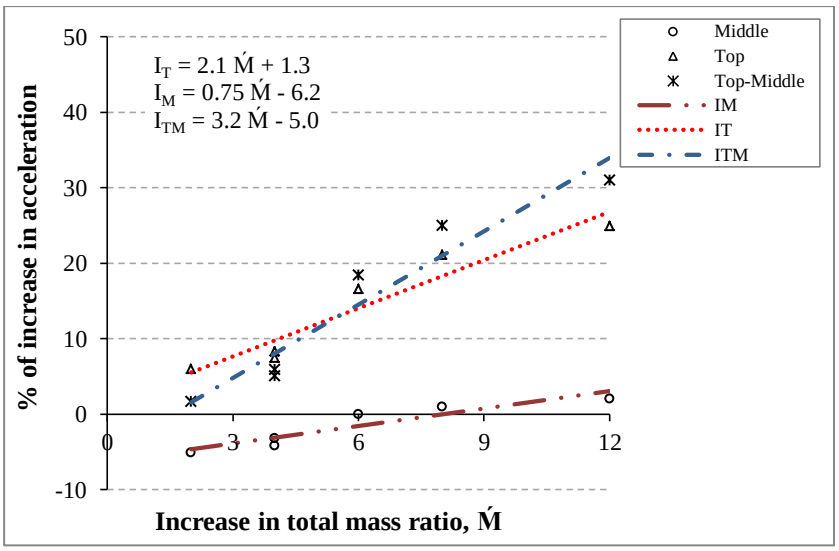

(b)

Figure 7.27 Relationships between the percentage increase in accelerations of the NSCs with $T_C = T_3$ and the increase in total mass ratio: (a) top and bottom floors and (b) top and middle floors.

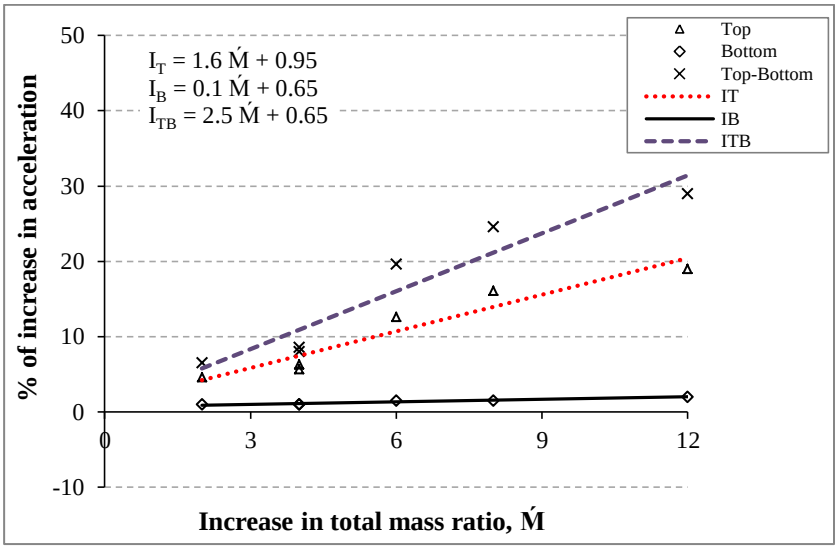

(a)

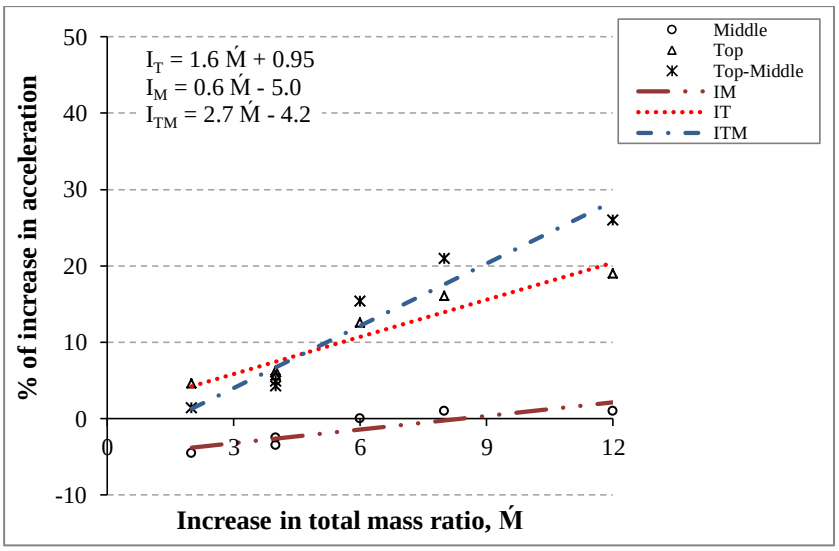

(b)

Figure 7.28 Relationships between the percentage increase in accelerations of the NSCs with $T_C \approx 0$ s and the increase in total mass ratio: (a) top and bottom floors and (b) top and middle floors.

Table 7.5 Proposed equations for the calculation of the increase percentages in the values of PCA_{xy} at the top floor of the P-structure due to the increase in the total mass ratios for different locations of mass irregularities.

NSCs period	Mass Location	% of increase in PCA_{xy}	Equation's No.
T_1	Top	$I_T = 2.8\,\acute{M} + 1.8$	(7-1)
	Bottom	$I_B = 0.7\,\acute{M} - 0.8$	
	Top-Bottom	$I_{TB} = 3.65\,\acute{M} + 0.85$	
	Middle	$I_M = 1.1\,\acute{M} - 8.0$	
	Top-Middle	$I_{TM} = 4.1\,\acute{M} - 7.8$	
T_2	Top	$I_T = 2.5\,\acute{M} + 1.6$	(7-2)
	Bottom	$I_B = 0.5\,\acute{M} - 0.55$	
	Top-Bottom	$I_{TB} = 3.25\,\acute{M} + 0.90$	
	Middle	$I_M = 0.95\,\acute{M} - 7.5$	
	Top-Middle	$I_{TM} = 3.6\,\acute{M} - 5.5$	
T_3	Top	$I_T = 2.1\,\acute{M} + 1.3$	(7-3)
	Bottom	$I_B = 0.4\,\acute{M} - 0.4$	
	Top-Bottom	$I_{TB} = 3.0\,\acute{M} + 0.8$	
	Middle	$I_M = 0.75\,\acute{M} - 6.2$	
	Top-Middle	$I_{TM} = 3.2\,\acute{M} - 5.0$	
T_0	Top	$I_T = 1.6\,\acute{M} + 0.95$	(7-4)
	Bottom	$I_B = 0.1\,\acute{M} + 0.65$	
	Top-Bottom	$I_{TB} = 2.5\,\acute{M} + 0.65$	
	Middle	$I_M = 0.6\,\acute{M} - 5.0$	
	Top-Middle	$I_{TM} = 2.7\,\acute{M} - 4.2$	

7.7 Torsional Amplification Factor for NSCs Accelerations

In this section, torsional amplification factors of NSCs (F_T) were evaluated under the effect of base motions with PGA values corresponding to the elastic and maximum seismic capacities of the P-structures (as given in Tables 7.4 and 7.3). Figure 7.29 shows values of peak

component accelerations at the flexible sides ($PCA_{xy,FS}$) and the corresponding values at the centres of rigidity ($PCA_{xy,CR}$) for NSCs with vibration periods equal to T_1 and attached to the top floors (see Figure 7.3 – locations of FS and CR) of the studied cases of vertical mass irregularities. Moreover, under the effect of the same values of the PGA (i.e. elastic and maximum seismic capacities), values of the top floors rotational displacements (θ) of the P-structure that had different cases of vertical mass irregularities were also reported, as shown in Figure 7.30.

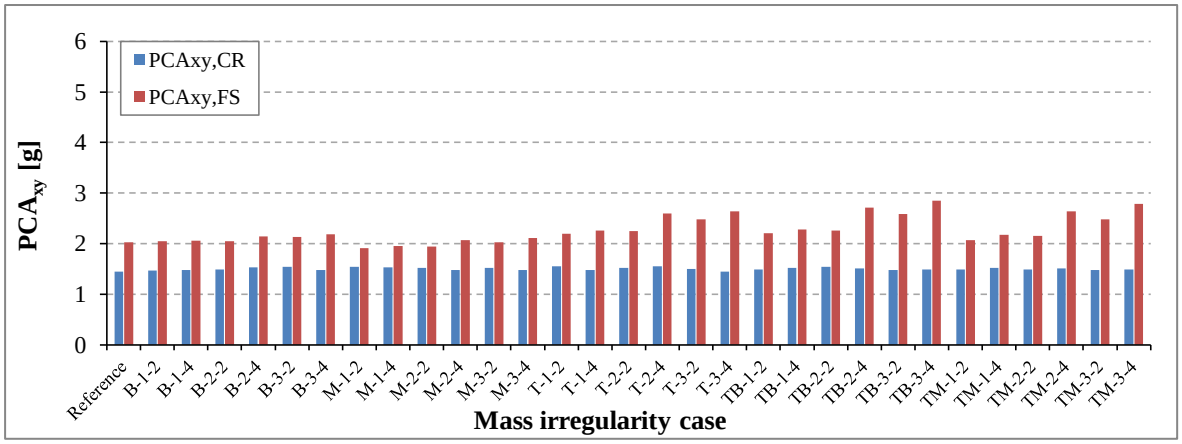

(a)

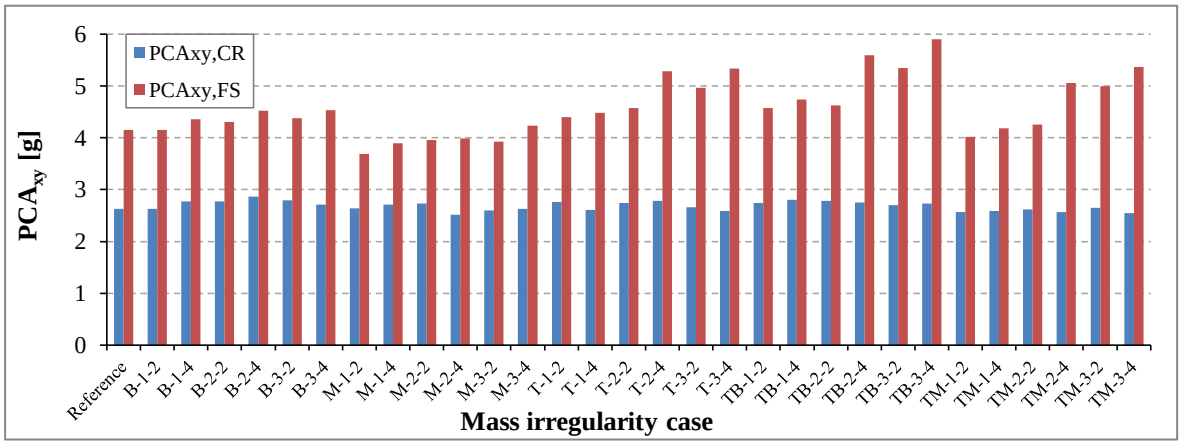

(b)

Figure 7.29 Values of peak component accelerations (PCA_{xy}) for the NSCs with $T_C = T_1$ and attached to the centres of rigidity (CR) and the flexible sides (FS) of the top floor of the P-structure that had different vertical mass irregularities at the PGA values corresponding to (a) the elastic seismic capacities and (b) the maximum seismic capacities.

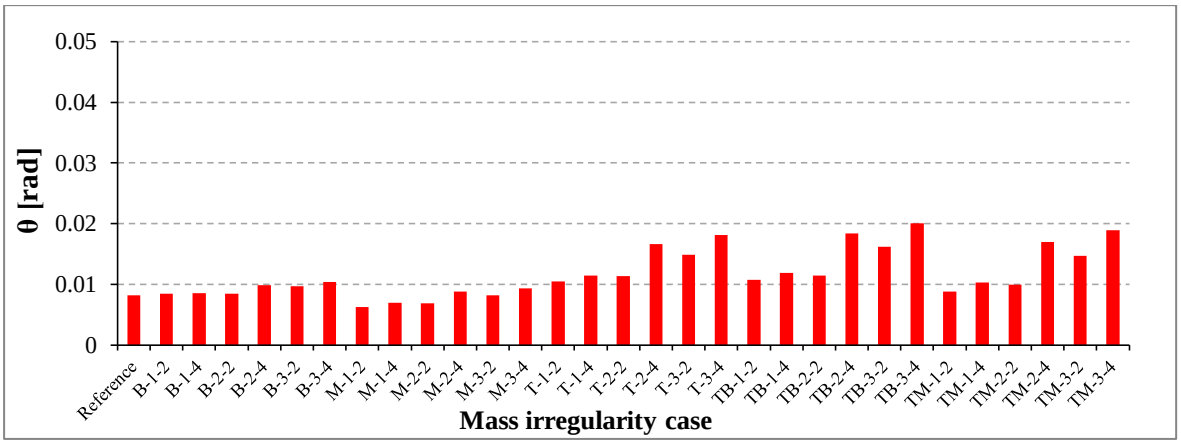

(a)

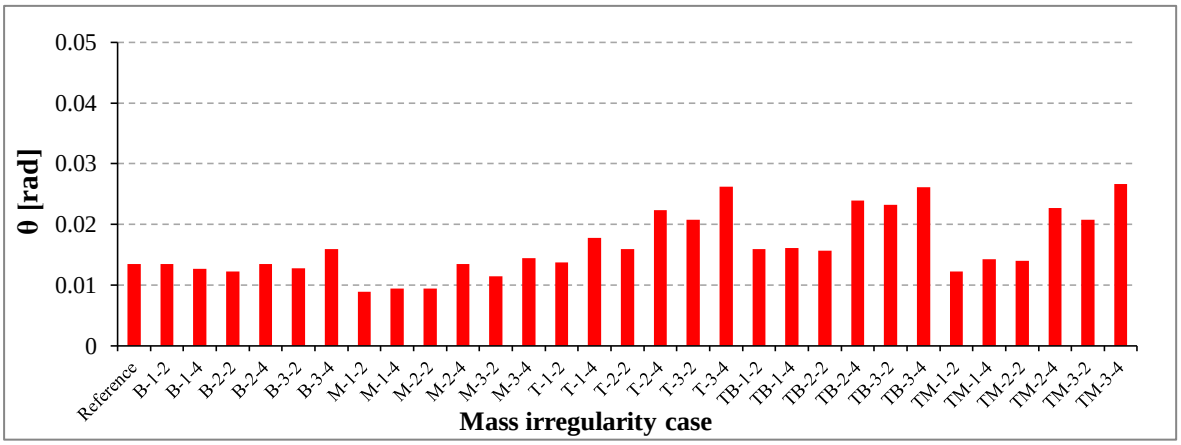

(b)

Figure 7.30 Values of top floors rotations (θ) of the P-structures with different vertical mass irregularities at the PGA values corresponding to the (a) elastic seismic capacities and (b) maximum seismic capacities.

According to the results presented in Figures 7.29 and 7.30, relation has been developed between the torsional amplification factor ($F_T = PCA_{xy,FS}/PCA_{xy,CR}$) and the top floor rotation θ. Shown in Figure 7.31 is the relation between the resulting values of F_T for NSCs having a period equal to T_1 and the values of θ. This relation can be expressed as follows:

$$F_T = 42.40\,\theta + 1.0 \qquad (7\text{-}5)$$

Equation (7-5) is valid for both symmetrical and asymmetrical P-structures. This equation results a value of F_T equal to 1.0 for the case of NSCs attached to the P-systems that can be classified as a plan and vertical regularity. Maximum standard deviations of 0.017 and 0.056 were found between Eq. (7-5) above and the corresponding relationship given in Eqs. (5-1) and (6-3) respectively.

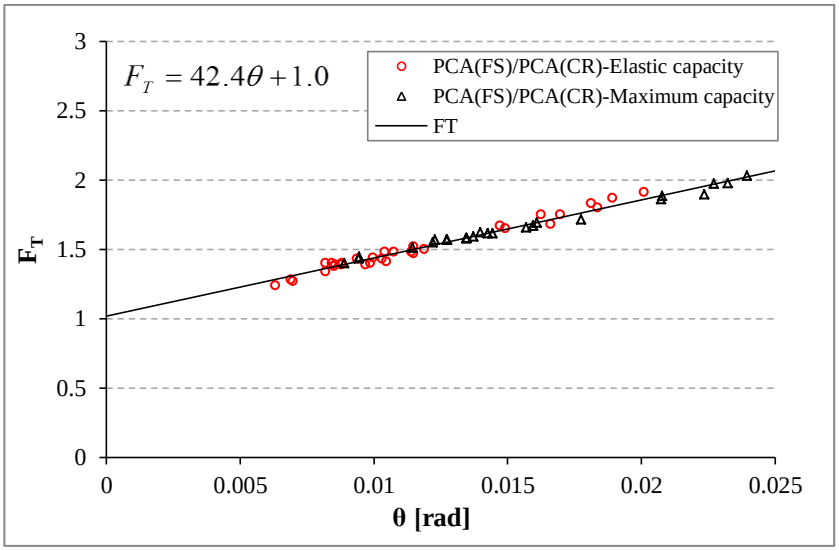

Figure 7.31 Relationship between the torsional amplification factor (F_T) for the NSCs with $T_C = T_1$ and top floor rotation (θ) of the P-structure with different vertical mass irregularities.

7.8 Comparison between the Dynamic Analysis Results and EC8 Predictions

One of the main objectives of the current investigation is to evaluate the adequacy of the EC8 (2004) provisions for the design of NSCs. This section reports on the comparison between the dynamic analysis results and EC8 (2004) predictions for NSCs accelerations. EC8 (2004) suggests the expression that given in Chapter 1 (see Eq. (1-1)) for the evaluating of the dynamic coefficient (S_a) viable to NSCs. The P-structures in this chapter (i.e. 20-storey, multi-bay RC buildings) were designed for a reference peak-ground acceleration a_{gR} value of 0.25 g on ground type A. An importance category III with a factor of γ_I equal 1.2 was used. Considering the soil factor of 1.15 for ground type C; hence, the term αS in Eq. (1-1) was taken as 0.345. Therefore, for comparison purposes between the FE results and the predictions of EC8 (2004), the earthquake records were scaled in such a way that their PGAs were equal to 0.345 g. Five critical cases of mass distribution; namely B-3-4; M-3-4; T-3-4; TB-3-4, and TM-3-4; in addition to the reference case were chosen for comparison purposes. Furthermore, NSCs with T_C = 0, T_1, T_2, and T_3 (see Table 7.2) and attached at varying heights along P-structures with different vertical mass irregularities were adopted in the comparison.

Figures 7.32, 7.33, 7.34, and 7.35 compare the dynamic analysis results with the predictions of EC8 (2004) for the acceleration of the NSCs with T_C = T_1, T_2, T_3, and 0s respectively. This is for NSCs with damping ratio of 3%. The PCA_{xy} values reported in Figures 7.32 to 7.35 are for those NSCs attached to the flexible side (FS) (see Figure 7.3) along the heights of the P-structures.

Figures 7.32 and 7.33 clearly show that EC8 (2004) underestimates the acceleration response of the NSCs (with $T_C = T_1$ and T_2 respectively) mounted on the flexible sides of the P-structures with the above-mentioned six vertical mass distributions. According to Eq. (1-1), EC8 (2004) predicts an acceleration of about 1.9 g for the NSCs attached to the top floors of the P-structures when the NSCs vibration periods match one of the P-structures vibration periods. The corresponding numerical results were 3.04 g, 3.26 g, 3.16 g, 4.03 g, 4.26 g, and 4.15 g for T_1-Reference, T_1-B-3-4, T_1-M-3-4, T_1-T-3-4, T_1-TB-3-4, and T_1-TM-3-4 respectively. These results show that EC8 (2004) underestimate the acceleration response of the NSC with $T_C = T_1$ with a mean predicted-to-numerical ratio of 0.53 and a standard deviation of 0.08. A comparable trend can be observed for the NSCs with $T_C = T_2$. EC8 (2004) underestimate the acceleration response of these NSCs with a mean predicted-to-numerical ratio of 0.63 and a standard deviation of 0.09. In addition, it can be seen from the results presented in Figure 7.29(b) that, EC8 (2004) predictions underestimated the values of PCA_{xy} (for NSCs with $T_C = T_1$) at the flexible side of the top floor up to 68% at the PGA value corresponding to the maximum seismic capacity of the P-structure had different cases of vertical mass irregularities.

For the NSCs with $T_C = T_3$, the acceleration values increased gradually from the lower to the upper floors, as shown in Figure 7.34. The dynamic analysis results for the accelerations of the NSCs with $T_C = T_3$ and attached to the flexible side of the top floors of the above-mentioned P-structures were 2.11 g, 2.21 g, 2.16 g, 2.65 g, 2.85 g, and 2.79 g for T_3-Reference, T_3-B-3-4, T_3-M-3-4, T_3-T-3-4, T_3-TB-3-4, and T_3-TM-3-4 respectively. The EC8 (2004) predictions underestimate the acceleration response of these NSCs with a mean predicted-to-numerical ratio of 0.78 and a standard deviation of 0.11.

For rigid NSCs with $T_C \approx 0$ s, EC8 (2004) predicts that the NSCs accelerations vary between 0.345 g and 0.863 g at the ground (z_c/H=0) and top floor (z_c/H=1) levels respectively. According to the EC8 provisions, these two values of accelerations are equivalent to the values of acceleration amplification factors of NSCs equal to 1.0 and 2.5 at the ground and roof levels respectively. It can be noted from Figure 7.35 that the FE predictions for the accelerations of T_0-reference, T_0-B-3-4, and T_0-M-3-4 are generally within the prediction range of EC8 (2004). However, EC8 (2004) underestimate the accelerations of T_0-T-3-4, T_0-TB-3-4, and T_0-TM-3-4 when the NSCs are attached at the lower third of the P-structures. At the 6th floor level (z_c/H = 0.31), EC8 (2004) predictions underestimate the acceleration response of these NSCs with a mean predicted-to-numerical ratio of 0.80 and a standard deviation of 0.03.

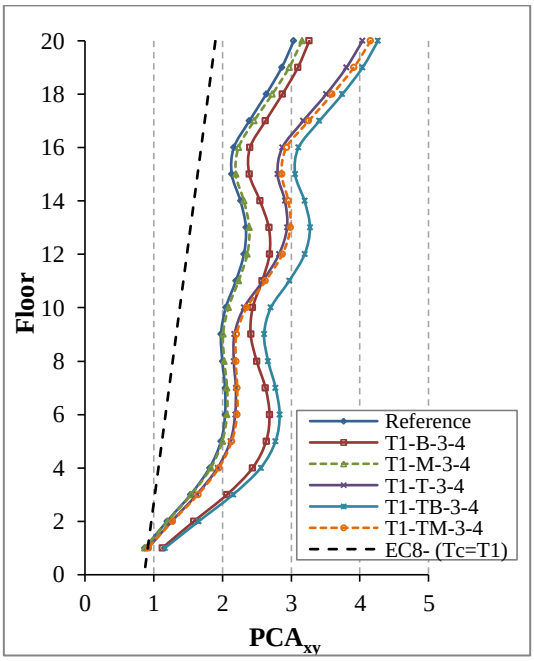

Figure 7.32 Comparison between the dynamic analysis results and EC8 (2004) predictions for the accelerations of the NSCs with $T_C = T_1$.

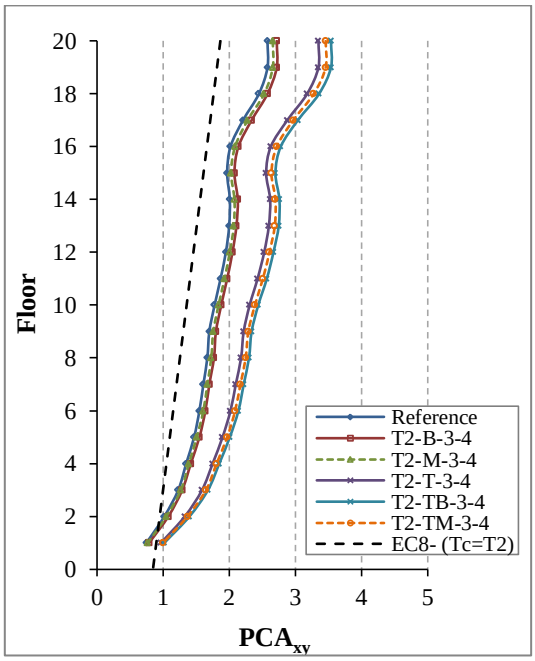

Figure 7.33 Comparison between the dynamic analysis results and EC8 (2004) predictions for the accelerations of the NSCs with $T_C = T_2$.

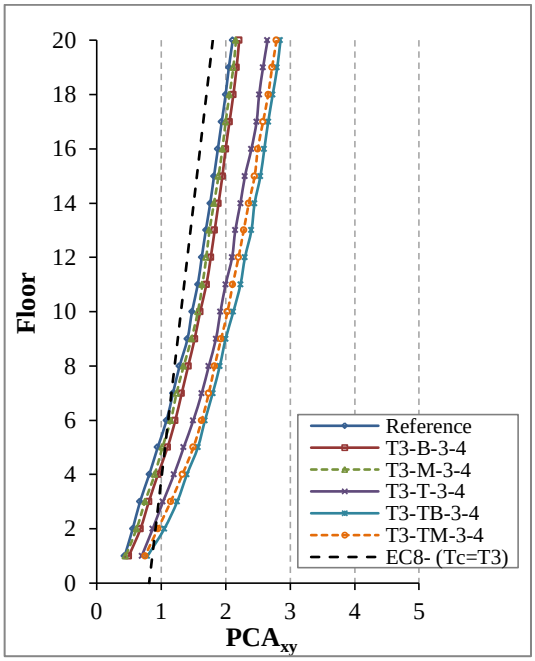

Figure 7.34 Comparison between the dynamic analysis results and EC8 (2004) predictions for the accelerations of the NSCs with $T_C = T_3$.

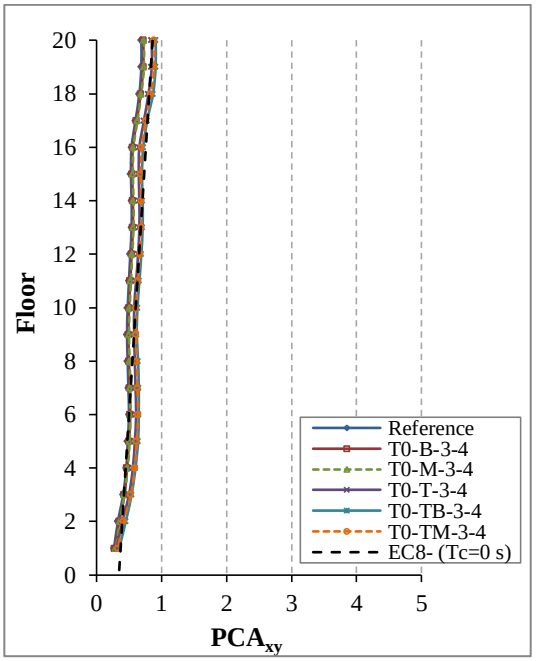

Figure 7.35 Comparison between the dynamic analysis results and EC8 (2004) predictions for the accelerations of the NSCs with $T_C \approx 0$ s.

To sum up, for the NSCs having periods equal to T_1, T_2, T_3, and $T_C \approx 0$ s and attached to the FS and CRs of the top floors of the reference and thirty cases of vertical mass irregularities, the comparison results between the predictions of EC8 (2004) and the numerical results are explained in Figures 7.36(a) to 7.36(d). It can be seen that the EC8 (2004) underestimates in the predictions of NSCs attached to the FS on average by 43.4%, 33.3%, and 19.9% for those having periods equal to T_1, T_2, and T_3, respectively. However, the majority values of PCA_{xy} for NSCs attached to the CRs for those having periods equal to T_2 and T_3 were found within the range of the predictions of the EC8 (2004), as shown in Figures 7.36(b) and 7.36(c) respectively. On the other hand, most of PCA_{xy} values for rigid NSCs ($T_C \approx 0$ s) attached to the FS and CRs of the top floors were found within the predictions of EC8 provisions under the effect of the PGA value corresponding the design value (0.345 g) for all the studied cases as shown in Figure 7.36(d). At the flexible sides of the top floors, EC8

(2004) predictions were observed to be overestimated the seismic response of the rigid NSCs on average by about 15.8%.

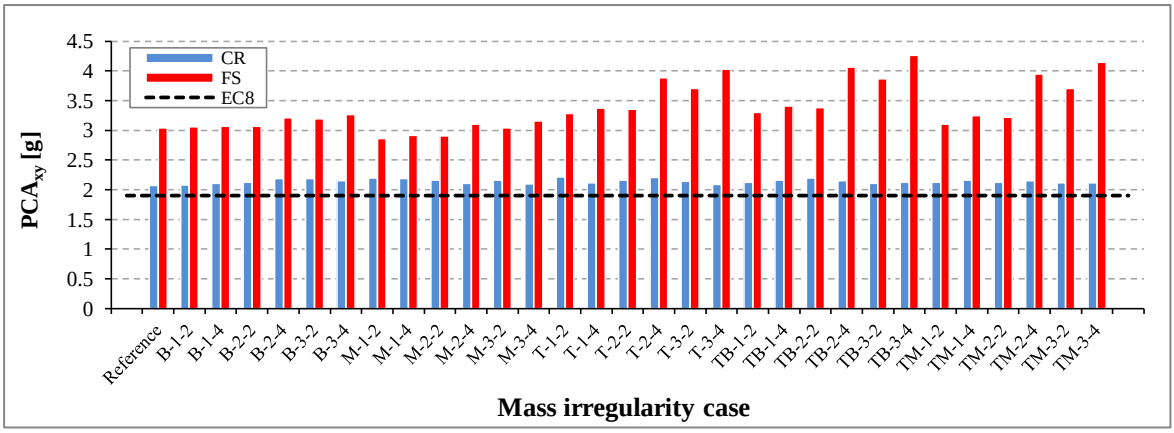

(a)

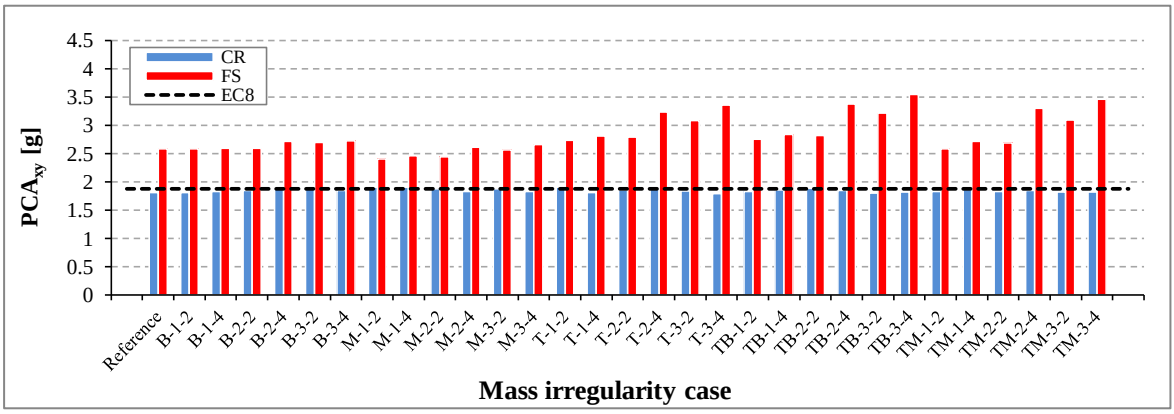

(b)

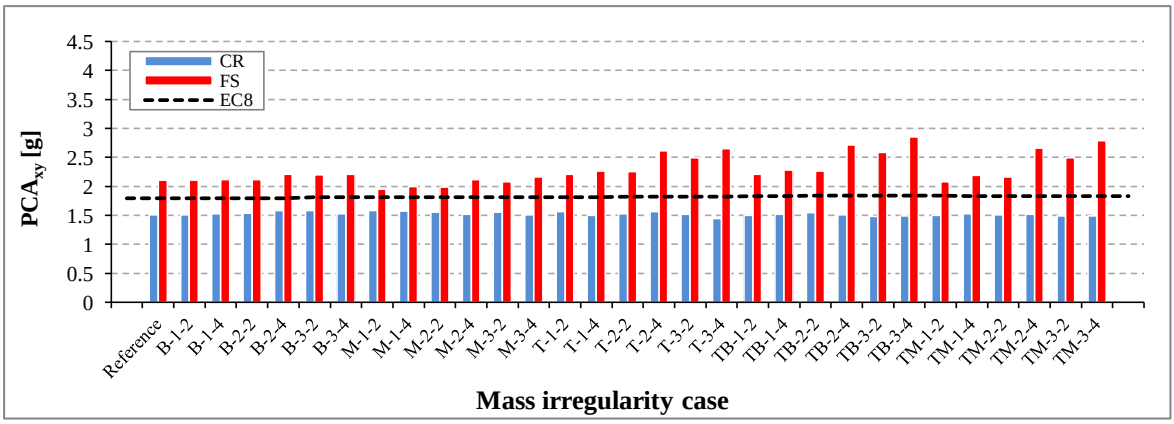

(c)

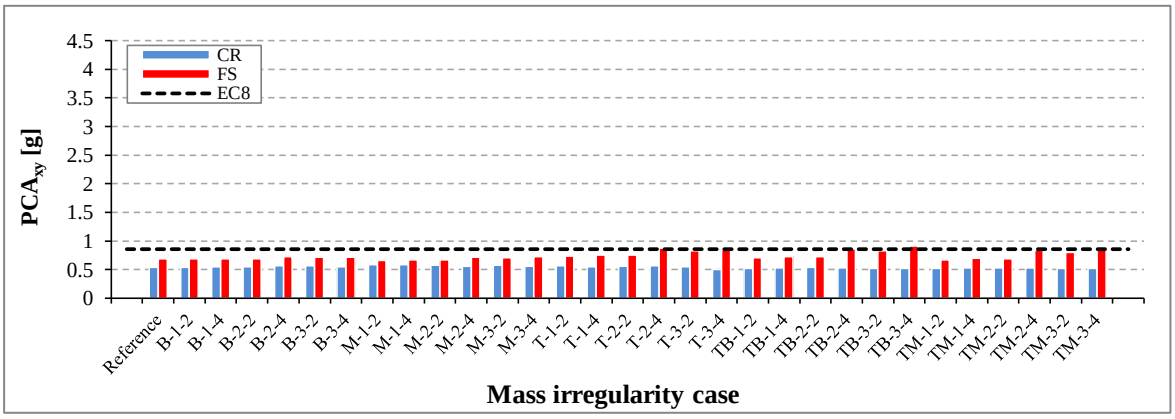

(d)

Figure 7.36 Comparison between FE and EC8 acceleration predictions for the NSCs attached to the centre of rigidity (CR) and the flexible side (FS) of the top floor of the P-structure with different cases of vertical mass irregularities, for the NSCs having periods equal to (a) T_1, (b) T_2, (c) T_3, and (d) $T_C \approx 0$ s.

7.9 Summary

Variation in the values of the acceleration responses of NSCs integrated on irregular 20-storey, multi-bay RC P-structure that had different cases of vertical mass irregularities with significant torsional modes was investigated in Chapter 7. Values of NSCs periods that were resonant with the first, second and third fundamental periods of the P-structures, as well as rigid NSCs were adopted.

The numerical results in Chapter 7 were evaluated based on the average of seven artificial ground motion inputs in the two horizontal directions (X and Y). Based on the numerical results, a number of expressions for the calculation of the percentages of increase in the values of peak component accelerations PCA_{xy} along the heights of the buildings due to the increases in the total mass ratios for different locations of mass irregularities were proposed. One of the more significant conclusions that can be found is that the percentages of

increase in the values of PCA_{xy} at the roof levels increased linearly as a result of increase in the total masses. In the case of the NSCs with vibration periods equal to T_1, the maximum percentages of increase in the values of PCA_{xy} were 44.7% and 41.4% for the NSCs termed as T_1-TB-3-4 and T_1-TM-3-4 respectively.

Furthermore, torsional amplification factor F_T of NSCs acceleration was proposed in terms of the top floors rotational displacements at PGA values corresponding to both the elastic and maximum seismic capacities of the P-structure with different cases of vertical mass irregularities.

The numerical results of the NSCs accelerations along the height of the P-structure with thirty cases of vertical mass irregularities were compared with the predictions of the EC8 at the PGA value corresponding to the design ground acceleration. Overall, the most obvious finding to emerge from these comparisons is that the current recommendations of EC8 (2004) underestimated the acceleration responses of NSCs that were attached to the flexible sides. For the NSCs with periods equal to T_1 and damping ratio of 3%, the current EC8 provisions underestimated the NSCs accelerations on average by 43.4%.

Therefore, according to the findings presented in Chapters 5 and 6, as well as in Chapter 7, the current EC8 equation for the seismic design of the NSCs at resonant condition with the fundamental vibration periods of the P-structures would need to be modified to consider the effects of both the torsional behaviours and maximum seismic capacities of irregular P-structures.

CHAPTER EIGHT: MODIFICATION OF THE EC8 EXPRESSION FOR THE DESIGN OF NSCs

8.1 General

In most of the seismic provision codes such as UBC (1997), EC8 (2004), and ASCE (2010), the importance of the acceleration amplification factor in the design of the S-systems is for both safety and functional purposes when the P-S systems are subjected to base motions with PGA value either equal to or larger than the design ground acceleration of the P-structure. Therefore, critical NSCs such as mechanical, electrical, or medical equipment should be designed so as they can remain operational in lifeline structures such as power and chemical plants, and hospitals during and after earthquakes. Therefore, such as NSCs may require to be designed to withstand earthquakes without failure or damage up to the PGA value corresponding to the maximum seismic capacity of the P-structure.

The comparisons between the finite element analyses FEA results and the predictions of EC8, which were implemented in Chapters 5, 6, and 7 showed that the EC8 (2004) underestimated the seismic responses of the NSCs at the design ground acceleration values when they were mounted on the flexible sides of different cases of irregular RC P-structures subjected to bi-directional earthquakes. The perceived cause of these discrepancies is that EC8 does not explicitly consider the increase in the NSCs accelerations caused by the torsional behaviour of the P-structure. In addition, it was observed from the numerical results

that NSCs have also been affected by the seismic capacities of the P-structures when they designed on different ground types. Based on the design provisions of the EC8 (2004), the NSCs can be designed using only the fundamental vibration periods of the primary and secondary systems. Therefore, the current equation of EC8 for the design of the NSCs is to be extended by taking into consideration the effects of the torsion and the maximum seismic capacity of the supporting structure. According to the EC8 (2004) provisions, the maximum values of the acceleration amplification factors, i.e. PCA/PGA at the top floor are taken as 2.5 and 5.5 respectively for rigid NSC with period approximately equal to zero and for the flexible NSC with period equal to the first fundamental vibration of the P-structure.

The value of the ductility factor μ may be used as an indicator of the degree of nonlinearity of each case of the building. The P-structures can be considered in the elastic range when the value of μ is within the range of 0.0 to 1.0; however, beyond this range, the value of μ can be used to evaluate the level of nonlinearity (EC8, 2004). Therefore, the value of the PGA that corresponds to the value of μ equal to 1.0 may be used to evaluate the maximum amplification factors of the accelerations of the NSCs. This trend was clearly observed in the results of Chapters 5, 6, and 7. It was observed that the maximum values of the acceleration amplification factors of the NSCs occurred when the P-S systems subjected to the base motions with PGA equal to the values of elastic seismic capacitates corresponding to the values of μ equal to 1.0.

In the following section, the methodology that adopted to extend the expression of EC8 (2004) for the design of the NSCs to account the effects of the torsional behaviour and the seismic capacities of the P-structures is explained.

8.2 Methodology on Modifying the EC8 Design Equation for NSCs

This section summarises the adopted methodology for the calculation of the maximum values of the acceleration amplification factors for NSCs attached to the flexible sides of the floors of irregular (vertical mass or/and plan irregularities) multi-storey RC P-structures. It also sets the basis of comparison between the FEA results and the predictions of the proposed formula for the seismic response of the considered cases of the NSCs. The adopted methodology suggests that the attached NSCs to the flexible sides of the irregular RC buildings can be influenced by the torsional behaviour and maximum seismic capacity of a P-structure. This methodology can be described as follows:

Step 1 (evaluate the elastic and maximum seismic capacities): values of both the elastic (i.e. PGA at μ = 1.0) and maximum (i.e. PGA at d_m/d_t = 1.0) seismic capacities of each case of the P-structure that the NSCs attached to its floors should be estimated. For each case of the considered P-structures, these two values of the seismic capacities have been estimated in Chapter 5 (see Tables 5.7 to 5.10) for the three groups of buildings. However, for buildings that had different eccentricity ratios for those investigated in Chapter 6, the elastic and maximum seismic capacities were reported in Tables 6.5 and 6.6. Furthermore, for buildings that characterised as vertical mass irregularities, these values of the seismic capacities were given in Chapter 7 (see Tables 7.3 and 7.4).

Step 2 (evaluate the values of the top floor rotations of the P-structures): values of the top floors rotational displacements should be evaluated under the effect of PGA value corresponding to the elastic seismic capacity of each case of the considered buildings. Linear

time-history analysis can be adopted to evaluate the values of the top floors rotations of the P-structures.

Step 3 (evaluate the torsional amplification factor): the mean value of the torsional amplification factors $F_{T\,mean}$ of the NSCs can be calculated from the mean of the relationships that were given in Eqs. (5-6), (6-3), and (7-5), as presented in Chapters 5, 6, and 7, respectively. Figure 8.1 shows the relations between the values of F_T and top floors rotations of the P-structures together with the expression of the $F_{T\,mean}$, as given as follows:

$$F_{T\,mean} = 43.8\,\theta + 1.0 \tag{8-1}$$

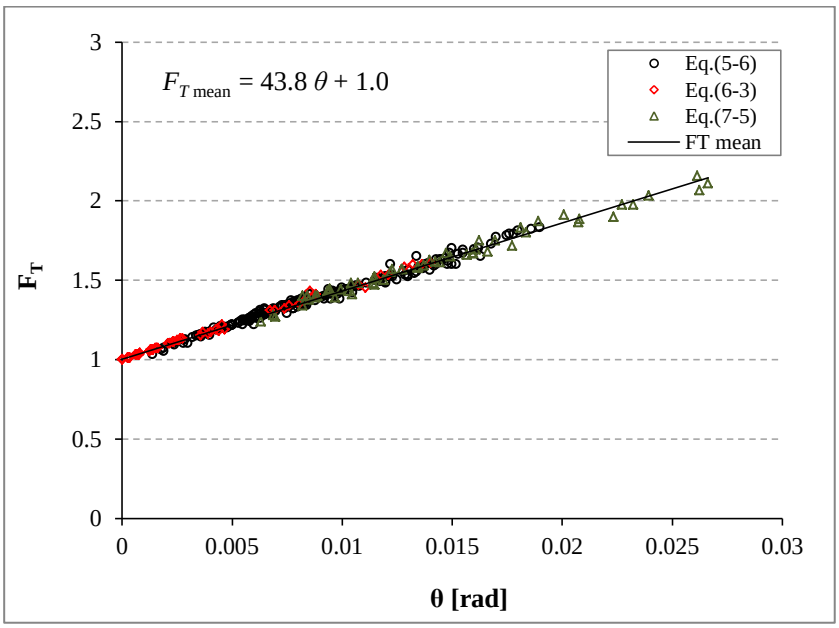

Figure 8.1 Relationship between the torsional amplification factor (F_T) for the NSCs with T_C equal to T_1 and top floor rotation (θ) of the adopted irregular RC P-structures.

Step 4 (modify the current expression of EC8, as presented in Eq. (1-1) for the design of the NSCs): the modification of the EC8 (2004) formula for the design of the NSCs can be

made by taking into account the effect of both the torsional amplification factor of NSC and the maximum seismic capacity factor of P-structure.

In the next sections, the FEA results of peak component accelerations of the NSCs attached to flexible sides of the first group of buildings (i.e. RC P-structures that physically tested or previously modelled by Negro *et al.* (2004) or by Rozman and Fajfar (2009) respectively), which presented in Chapter 5 are used to extend the current expression of the EC8 (2004) for the design of the NSCs. However, to assess the accuracy of the extended formula for the design of the NSCs, the FEA results of the acceleration responses of the NSCs attached to the other remaining P-structures are used. These buildings can be described as follows: (i) the second and third groups, which studied in Chapter 5; (ii) eight cases of the buildings that had different values of eccentricity ratios, which presented in Chapter 6; (iii) the thirty-one cases of vertical mass irregularities that investigated in Chapter 7.

8.3 Extension of the EC8 Expression for the Design of NSCs

The required parameters for the evaluating of the acceleration amplification factors of NSCs, are reported in Table 8.1. These parameters are obtained from the adopted cases of the primary and secondary systems. Except the values of the top floors rotations (θ) of the considered cases of the P-structures and their corresponding values of the torsional amplification factor ($F_{T\,mean}$), the values presented in Table 8.1 can be found in various Tables (5.3-5.10), (6.3-6.6), and (7.1-7.4) in Chapters 5, 6, and 7, respectively. The values of the factor (F_{Sc}) in Table 8.1 are equal to the corresponding values of the maximum seismic

capacities of the studied P-structures. Based on the results presented in Section 5.6.4 (see Figures 5.21 and 5.22), the values of θ in Table 8.1 were evaluated using linear time-history analyses of the P-structures under the effect of base motions with PGA value corresponding to the elastic seismic capacity of each case of the considered buildings. Thereafter, the values of θ that derived from the linear time-history analyses were substituted in Eq. (8-1) to evaluate the values of $F_{T\,mean}$, as presented in Table 8.1.

Table 8.1 The required parameters for the evaluating of the maximum acceleration amplification factors of NSCs integrated on different studied cases of irregular RC P-structures.

Building		Ground type	Fund. period, T [s]	Elastic capacity [g]	Max. capacity [g] F_{Sc}	Top rotation, θ [rad]	$F_{T\ mean}$ Eq. (8-1)	T_C		
								T_1	T_2	T_3
First group	Test	--	0.82	0.070	0.26	0.0084	1.37	0.82	0.73	0.65
	Test 0.15	C	0.82	0.100	0.46	0.0084	1.37	0.82	0.73	0.65
	Test 0.25	C	0.82	0.120	0.51	0.0077	1.34	0.82	0.73	0.65
	EC8 M	C	0.55	0.135	0.76	0.0038	1.17	0.55	0.52	0.42
Second group	EC8 M5	C	0.66	0.160	0.74	0.0045	1.20	0.66	-	0.51
	EC8 M7	C	0.84	0.160	0.69	0.0059	1.26	0.84	-	0.66
	EC8 M10	C	1.17	0.160	0.63	0.0090	1.39	1.17	-	0.92
	EC8 M13	C	1.29	0.170	0.58	0.0106	1.46	1.29	-	1.02
	EC8 M15	C	1.39	0.170	0.58	0.0117	1.51	1.39	-	1.12
Third group	EC8 M	A	0.620	0.120	0.69	0.0052	1.23	0.62	-	-
		B	0.590	0.131	0.72	0.0046	1.20	0.59	-	-
		D	0.470	0.149	0.83	0.0024	1.11	0.47	-	-
		E	0.520	0.143	0.79	0.0029	1.13	0.52	-	-
	EC8 M5	A	0.750	0.142	0.64	0.0067	1.29	0.75	-	-
		B	0.710	0.156	0.68	0.0057	1.25	0.71	-	-
		D	0.610	0.179	0.78	0.0032	1.14	0.61	-	-
		E	0.660	0.160	0.74	0.0047	1.21	0.66	-	-
	EC8 M10	A	1.250	0.135	0.57	0.0102	1.45	1.25	-	-
		B	1.220	0.150	0.59	0.0096	1.42	1.22	-	-
		D	1.080	0.178	0.70	0.0057	1.25	1.08	-	-
		E	1.170	0.160	0.63	0.0091	1.4	1.17	-	-
	EC8 M15	A	1.500	0.148	0.50	0.0163	1.71	1.50	-	-
		B	1.450	0.168	0.54	0.0140	1.61	1.45	-	-
		D	1.280	0.192	0.64	0.0081	1.35	1.28	-	-
		E	1.390	0.170	0.58	0.0117	1.51	1.39	-	-
One-bay three-storey	Reference	C	0.385	0.15	0.57	0.0000	1.00	0.385	0.379	0.261
	Modified 1	C	0.385	0.14	0.57	0.0003	1.01	0.385	0.379	0.261
	Modified 2	C	0.385	0.14	0.56	0.0007	1.03	0.385	0.379	0.261
	Modified 3	C	0.385	0.14	0.55	0.0013	1.06	0.385	0.379	0.261
	Modified 4	C	0.385	0.14	0.55	0.0022	1.10	0.385	0.379	0.261
	Modified 5	C	0.385	0.15	0.55	0.0038	1.17	0.385	0.379	0.261
	Modified 6	C	0.385	0.15	0.54	0.0072	1.31	0.385	0.379	0.261
	Modified 7	C	0.385	0.15	0.54	0.0114	1.50	0.385	0.379	0.261
Vertical mass irregularity	Reference	C	2.13	0.213	0.65	0.0082	1.36	2.13	1.87	1.66
	B-1-2	C	2.13	0.216	0.66	0.0084	1.37	2.13	1.88	1.69
	B-1-4	C	2.13	0.222	0.67	0.0085	1.37	2.13	1.89	1.71
	B-2-2	C	2.13	0.218	0.66	0.0085	1.37	2.13	1.89	1.71
	B-2-4	C	2.15	0.224	0.67	0.0099	1.43	2.15	1.90	1.72
	B-3-2	C	2.14	0.218	0.66	0.0097	1.42	2.14	1.89	1.71
	B-3-4	C	2.17	0.219	0.66	0.0104	1.46	2.17	1.92	1.72
	M-1-2	C	2.15	0.210	0.64	0.0063	1.28	2.15	1.91	1.73
	M-1-4	C	2.20	0.205	0.63	0.0070	1.31	2.20	1.95	1.75
	M-2-2	C	2.18	0.208	0.64	0.0069	1.30	2.18	1.93	1.74
	M-2-4	C	2.29	0.199	0.62	0.0088	1.39	2.29	2.00	1.80
	M-3-2	C	2.20	0.205	0.63	0.0082	1.36	2.20	1.95	1.75
	M-3-4	C	2.35	0.209	0.64	0.0094	1.41	2.35	2.14	1.85
	T-1-2	C	2.18	0.213	0.64	0.0105	1.46	2.18	1.92	1.75
	T-1-4	C	2.28	0.210	0.64	0.0115	1.50	2.28	2.00	1.82
	T-2-2	C	2.23	0.211	0.64	0.0114	1.50	2.23	1.97	1.80
	T-2-4	C	2.42	0.204	0.63	0.0166	1.73	2.42	2.12	1.95
	T-3-2	C	2.27	0.208	0.63	0.0149	1.65	2.27	2.01	1.83
	T-3-4	C	2.55	0.199	0.62	0.0181	1.79	2.55	2.29	2.05
	TB-1-2	C	2.18	0.216	0.66	0.0107	1.47	2.18	1.92	1.83
	TB-1-4	C	2.28	0.219	0.66	0.0119	1.52	2.28	2.03	1.91
	TB-2-2	C	2.23	0.216	0.66	0.0115	1.50	2.23	1.97	1.88
	TB-2-4	C	2.43	0.218	0.67	0.0184	1.81	2.43	2.15	2.02
	TB-3-2	C	2.28	0.214	0.65	0.0162	1.71	2.28	2.03	1.92
	TB-3-4	C	2.57	0.214	0.64	0.0201	1.88	2.57	2.34	2.15
	TM-1-2	C	2.20	0.210	0.64	0.0088	1.39	2.20	1.96	1.82
	TM-1-4	C	2.35	0.203	0.62	0.0103	1.45	2.35	2.07	1.93
	TM-2-2	C	2.28	0.206	0.63	0.0100	1.44	2.28	2.00	1.87
	TM-2-4	C	2.56	0.196	0.62	0.0170	1.74	2.56	2.25	2.10
	TM-3-2	C	2.34	0.214	0.65	0.0147	1.64	2.34	2.05	1.93
	TM-3-4	C	2.73	0.214	0.64	0.0189	1.83	2.73	2.50	2.23

As described in Chapter 5 (see Section 5.2.1), the first group of buildings is consisted of four irregular three-storey RC P-structures termed as Test, Test 0.15, Test 0.25, and EC8 M which had the same plan layout and number of storeys, but they were designed due to different conditions of EC8 provisions (seismic or non-seismic conditions). Under the effect of the base motions with PGA value corresponding to the elastic seismic capacity of each case of the first group of buildings, Figure 8.2 presents the variations of maximum acceleration amplification factor A_p^a with values of T_C/T_1. Although the buildings Test, Test 0.15, and Test 0.25 had the same fundamental periods (see Table 8.1), Figure 8.2 shows that the NSCs attached to these buildings had different seismic behaviours during earthquakes. Therefore, it would be inaccurate to evaluate the behaviour of the NSCs mounted on these or similar buildings using only the fundamental vibration periods of the P-structures as it is considered in the current EC8 (2004) provisions.

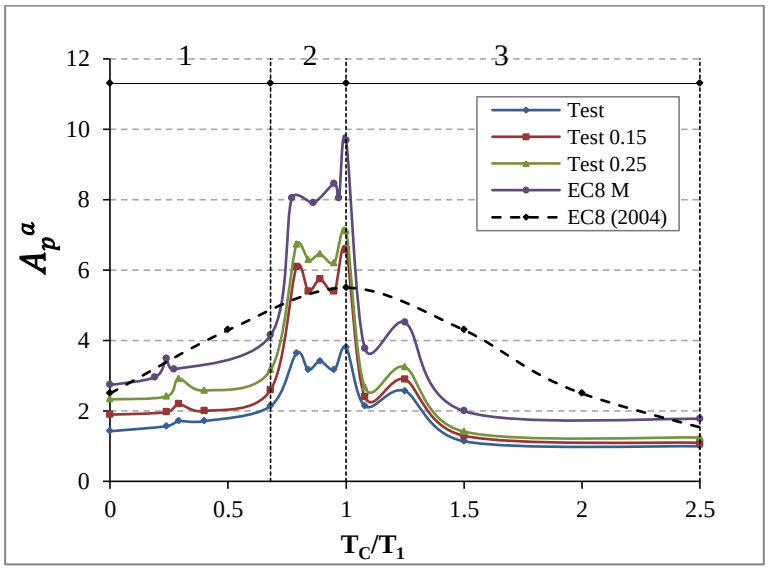

Figure 8.2 Variations of maximum acceleration amplification factor (A_p^a) predicted from FEA results and the EC8 vs. NSC to P-structure period ratio (T_C/T_1) for the NSCs attached to the flexible sides of the top floors of the first group of buildings at PGA values corresponding to the elastic seismic capacities.

As can be seen from Figure 8.2, the amplifications evaluated by EC8 (2004) provisions for the design of NSCs seem more appropriate to those NSCs attached to buildings designed for gravity loads only (i.e. building Test). Furthermore, it can be observed that EC8 underestimates the amplification factors at Zone 2 more than those at Zones 1 and 3. Therefore, the methodology that was used to extend the current EC8 formula for the design of NSCs would need a significant modification on the values of the acceleration amplification factors located in Zone 2 more than those in Zones 1 and 3. It is worth to note that the results of the comparison between FEA and EC8 suggest that the majority of the peak component accelerations for NSCs with $T_C \approx 0$ (i.e. rigid NSCs) were found within the range of the predictions of the EC8 (2004). Therefore, the modification on EC8 formula includes only flexible NSCs especially for those in resonance with the vibration period of the P-structure, as well as for long periods of NSCs.

To account for the effect of both the torsional amplification factor F_T of the NSC and the maximum seismic capacity of the P-structure, the first modification attempt to the EC8 (2004) formula is based on the FEA results of the maximum acceleration amplification factors for the NSCs attached to the EC8 M building. This building was designed in full compliance with the EC8 (2004) provisions. The EC8 (2004) formula (i.e. Eq. (1-1), as presented in Chapter 1) is modified in this chapter as given in Eq. (8-2). The modification is made in such a way that the acceleration amplification factor at $(\frac{T_C}{T_1} = 1.0)$ matches with that of the FEA result of the NSC that had a period equal to T_1 and attached to the top floor of EC8 M building as shown in Figure 8.3.

$$\frac{S_a}{\alpha.S} = \left[\frac{6.\left(1+\frac{z_c}{H}\right).F_T.F_{Sc}}{1+\left(1-\frac{T_C}{T_1}\right)^2} - 0.5\right] \quad (8\text{-}2)$$

where $(S_a/\alpha.S)$ is the acceleration amplification factor for the NSC; however, F_T and F_{Sc} are, respectively, the torsional amplification factor of the NSC and the maximum seismic capacity factor of the P-structure. Furthermore, the terms T_C, T_1, z_c, and H were defined in Chapter 1 (see Eq. (1-1)). The values of F_T and F_{Sc} corresponding to the EC8 M building can be found in Table 8.1.

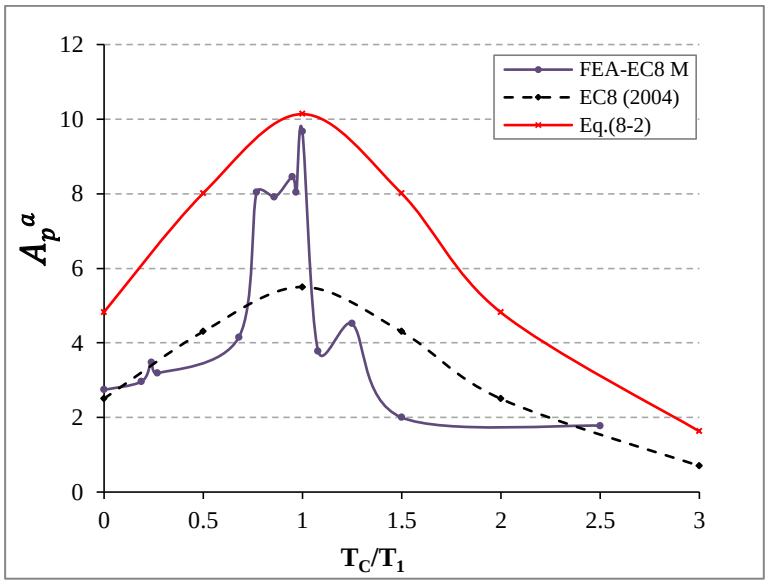

Figure 8.3 Variations of maximum acceleration amplification factor (A_p^a) predicted from FEA results, EC8 and Eq. (8-2) vs. NSC to P-structure period ratio (T_C/T_1) for the NSCs attached to the flexible sides of the top floors of the EC8 M building at PGA value corresponding to the elastic seismic capacity.

Shown in Figure 8.3 are the FEA results of the acceleration amplification factors of NSCs attached to the EC8 M building and the predictions of the proposed Eq. (8-2), as well as the predictions of EC8 (2004). It can be seen from Figure 8.3 that the predictions of Eq. (8-2)

are over- conservative for NSCs with frequencies out-of-tune with the first three fundamental periods of the EC8 M building. Hence, Eq. (8-2) is further modified by multiplying the term $(1 - T_C/T_1)^2$ by the term $(4.F_T.F_{Sc}-1)$ so as to obtain an acceleration amplification value of 2.5 for rigid NSCs with $T_C = 0$ s, as suggested by the EC8 (2004) recommendation. Moreover, an exponent of 3/5 is applied to the term $(1 - T_C/T_1)^2$ in order to obtain acceleration amplification factor values comparable with the predictions of the EC8 and the FEA results for NSCs with frequencies out-of-tune with the first three vibration periods of the EC8 M building, as shown in Figure 8.4. Hence, Eq. (8-2) can be re-written as follows:

$$\frac{S_a}{\alpha . S} = \left[\frac{6.\left(1 + \frac{z_c}{H}\right).F_T.F_{Sc}}{1 + (4.F_T.F_{Sc} - 1)\left[\left(1 - \frac{T_C}{T_1}\right)^2\right]^{3/5}} - 0.5 \right] \tag{8-3}$$

Figures 8.4 to 8.7 show the variations of maximum acceleration amplification factor (A_p^a) predicted from the FEA results and EC8, as well as from Eq. (8-3) versus NSC to P-structure period ratio (T_C/T_1) for the NSCs attached to the flexible sides of the top floors of the first group of buildings at the PGA values corresponding to the elastic seismic capacities. The values of F_T and F_{Sc} corresponding to the buildings: Test 0.25, Test 0.15, and Test that were used to evaluate the predictions of A_p^a using the modified Eq. (8-3), can be found in Table 8.1.

It can be seen from Figures 8.4 to 8.7 that Eq. (8-3) provides better predictions than the EC8 (2004) for the evaluating of the A_p^a values when the NSCs mounted on the top floors of all the considered buildings. Furthermore, another trend can be observed that Eq. (8-3) predicts a lower response than the EC8 provision when the NSCs attached to building Test, as

shown in Figure 8.7. This response is produced due to a low value of the maximum seismic capacity factor (0.26 g) of building Test which was substituted in Eq. (8-3).

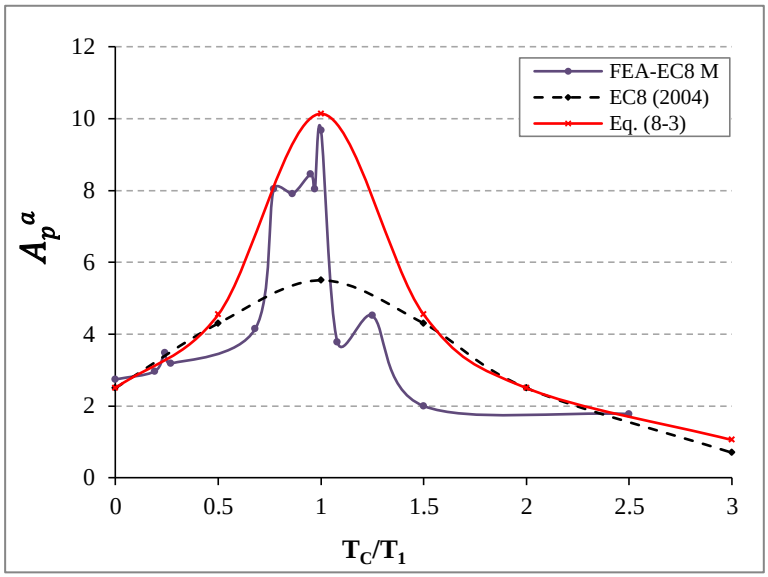

Figure 8.4 Variations of maximum acceleration amplification factor (A_p^a) predicted from FEA results, EC8, and Eq. (8-3) vs. NSC to P-structure period ratio (T_C/T_1) for the NSCs attached to the flexible sides of the top floors of the EC8 M building at PGA value corresponding to the elastic seismic capacity.

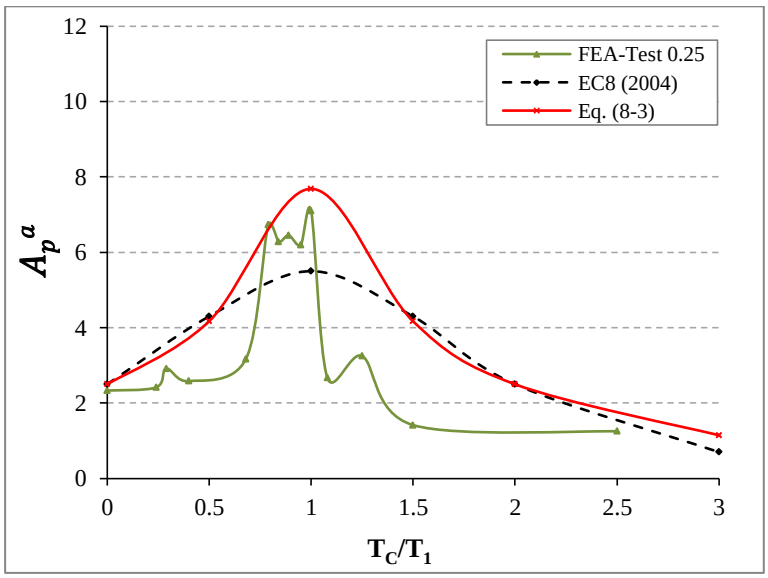

Figure 8.5 Variations of maximum acceleration amplification factor (A_p^a) predicted from FEA results, EC8, and Eq. (8-3) vs. NSC to P-structure period ratio (T_C/T_1) for the NSCs attached to the flexible sides of the top floors of the Test 0.25 building at PGA value corresponding to the elastic seismic capacity.

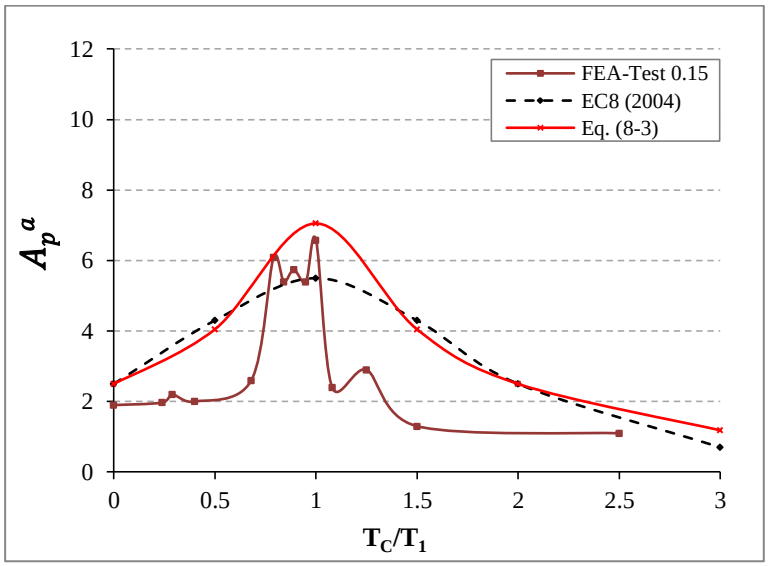

Figure 8.6 Variations of maximum acceleration amplification factor (A_p^a) predicted from FEA results, EC8, and Eq. (8-3) vs. NSC to P-structure period ratio (T_C/T_1) for the NSCs attached to the flexible sides of the top floors of the Test 0.15 building at PGA value corresponding to the elastic seismic.

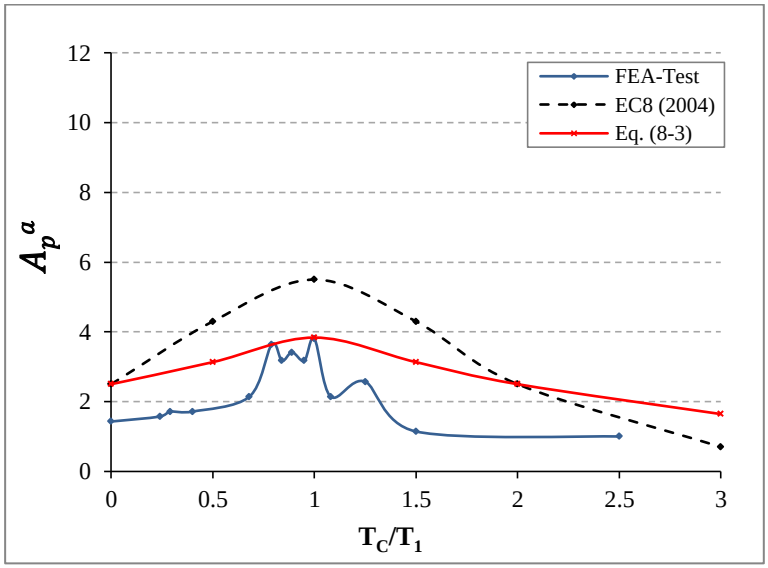

Figure 8.7 Variations of maximum acceleration amplification factor (A_p^a) predicted from FEA results, EC8, and Eq. (8-3) vs. NSC to P-structure period ratio (T_C/T_1) for the NSCs attached to the flexible sides of the top floors of the Test building at PGA value corresponding to the elastic seismic.

In order to generalise the modified Eq. (8-3) and to use in the wider context for other cases of NSCs attached to different P-structures, this equation should be verified against an

extensive range of P-structures. Therefore, the other remaining studied cases of the P-structures (i.e. sixty cases of irregular RC buildings), were used to validate Eq. (8-3) for the design of NSCs attached to buildings experiencing torsional behaviours during earthquakes, as clearly explained in Section 8.4.

8.4 Assessment of Accuracy of the Modified EC8 Formula for the Design of the NSCs

In the following sections, the assessment of accuracy of the proposed Eq. (8-3) is based on the FEA results of NSCs attached to different cases of P-structures that were studied in Chapters 5, 6, and 7. The FEA results presented hereinafter as maximum acceleration amplification factors of the NSCs under the effect of the base motions with PGA values corresponding to the elastic seismic capacities of the P-structures.

8.4.1 NSCs Attached to the Second Group of Buildings

This section focuses on evaluating the accuracy of the proposed Eq. (8-3) for the design of NSCs mounted on irregular multi-storey RC buildings with different heights. Five irregular RC buildings, namely EC8 M5, EC8 M7, EC8 M10, EC8 M13, and EC8 M15, as described in Chapter 5, were considered. These buildings were designed according to EC8 (2004) seismic provisions and then subjected to seven artificial earthquake records. These records were scaled so their PGAs (0.16 g for EC8 M5, EC8 M7, and EC8 M10; and 0.17 g for EC8 M13 and EC8 M15) give a value of μ equal to 1.0.

To assess the precision of the proposed Eq. (8-3) in evaluating the acceleration amplification factors along the heights of the second group of buildings, values of the F_T and F_{Sc} corresponding to each building of the second group as given in Table 8.1 were substituted into Eq. (8-3). Along the heights of each case of buildings EC8 M5, EC8 M7, EC8 M10, EC8 M13, and EC8 M15, the comparisons between the FEA results and the predictions of the proposed Eq. (8-3) are shown in Figures 8.8 to 8.10. The FEA results are presented as the values of the maximum acceleration amplification factors A_p^a at CR and FS under the effect of the base motions with PGA values corresponding to the elastic capacities of the P-structures. It can be observed from Figure 8.8 that, for rigid NSCs (i.e. $T_C \approx 0$ s), most of the A_p^a values at the centres of rigidity along the heights of the second group of buildings are within the recommended values by the proposed Eq. (8-3). Whereas, the acceleration amplification factors at the flexible sides, when the NSCs are attached to the lower third of the height of the buildings that had 10, 13, and 15-storey, are slightly exceeding the proposed equation by a maximum value of 17%. In order to avoid damage to such NSCs, based on the FEA results it can be suggested that these NSCs should be designed by adopting values of A_p^a that are suitable for the design of the corresponding NSCs attached to the upper floors (i.e. values of A_p^a in the range of 1.8 to 2.0). However, for NSCs having a period equal to T_1, Eq. (8-3) provided good predictions for the values of A_p^a for the NSCs attached to the floors along the heights of the second group of buildings, as shown in Figure 8.9.

For NSCs that had periods equal to the torsional fundamental periods (i.e. $T_C = T_3$) of the second group of buildings, the A_p^a values estimated from the proposed Eq. (8-3) were found to have predicted well the corresponding values of the NSCs attached to the flexible sides and are conservative for NSC attached to centres of rigidity, as shown in Figure 8.10.

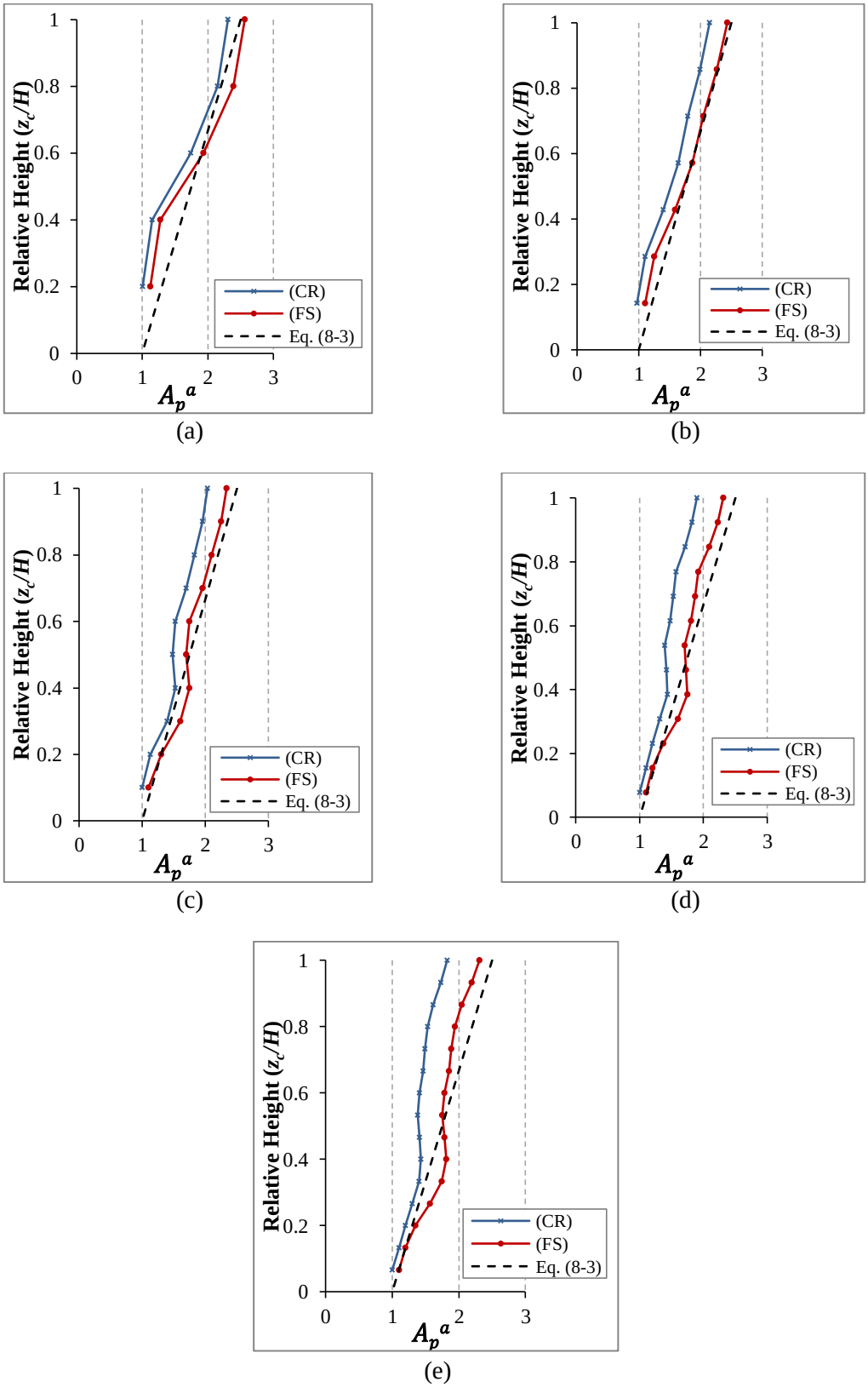

Figure 8.8 Comparison between FE and Eq. (8-3) predictions of maximum acceleration amplification factors (A_p^a) for the NSCs with $T_C \approx 0$ s and attached to buildings: (a) EC8 M5, (b) EC8 M7, (c) EC8 M10, (d) EC8 M13, and (e) EC8 M15.

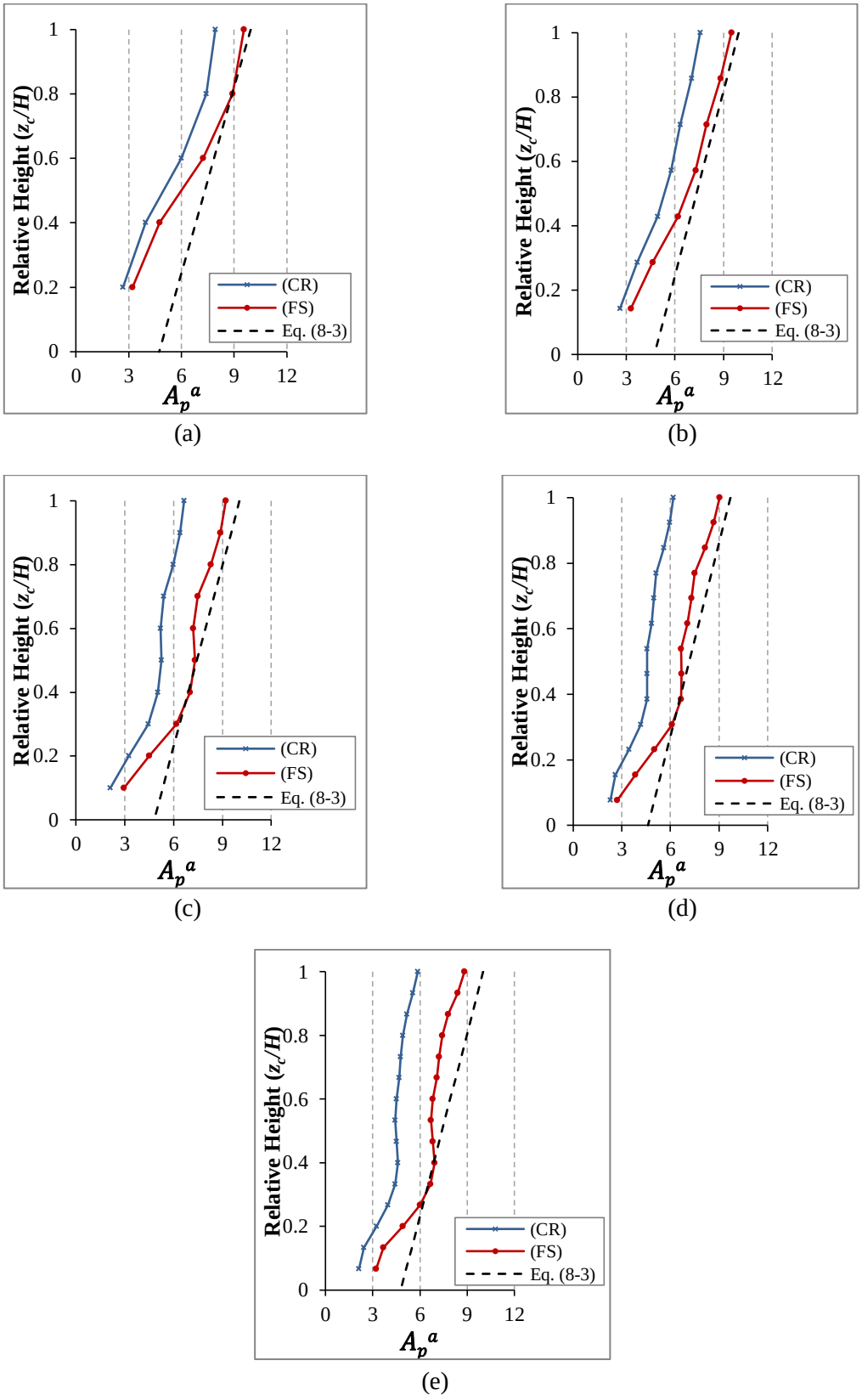

Figure 8.9 Comparison between FE and Eq. (8-3) predictions of maximum acceleration amplification factors (A_p^a) for the NSCs with $T_C = T_1$ and attached to buildings: (a) EC8 M5, (b) EC8 M7, (c) EC8 M10, (d) EC8 M13, and (e) EC8 M15.

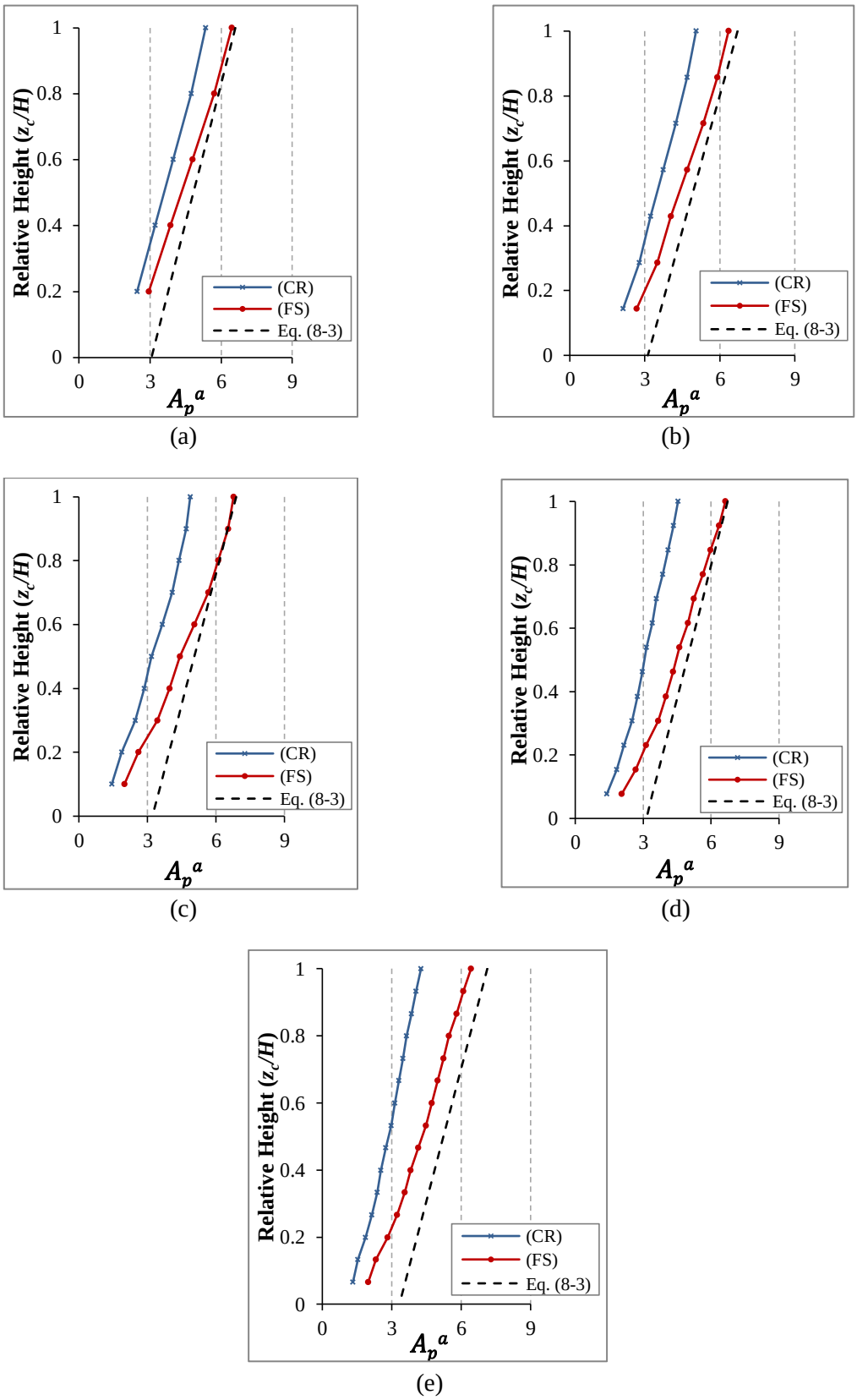

Figure 8.10 Comparison between FE and Eq. (8-3) predictions of maximum acceleration amplification factors (A_p^a) for the NSCs with $T_C = T_3$ and attached to buildings: (a) EC8 M5, (b) EC8 M7, (c) EC8 M10, (d) EC8 M13, and (e) EC8 M15.

Figure 8.11 compares the numerical results of the NSCs accelerations with the predictions of both the EC8 (2004) and the proposed Eq. (8-3). These accelerations are measured at 3% damping ratio for NSCs with $T_C = T_1$ and attached to the flexible sides of the top floors of the second group of buildings designed in full compliance with the EC8 (2004), as presented in Figures 5.13(a) and 5.14(a). It can be seen from Figure 8.11 that the predictions of the EC8 underestimate the seismic responses on average by about 50.4% of the corresponding numerical values at the PGA values corresponding to the maximum seismic capacities of the studied buildings. However, Eq. (8-3) underestimates the corresponding dynamic responses of the NSCs on average by about 8.7% of the numerical results at the maximum seismic capacities. Overall, Figures 8.8 to 8.11 clearly demonstrate that the proposed Eq. (8-3) provided a good improvement and conservative predictions in comparison with those of the EC8 (2004) for NSCs attached to the flexible sides of irregular RC structures.

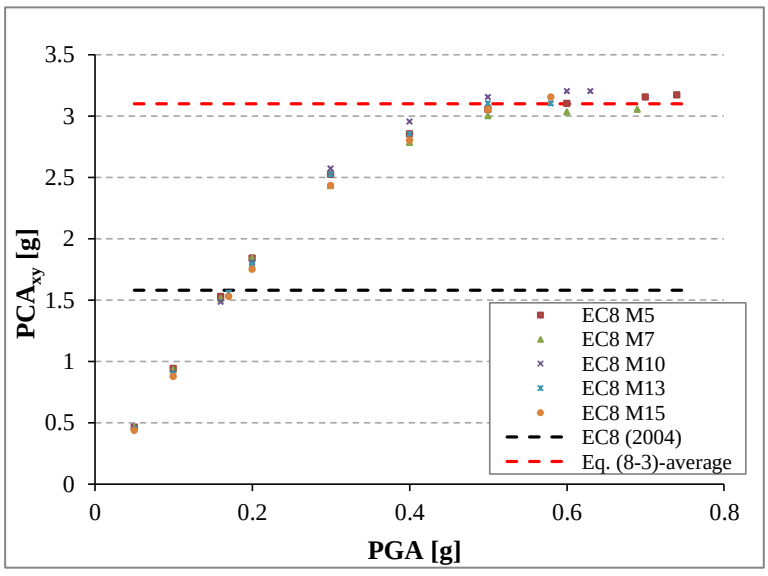

Figure 8.11 Comparison between FEA results of PCA_{xy} and the predictions of EC8, as well as the proposed Eq. (8-3) at different values of PGA, for the NSCs with periods equal to T_1 and attached to the flexible sides of the top floors of the second group of buildings designed on ground type C.

8.4.2 NSCs Attached to the Third Group of Buildings

The buildings in the third group were designed on ground types A, B, D, and E, as described in Chapter 5 (see Section 5.2.3). For each case of the buildings in this group, Table 8.1 gives the value of the seismic capacity factor F_{Sc} (i.e. maximum seismic capacity of a given P-structure) and the value of the top floor rotation that was evaluated from the linear time-history analyses at PGA value corresponding to the elastic seismic capacity. Value of the torsional amplification factor F_T corresponding to each value of the top floor rotation calculated using Eq. (8-1) is also presented in Table 8.1. Accordingly, values of F_T and F_{Sc} for different cases of buildings in the third group were substituted into Eq. (8-3) to evaluate the maximum values of the acceleration amplification factors of NSCs and for different types of ground.

Figure 8.12 shows the comparison between the FEA results and the predictions of Eq. (8-3) of values of A_p^a for the NSCs having a period equal to T_1 and attached to the flexible sides of the top floors of buildings designed on ground types A, B, D, and E. It can be seen from Figure 8.12 that the proposed Eq. (8-3) provides good estimations of the maximum acceleration amplification factors for such NSCs and for different ground types. Furthermore, when the P-S systems are subjected to base motions with PGA values corresponding to the maximum seismic capacities of the P-structures, the proposed Eq. (8-3) provides underestimation values of PCA_{xy} on average by about 15.5%, 10.0%, and 12.9% for the NSCs attached to the flexible sides of the top floors of the buildings designed on ground types A, B, and D respectively, as shown in Figures 8.13(a) to 8.13(c). However, it seems that the proposed Eq. (8-3) was observed to overestimate these values of PCA_{xy} on average by about 9.2% for the NSCs attached to the buildings designed on ground type E, as displayed in

Figure 8.13(d). This overestimation of the values of PCA_{xy} according to the proposed Eq. (8-3), is produced due to the high value of the design ground acceleration of 0.35 g used for buildings founded on ground type E.

On the other hand, the recommendations of EC8 (2004) underestimated the seismic responses of the NSCs with periods equal to T_1 on average by about 51.4%, 49.3%, 52.8%, and 40.5% when attached to the P-structures designed on ground types A, B, D, and E respectively; and at PGA values corresponding to the maximum seismic capacities of the studied buildings, as shown in Figures 8.13(a) to 8.13(d).

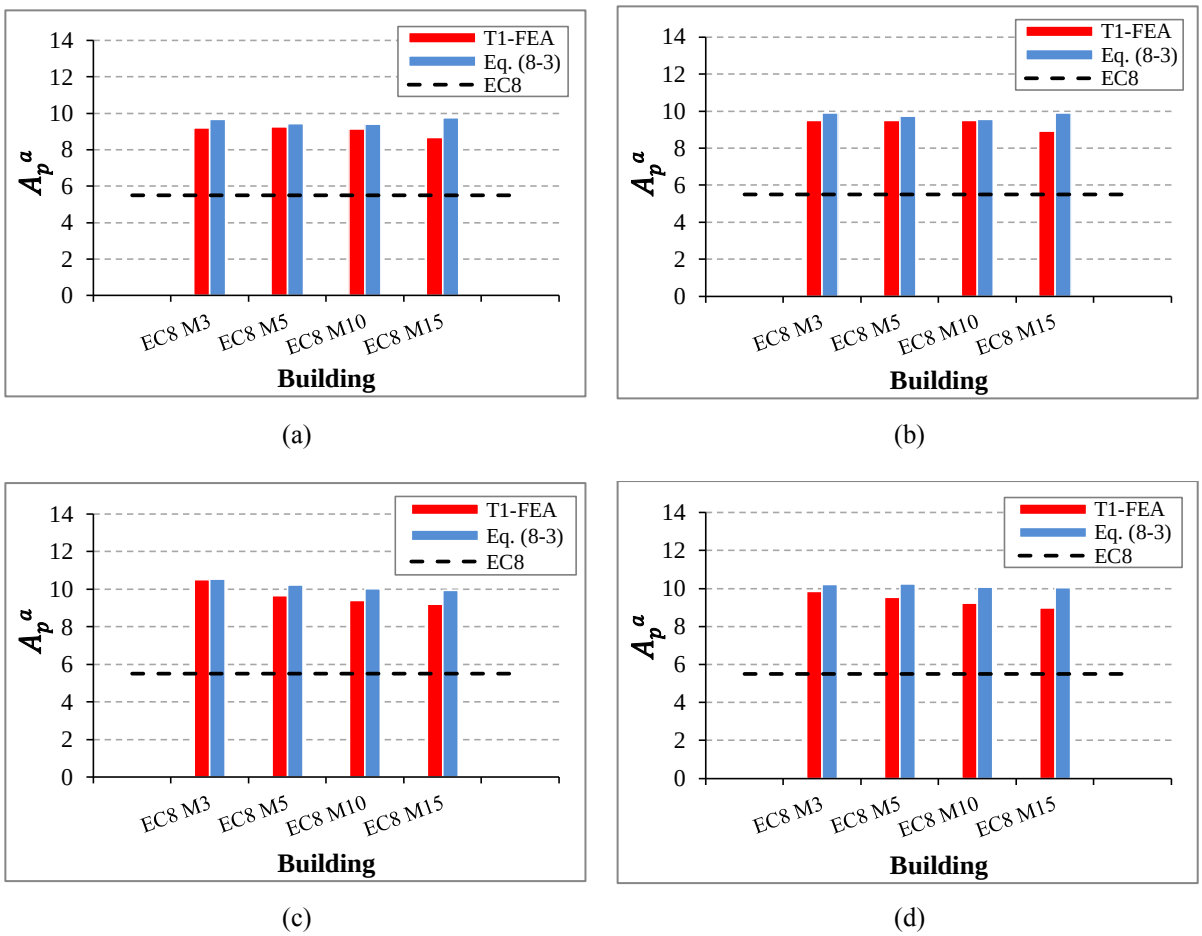

Figure 8.12 Comparison between FEA results and the prediction of Eq. (8-3), as well as the EC8 of the maximum acceleration amplification factors (A_p^a) for the NSCs with periods equal to T_1 and attached to the flexible sides of the top floors of the buildings designed on ground types (a) A, (b) B, (c) D, and (d) E.

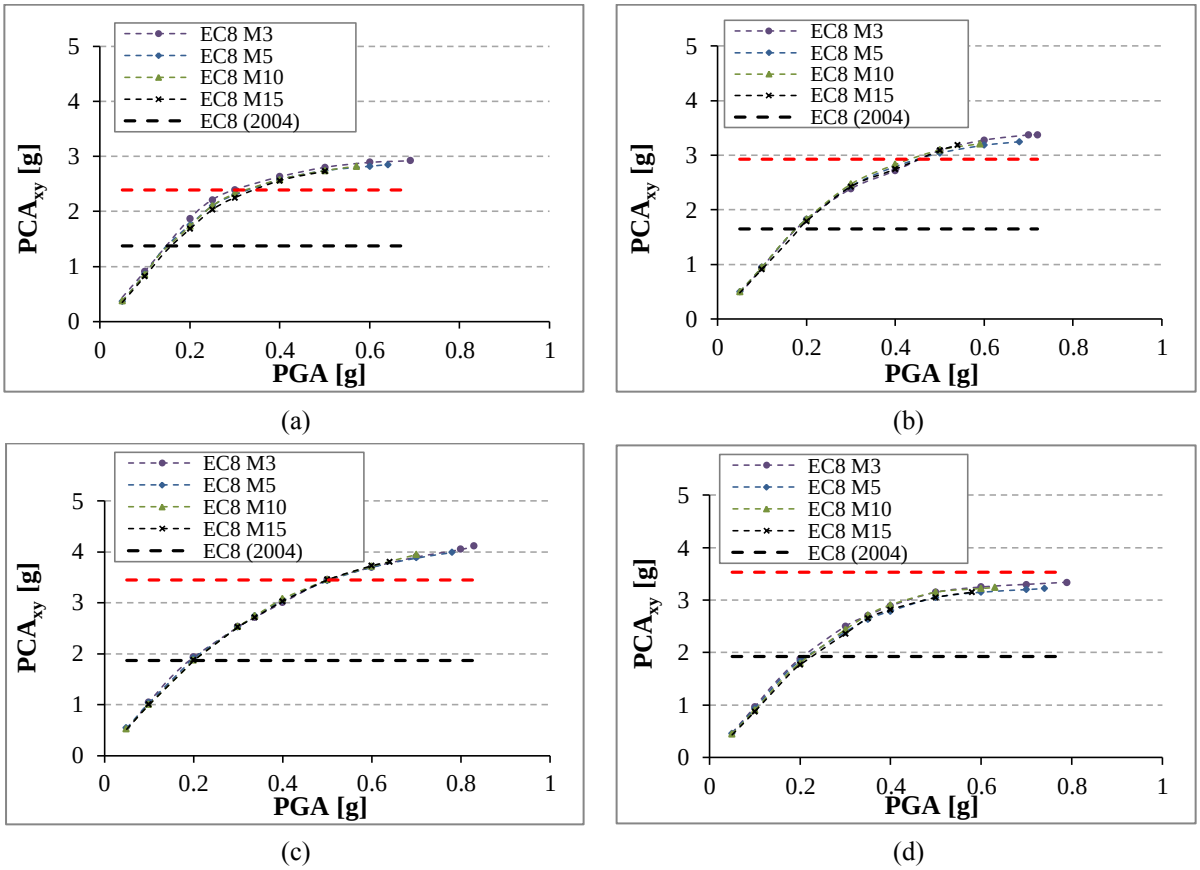

Figure 8.13 Comparison between FEA results of PCA_{xy} and the predictions of the EC8, as well as the proposed Eq. (8-3) at different values of PGA, for the NSCs with periods equal to T_1 and attached to the flexible sides of the top floors of the P-structures designed on ground types: (a) A, (b) B, (c) D, and (d) E.

8.4.3 NSCs Attached to the RC Buildings having Different Eccentricity Ratios

In this section, the accuracy level of the proposed Eq. (8-3) in predicting the maximum acceleration amplification factors for the NSCs attached to the P-structures with different values of eccentricity ratios are assessed. The considered P-structures are one-bay three-storey RC buildings. General description and modelling of these structures can be found in Chapter 6 (see Section 6.2). Values of F_T and F_{Sc} corresponding to each case of the P-structures as reported in Table 8.1 were substituted into Eq. (8-3). Figures 8.14 to 8.16 show comparisons between the FEA results and the predictions of both the EC8 and the proposed Eq. (8-3) for the NSCs attached to the flexible sides of the first and second, as well as the top floors of the P-structures; and for different values of NSCs periods. The FEA results are presented as the

values of the maximum acceleration amplification factors at the FS under the effect of base motion with PGA values corresponding to the elastic capacities of the P-structures. In general, it can be observed from Figures 8.14 to 8.16 that the predictions of the maximum acceleration factors of NSCs attached to the considered floors that estimated by the proposed Eq. (8-3) were found more appropriate (i.e. matched with FEA results) than those values were calculated by the recommendations of the EC8 (2004). The proposed equation was more applicable than the EC8 especially for those NSCs either their natural periods were tuned with the first fundamental vibration periods of the P-structures or having a long value of period (i.e. at T_C/T_1 equal to 4.0).

Moreover, as shown in Figure 8.17, the predictions of the EC8 (2004) underestimate the seismic response of the NSCs with periods equal to T_1 by about 32.3% and 61.5% at PGA values corresponding to the maximum seismic capacities. This is for NSCs attached to the flexible side of the top floors of the P-structures with eccentricity ratios respectively equal to 0.0 (i.e. P-structure without eccentricity) and 0.372 (i.e. the highest considered value of the eccentricity ratio). However, the proposed Eq. (8-3) gives underestimations of the corresponding dynamic responses of the NSCs by about 21.9% and 35.4% when attached to the top floors of the RC P-structures having eccentricity ratios equal to 0.0 (i.e. plan-regular P-structure without eccentricity) and 0.372 respectively. It can be concluded from the results presented in Figure 8.17 that the modified design formula provides better predictions of the NSCs accelerations than the current EC8 formula at values of maximum peak ground accelerations. In addition, it seems that the modified formula is more appropriate for those NSCs attached to weak torsional P-structures (i.e. low values of eccentricity ratios) than those of NSCs attached to strong torsional P-structures (i.e. high values of eccentricity ratios).

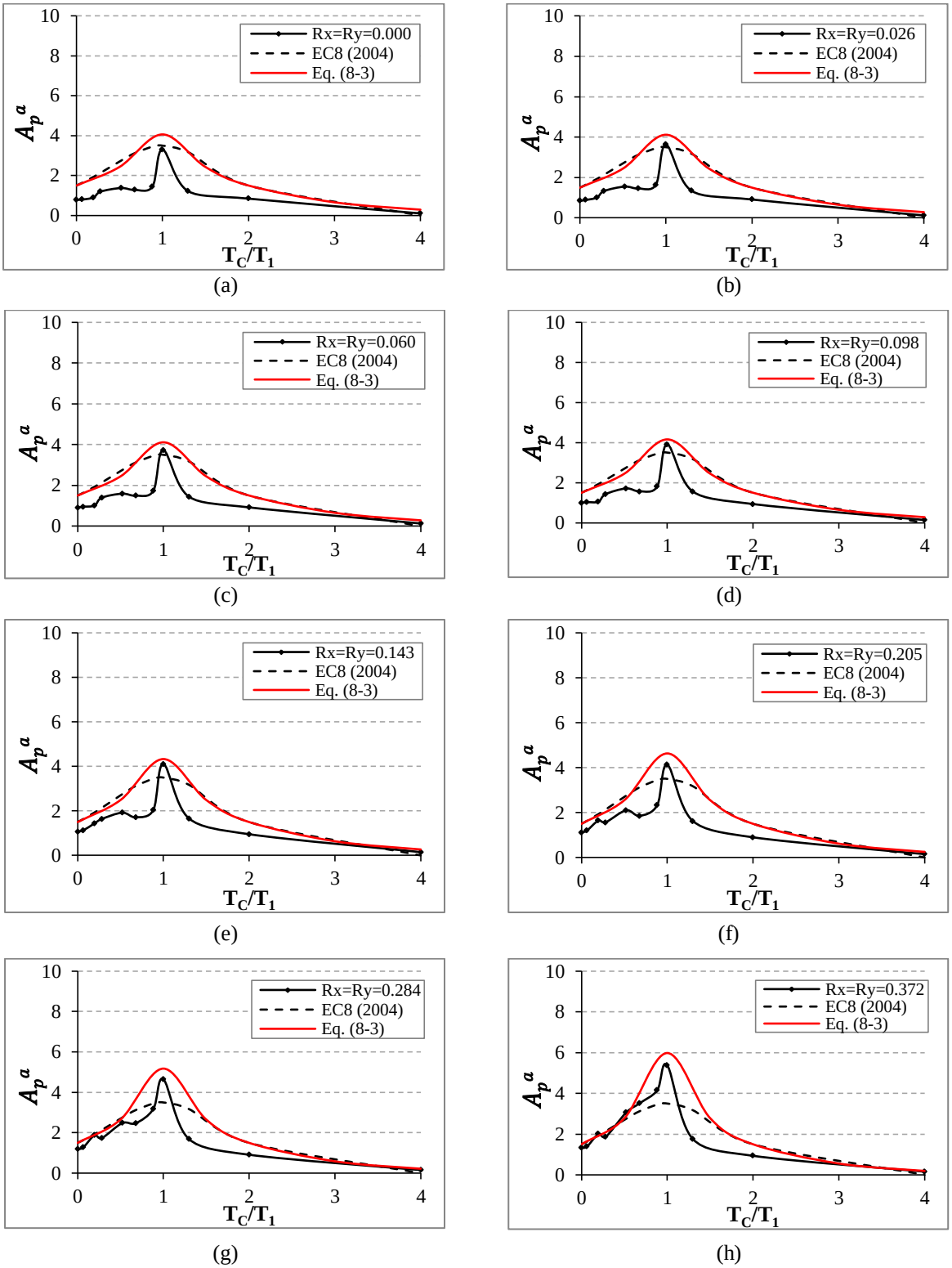

Figure 8.14 Predictions of Eq. (8-3) and the FEA results of the maximum acceleration amplification factors (A_p^a) for the NSCs having different periods and attached to the first floors of the buildings with eccentricity ratios equal to (a) 0.000, (b) 0.026, (c) 0.060, (d) 0.098, (e) 0.143, (f) 0.205, (g) 0.284, and (h) 0.372.

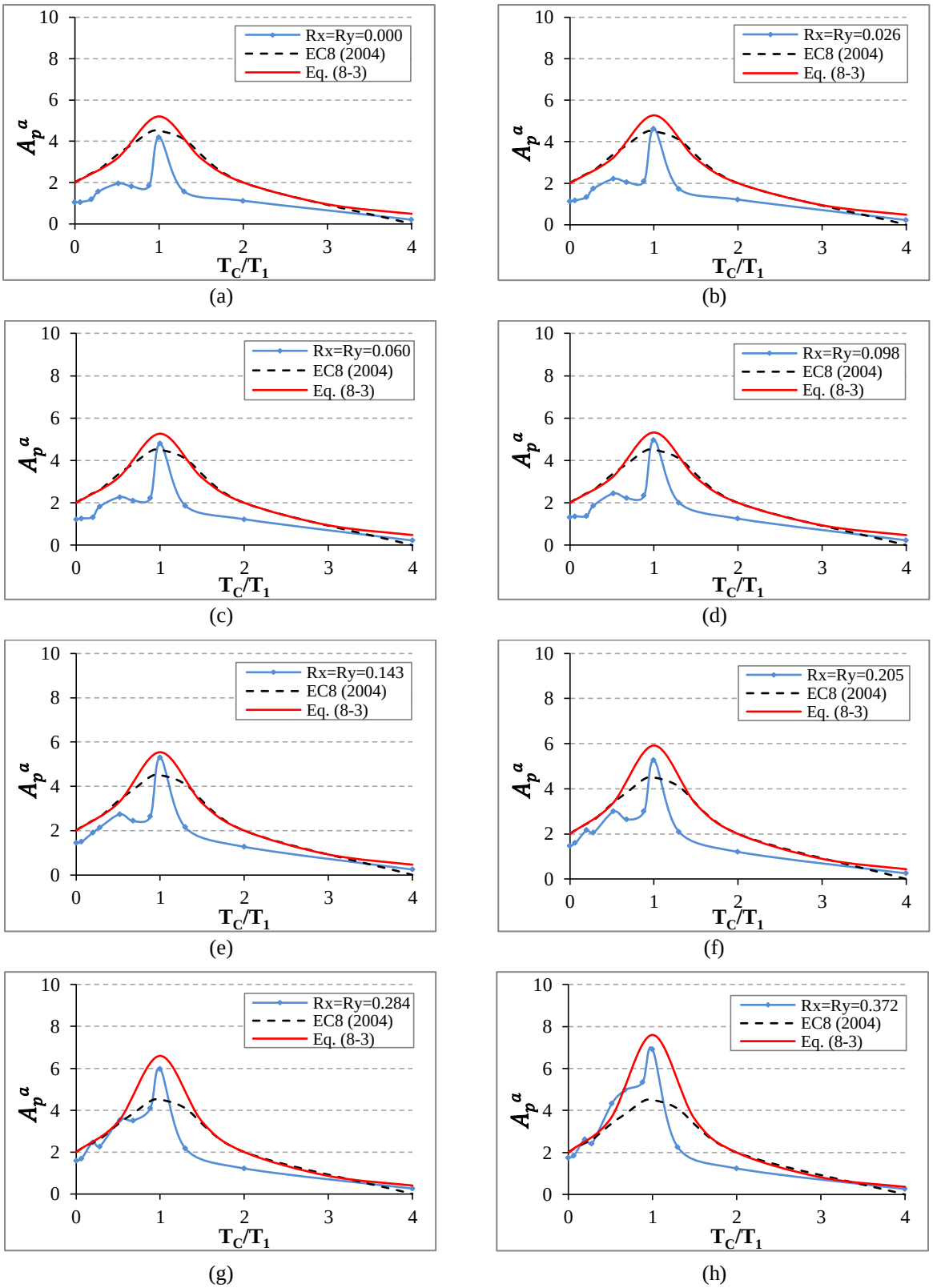

Figure 8.15 Predictions of Eq. (8-3) and the FEA results of the maximum acceleration amplification factors (A_p^a) for the NSCs having different periods and attached to the second floors of the buildings with eccentricity ratios equal to (a) 0.000, (b) 0.026, (c) 0.060, (d) 0.098, (e) 0.143, (f) 0.205, (g) 0.284, and (h) 0.372.

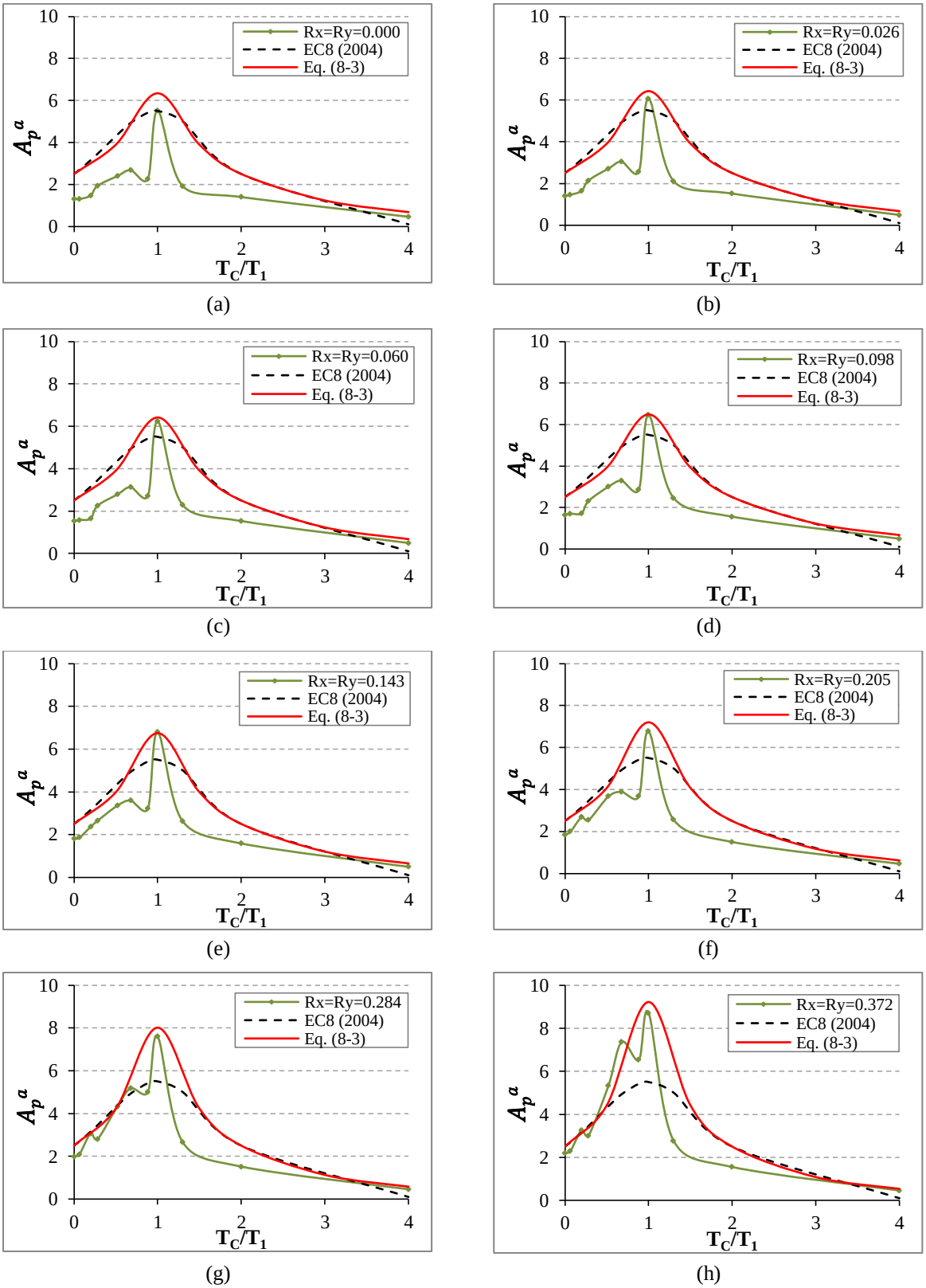

Figure 8.16 Predictions of Eq. (8-3) and the FEA results of the maximum acceleration amplification factors (A_p^a) for the NSCs having different periods and attached to the top floors of the buildings with eccentricity ratios equal to (a) 0.000, (b) 0.026, (c) 0.060, (d) 0.098, (e) 0.143, (f) 0.205, (g) 0.284, and (h) 0.372.

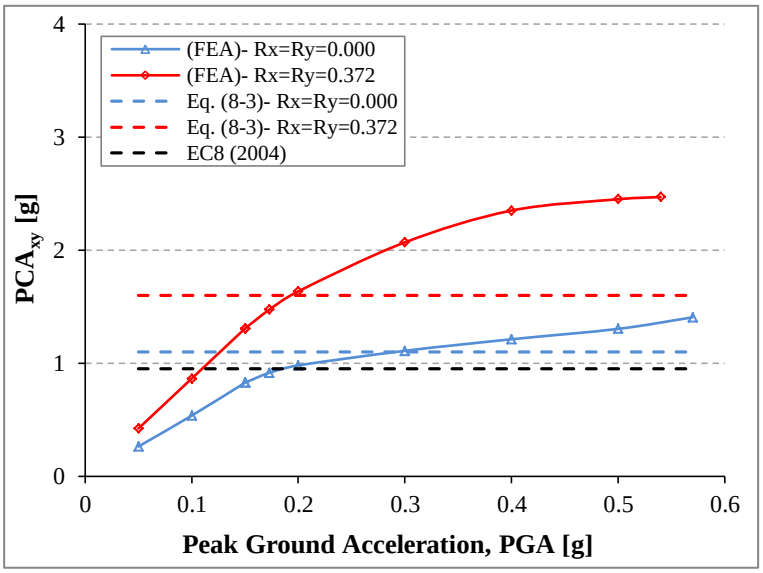

Figure 8.17 Comparison between FEA results of PCA_{xy} and the predictions of the EC8, as well as the proposed Eq. (8-3) at different values of PGA, for the NSCs with periods equal to T_1 and attached to the flexible sides of the top floors of the P-structures having eccentricity ratios equal to 0.0 and 0.372.

8.4.4 NSCs Attached to the RC Building with Vertical Mass Irregularities

This section evaluates the accuracy of Eq. (8-3) in estimating the maximum acceleration amplification factors of NSCs attached to the flexible sides at different height levels of a complicated irregular 20-storey, multi-bay RC building that had thirty different cases of vertical mass irregularities. Further information on these cases of mass irregularities can be found in Chapter 7 (see Section 7.2.2).

Comparisons are made between the FEA results and the predictions of Eq. (8-3) of the value of A_p^a for the NSCs attached to the flexible sides of different floors along the height of the selected cases of the P-structures under the effect of earthquakes with values of PGAs equal to the elastic capacities of the P-structures (see Table 8.1). Five critical mass irregularity

cases (i.e. B-3-4; M-3-4; T-3-4; TB-3-4; and TM-3-4) in addition to the reference case were chosen in these comparisons, as shown in Figures 8.18 to 8.21. While, the remaining cases of vertical mass irregularities (i.e. 25 cases of vertical mass irregularities) were used only for the comparison of the values of A_p^a at the top floors of the P-structures, as displayed in Figures 8.22 to 8.25.

Values of F_T and F_{Sc} that can be used for the design of the NSCs attached to the selected cases of the P-structures that had different cases of vertical mass irregularities are presented in Table 8.1. It can be seen from Figure 8.18 that, for the NSCs with periods equal to T_1, Eq. (8-3) gives well-predictions of the seismic responses for those NSCs were mounted on the flexible sides of the selected cases (T_1-M-3-4; T_1-T-3-4; T_1-TB-3-4; and T_1-TM-3-4, as well as the reference case). Whereas, the maximum acceleration amplification factors for the NSCs termed as T_1-B-3-4 and attached to the flexible sides at the lower third levels of the building, are exceeding the predictions of Eq. (8-3). The main reason behind this underestimation in the responses estimated by the proposed Eq. (8-3) for the case of T_1-B-3-4 is that the values of the floors rotations were increased at the bottom floors; and therefore, the values of accelerations of the NSCs attached to these specific irregular floors were also increased. In order to prevent the failure of NSCs that may have periods equal to T_1 and attached to the lower third floors of a building, they should be designed by adopting the same acceleration amplification factors value of the corresponding NSCs expected to be attached to the upper third floors of the building.

For NSC with periods equal to T_2 and attached to the considered cases of the P-structures, the values of A_p^a for such NSCs that evaluated using of Eq. (8-3) were observed

quite well-predicted the dynamic responses of the NSCs attached to the flexible sides, as shown in Figure 8.19. However, for NSCs with periods equal to T_3, the maximum acceleration amplification factors increase gradually from the lower to the higher floors as shown in Figure 8.20. Furthermore, Eq. (8-3) gives good estimates for the dynamic responses, especially for the NSCs attached to the upper two thirds floor levels; whereas Eq. (8-3) gives conservative predictions for the NSCs with $T_C = T_3$ and attached to the lower third floor levels.

For rigid NSCs (i.e. $T_C \approx 0$ s), the proposed Eq. (8-3) gives values of acceleration amplification factors equal to 2.5 and 1.0 at roof and ground levels, respectively. It can be noted from Figures 8.21(a), 8.21(b), and 8.21(c) that most of the acceleration amplification factors (for rigid NSCs attached to the flexible sides along the upper two thirds of the heights of the selected cases of the buildings) were observed within the range of the corresponding values estimated by Eq. (8-3). Whereas, the acceleration amplification factors for the NSCs attached to the lower third floor levels of these cases were exceeded the predictions accounted by Eq. (8-3) by a maximum value of 15%. In order to avoid the failure of rigid NSCs, it should not be attached to such locations (i.e. the lower third floor levels of the P-structures), or should be designed by adopting the same factors of A_p^a that are used for rigid NSCs attached to the upper floors of the buildings (i.e. values of A_p^a in the range of 1.8 to 2.0).

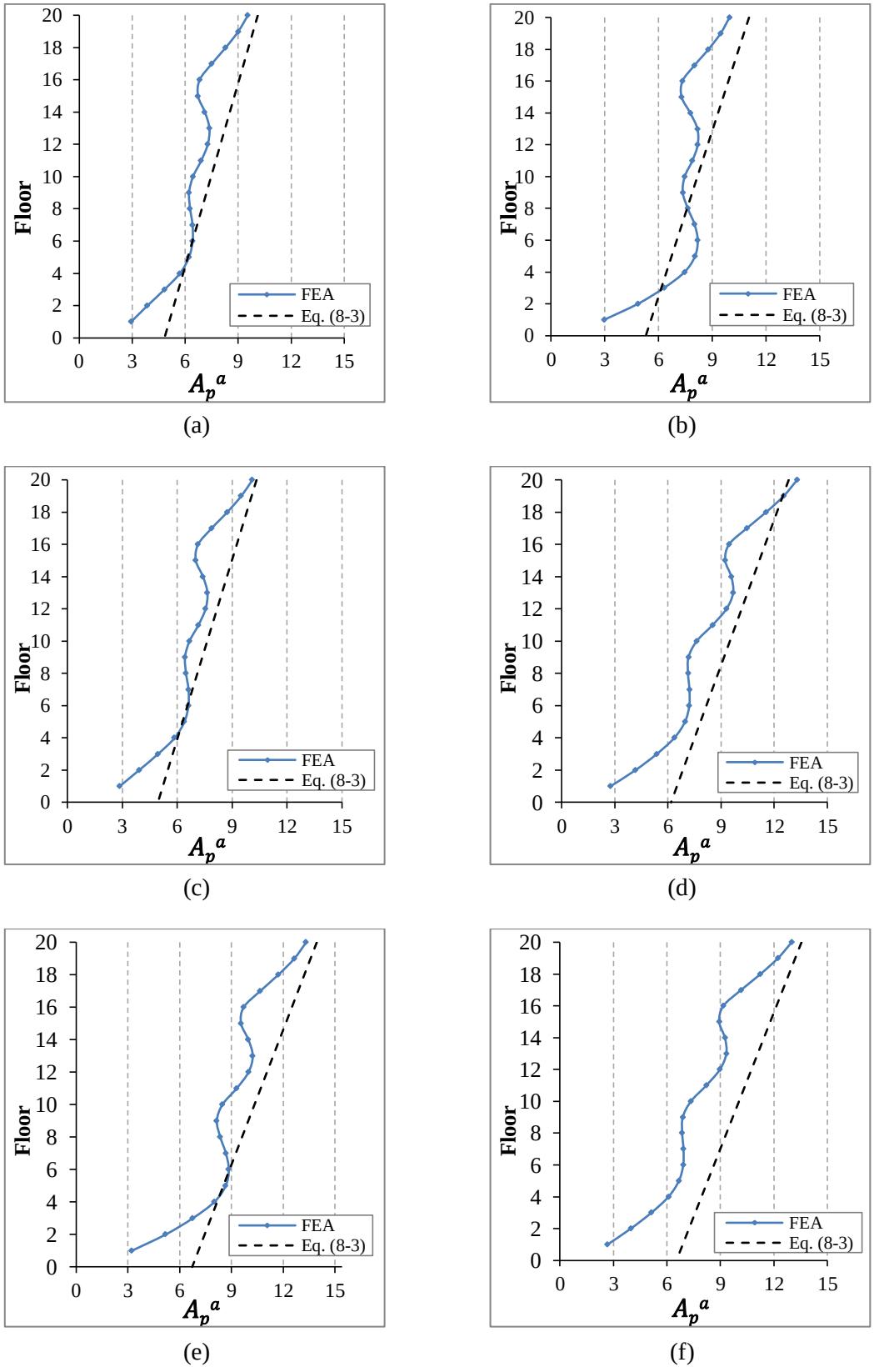

Figure 8.18 Predictions of Eq. (8-3) and FE results of the maximum acceleration amplification factors (A_p^a) for the NSCs with periods equal to $T_C = T_1$ for those termed as (a) T_1-Reference, (b) T_1-B-3-4, (c) T_1-M-3-4, (d) T_1-T-3-4, (e) T_1-TB-3-4, and (f) T_1-TM-3-4.

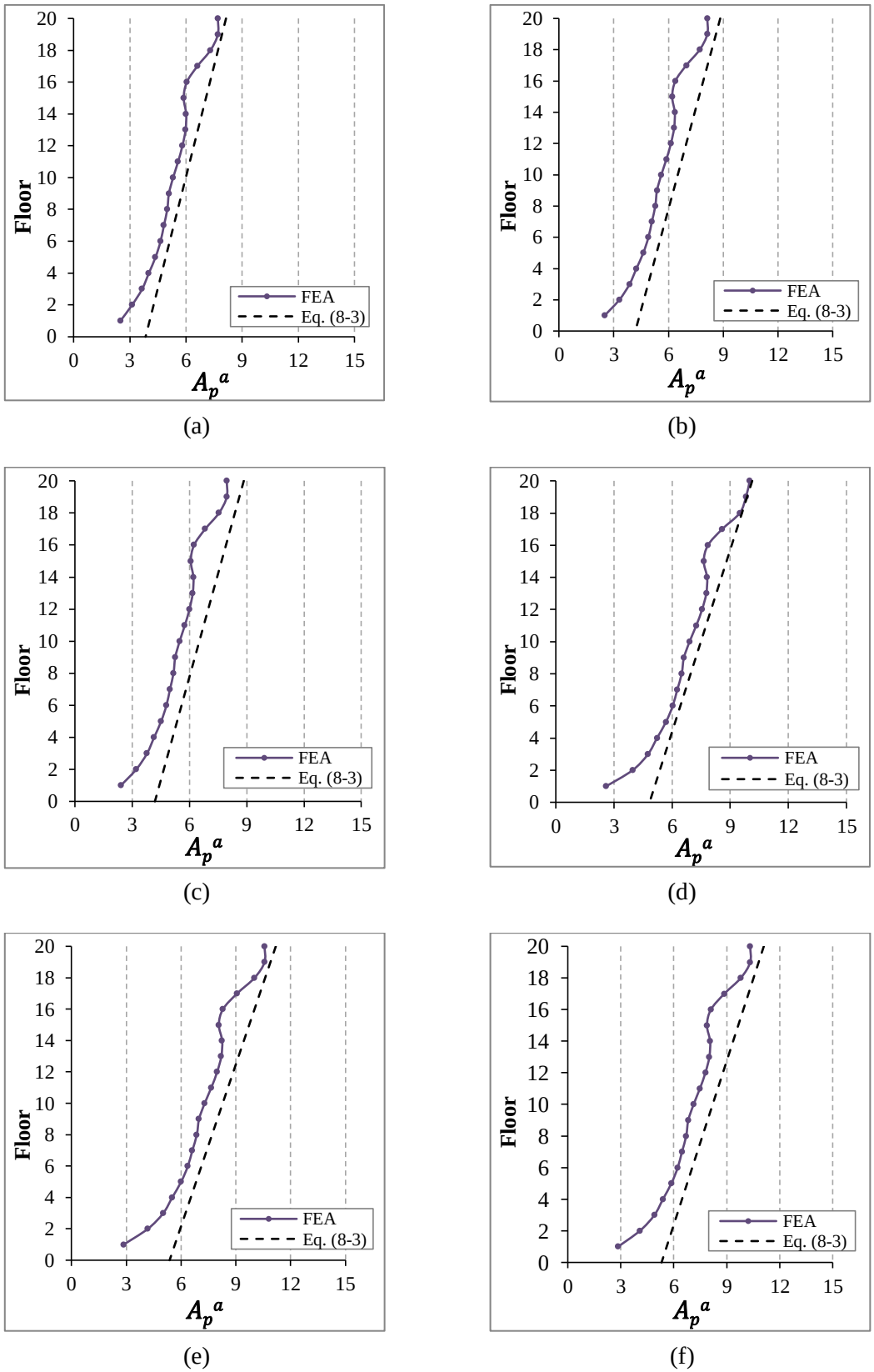

Figure 8.19 Predictions of Eq. (8-3) and FE results of the maximum acceleration amplification factors (A_p^a) for the NSCs with periods equal to $T_C = T_2$ for those termed as (a) T_2-Reference, (b) T_2-B-3-4, (c) T_2-M-3-4, (d) T_2-T-3-4, (e) T_2-TB-3-4, and (f) T_2-TM-3-4.

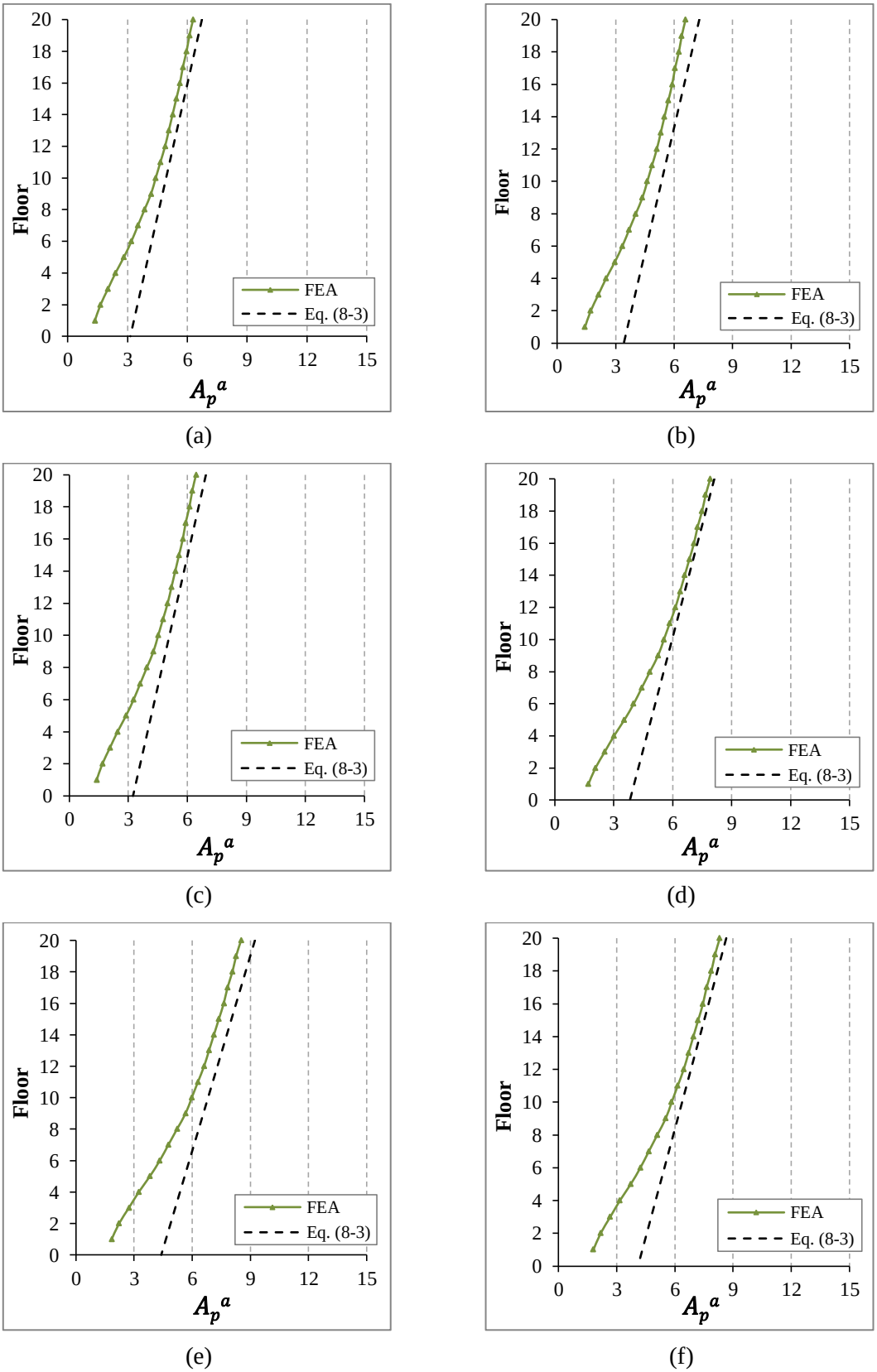

Figure 8.20 Predictions of Eq. (8-3) and FE results of the maximum acceleration amplification factors (A_p^a) for the NSCs with periods equal to $T_C = T_3$ for those termed as (a) T_3-Reference, (b) T_3-B-3-4, (c) T_3-M-3-4, (d) T_3-T-3-4, (e) T_3-TB-3-4, and (f) T_3-TM-3-4.

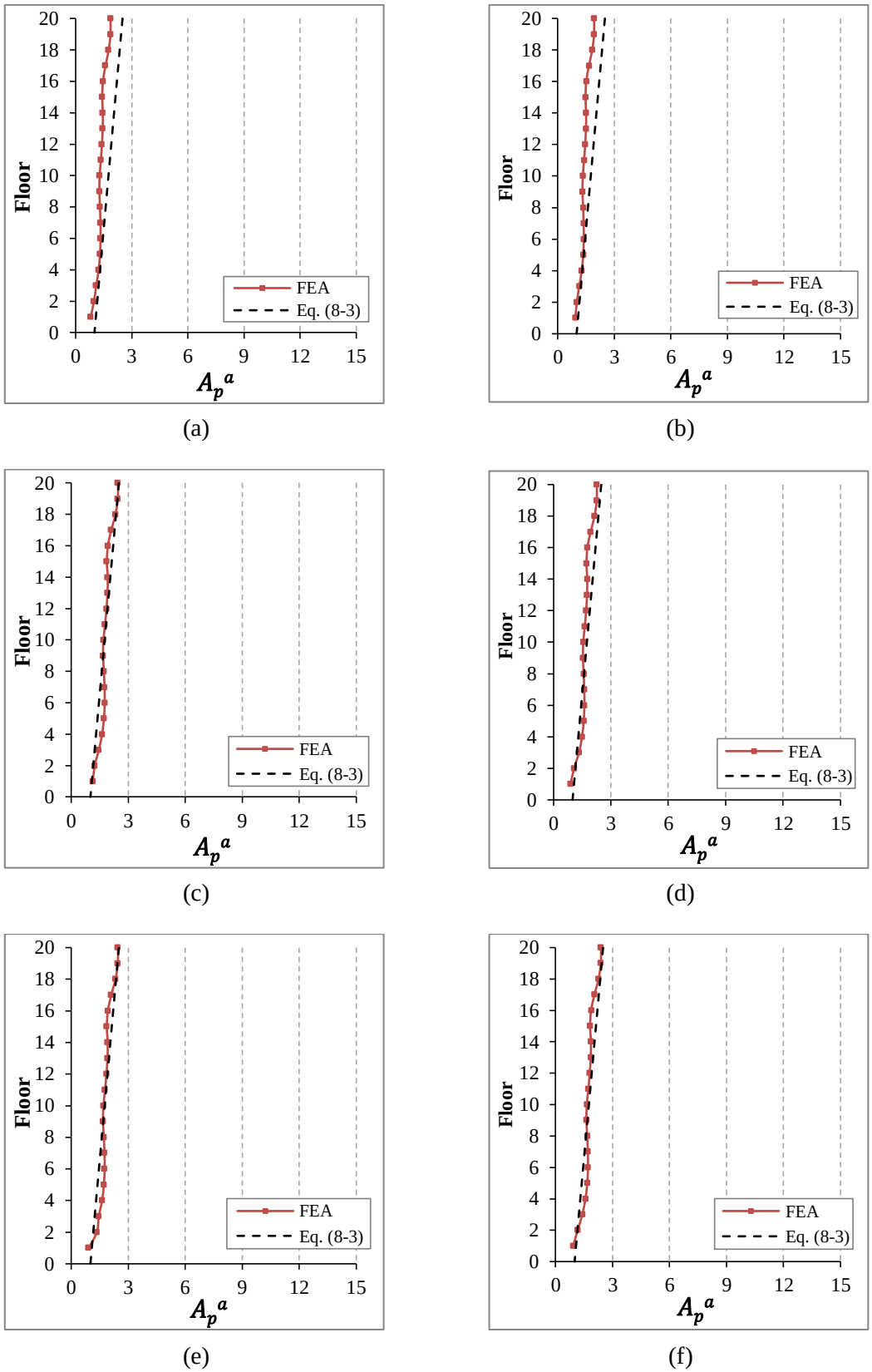

Figure 8.21 Predictions of Eq. (8-3) and FE results of the maximum acceleration amplification factors (A_p^a) for the NSCs with periods equal to $T_C \approx 0$ s, for those termed as (a) T_0-Reference, (b) T_0-B-3-4, (c) T_0-M-3-4, (d) T_0-T-3-4, (e) T_0-TB-3-4, and (f) T_0-TM-3-4.

Because of the values of the acceleration amplification factors were observed maximum at the top floors of the selected five critical and the reference cases, additional comparisons at the roof levels are made for all the adopted cases of vertical mass irregularities. Figures 8.22, 8.23, 8.24, and 8.25 illustrated the comparisons between the numerical values of A_p^a for the NSCs mounted on the flexible sides of the top floors for those having periods equal to T_1, T_2, T_3, and $T_C \approx 0$ s, respectively. Overall, Figures 8.22 to 8.25 have clearly demonstrated that Eq. (8-3) provides good predictions of the values of A_p^a in comparison with those estimated using the expression of the EC8 (2004). It can be seen from Figure 8.25 that the predictions of EC8 and Eq. (8-3) have the same line style, as well as have similar predictions. This is attributable to the fact that the modification on EC8 i.e. Eq. (8-3), is made only for the NSCs that have periods larger than $T_C = 0.0$. However, the predictions of the rigid NSCs were kept the same as the EC8 provision.

Furthermore, it can be seen from Figure 8.26 that the proposed Eq. (8-3) underestimated the seismic responses on average by 15.6% for the NSCs with $T_C = T_1$ and attached to the flexible sides of the top floors of different cases of vertical mass irregularities under the effect of the base motions with PGA values corresponding to the maximum seismic capacities. However, the EC8 (2004) recommendations give an average value of the underestimation by about 58% at values of PGA values corresponding to the maximum seismic capacities.

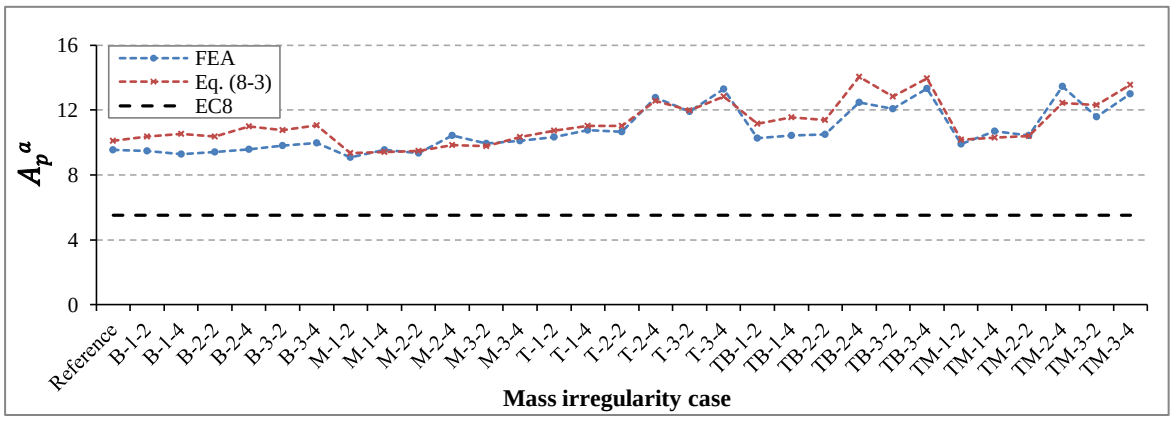

Figure 8.22 Predictions of FEA results and Eq. (8-3) of the maximum acceleration amplification factors (A_p^a) for the NSCs with periods equal to T_1 for those NSCs attached to the flexible sides of the top floors of the P-structure that had different cases of vertical mass irregularities.

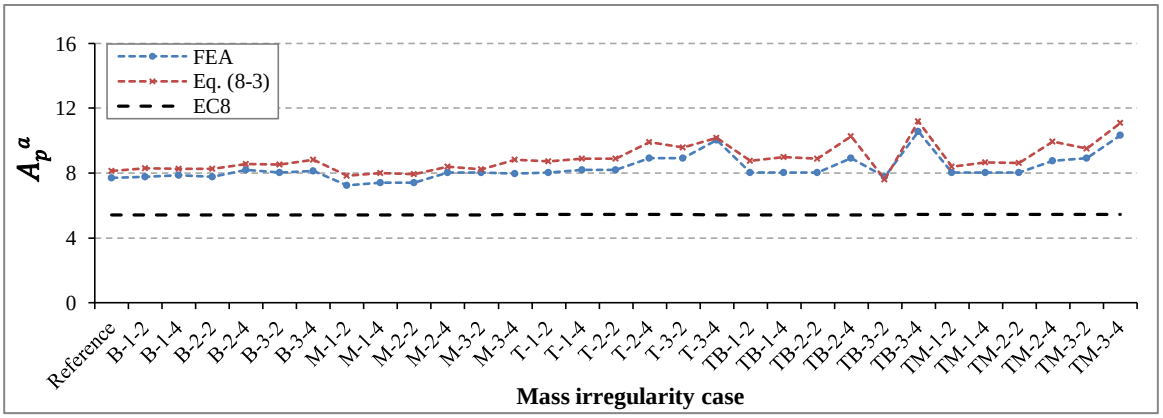

Figure 8.23 Predictions of FEA results and Eq. (8-3) of the maximum acceleration amplification factors (A_p^a) for the NSCs with periods equal to T_2 for those NSCs attached to the flexible sides of the top floors of the P-structure that had different cases of vertical mass irregularities.

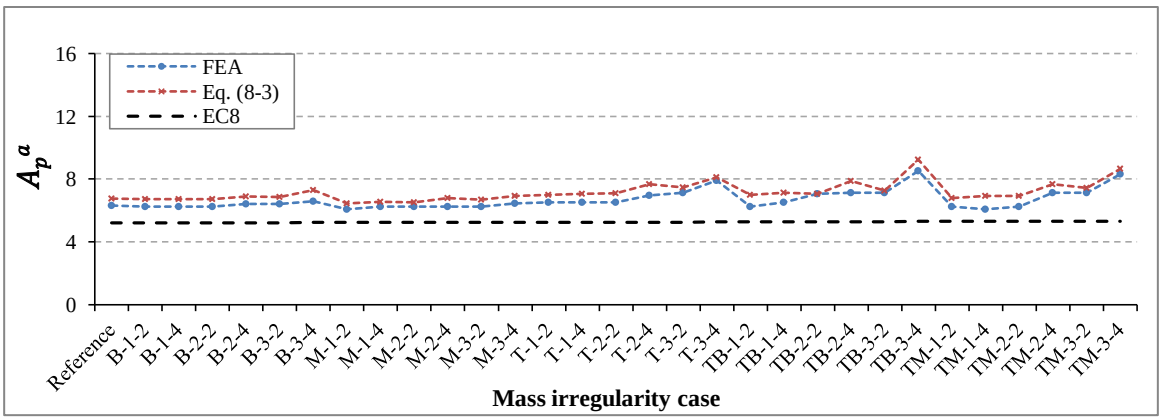

Figure 8.24 Predictions of FEA results and Eq. (8-3) of the maximum acceleration amplification factors (A_p^a) for the NSCs with periods equal to T_3 for those NSCs attached to the flexible sides of the top floors of the P-structure that had different cases of vertical mass irregularities.

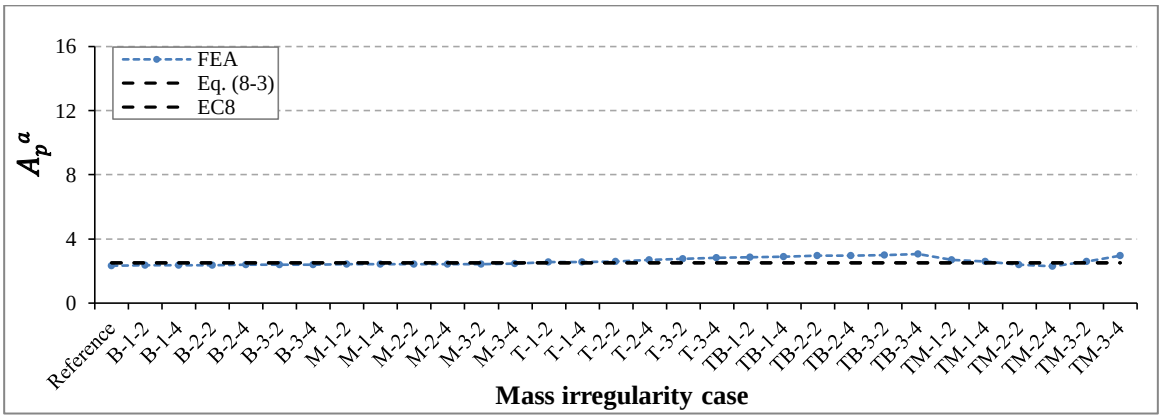

Figure 8.25 Predictions of FEA results and Eq. (8-3) of the maximum acceleration amplification factors (A_p^a) for the NSCs with $T_C \approx 0$ s for those NSCs attached to the flexible sides of the top floors of the P-structure that had different cases of vertical mass irregularities.

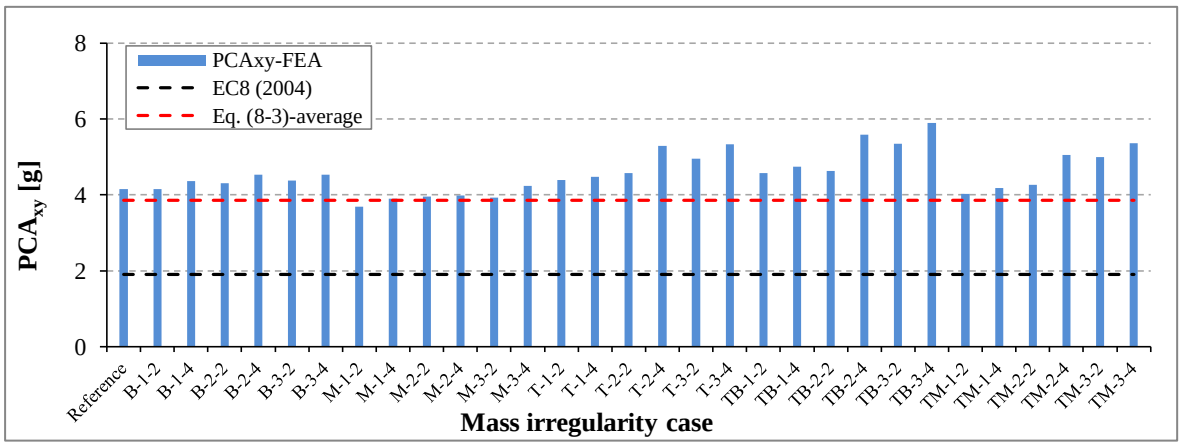

(b)

Figure 8.26 Comparison between FEA results of PCA_{xy} and the predictions of the EC8, as well as the proposed Eq. (8-3) for the NSCs with periods equal to T_1 and attached to the flexible sides of the top floors of the P-structure that had different cases of vertical mass irregularities at the PGA values corresponding to the maximum seismic capacities.

For periods of the NSCs equal to T_1, T_2, T_3, and $T_C \approx 0$ s, shown in Figure 8.27 are the ratios between the values of A_p^a at the relative height equal to zero and those value of A_p^a at the relative height equal to 1.0 (i.e. $A_p^a{}_{(z_c/H=0)}/A_p^a{}_{(z_c/H=1)}$) which estimated by Eq. (8-3). It can be observed that in the case of the NSCs, which had periods equal to T_1, T_2, and T_3, the average of the ratio $A_p^a{}_{(z_c/H=0)}/A_p^a{}_{(z_c/H=1)}$ was found approximately equal to 0.48. However, this ratio

value was observed equal to 0.4 for rigid NSCs with $T_C \approx 0$ s. These two values can be used to modify the expressions presented in Chapter 7 (see Table 7.5) to account in general the percentages of the increase in the values of PCA_{xy} along the buildings heights due to the increase in total mass ratios for different locations of the mass irregularities. Table 8.2 shows the expressions for the calculation of the percentages of the increases in the accelerations of the NSCs that are attached to the floors of the P-structures along their heights.

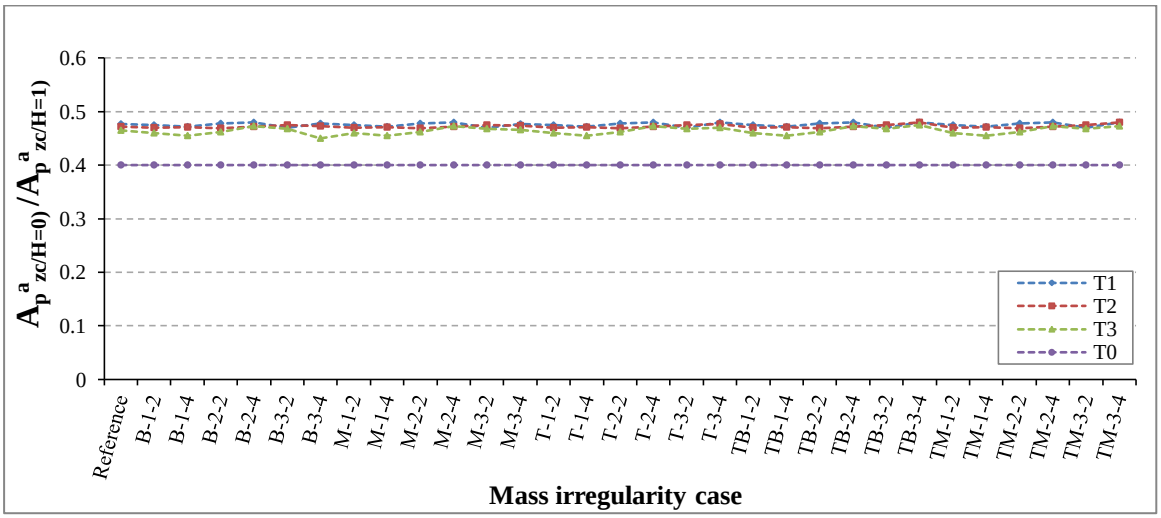

Figure 8.27 Ratio values of the maximum acceleration amplification factors (A_p^a) at ground levels with respect to those values at the roof levels estimated by to the proposed Eq. (8-3) for the NSCs periods equal to T_1, T_2, T_3, and $T_C \approx 0$ s.

Table 8.2 Modified expressions for the calculation of the increase percentages in the values of PCA_{xy} along the height of the P-structures due to the increase in the total mass ratios for different locations of mass irregularities.

NSCs period	Mass Location	% of increase in PCA_{xy}	Equation's No.
T_1	Top	$I_T = \left(0.48 + 0.52\,\frac{z_c}{H}\right)(2.8\,\acute{M} + 1.8)$	(8-4)
	Bottom	$I_B = \left(0.48 + 0.52\,\frac{z_c}{H}\right)(0.7\,\acute{M} - 0.8)$	
	Top-Bottom	$I_{TB} = \left(0.48 + 0.52\,\frac{z_c}{H}\right)(3.65\,\acute{M} + 0.85)$	
	Middle	$I_M = \left(0.48 + 0.52\,\frac{z_c}{H}\right)(1.1\,\acute{M} - 8.0)$	
	Top-Middle	$I_{TM} = \left(0.48 + 0.52\,\frac{z_c}{H}\right)(4.1\,\acute{M} - 7.8)$	
T_2	Top	$I_T = \left(0.48 + 0.52\,\frac{z_c}{H}\right)(2.5\,\acute{M} + 1.6)$	(8-5)
	Bottom	$I_B = \left(0.48 + 0.52\,\frac{z_c}{H}\right)(0.5\,\acute{M} - 0.55)$	
	Top-Bottom	$I_{TB} = \left(0.48 + 0.52\,\frac{z_c}{H}\right)(3.25\,\acute{M} + 0.90)$	
	Middle	$I_M = \left(0.48 + 0.52\,\frac{z_c}{H}\right)(0.95\,\acute{M} - 7.5)$	
	Top-Middle	$I_{TM} = \left(0.48 + 0.52\,\frac{z_c}{H}\right)(3.6\,\acute{M} - 5.5)$	
T_3	Top	$I_T = \left(0.48 + 0.52\,\frac{z_c}{H}\right)(2.1\,\acute{M} + 1.3)$	(8-6)
	Bottom	$I_B = \left(0.48 + 0.52\,\frac{z_c}{H}\right)(0.4\,\acute{M} - 0.4)$	
	Top-Bottom	$I_{TB} = \left(0.48 + 0.52\,\frac{z_c}{H}\right)(3.0\,\acute{M} + 0.8)$	
	Middle	$I_M = \left(0.48 + 0.52\,\frac{z_c}{H}\right)(0.75\,\acute{M} - 6.2)$	
	Top-Middle	$I_{TM} = \left(0.48 + 0.52\,\frac{z_c}{H}\right)(3.2\,\acute{M} - 5.0)$	
T_0	Top	$I_T = \left(0.4 + 0.6\,\frac{z_c}{H}\right)(1.6\,\acute{M} + 0.95)$	(8-7)
	Bottom	$I_B = \left(0.4 + 0.6\,\frac{z_c}{H}\right)(0.1\,\acute{M} + 0.65)$	
	Top-Bottom	$I_{TB} = \left(0.4 + 0.6\,\frac{z_c}{H}\right)(2.5\,\acute{M} + 0.65)$	
	Middle	$I_M = \left(0.4 + 0.6\,\frac{z_c}{H}\right)(0.6\,\acute{M} - 5.0)$	
	Top-Middle	$I_{TM} = \left(0.4 + 0.6\,\frac{z_c}{H}\right)(2.7\,\acute{M} - 4.2)$	

8.5 Summary

In Chapter 8, an extended design equation of NSCs was proposed to improve the EC8 (2004) predictions. Two factors have been used to extend the EC8 formula for NSCs that are expected to be attached to the flexible sides of irregular RC buildings. The effects of both the torsion and maximum seismic capacity of irregular RC P-structure were suggested in this extension. The proposed expression demonstrated to be applicable to NSC with different periods mounted on irregular RC multi-storey buildings designed with different heights, eccentricity ratios, ground types, and different seismic capacities, as well as different distributions of masses along the heights of asymmetrical P-structures. In general, the proposed formula provides: (i) good estimates of the dynamic response of NSCs that can be affected by the torsional behaviour of the P-structures; (ii) accurate estimates of the maximum acceleration amplification factors of NSCs under the effect of base motions having PGA values corresponding to the elastic seismic capacities of the P-structures; and (iii) safer predictions of the NSCs accelerations than those of the EC8 under the effect of PGA values corresponding to the maximum seismic capacities of the P-structures. Therefore, it is expected that when the NSCs are designed using the proposed expression, they can remain functional without damage under the effect of earthquakes having PGA in the range of 70% to 80% of the maximum seismic capacities of the P-structures.

CHAPTER NINE: CONCLUSIONS AND FUTURE RESEARCH

9.1 Conclusions

This section presents the most significant conclusions that can be drawn from the analyses (i.e. average numerical results of 6755 nonlinear dynamic finite element analyses of P-S systems) presented in Chapters 5 to 8. In general, for a given P-structure, the numerical results suggest that there is a strong correlation between the NSCs torsional amplification factors and top floor rotations of the P-structures. EC8 (2004) seems to underestimate the acceleration response of the NSCs attached to the flexible sides of the P-structures. Based on the results of this research, the following specific conclusions are drawn:

- Accelerations of NSCs exhibited three zones for different ranges of fundamental periods; in Zone 1, NSCs accelerations increased gradually with the increase in the values of T_C/T_1 from 0.0 to the values slightly lower than the value of T_3/T_1. In Zone 2, a sharp increase in the dynamic response of the NSCs was observed for those values of T_C/T_1 in the range between the values of T_3/T_1 and 1.0 (i.e. when NSCs periods matched the fundamental vibration periods of the P-structures). However, Zone 3 was marked by a sudden drop in the NSCs accelerations at values of T_C/T_1 greater than 1.0.

- For a given P-structure, the accelerations of the NSCs varied approximately linearly with the base excitations up to the peak ground acceleration (PGA) values corresponding to the elastic seismic capacities of the P-structures. At higher PGA values, damage reduces

the global stiffness of the P-structures and consequently changes their dynamic characteristics. This, in turn, reduces the rate of the increase of the accelerations of both the P-structures and NSCs resulting in a nonlinear relationship between NSCs accelerations and PGA.

- The torsional amplification factors of NSCs increased with the increase in the height of the buildings. This trend seems to be affected by the floor rotation values of the P-structures. The higher the value of the top floor rotations, the higher the values of the torsional amplification factors. Therefore, it can be concluded that the increase in the torsional behaviour of the P-structure results in a corresponding increase in the acceleration of the NSC that is attached to the flexible sides of the P-structure.

- For NSCs with damping ratio of 3% and having vibration periods equal to the first fundamental periods of the P-structures (i.e. $T_C = T_1$), the values of peak component accelerations (PCA_{xy}) at the centres of rigidity of the P-structures designed on ground type D were higher than the corresponding values on ground types A, B, and E by about 61.5%, 37.4%, and 33.0%, respectively. However, these values were found equal to 40.0%, 21.8%, and 22.2%, respectively, when the NSCs were attached to the flexible sides.

- For the NSCs under tuned conditions and attached to the flexible side of the top floor of the P-structure with a high eccentricity ratio (0.372), the accelerations of the NSCs with damping ratio of 3% at the PGA values corresponding to the elastic seismic capacities of the P-structure were 57.8% higher than those accelerations of the NSCs attached to the P-structure without eccentricity. The NSCs accelerations at the PGA values corresponding to the maximum seismic capacities were 77% higher than the corresponding accelerations at the elastic seismic capacities of the P-structures.

- The NSCs located between the stiff sides (SS) and the centres of rigidity (CRs) of the P-structures had approximately equal accelerations. Beyond the CRs, the acceleration response increased with the increase in the relative distance from the SS. This result suggests that there is no de-amplification in the acceleration response of the NSCs attached to the SS with respect to the corresponding value at CR.

- The accelerations of the NSCs with vibration periods equal to T_1 decreased with the increase in NSC damping ratio from 0.01% to 3%. The percentage decreases varied from 48% to 40% and from 50% to 41% at the PGA values corresponding to the elastic and maximum seismic capacities of the P-structures respectively. The accelerations of the NSCs with un-tuned conditions were less affected by the increase in NSC damping ratio from 0.01% to 3%. The percentage decreases for such NSCs varied from 23% to 21% and from 26% to 22% at the PGA values corresponding to the elastic and maximum seismic capacities of the P-structures, respectively. At higher NSC damping ratios (i.e. from 3% to 5%), the NSCs accelerations were not significantly affected by the increase in NSC damping ratio.

- The trend and value of the increase in the seismic response of NSCs due to the increase in NSC damping ratio from 0.01% to 3% were found unequal when they are attached to different irregular buildings. The largest value of the increase in the value of PCA_{xy} was found for the NSCs attached to the buildings with the highest torsional behaviour (i.e. the highest floor rotations).

- The minimum value of the amplification of peak component acceleration due to a reduction in the damping ratio from 3% to 0.01% was observed equal to 1.65 for the NSCs attached to regular building (i.e. non-torsional RC P-structure).

- It was observed that there is a strong relation between the NSCs accelerations and the torsional behaviour of P-structures with different vertical mass irregularities. Except for some P-structures with vertical mass irregularities at the middle floors, the values of the top floor rotations were found higher than the corresponding values for the P-structure with uniform mass distribution along its height (i.e. vertical mass ratio equal to 1.0). The percentage increases in the top floor rotations of the buildings termed as B-3-4, M-3-4, T-3-4, TB-3-4, and TM-3-4 were found higher by 1.27, 1.14, 2.21, 2.45, and 2.3 respectively than those of the building with uniform mass distribution along its height. Accordingly, at the flexible side, the corresponding accelerations of the NSCs with periods equal to T_1 and 3% damping ratio were higher by 1.074, 1.04, 1.30, 1.404, and 1.37, respectively, than the accelerations of the NSCs attached to the building with uniform mass distribution.

- For the cases of mass irregularities at the bottom floors of the P-structures, the percentages of the increase in the values of NSCs accelerations at these floors were higher than the corresponding values at the top floors. The major cause for this trend is due to higher percentages of the increase in the values of floor rotations at the bottom floors when the mass irregularities were also at the bottom floors. When the total ratio of a mass irregularity at the bottom levels was 12 (i.e. B-3-4), an increase of 34.5% was observed in PCA_{xy} for the NSCs with $T_C = T_1$ and 3% damping ratio with respect to the reference case due to the increase in the values of the floor rotations by 59%.

- One of the more significant conclusions that can be found is that the percentages of the increase in the values of peak component accelerations at the flexible side of the roof levels were increased linearly as a result of the increase in the total mass. In the case of the NSCs with periods equal to T_1 and 3% damping ratio, the maximum percentages of the

increase in the NSCs acceleration values were 44.65% and 41.4% for the NSCs termed as T_1-TB-3-4 and T_1-TM-3-4 respectively (i.e. for the cases of total mass ratio equal to 12).

- Comparison of the EC8 (2004) predictions for NSCs accelerations with the corresponding numerical results suggests that, when the fundamental periods and heights of the NSCs matched those of the P-structures (i.e. NSCs with periods equal to T_1 and attached to the roof levels), EC8 design provisions underestimate the seismic response of the NSCs attached to the flexible sides of irregular RC P-structures designed on ground types A, B, C, D, and E. Predictions of the EC8 were on average 32.5% less than the numerical results when the P-S systems were subjected to the PGA values corresponding to the design ground accelerations of the P-structures.

- For rigid NSCs ($T_C \approx 0$ s) attached to the centres of rigidity along the heights of the RC P-structures, the majority of peak component acceleration values at the design ground accelerations were found within the range of the predictions of the EC8 (2004). However, the values of the peak component accelerations for the rigid NSCs attached to the flexible sides at the lower third of the P-structures exceeded the EC8 predictions. On average, the EC8 underestimated the finite element dynamic response of the NSCs attached to such locations by about 16%. Therefore, it is suggested that rigid NSCs attached at the lower third of the P-structures should be designed by implementing the acceleration amplification factors for the corresponding NSCs attached to the upper floors.

- For the NSCs that had periods equal to $4T_1$ (i.e. very long NSCs period) and attached to both the centres of rigidity and flexible sides along the height of the P-structures, EC8 predicted unconservative values for the NSCs accelerations. This fact is recognised in the manual for design of buildings according to Eurocode 8 (IStructE, 2010), where it is stated

that the design formula of the NSCs according to EC8 (2004) may be unconservative for very long periods of NSCs. Therefore, it is recommended that the value of (T_C/T_1) should be limited to a maximum of 2.0 for design purposes of the NSCs.

- The perceived cause of the underestimations in the seismic response of NSCs according to the EC8 provisions is that EC8 does not take into account the amplification in the NSCs accelerations caused by the torsional modes of the P-systems. Accordingly, the current EC8 design provision for NSCs is modified by taking into consideration the influence of both the torsion and the maximum seismic capacity of the supporting structure. It was clearly demonstrated that the proposed formula (i.e. modification of the EC8 equation) provided good predictions in comparison with that of EC8 (2004) for the NSCs mounted on the flexible sides along the heights of the P-structures. The proposed formula predicted well the response of the NSCs that had periods equal to or larger than the torsional vibration periods of the P-structures.

- The recommendations of EC8 (2004) underestimated the seismic response of the NSCs with $T_C = T_1$ and 3% damping ratio by about 50% on average compared with the corresponding numerical results at the PGAs equal to the maximum seismic capacities of the P-structures. However, the proposed formula underestimated the corresponding dynamic response on average by about 17% compared with the numerical results at the PGA values corresponding to the maximum seismic capacities of the P-structures.

9.2 Recommendations for Further Research

The current research has attempted to investigate the influence of the torsional and seismic capacity of the P-structure on the seismic response of the attached lightweight acceleration-sensitive NSCs using a three-dimensional numerical model. Accordingly, this research has modified the formula of the EC8 (2004) for the design of the NSCs. In addition, several expressions have been proposed which can be used to calculate the percentages of the increase in the values of the NSCs accelerations when the NSCs are mounted on an RC P-structure with plan and/or vertical mass irregularities. Furthermore, the conclusions of the current research gave useful insights into the global response of the NSCs attached to irregular RC buildings. Although that more than 6500 nonlinear dynamic analyses were used to generalise the results, but these results could not be applied to other types of NSCs such as deformation-sensitive NSCs, as well as may not be applied to NSCs when they are mounted on other types of P-structures such as irregular steel frames. The numerical results of the current investigation are appropriate for non-structural components that can be classified as lightweight acceleration-sensitive systems mounted on fixed-base irregular RC buildings designed according to the modern seismic provisions. In this investigation, the NSCs were idealised as cantilevers with masses on the top and in contact with the P-structure at a single point. However, it is recommended that additional research studies are carried out in the following areas using a 3D numerical model:

1) Seismic response of multi-support non-structural components: for flexible secondary elements attached to the main supporting structure at multi-points, it may be more appropriate to model these elements as a MDOF system with multi-supports. Some examples of these S-

systems are pipelines and signboards, which may be connected either horizontally or vertically to the P-structures. Therefore, it would be interesting to investigate numerically the effect of torsion on the NSCs accelerations when the NSCs are attached to the flexible sides at multi-points along the height of asymmetrical supporting structures.

2) Seismic behaviour of deformation-sensitive non-structural components: most of the current studies on deformation-sensitive NSCs focus on their behaviour using 2-D models while neglecting the torsional response of the P-structure (Colangelo, 2013). Therefore, those S-systems classified as deformation-sensitive elements, such as infill masonry walls, need to be investigated to explore how they can be affected when they are attached to or built within RC multi-storey buildings with significant torsional behaviour. Furthermore, the effect of the vertical component of an earthquake may have a considerable influence on the seismic response of such NSCs; therefore, the effect of vertical accelerograms could also be the subject of further research.

3) Non-structural components integrated on base-isolated structures: seismic base-isolation devices can provide an improvement to the behaviour of the S-systems mounted on torsional buildings during earthquakes. This approach can be used to increase the fundamental vibration period of the main structure and thus reduce the floor acceleration values of the P-structure. Furthermore, a base isolation technique can be used to decrease the rotations of the floors of the irregular buildings, so this can result in a reduction of the transmitted accelerations into the structures and their attachments under the effect of the seismic actions. Therefore, it is recommended to investigate numerically the seismic response of NSCs attached to irregular buildings designed as base-isolated structures.

4) Seismic response of NSCs integrated on an RC multi-storey building constructed using recycled aggregates: for a variety of purposes such as environmental conservation and a rise in the cost of the waste treatment, recycling of the construction and destruction materials has become more prevalent. Therefore, some countries have developed some guides and provisions for using recycled materials such as aggregates in the construction of RC structures (Xiao *et al.*, 2006). Due to the expectation of a growing use of recycled materials to construct low to medium rise RC multi-storey buildings, further research needs to be undertaken, using the Finite Element Method, to investigate the dynamic response of NSCs attached to different floors along the height of an RC buildings constructed using different percentages of recycled aggregate materials.

5) Dynamic response of NSCs integrated on RC multi-storey structures strengthened by different seismic rehabilitation approaches: one of the main causes of hazards in some seismic areas is under-designed RC buildings, which are incompatible with modern provisions of the seismic design codes. These buildings may have been designed to resist gravity loads only according to the old codes provisions and they do not meet the requirements of the modern seismic codes. Among them, plan-irregular buildings are common P-structures (Di Ludovico *et al.*, 2008; Ferraioli *et al.*, 2010). Due to the economic costs of demolishing and reconstructing such buildings, different seismic recovery methods are used to improve their seismic capacities. Based on the classification of FEMA 356 (2000), seismic rehabilitation approaches can be identified as follows: components local adjustment, modification in the irregularity of plan or discontinuity along the height of the existing buildings, strengthening of the structural members, reduction of the masses, and base isolation techniques. Therefore, it is recommended to extend the current research by investigating the dynamic response of NSCs

integrated on non-seismic designed buildings strengthened using one of the above-mentioned techniques.

It can be seen that the recommended research studies presented above in (1) and (2) are dealing with the dynamic characteristics of the secondary systems that may be affected by the displacement values of the P-structures (i.e. lateral and torsional displacements). Therefore, validation of the EC8 recommendations for the design of deformation-sensitive non-structural components is worthy of investigation when they are attached to asymmetrical structures.

However, those studies recommended above in (3) to (5) are dealing with the dynamic characteristics of the primary structures such as their stiffness and seismic performance during earthquakes, as well as their base conditions. As the modified equation proposed in this research (i.e. Eq. (8-3)) considers the maximum seismic capacity of the P-structure, therefore, this equation can also be used for the design of the acceleration-sensitive NSCs when they are attached to the buildings mentioned above in (3) to (5). In this case, the main purpose of these recommended studies is to examine the validity of the proposed equation (8-3) for the design of the NSCs attached to P-structure with various dynamic characteristics.

REFERENCES

Adam, C. and Fotiu, P. (2000). Dynamic analysis of inelastic primary-secondary systems. *Engineering Structures*, 22 (1): 58-71. Available online: http://www.sciencedirect.com/science/article/pii/S014102969800073X, (last accessed on 06.12.2014).

Adam, C. and Furtmüller, T. (2008). Response of nonstructural components in ductile load-bearing structures subjected to ordinary ground motions. In *Proceedings of the 14th World Conference on Earthquake Engineering*, October 12-17, Beijing, China, 8pp. Available online: http://www.iitk.ac.in/nicee/wcee/article/14_05-01-0327.PDF, (last accessed on 06.12.2014).

Agrawal, A. and Datta, T. (1997). Behavior of secondary system attached to a torsionally coupled primary system. *European Earthquake Engineering*, 11: 47-53.

Agrawal, A. and Datta, T. (1998). Seismic response of a secondary system mounted on a torsionally coupled non-linear primary system. *Journal of Earthquake Engineering*, 2 (3): 339-356. Available online: http://www.iiees.ac.ir/iiees/English/Publication/jsee/Jsee2_3.pdf, (last accessed on 06.12.2014).

Agrawal, A. K. (1999). Non-linear response of light equipment system in a torsional building to bi-directional ground excitation. *Shock & Vibration*, 6 (5-6): 223-236. Available online: http://www.hindawi.com/journals/sv/1999/948265/abs/, (last accessed on 06.12.2014).

Agrawal, A. K. (2000a). Response of light equipment on torsional building with passive tuned mass damper. *Computers & Structures*, 78 (4): 591-602. Available online: http://www.sciencedirect.com/science/article/pii/S0045794900000377, (last accessed on 06.12.2014).

Agrawal, A. K. (2000b). Behaviour of equipment mounted over a torsionally coupled structure with sliding support. *Engineering Structures*, 22 (1): 72-84. Available online: http://www.sciencedirect.com/science/article/pii/S0141029698000662, (last accessed on 06.12.2014).

Agrawal, A. K. and Datta, T. (1999a). Seismic behavior of secondary system on yielding torsionally coupled primary system. *Journal of Seismology and Earthquake Engineering-JSEE*, 2 (1): 35-46. Available online: http://www.iiees.ac.ir/iiees/English/Publication/jsee/Jsee2_3.pdf, (last accessed on 06.12.2014).

Agrawal, A. K. and Datta, T. (1999b). Seismic response of a secondary system attached to a torsionally coupled primary system under bi-directional ground motion. *Journal of Earthquake Technology-ISET*, 36 (1): 27-42. Available online: http://home.iitk.ac.in/~vinaykg/Iset389.pdf, (last accessed on 06.12.2014).

Agrawal, A. K. and Datta, T. (2001). Behavior of multiple supported secondary system mounted on a torsionally coupled primary system. *Journal of Seismology and Earthquake Engineering*, 3 (1): 13-22. Available online: http://www.iiees.ac.ir/iiees/English/Publication/jsee/Jsee6_2.pdf, (last accessed on 06.12.2014).

Al Ali, A. A. K. and Krawinkler, H. (1998). Effect of vertical irregularities on seismic behavior of building structure. *Report No. 130*, Stanford University: Blume Earthquake Engineering Center. Available online: https://blume.stanford.edu/content/effects-vertical-irregularities-seismic-behavior-building-structures, (last accessed on 06.12.2014).

ASCE (2005). Seismic design criteria for structures, systems, and components in nuclear facilities. *American Society of Civil Engineers*, ASCE Standard 43-05, Reston, VA. Available online: http://www.civil.utah.edu/~bartlett/NEUP/Guidance%20Documents/ASCE%204305%20020713.pdf, (last accessed on 06.12.2014).

ASCE (2010). Minimum design loads for buildings and other structures. *American Society of Civil Engineers*, ASCE/SEI Standard 7-10, Reston, VA.

ATC (1978). Tentative provisions for the development of seismic regulations for buildings. *ATC-3-06*, Redwood City, CA: Applied Technology Council - Structural Engineers Association of California.

Biggs, J. M. (1971). Seismic response spectra for equipment design in nuclear power plants. In *Proceedings of the 1st International Conference on Structural Mechanics in Reactor Technology*, September 20-24, Berlin, Germany, 329-343. Available online: http://nisee.berkeley.edu/elibrary/Text/S22519, (last accessed on 06.12.2014).

Booth, E. (1999). SIMQKE1-Generation of artificial time histories compatible with a specified target spectrum. Available online: http://www.booth-seismic.co.uk/page3.html, (last accessed on 06.12.2014).

BSSC (1992). NEHRP Handbook for the seismic evaluation of existing buildings. *FEMA 178*, Washington, DC: Building Seismic Safety Council. Available online: http://mitigation.eeri.org/resource-library/building-professionals/nehrp-handbook-for-seismic-evaluation-of-existing-buildings-fema-178, (last accessed on 06.12.2014).

BSSC (1994). NEHRP Recommended provisions for the development of seismic regulations for new buildings. Washington, DC: Building Seismic Safety Council.

BSSC (2001). NEHRP Recommended provisions for seismic regulations for new buildings and other structures, 2000 Ed. *Report FEMA 368*, Washington, DC: Building Seismic Safety Council. Available online: https://www.wbdg.org/ccb/DHS/ARCHIVES/fema368.pdf, (last accessed on 06.12.2014).

BSSC (2003). Part 1: Provisions-NEHRP Recommended provisions for seismic regulations for new buildings and other structures, 2003 Ed. *FEMA 450*, Washington, DC: Building Seismic Safety Council. Available online: http://www.nehrp.gov/pdf/fema450provisions.pdf, (last accessed on 06.12.2014).

Cetisli, F. and Naito, C. J. (2003). State of the art of analytical prediction for confined concrete. *Report No. 0.3-24*, Lehigh University: National Center for Engineering Research on Advanced Technology for Large Structural Systems ATLSS. Available online: http://preserve.lehigh.edu/cgi/viewcontent.cgi?article=1034&context=engr-civil-environmental-atlss-reports, (last accessed on 06.12.2014).

Chandler, A. and Hutchinson, G. (1986). Torsional coupling effects in the earthquake response of asymmetric buildings. *Engineering Structures*, 8 (4): 222-236.

Chandler, A. M. (1986). Building damage in Mexico City earthquake. *Nature,* 320: 497-501. Available online: http://www.nature.com/nature/journal/v320/n6062/pdf/320497a0.pdf, (last accessed on 06.12.2014).

Chaudhuri, S. R. and Villaverde, R. (2008). Effect of building nonlinearity on seismic response of nonstructural components: a parametric study. *Journal of Structural Engineering,* 134 (4): 661-670. Available online: http://cedb.asce.org/cgi/WWWdisplay.cgi?163578, (last accessed on 06.12.2014).

Chen, D. C. and Lutes, L. D. (1990). Nonnormal secondary response due to yielding in a primary structure. *Technical Report NCEER-90-0002,* State University of New York, Buffalo: National Center for Earthquake Engineering Research (NCEER). Available online: http://mceer.buffalo.edu/publications/catalog/reports/Nonnormal-Secondary-Response-Due-To-Yielding-in-a-Primary-Structure-NCEER-90-0002.html, (last accessed on 06.12.2014).

Chen, W. F. (2007). *Plasticity in reinforced concrete.* New York: J. Ross Publishing. Available online: http://books.google.co.uk/books, (last accessed on 06.12.2014).

Chen, Y. and Soong, T. (1988). State-of-the-art review Seismic response of secondary systems. *Engineering Structures,* 10 (4): 218-228. Available online: http://www.sciencedirect.com/science/article/pii/0141029688900430, (last accessed on 06.12.2014).

Chintanapakdee, C. and Chopra, A. K. (2004). Seismic response of vertically irregular frames: response history and modal pushover analyses. *Journal of Structural Engineering,* 130 (8): 1177-1185. Available online: http://ascelibrary.org/doi/abs/10.1061/%28ASCE%290733-9445%282004%29130:8%281177%29, (last accessed on 06.12.2014).

Choi, B. J. (2004). Hysteretic energy response of steel moment-resisting frames with vertical mass irregularities. *The Structural Design of Tall and Special Buildings,* 13 (2): 123-144.

Chopra, A. K. and De la Llera, J. C. (1996). Accidental and natural torsion in earthquake response and design of buildings. In *Proceedings of the 11th World Conference on Earthquake Engineering*, June 23-28, Acapulco, Mexico, 15pp. Available online: http://www.iitk.ac.in/nicee/wcee/article/11_2006.PDF, (last accessed on 06.12.2014).

Chopra, A. K. and Goel, R. K. (2004). A modal pushover analysis procedure to estimate seismic demands for unsymmetric-plan buildings. *Earthquake Engineering & Structural Dynamics*, 33 (8): 903-927. Available online: http://onlinelibrary.wiley.com/doi/10.1002/eqe.380/abstract, (last accessed on 06.12.2014).

Ciampi, V. and Carlesimo, L. (1986). A nonlinear beam element for seismic analysis of structures. In *Proceedings of the 8th European Conference on Earthquake Engineering*, Lisbon, Portugal, 73-80.

Colangelo, F. (2013). Drift-sensitive non-structural damage to masonry-infilled reinforced concrete frames designed to Eurocode 8. *Bulletin of Earthquake Engineering*, 11 (6): 2151-2176. Available online: http://link.springer.com/article/10.1007/s10518-013-9503-y#page-1, (last accessed on 06.12.2014).

D'Ambrisi, A., De Stefano, M. and Viti, S. (2008). Seismic performance of irregular 3D RC frames. In *Proceedings of the 14th World Conference on Earthquake Engineering*, October 12-17, Beijing, China, 7pp. Available online: http://www.iitk.ac.in/nicee/wcee/article/14_05-01-0116.PDF, (last accessed on 06.12.2014).

De la Llera, J. C. and Chopra, A. K. (1994a). Evaluation of code accidental-torsion provisions from building records. *Journal of Structural Engineering*, 120 (2): 597-616. Available online: http://ascelibrary.org/doi/abs/10.1061/%28ASCE%290733-9445%281994%29120%3A2%28597%29?journalCode=jsendh, (last accessed on 06.12.2014).

De la Llera, J. C. and Chopra, A. K. (1994b). Accidental and natural torsion in earthquake response and design of buildings. University of California at Berkeley: Earthquake Engineering Research Center. Available online: http://nisee.berkeley.edu/elibrary/Text/239416, (last accessed on 06.12.2014).

Der Kiureghian, A., Sackman, J. L. and Nour-Omid, B. (1983). Dynamic analysis of light equipment in structures: response to stochastic input. *Journal of Engineering Mechanics*, 109 (1): 90-110. Available online: http://cedb.asce.org/cgi/WWWdisplay.cgi?36527, (last accessed on 06.12.2014).

Di Ludovico, M., Manfredi, G., Mola, E., Negro, P. and Prota, A. (2008). Seismic behavior of a full-scale RC structure retrofitted using GFRP laminates. *Journal of structural engineering*, 134 (5): 810-821. Available online: http://ascelibrary.org/doi/abs/10.1061/%28ASCE%290733-9445%282008%29134:5%28810%29, (last accessed on 06.12.2014).

EC1 (2002). EN 1991-1-1 Eurocode 1: Actions on structures - Part 1-1: General actions - Densities, self-weight, imposed loads for buildings. *European Committee for Standardization*, Brussels, Belgium. Available online: http://eurocodes.jrc.ec.europa.eu/showpage.php?id=13, (last accessed on 06.12.2014).

EC2 (2004). EN 1992-1-1 Eurocode 2: Design of concrete - Part 1-1: General rules and rules for buildings. *European Committee for Standardization*, Brussels, Belgium. Available online: http://eurocodes.jrc.ec.europa.eu/showpage.php?id=13, (last accessed on 06.12.2014).

EC8 (2004). EN 1998-1 Eurocode 8: Design of structures for earthquake resistance - Part 1: General rules, seismic actions and rules for buildings. *European Committee for Standardization*, Brussels, Belgium. Available online: http://eurocodes.jrc.ec.europa.eu/showpage.php?id=13, (last accessed on 06.12.2014).

ESD European Strong motion Database. < http://www.isesd.cv.ic.ac.uk/>.

Fajfar, P. (2002). Structural analysis in earthquake engineering - a breakthrough of simplified non-linear methods. In *Proceedings of the12th European Conference on Earthquake Engineering*, September 9-13, London, UK, 20pp. Available online: http://www.ikpir.com/data/bibliografije/att/88a2.fulltext.pdf, (last accessed on 06.12.2014).

Fajfar, P., Dolšek, M., Marušić, D. and Stratan, A. (2006). Pre-and post-test mathematical modelling of a plan-asymmetric reinforced concrete frame building. *Earthquake engineering & structural dynamics*, 35 (11): 1359-1379.

Fajfar, P., Kilar, V., Marusic, D., Perus, I. and Magliulo, G. (2005a). The extension of the N2 method to asymmetric buildings. In *Proceedings of the 4th European Workshop on the Seismic Behaviour of Irregular and Complex Structures*, August 26-27, Thessaloniki, Greece, 16pp. Available online: http://eventos.iingen.unam.mx/SimposioLE/Documentos/Fajfar.pdf, (last accessed on 06.12.2014).

Fajfar, P., Marušić, D. and Peruš, I. (2005b). Torsional effects in the pushover-based seismic analysis of buildings. *Journal of Earthquake Engineering*, 9 (6): 831-854. Available online: http://www.worldscientific.com/doi/abs/10.1142/S1363246905002249, (last accessed on 06.12.2014).

FEMA (1997a). NEHRP guidelines for the seismic rehabilitation of buildings. *FEMA 273*, Washington, DC: Federal Emergency Management Agency. Available online: https://www.wbdg.org/ccb/DHS/ARCHIVES/fema273.pdf, (last accessed on 06.12.2014).

FEMA (1997b). NEHRP Commentary on the guidelines for the seismic rehabilitation of buildings. *FEMA 274*, Washington, DC: Federal Emergency Management Agency. Available online: https://www.wbdg.org/ccb/DHS/ARCHIVES/fema274.pdf, (last accessed on 06.12.2014).

FEMA (2000). Prestandard and commentary for the seismic rehabilitation of buildings. *FEMA 356*, Washington, DC: Federal Emergency Management Agency. Available online: http://www.conservationtech.com/FEMA-publications/FEMA356-2000.pdf, (last accessed on 06.12.2014).

FEMA (2007). Design guide for improving hospital safety in earthquakes, floods, and high winds. *FEMA 577*, US Department of Homeland Security: Federal Emergency Management Agency. Available online: https://www.discountpdh.com/course/hospitalsafety/Design%20Guide%20in%20improving%20hospital%20safety.pdf, (last accessed on 06.12.2014).

Ferraioli, M., Abruzzese, D., Miccoli, L., Vari, A. and Di Lauro, G. (2010). Structural identification from environmental vibration testing of an asymmetric-plan hospital building in Italy. In: *International Conference Urban Habitat Constructions under catastrophic events, COST ACTION C*. Available online: http://www.airesingegneria.it/ita/pubblicazioni/dilauro_2010_avezzano.pdf, (last accessed on 06.12.2014).

Filiatrault, A., Christopoulos, C. and Stearns, C. (2002). Guidelines, specifications, and seismic performance characterization of nonstructural building components and equipment. *PEER Report 2002/05*, College of Engineering, University of California, Berkeley: Pacific Earthquake Engineering Research Center. Available online: http://nisee.berkeley.edu/elibrary/Text/1276078, (last accessed on 06.12.2014).

Filippou, F. C., Popov, E. P. and Bertero, V. V. (1983). Effects of bond deterioration on hysteretic behavior of reinforced concrete joints. *Report No. UCB/EERC-83/19*, College of Engineering, University of California, Berkeley, California: Earthquake Engineering Research Center. Available online: http://www.ce.berkeley.edu/~filippou/Research/Publications/Reports/EERC-83-19.pdf, (last accessed on 06.12.2014).

Fujii, M., Kobayashi, K., Miyagawa, T., Inoue, S. and Matsumoto, T. (1988). A study on the application of a stress-strain relation of confined concrete. In *JCA Proceedings of Cement and Concrete*, Vol. 42, Tokyo, Japan, 311-314.

Gasparini, D. and Vanmarcke, E. (1976). Simulated earthquake motions compatible with prescribed response spectra-Evaluation of seismic safety of buildings. *Report No. 2*, Cambridge, Massachusetts: Massachusetts Institute of Technology. Available online: http://nisee.berkeley.edu/elibrary/Text/S26762, (last accessed on 06.12.2014).

Gelfi, P. (2007). SIMQKE-GR, Programma per la generazione di accelerogrammi artificiali spettro-compatibili. Italy: University of Brescia. Available online: http://dicata.ing.unibs.it/gelfi/software/simqke/simqke_gr.htm, (last accessed on 06.12.2014).

Gillengerten, J. D. 2001. Design of nonstructural systems and components. *The seismic design handbook.* Springer. 681-721. Available online: http://link.springer.com/chapter/10.1007%2F978-1-4615-1693-4_13#page-1, (last accessed on 06.12.2014).

Graves, H. and Morante, R. (2006). Recommendations for revision of seismic damping values in regulatory guide 1.61. *Report BNL-NUREG-77174*, Office of Nuclear Regulatory Research, Washington, DC: U.S. Nuclear Regulatory Commission. Available online: http://www.vibrationdata.com/tutorials/seismic_damping.pdf, (last accessed on 06.12.2014).

Griffin, M. (2006). Earthquake performance of nonstructural components and systems: difficulties in achieving enhanced earthquake performance. In *Proceedings of the 8th US National Conference on Earthquake Engineering*, April 18-22, San Francisco, California, USA, 10pp. Available online: http://nisee.berkeley.edu/elibrary/Text/201402058, (last accessed on 06.12.2014).

Guragain, R., Pandey, B. H. and Shrestha, S. N. (2004). Guidelines for seismic vulnerability assessment of hospitals in Nepal. Kathmandu, Nepal: National Society for Earthquake Technology (NSET). Available online: http://www.preventionweb.net/files/1954_VL206311.pdf, (last accessed on 06.12.2014).

Halldorsson, B., Dong, G. and Papageorgiou, A. S. (2002). Earthquake motion input and its dissemination via the Internet. *Earthquake Engineering & Engineering Vibration*, 1 (1): 20-26. Available online: http://link.springer.com/article/10.1007%2Fs11803-002-0003-3#page-1, (last accessed on 06.12.2014).

Hart, G. C. and DiJulio, R. M. (1974). Torsional response and design of high-rise buildings. *Report ULCA-ENG-7373*, University of California, Los Angeles: Mechanics and Structures Department. Available online: http://nisee.berkeley.edu/elibrary/Text/S24944, (last accessed on 06.12.2014).

Hart, G. C., Lew, M. and DiJulio, R. M. (1975). Torsional response of high-rise buildings. *Journal of the Structural Division*, 101 (2): 397-416. Available online: http://cedb.asce.org/cgi/WWWdisplay.cgi?5814, (last accessed on 06.12.2014).

Hutchinson, G., Chandler, A. and Rady, M. (1993). Effect of vertical distribution of mass and translational stiffness on dynamic eccentricities for a special class of multi-storey buildings. *Bulletin of the New Zealand National Society for Earthquake Engineering*, 26 (1): 42-48. Available online: http://www.nzsee.org.nz/db/Bulletin/Archive/26%281%290042.pdf, (last accessed on 06.12.2014).

IBC (2012). International Building Code. *International Code Council*, Washington, DC.

Iervolino, I., Galasso, C. and Cosenza, E. (2010a). REXEL: Computer aided record selection for code-based seismic structural analysis. *Bulletin of Earthquake Engineering*, 8 (2): 339-362.

Iervolino, I., Galasso, C. and Cosenza, E. (2010b). New features of REXEL 2.61 beta, a tool for automated record selection. In *Proceedings of 14th European Conference on Earthquake Engineering (ECEE)*, 30 Aug. - 3 Sep., Ohrid, Republic of Macedonia, 7pp. Available online: http://wpage.unina.it/iuniervo/papers/394.pdf, (last accessed on 06.12.2014).

Iervolino, I., Galasso, C., Paolucci, R. and Pacor, F. (2010c). REXELite, online record selection for the ITalian ACcelerometric Archive. In *Proceedings of 14th European Conference on Earthquake Engineering (ECEE)*, 30 Aug. - 3 Sep., Ohrid, Republic of Macedonia, 8pp. Available online: http://wpage.unina.it/iuniervo/papers/391.pdf, (last accessed on 06.12.2014).

Iervolino, I., Maddaloni, G. and Cosenza, E. (2008). Eurocode 8 compliant real record sets for seismic analysis of structures. *Journal of Earthquake Engineering*, 12 (1): 54-90. Available online: http://www.reluis.it/doc/pdf/AccelerogrammiEC8/Eurocode_8_Compliant_Real_Record_Sets_for_Seismic_Analysis_of_Structures.pdf, (last accessed on 06.12.2014).

Iervolino, I., Maddaloni, G. and Cosenza, E. (2009). A note on selection of time-histories for seismic analysis of bridges in Eurocode 8. *Journal of Earthquake Engineering*, 13 (8): 1125-1152. Available online: http://wpage.unina.it/iuniervo/papers/Iervolino_et_al_RECORDS2_JEE.pdf, (last accessed on 06.12.2014).

Igusa, T. and Der Kiureghian, A. (1985). Dynamic response of multiply supported secondary systems. *Journal of Engineering Mechanics-ASCE*, 111 (1): 20-41. Available online: http://ascelibrary.org/doi/abs/10.1061/%28ASCE%290733-9399%281985%29111%3A1%2820%29?journalCode=jenmdt, (last accessed on 06.12.2014).

IStructE (2010). Manual for the design of steel and concrete buildings to Eurocode 8. London and Association Française du Génie Parasismique, Paris: Institution of Structural Engineers.

Kalkan, E. and Kunnath, S. (2006). Adaptive modal combination procedure for predicting seismic response of vertically irregular structural systems. In *Proceedings of the 8th US National Conference on Earthquake Engineering*, April 18-22, San Francisco, California, USA, 10pp. Available online: http://nsmp.wr.usgs.gov/ekalkan/PDFs/A35_Kalkan_Kunnath.pdf, (last accessed on 06.12.2014).

Karavasilis, T. L., Bazeos, N. and Beskos, D. (2008). Estimation of seismic inelastic deformation demands in plane steel MRF with vertical mass irregularities. *Engineering Structures*, 30 (11): 3265-3275. Available online: http://www.sciencedirect.com/science/article/pii/S0141029608001776, (last accessed on 06.12.2014).

Kaynia, A. (2013). Guidelines for deriving seismic fragility functions of elements at risk: buildings, lifelines, transportation networks and critical facilities. *SYNER-G Reference Report 4*: Publications Office of the European Union, Joint Research Centre. Available online: http://www.vce.at/SYNER-G/pdf/deliverables/D8.10_RR4-LB-NA-25880-EN-N.pdf, (last accessed on 06.12.2014).

Kent, D. C. and Park, R. 1969. *Inelastic behaviour of reinforced concrete members with cyclic loading*. Ph.D. Thesis, University of Canterbury. Available online: http://www.nzsee.org.nz/db/Bulletin/Archive/04%281%290108.pdf, (last accessed on 06.12.2014).

Kent, D. C. and Park, R. (1971). Flexural members with confined concrete. *Journal of the Structural Division,* 97 (7): 1969-1990. Available online: http://cedb.asce.org/cgi/WWWdisplay.cgi?18246, (last accessed on 06.12.2014).

Kreslin, M. and Fajfar, P. (2010). Seismic evaluation of an existing complex RC building. *Bulletin of Earthquake Engineering,* 8 (2): 363-385. Available online: http://link.springer.com/article/10.1007%2Fs10518-009-9155-0#page-1, (last accessed on 06.12.2014).

Lepage, A., Shoemaker, J. M. and Memari, A. M. (2012). Accelerations of nonstructural components during nonlinear seismic response of multi-story structures. *Journal of Architectural Engineering,* 18 (4): 285-297.

Lin, J. and Mahin, S. A. (1985). Seismic response of light subsystems on inelastic structures. *Journal of Structural Engineering-ASCE,* 111 (2): 400-417. Available online: http://ascelibrary.org/doi/abs/10.1061/%28ASCE%290733-9445%281985%29111%3A2%28400%29, (last accessed on 06.12.2014).

Mander, J., Priestley, M. N. and Park, R. (1988). Theoretical stress-strain model for confined concrete. *Journal of Structural Engineering-ASCE,* 114 (8): 1804-1826.

McKevitt, W. (2004). Reply to the discussion by RD Watts on" Proposed Canadian code provisions for seismic design of elements of structures, nonstructural components, and equipment". *Canadian Journal of Civil Engineering,* 31 (2): 392-392. Available online: http://www.nrcresearchpress.com/doi/abs/10.1139/l04-010?journalCode=cjce#.VIM7K2d_2_w, (last accessed on 06.12.2014).

Medina, R. A., Sankaranarayanan, R. and Kingston, K. M. (2006). Floor response spectra for light components mounted on regular moment-resisting frame structures. *Engineering Structures*, 28 (14): 1927-1940. Available online: http://www.sciencedirect.com/science/article/pii/S0141029606001325, (last accessed on 06.12.2014).

Menegotto, M. and Pinto, P. E. (1973). Method of analysis for cyclically loaded RC plane frames including changes in geometry and non-elastic behaviour of elements under combined normal force and bending. In *Proceedings of IABSE Symposium on the Resistance and Ultimate Deformability of Structures Acted on by Well Defined Repeated Loads*: International Association for Bridge and Structural Engineering, Zurich, Switzerland, 15-22. Available online: http://nisee.berkeley.edu/elibrary/Text/200603092, (last accessed on 06.12.2014).

Michalis, F., Dimitrios, V. and Manolis, P. (2006). Evaluation of the influence of vertical irregularities on the seismic performance of a nine-storey steel frame. *Earthquake Engineering & Structural Dynamics*, 35 (12): 1489-1509. Available online: http://onlinelibrary.wiley.com/doi/10.1002/eqe.591/abstract, (last accessed on 06.12.2014).

MIDAS-Gen (2013). Analysis manual. Available online: http://manual.midasuser.com, (last accessed on 06.12.2014).

Mohammed, H., Ghobarah, A. and Aziz, T. (2008). Seismic response of secondary systems supported by torsionally yielding structures. *Journal of Earthquake Engineering*, 12 (6): 932-952. Available online: http://www.tandfonline.com/doi/abs/10.1080/13632460701758588?journalCode=ueqe20, (last accessed on 06.12.2014).

Mondal, G. and Jain, S. K. (2005). Design of non-structural elements for buildings: a review of codal provisions. *Indian Concrete Journal*, 79 (8): 22-28.

Muguruma, H., Watanabe, S., Katsuta, S. and Tanaka, S. (1980). A stress-strain model of confined concrete. In *JCA Proceedings of Cement and concrete*, Vol. 34, Tokyo, Japan, 429-432.

Myrtle, R. C., Masri, S. F., Nigbor, R. L. and Caffrey, J. P. (2005). Classification and prioritization of essential systems in hospitals under extreme events. *Earthquake Spectra*, 21 (3): 779-802. Available online: http://www.earthquakespectra.org/doi/abs/10.1193/1.1988338,(last accessed on 06.12.2014).

Naeim, F. (2000). Learning from structural and nonstructural seismic performance of 20 extensively instrumented buildings. In *Proceedings of the 12th World Conference on Earthquake Engineering*, 30 Jan. - 4 Feb., Auckland, New Zealand, 8pp. Available online: http://www.johnmartin.com/publications/Instrumented%20Paper/Instrumented%20Paper.pdf, (last accessed on 06.12.2014).

Naeim, F., Alimoradi, A. and Pezeshk, S. (2004). Selection and scaling of ground motion time histories for structural design using genetic algorithms. *Earthquake Spectra*, 20 (2): 413-426. Available online: http://www.earthquakespectra.org/doi/abs/10.1193/1.1719028,(last accessed on 06.12.2014).

Naiem, F. (2001). *The seismic design handbook.* Boston, London: Kluwer Academic Publishers. Available online: http://books.google.co.uk/books, (last accessed on 06.12.2014).

NBCC (2005). National Building Code of Canada. *National Research Council of Canada*, Ottawa, Ontario, Canada. Available online: http://www.nrc-cnrc.gc.ca/eng/solutions/advisory/codes_centre_index.html, (last accessed on 06.12.2014).

Negro, P., Mola, E., Molina, F. J. and Magonette, G. E. (2004). Full-scale PSD testing of a torsionally unbalanced three-storey non-seismic RC frame. In *Proceedings of the 13th World Conference on Earthquake Engineering (WCEE)*, August 1-6, Vancouver, B.C., Canada, 15pp. Available online: http://www.iitk.ac.in/nicee/wcee/article/13_968.pdf, (last accessed on 06.12.2014).

Neuenhofer, A. and Filippou, F. C. (1997). Evaluation of nonlinear frame finite-element models. *Journal of Structural Engineering*, 123 (7): 958-966. Available online: http://www.ce.berkeley.edu/~filippou/Research/Publications/Papers/Force_Formulation_ASCE_Paper_1997.pdf, (last accessed on 06.12.2014).

Newmark, N. M. (1959). A method of computation for structural dynamics. *Journal of Engineering Mechanics Division*, 85: 67-94. Available online: https://engineering.purdue.edu/~ce573/Documents/Newmark_A%20Method%20of%20Computation%20for%20Structural%20Dynamics.pdf, (last accessed on 06.12.2014).

Newmark, N. M. and Rosenblueth, E. (1971). *Fundamentals of earthquake engineering*. Englewood Cliffs, N.J.: Prentice-Hall.

Nguyen, V. B. 2006. *Numerical modelling of reinforced concrete bridge pier under artificially generated earthquake time-histories.* Ph.D. Thesis, The University of Birmingham. Available online: http://etheses.bham.ac.uk/25/, (last accessed on 06.12.2014).

NRC (1973). Damping values for seismic design of nuclear power plants. Regulatory Guide 1.61, US Nuclear Regulatory Commission: Washington, D.C. Available online: http://pbadupws.nrc.gov/docs/ML0037/ML003740213.pdf, (last accessed on 06.12.2014).

NZS3101 (1995). Concrete structures standard. Part 1-the design of concrete structures. *Standard New Zealand,* Wellington. Available online: https://law.resource.org/pub/nz/ibr/nzs.3101.1.2006.pdf, (last accessed on 06.12.2014).

NZS4203 (1992). Code of practice for general structural design and design loadings for buildings. *Standard New Zealand,* Wellington.

Oropeza, M., Favez, P. and Lestuzzi, P. (2010). Seismic response of nonstructural components in case of nonlinear structures based on floor response spectra method. *Bull Earthquake Engineering,* 8: 387-400. Available online: http://link.springer.com/article/10.1007%2Fs10518-009-9139-0, (last accessed on 06.12.2014).

Park, R. and Priestley, M. (1980). Code provisions for confining steel in seismic design. *Bulletin of the New Zealand National Society for Earthquake Engineering,* 13 (1): 60-70. Available online: http://www.nzsee.org.nz/db/Bulletin/Archive/13%281%290060.pdf, (last accessed on 06.12.2014).

Pavlou, E. and Constantinou, M. C. (2006). Response of nonstructural components in structures with damping systems. *Journal of Structural Engineering,* 132 (7): 1108-1117.

Paz, M. (1994). *International handbook of earthquake engineering: codes, programs, and examples.* New York: Chapman & Hall. Available online: http://books.google.co.uk/books, (last accessed on 06.12.2014).

Petersson, H. and Popov, E. P. (1977). Constitutive relations for generalized loadings. *Journal of the Engineering Mechanics Division,* 103 (4): 611-627. Available online: http://cedb.asce.org/cgi/WWWdisplay.cgi?7544, (last accessed on 06.12.2014).

Phan, L. T. and Taylor, A. W. (1996). State of the art report on seismic design requirements for nonstructural building components. *Report NISTIR-5857*, Gaithersburgh, MD: National Institute of Standards and Technology. Available online: http://fire.nist.gov/bfrlpubs/build96/PDF/b96132.pdf, (last accessed on 06.12.2014).

Poncet, L. and Tremblay, R. (2004). Influence of mass irregularity on the seismic design and performance of multi-storey braced steel frames. *Proceedings of the13th World Conference on Earthquake Engineering.* August 1-6, Vancouver, B.C., Canada. Available online: http://www.iitk.ac.in/nicee/wcee/article/13_2896.pdf, (last accessed on 06.12.2014).

Poonam, Anil, K. and Ashok, K. G. (2012). Study of response of structurally irregular building frames to seismic excitations. *International Journal of Civil, Structural, Environmental and Infrastructure Engineering,* 2 (2): 25-31. Available online: http://www.tjprc.org/search.php, (last accessed on 06.12.2014).

Popovics, S. (1973). A numerical approach to the complete stress-strain curve of concrete. *Cement and Concrete Research,* 3 (5): 583-599. Available online: http://www.sciencedirect.com/science/article/pii/0008884673900963, (last accessed on 06.12.2014).

Ramberg, W. and Osgood, W. R. (1943). Description of stress-strain curves by three parameters. *Technical Note No. 902*, National Advisory Committee for Aeronautics, Washington. Available online: http://www.apesolutions.com/spd/public/NACA-TN902.pdf, (last accessed on 06.12.2014).

Richart, F. E., Brandtzaeg, A. and Brown, R. L. (1928). A study of the failure of concrete under combined compressive stresses. *Bulletin No. 185*, University of Illinois, Urbana-Champaign: Engineering Experiment Station.

Rodriguez, M., Restrepo, J. and Carr, A. (2002). Earthquake-induced floor horizontal accelerations in buildings. *Earthquake Engineering & Structural Dynamics,* 31 (3): 693-718. Available online: http://onlinelibrary.wiley.com/doi/10.1002/eqe.149/abstract, (last accessed on 06.12.2014).

Rosenblueth, E. (1980). *Design of earthquake resistant structures.* London: Pentech Press. Available online: http://books.google.co.uk/books, (last accessed on 06.12.2014).

Rozman, M. and Fajfar, P. (2009). Seismic response of a RC frame building designed according to old and modern practices. *Bulletin of Earthquake Engineering*, 7 (3): 779-799. Available online: http://link.springer.com/article/10.1007%2Fs10518-009-9119-4, (last accessed on 06.12.2014).

Ruiz, P. and Penzien, J. (1969). Probabilistic study of the behavior of structures during earthquakes. *Report No. EERC 69-3*, Berkeley, California: Earthquake Engineering Research Center. Available online: http://nisee.berkeley.edu/elibrary/Text/3112, (last accessed on 06.12.2014).

Saatcioglu, M. and Razvi, S. R. (1992). Strength and ductility of confined concrete. *Journal of structural engineering*, 118 (6): 1590-1607. Available online: http://ascelibrary.org/doi/abs/10.1061/%28ASCE%290733-9445%281992%29118%3A6%281590%29, (last accessed on 06.12.2014).

Sackman, J. L., Der Kiureghian, A. and Nour-Omid, B. (1983). Dynamic analysis of light equipment in structures-modal properties of the combined system. *Journal of Engineering Mechanics-ASCE*, 109 (1): 73-89. Available online: http://cedb.asce.org/cgi/WWWdisplay.cgi?36526, (last accessed on 06.12.2014).

Sackman, J. L. and Kelly, J. M. (1979). Seismic analysis of internal equipment and components in structures. *Engineering Structures*, 1 (4): 179-190. Available online: http://www.sciencedirect.com/science/article/pii/0141029679900452, (last accessed on 06.12.2014).

Sadashiva, V. K., MacRae, G. A. and Deam, B. L. (2009). Determination of structural irregularity limits-Mass irregularity example. *Bulletin of the New Zealand Society for Earthquake Engineering*, 42 (4): 288-301. Available online: http://www.nzsee.org.nz/db/Bulletin/Archive/42%284%290288.pdf, (last accessed on 06.12.2014).

Sakai, K. and Sheikh, S. A. (1989). What do we know about confinement in R.C. columns? a critical review of previous work and code provisions. *ACI Structural Journal*, 86 (2): 192-207. Available online: http://www.concrete.org/Publications/InternationalConcreteAbstractsPortal.aspx?m=details&i=2705, (last accessed on 06.12.2014).

Sankaranarayanan, R. and Medina, R. A. (2007). Acceleration response modification factors for nonstructural components attached to inelastic moment-resisting frame structures. *Earthquake Engineering & Structural Dynamics,* 36 (14): 2189-2210. Available online: http://onlinelibrary.wiley.com/doi/10.1002/eqe.724/abstract, (last accessed on 06.12.2014).

Sankaranarayanan, R. and Medina, R. A. (2008). Statistical models for a proposed acceleration-response modification factor for nonstructural components attached to inelastic structures. In *Proceedings of the 14th World Conference on Earthquake Engineering (WCEE)*, October 12-17, Beijing, China, 8pp. Available online: http://www.iitk.ac.in/nicee/wcee/article/14_S20-013.PDF, (last accessed on 06.12.2014).

Schroeder, M. E. and Backman, R. (1994). Analytical studies in support of the 1994 NEHRP provisions for nonstructural components. In *Proceedings of the 5th US National Conference on Earthquake Engineering*, July 10-14, Chicago, Illinois, 755-764. Available online: http://www.fwcse.com/wp-content/themes/FWC/Publications/Earthquake.pdf, (last accessed on 06.12.2014).

Seckin, M. 1981. *Hysteretic behaviour of cast-in-place exterior beam-column slab-subassemblies.* Ph.D. Thesis, Department of Civil Engineering, University of Toronto.

Segal, D. and Hall, W. J. (1989). Experimental seismic investigation of appendages in structures. *Structural Research Series No. 545*, College of Engineering, University of Illinois, Urbana-Champaign: Engineering Experiment Station. Available online: https://www.ideals.illinois.edu/handle/2142/14170, (last accessed on 06.12.2014).

Seismosoft (2009). SeismoMatch version 2.1. Available online: http://www.seismosoft.com/, (last accessed on 06.12.2014).

Sewell, R. T., Cornell, C. A., Toro, G. R. and McGuire, R. K. (1986). A study of factors influencing floor response spectra in nonlinear multi-degree-of-freedom structures. *Report No. 82*, Department of Civil and Environmental Engineering, Stanford University, Palo Alto, CA: John A. Blume Earthquake Engineering Center (JABEEC). Available online: https://blume.stanford.edu/content/study-factors-influencing-floor-response-spectra-nonlinear-multi-degree-freedom-structures, (last accessed on 06.12.2014).

Sheikh, S. A. and Uzumeri, S. (1982). Analytical model for concrete confinement in tied columns. *Journal of the Structural Division*, 108 (12): 2703-2722. Available online: http://cedb.asce.org/cgi/WWWdisplay.cgi?34966, (last accessed on 06.12.2014).

Sheikh, S. A. and Uzumeri, S. M. (1980). Strength and ductility of tied concrete columns. *Journal of the Structural Division*, 106 (5): 1079-1102. Available online: http://cedb.asce.org/cgi/WWWdisplay.cgi?9470, (last accessed on 06.12.2014).

SIA (2003). Swiss Standards Association -261: Actions on structures. *Swiss Society of Engineers and Architects*, Zurich, Switzerland.

Silva, W. and Lee, K. (1987). WES RASCAL code for synthesizing earthquake ground motions. *Report 24, Paper S-73-1*, Washington, DC: Department of the Army, US Army Crops of Engineers. Available online: http://www.pacificengineering.org/Rascal%20Code/RASCAL%20CODE.pdf, (last accessed on 06.12.2014).

SIMQKE (1976). User manual *NISEE Software Library, University of California*, Berkeley, USA. Available online: http://nisee.berkeley.edu/elibrary/getpkg?id=SIMQKE2, (last accessed on 06.12.2014).

Singh, A. and Ang, A.-S. (1974). Stochastic prediction of maximum seismic response of light secondary systems. *Nuclear Engineering and Design*, 29 (2): 218-230. Available online: http://www.sciencedirect.com/science/article/pii/0029549374901241, (last accessed on 06.12.2014).

Singh, M., Moreschi, L., Suarez, L. and Matheu, E. (2006a). Seismic design forces. I: Rigid nonstructural components. *Journal of Structural Engineering-ASCE*, 132 (10): 1524-1532. Available online: http://cedb.asce.org/cgi/WWWdisplay.cgi?154822, (last accessed on 06.12.2014).

Singh, M., Moreschi, L., Suárez, L. and Matheu, E. (2006b). Seismic design forces. II: Flexible nonstructural components. *Journal of Structural Engineering-ASCE*, 132 (10): 1533-1542. Available online: http://ascelibrary.org/doi/abs/10.1061/%28ASCE%290733-9445%282006%29132%3A10%281533%29, (last accessed on 06.12.2014).

Singh, M. P., Suarez, L., Matheu, E. and Maldonado, G. (1993). Simplified procedures for seismic design of nonstructural components and assessment of current code provisions. *Technical Report: 93-0013*, State University of New York at Buffalo, Buffalo: National Center for Earthquake Engineering Research NCEER. Available online: http://mceer.buffalo.edu/publications/catalog/reports/Simplified-Procedures-for-Seismic-Design-of-Nonstructural-Components-and-Assessment-of-Current-Code-Provisions-NCEER-93-0013.html, (last accessed on 06.12.2014).

Spacone, E., Ciampi, V. and Filippou, F. (1996a). Mixed formulation of nonlinear beam finite element. *Computers & Structures,* 58 (1): 71-83. Available online: http://www.sciencedirect.com/science/article/pii/004579499500103N, (last accessed on 06.12.2014).

Spacone, E., Filippou, F. C. and Taucer, F. F. (1996b). Fibre beam-column model for non-linear analysis of R/C frames: Part I. Formulation. *Earthquake Engineering & Structural Dynamics,* 25 (7): 711-726. Available online: http://onlinelibrary.wiley.com/doi/10.1002/%28SICI%291096-9845%28199607%2925:7%3C711::AID-EQE576%3E3.0.CO;2-9/abstract, (last accessed on 06.12.2014).

Spacone, E., Filippou, F. C. and Taucer, F. F. (1996c). Fibre beam-column model for non-linear analysis of R/C frames: Part II. Applications. *Earthquake Engineering & Structural Dynamics,* 25 (7): 727-742. Available online: http://onlinelibrary.wiley.com/doi/10.1002/%28SICI%291096-9845%28199607%2925:7%3C727::AID-EQE577%3E3.0.CO;2-O/abstract, (last accessed on 06.12.2014).

Stefano, D. M. and Pintucchi, B. (2010). Predicting torsion-induced lateral displacements for pushover analysis: Influence of torsional system characteristics. *Earthquake Engineering & Structural Dynamics,* 39 (12): 1369-1394. Available online: http://onlinelibrary.wiley.com/doi/10.1002/eqe.1002/abstract, (last accessed on 06.12.2014).

Suidan, M. and Schnobrich, W. C. (1973). Finite element analysis of reinforced concrete. *Journal of the Structural Division,* 99 (10): 2109-2122. Available online: http://cedb.asce.org/cgi/WWWdisplay.cgi?20365, (last accessed on 06.12.2014).

Taucer, F., Spacone, E. and Filippou, F. C. (1991). A fiber beam-column element for seismic response analysis of reinforced concrete structures. *Report No. UCB/EERC-91/17*, Berkeley, CA: Earthquake Engineering Research Center, College of Engineering, University of California. Available online: http://www.ce.berkeley.edu/~filippou/Research/Publications/Reports/EERC91-17.pdf, (last accessed on 06.12.2014).

Tremblay, R. and Poncet, L. (2005). Seismic performance of concentrically braced steel frames in multistory buildings with mass irregularity. *Journal of Structural Engineering*, 131 (9): 1363-1375. Available online: http://cedb.asce.org/cgi/WWWdisplay.cgi?148793, (last accessed on 06.12.2014).

UBC (1927). International Conference of Building Officials, Uniform Building Code. Whittier, California, USA.

UBC (1935). International Conference of Building Officials, Uniform Building Code. Whittier, California, USA.

UBC (1994). International Conference of Building Officials, Uniform Building Code. Whittier, California, USA.

UBC (1997). International Conference of Building Officials, Uniform Building Code. Whittier, California, USA.

Valmundsson, E. V. and Nau, J. M. (1997). Seismic response of building frames with vertical structural irregularities. *Journal of Structural Engineering*, 123 (1): 30-41.

Vanmarke, E. 1976. Structural response to earthquake. In Lomnitz, C. (ed.) *Seismic risk and engineering decisions.* Amsterdam: Elsevier. pp. 287-334. Available online: http://books.google.co.uk/books, (last accessed on 06.12.2014).

Villaverde, R. (1987). Simplified approach for the seismic analysis of equipment attached to elasto-plastic structures. *Nuclear Engineering and Design*, 103 (3): 267-279. Available online: http://www.sciencedirect.com/science/article/pii/0029549387903104, (last accessed on 06.12.2014).

Villaverde, R. (1991). Approximate formulas to calculate the seismic response of light attachments to buildings. *Nuclear Engineering and Design*, 128 (3): 349-368. Available online: http://www.sciencedirect.com/science/article/pii/002954939190172E, (last accessed on 06.12.2014).

Villaverde, R. (1997a). Method to improve seismic provisions for nonstructural components in buildings. *Journal of Structural Engineering*, 123 (4): 432-439. Available online: http://ascelibrary.org/doi/abs/10.1061/%28ASCE%290733-9445%281997%29123:4%28432%29, (last accessed on 06.12.2014).

Villaverde, R. (1997b). Seismic design of secondary structures: state of the art. *Journal of Structural Engineering-ASCE*, 123 (8): 1011-1019. Available online: http://ascelibrary.org/doi/abs/10.1061/%28ASCE%290733-9445%281997%29123%3A8%281011%29?journalCode=jsendh, (last accessed on 06.12.2014).

Villaverde, R. (2005). Approximate procedure for the seismic nonlinear analysis of nonstructural components in buildings. *Journal of Seismology and Earthquake Engineering-JSEE*, 7 (1): 9-24. Available online: http://www.iiees.ac.ir/iiees/English/Publication/Jsee/jsee14_2.pdf, (last accessed on 06.12.2014).

Villaverde, R. (2006). Simple method to estimate the seismic nonlinear response of nonstructural components in buildings. *Engineering Structures*, 28 (8): 1209-1221. Available online: http://www.sciencedirect.com/science/article/pii/S0141029606000320, (last accessed on 06.12.2014).

Waller, C. L. 2010. *A Methodology for Probabilistic Performance-Based Seismic Risk Assessment of Bridge Inventories.* M.A.Sc Thesis, Carleton University, Ottawa.

Watts, R. E. (2004). Discussion of" Proposed Canadian code provisions for seismic design of elements of structures, nonstructural components, and equipment". *Canadian Journal of Civil Engineering*, 31 (2): 391-391. Available online: http://www.nrcresearchpress.com/doi/abs/10.1139/l04-009?journalCode=cjce#.VINMhWd_2_w, (last accessed on 06.12.2014).

Whittaker, A. and Soong, T. (2003). An overview of nonstructural components research at three US earthquake engineering research centers. In *Proceedings of Seminar on Seismic Design, Performance, and Retrofit of Nonstructural Components in Critical Facilities*: Applied Technology Council-Multidisciplinary Center for Earthquake Engineering Research, Redwood City, California, 271-280. Available online: http://www.researchgate.net/publication/242693449, (last accessed on 06.12.2014).

Wilson, E. L. (1998). *Three dimensional static and dynamic analysis of structures: A physical approach with emphasis on earthquake engineering.* Berkeley, California, USA: Computers and Structures, Inc. Available online: http://www.edwilson.org/book/book.htm#Author, (last accessed on 06.12.2014).

Wu, H. 2007. *Constitutive model of concrete confined by advanced fiber composite materials and applications in seismic retrofitting.* Ph.D. Thesis, University of Southern California. Available online: http://cee.usc.edu/assets/025/85732.pdf, (last accessed on 06.12.2014).

Xiao, J., Sun, Y. and Falkner, H. (2006). Seismic performance of frame structures with recycled aggregate concrete. *Engineering Structures,* 28 (1): 1-8. Available online: http://www.sciencedirect.com/science/article/pii/S0141029605002579, (last accessed on 06.12.2014).

Yang, Y. B. and Huang, W. H. (1993). Seismic response of light equipment in torsional buildings. *Earthquake Engineering & Structural Dynamics,* 22 (2): 113-128.

Yang, Y. B. and Huang, W. H. (1998). Equipment-structure interaction considering the effect of torsion and base isolation. *Earthquake Engineering & Structural Dynamics,* 27 (2): 155-171.

Zeris, C. A. and Mahin, S. A. (1988). Analysis of reinforced concrete beam-columns under uniaxial excitation. *Journal of structural engineering,* 114 (4): 804-820. Available online: http://ascelibrary.org/doi/abs/10.1061/%28ASCE%290733-9445%281988%29114%3A4%28804%29?journalCode=jsendh, (last accessed on 06.12.2014).

Zeris, C. A. and Mahin, S. A. (1991). Behavior of reinforced concrete structures subjected to biaxial excitation. *Journal of structural engineering,* 117 (9): 2657-2673.

Zienkiewicz, O. C. and Taylor, R. L. (1989). *The Finite Element Method*. Volume 1. Basic Formulation and Linear Problems. Fourth Edition: McGraw Hill, London. Available online: http://books.google.co.uk/books, (last accessed on 06.12.2014).

Zienkiewicz, O. C. and Taylor, R. L. (1991). *The Finite Element Method*. Volume 2. Basic Formulation and Linear Problems. Fourth Edition: McGraw Hill, London. Available online: http://books.google.co.uk/books, (last accessed on 06.12.2014).

Zoghi, M. (2013). *The international handbook of FRP composites in civil engineering*. Boca Raton: Taylor & Francis Group. Available online: http://www.crcpress.com/product/isbn/9780849320132, (last accessed on 06.12.2014).

APPENDIX A

A1: The extension N2 method

The extended N2 procedure is a simplified nonlinear method for the seismic analysis of plan-asymmetric structures. It can be used to calculate the seismic capacities and the idealised force-displacement response of such structures by combining the results obtained by the push-over analysis of a 3D structural model with the results of an elastic dynamic analysis (Fajfar *et al.*, 2005b). The steps of this method can be described as follows: (1) Apply nonlinear static analysis by using a 3D numerical model. Individually in the two horizontal directions, X and Y, the horizontal forces are applied at the centres of the masses. The forces should be applied with + and – sign in each direction. Evaluate the larger magnitude of the target top floor displacement at the mass centre that can be determined for + and – sign. (2) Apply an elastic dynamic analysis of the 3D numerical model. Evaluate the value of the top floor displacement at the mass centre by combining the results of the two horizontal directions using the SQRSS method. (3) Calculate the displacement correction factor which can be obtained as the ratio of the normalised top floor displacement, estimated from elastic dynamic analysis (is taken as $\geq$ 1.0), to the corresponding normalised value, estimated from the nonlinear static analysis. The normalised top floor displacement can be determined as the ratio between the top floor displacement at a selected location and the corresponding displacement at the top floor mass centre. (4) Magnify the value of the top floor displacement, calculated from nonlinear static analysis by the displacement correction factor.

A2: The expressions of Annex B (EC8 2004)

The value of the effective mass m^* of an equivalent SDOF system depends on the normalised displacements Φ_i and the mass value m_i in the $i-th$ floor of the P-structure; thus value of m^* can be determined as follows:

$$m^* = \sum m_i \,.\, \Phi_i \tag{A-1}$$

and, the transformation factor Γ which can be used to transform the P-structure from MDOF (real system) to an equivalent SDOF system can be computed as:

$$\Gamma = \frac{\sum m_i \,.\, \Phi_i}{\sum m_i \,.\, \Phi_i^2} = \frac{m^*}{\sum m_i \,.\, \Phi_i^2} \tag{A-2}$$

The effective ultimate value of the base shear force at the development of the plastic state F_y^* of the equivalent SDOF system is calculated as follows:

$$F_y^* = \frac{F_y}{\Gamma} \tag{A-3}$$

where F_y represents the ultimate strength of a MDOF system.

As stated in EC8 (2004), *"the stiffness at the elastic range of the idealised SDOF system is defined in a way that the area under the real and the idealised strength-displacement curves are equivalent"*, as shown in Figure A2-1.

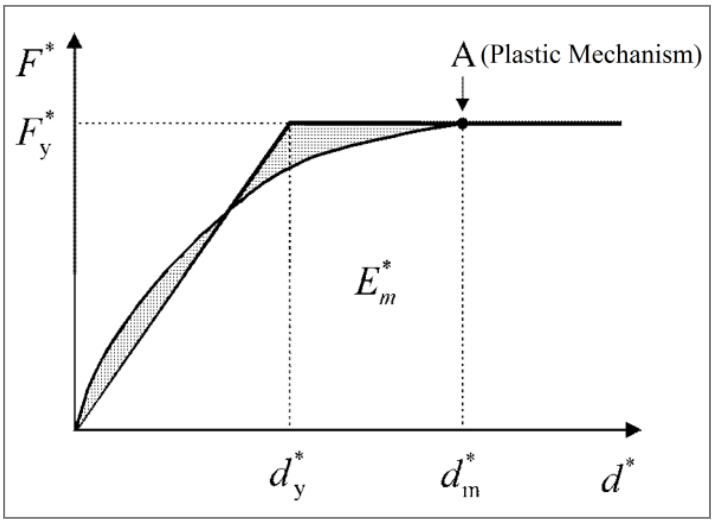

Figure A2-1 Determination of the idealised elasto-perfect plastic force-displacement relationship according to Annex B of EC8 (2004).

Subsequently, the effective yield deformation of the idealised equivalent SDOF system d_y^* is introduced by:

$$d_y^* = 2\left(d_m^* - \frac{E_m^*}{F_y^*}\right) \tag{A-4}$$

where,

$$d_m^* = \frac{d_m}{\Gamma} \tag{A-5}$$

and,

$$E_m^* = \frac{E_m}{\Gamma^2} \tag{A-6}$$

where d_m and E_m are, respectively, the ultimate displacement (i.e. near collapse deformation) and the actual energy up to the creation of the plastic mechanism of the MDOF system. However, d_m^* and E_m^* are, respectively, the effective ultimate displacement and the deformation energy of the equivalent SDOF system.

The effective period T^* of the idealised SDOF system can be defined as follows:

$$T^* = 2\pi \sqrt{\frac{m^* d_y^*}{F_y^*}} \tag{A-7}$$

Then, the target deformation d_{et}^* of the structure (MDOF) can be computed in terms of the value of the elastic response spectrum $S_{ae}(T^*)$ at the effective period T^*as follows:

$$d_{et}^* = S_{ae}(T^*) \left[\frac{T^*}{2\pi}\right]^2 \tag{A-8}$$

For structural systems that have short, or medium to long periods, the calculation of the target deformation values d_t^* can be expressed as follows:

a) For structures that have a short effective period $T^* < TC$; where TC is the upper period of the constant horizontal zone of the spectral shape as shown in Figure A2-2(a).

If the resulting acceleration from the limited strength of the structure, $(S_{ay} = F_y^*/m^*)$ is equal or larger than the elastic response spectrum $S_{ae}(T^*)$, i.e. $S_{ay} \geq S_{ae}(T^*)$, the behaviour is assumed within the elastic range; hence,

$$d_t^* = d_{et}^* \tag{A-9}$$

However, if $\left(S_{ay} = F_y^*/m^*\right) < S_{ae}(T^*)$, the behaviour is assumed in the nonlinear range and the value of the target deformation can be found as:

$$d_t^* = \frac{d_{et}^*}{\mu}\left(1 + (\mu - 1)\frac{TC}{T^*}\right) \geq d_{et}^* \tag{A-10}$$

where μ is the ductility factor and can be represented as the ratio between the elastic acceleration $S_{ae}(T^*)$ at the effective period $T^*$and the acceleration at the limited strength of the structure S_{ay} and can be expressed as follows:

$$\mu = \frac{S_{ae}}{S_{ay}} \tag{A-11}$$

b) For structures that have a medium or long effective period $T^* \geq TC$, as shown in Figure A2-2(b), then

$$d_t^* = d_{et}^* \tag{A-12}$$

For both cases of the periods in (a) and (b) above, the target deformation d_t of the MDOF system can be found as:

$$d_t = \Gamma d_t^* \tag{A-13}$$

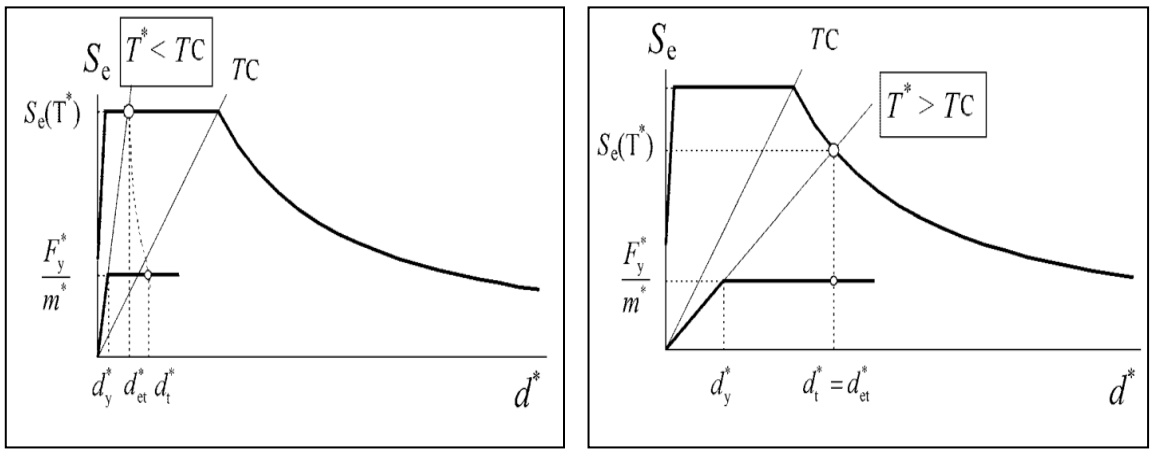

(a) (b)

Figure A2-2 Determination of the target displacement of the equivalent SDOF system for (a) short period range and (b) medium and long period range (EC8, 2004).

A3: Cross-section details of the three group of buildings presented in Chapter 5

Table A3-1 Cross-section details of the first group of buildings (all dimensions are in millimetres).

Building	Beams			Columns					
				C1,C2,C3,C4,C5,C7,C8,C9			C6		
	Cross section	Long. steel	Shear steel	Cross section	Long. steel	Shear steel	Cross section	Long. steel	Shear steel
Test	250×500	6Ø12	Ø8@200	250×250	4Ø12	Ø8@250	250×750	10Ø12	Ø8@250
Test 0.15	250×500	6Ø14	Ø8@100	250×250	8Ø16	Ø6@100	250×750	16Ø16	Ø6@80
Test 0.25	250×500	6Ø14	Ø8@100	250×250	8Ø20	Ø6@100	250×750	14Ø22	Ø6@80
EC8 M	350×450	9Ø16	Ø8@90	350×350	Table A3-2	Ø8@120	350×850	Table A3-2	Ø8@120

Table A3-2 Longitudinal steel reinforcement of the columns of EC8 M building (all dimensions are in millimetres).

Storey	C1	C2	C3	C4	C5	C6	C7	C8	C9
1st & 2nd	8Ø25	8Ø22	4Ø22+4Ø25	8Ø22	8Ø22	16Ø22	8Ø20	8Ø22	8Ø20
3rd	8Ø20	8Ø20	8Ø20	8Ø20	8Ø16	16Ø22	4Ø16+4Ø20	8Ø16	8Ø16

Table A3-3 Cross-section details of the second group of buildings (all dimensions are in millimetres).

Building	Storey	Columns						Beams		
		C1,C2,C3,C4, C5,C7,C8,C9		C6		Shear hoops (critical region)	Joint shear hoops	Cross section	Long. Steel: bottom* top+	Shear hoops
		Cross section	Long. steel	Cross section	Long. steel					
EC8 M5 (15 m high)	1-2	450×450	16Ø20	450×1000	20Ø20	2Ø8 @120	3Ø8 @100	350×500	5Ø16* 4Ø16+	Ø8 @90
	3-5	400×400	16Ø20	400×850	20Ø20					
EC8 M7 (21 m high)	1-2	550×550	24Ø20	550×1150	30Ø20	2Ø8 @110	3Ø8 @90	350×500	6Ø16* 4Ø16+	Ø8 @90
	3-4	500×500	24Ø20	500×1000	28Ø20					
	5-7	450×450	16Ø20	450×850	20Ø20					
EC8 M10 (30 m high)	1-2	650×650	30Ø20	650×1200	34Ø20	3Ø8 @110	3Ø8 @90	350×500	8Ø16* 5Ø16+	Ø8 @90
	3-4	600×600	30Ø20	600×1100	30Ø20					
	5-7	550×550	24Ø20	550×950	28Ø20	2Ø8 @110				
	8-10	500×500	16Ø20	500×800	22Ø20					
EC8 M13 (39 m high)	1-2	750×750	24Ø25	800×1200	26Ø25	3Ø8 @90	3Ø8 @90	400×600	10Ø16* 7Ø16+	Ø8 @100
	3-4	650×650	24Ø25	700×1000	24Ø25					
	5-7	650×650	24Ø25	700×1000	24Ø25					
	8-10	600×600	20Ø25	650×950	22Ø25					
	11-13	500×500	16Ø25	500×850	16Ø25	2Ø8 @90				
EC8 M15 (45 m high)	1-2	850×850	30Ø25	850×1250	32Ø25	3Ø8 @90	3Ø8 @90	450×650	7Ø20* 6Ø20+	Ø8 @100
	3-4	750×750	30Ø25	750×1000	32Ø25					
	5-6	700×700	28Ø25	700×900	28Ø25					
	7-9	650×650	24Ø25	650×800	24Ø25					
	10-12	600×600	20Ø25	600×700	18Ø25					
	13-15	500×500	16Ø25	500×550	16Ø25	2Ø8 @90				

Table A3-4 Cross-section details of the buildings designed on ground type A (all dimensions are in millimetres).

Building	Storey	Columns						Beams		
		C1,C2,C3,C4, C5,C7,C8,C9		C6		Shear hoops (critical region)	Joint shear hoops	Cross section	Long. Steel: bottom* top+	Shear hoops
		Cross section	Long. steel	Cross section	Long. steel					
EC8 M3 (9 m high)	1-3	300×300	8Ø20	300×750	16Ø20	2Ø8@90	3Ø8@8	300×450	4Ø16* 4Ø16+	Ø8 @90
EC8 M5 (15 m high)	1-2	350×350	10Ø20	350×780	14Ø20	2Ø8 @80	3Ø8 @70	300×500	5Ø16* 3Ø16+	Ø8 @90
	3-5	300×300	10Ø20	300×700	14Ø20					
EC8 M10 (30 m high)	1-2	500×500	18Ø20	500×900	22Ø20	3Ø8 @70	3Ø8 @65	300×500	7Ø16* 4Ø16+	Ø8 @90
	3-4	450×450	18Ø20	450×825	18Ø20					
	5-7	400×400	14Ø20	400×725	16Ø20	2Ø8 @70				
	8-10	375×375	10Ø20	375×600	12Ø20					
EC8 M15 (45 m high)	1-2	675×675	20Ø25	675×1000	22Ø25	3Ø8 @65	3Ø8 @65	350×550	7Ø20* 4Ø20+	Ø8 @80
	3-4	600×600	20Ø25	600×800	22Ø25					
	5-6	575×575	18Ø25	575×725	18Ø25					
	7-9	525×525	16Ø25	525×650	16Ø25					
	10-12	475×475	12Ø25	475×550	12Ø25					
	13-15	400×400	10Ø25	400×450	10Ø25	2Ø8 @65				

Table A3-5 Cross-section details of the buildings designed on ground type B (all dimensions are in millimetres).

Building	Storey	Columns						Beams		
		C1,C2,C3,C4, C5,C7,C8,C9		C6		Shear hoops (critical region)	Joint shear hoops	Cross section	Long. Steel: bottom* top+	Shear hoops
		Cross section	Long. steel	Cross section	Long. steel					
EC8 M3 (9 m high)	1-3	335×335	10Ø20	335×800	18Ø20	2Ø8 @100	3Ø8 @90	335×450	4Ø16* 4Ø16+	Ø8 @90
EC8 M5 (15 m high)	1-2	400×400	12Ø20	400×850	18Ø20	2Ø8 @100	3Ø8 @90	350×500	5Ø16* 4Ø16+	Ø8 @90
	3-5	350×350	12Ø20	350×750	16Ø20					
EC8 M10 (30 m high)	1-2	550×550	20Ø20	550×1000	24Ø20	3Ø8 @90	3Ø8 @80	350×500	7Ø16* 5Ø16+	Ø8 @90
	3-4	500×500	20Ø20	500×900	20Ø20					
	5-7	450×450	16Ø20	450×800	18Ø20	2Ø8 @90				
	8-10	400×400	10Ø20	400×700	14Ø20					
EC8 M15 (45 m high)	1-2	750×750	22Ø25	750×1100	26Ø25	3Ø8 @80	3Ø8 @80	350×600	7Ø20* 5Ø20+	Ø8 @90
	3-4	675×675	22Ø25	675×900	26Ø25					
	5-6	625×625	22Ø25	625×800	22Ø25					
	7-9	575×575	18Ø25	575×700	20Ø25					
	10-12	525×525	16Ø25	525×625	14Ø25					
	13-15	450×450	12Ø25	450×500	14Ø25	2Ø8 @80				

Table A3-6 Cross-section details of the buildings designed on ground type D (all dimensions are in millimetres).

Building	Storey	Columns						Beams		
		C1,C2,C3,C4, C5,C7,C8,C9		C6		Shear hoops (critical region)	Joint shear hoops	Cross section	Long. Steel: bottom* top+	Shear hoops
		Cross section	Long. steel	Cross section	Long. steel					
EC8 M3 (9 m high)	1-3	410×410	14Ø20	410×950	26Ø20	2Ø8 @140	3Ø8 @130	400×500	6Ø16* 5Ø16+	Ø8 @100
EC8 M5 (15 m high)	1-2	580×580	26Ø20	580×1150	20Ø20	2Ø8 @140	3Ø8 @130	400×500	5Ø18* 4Ø18+	Ø8 @100
	3-5	500×500	24Ø20	500×950	20Ø20					
EC8 M10 (30 m high)	1-2	750×750	26Ø25	750×1300	34Ø20	3Ø8 @120	3Ø8 @110	400×500	7Ø18* 4Ø18+	Ø8 @100
	3-4	700×700	26Ø25	700×1200	30Ø20					
	5-7	630×630	20Ø25	630×1100	28Ø20	2Ø8 @120				
	8-10	575×575	14Ø25	575×900	22Ø20					
EC8 M15 (45 m high)	1-2	1000×1000	40Ø25	1000×1300	40Ø25	3Ø8 @120	3Ø8 @110	450×650	8Ø20* 6Ø20+	Ø8 @110
	3-4	935×935	40Ø25	935×1200	40Ø25					
	5-6	875×875	38Ø25	875×1000	38Ø25					
	7-9	800×800	36Ø25	800×900	36Ø25					
	10-12	750×750	32Ø25	750×850	32Ø25					
	13-15	600×600	22Ø25	600×650	22Ø25	2Ø8 @120				

Table A3-7 Cross-section details of the buildings designed on ground type E (all dimensions are in millimetres).

Building	Storey	Columns						Beams		
		C1,C2,C3,C4, C5,C7,C8,C9		C6		Shear hoops (critical region)	Joint shear hoops	Cross section	Long. Steel: bottom* top+	Shear hoops
		Cross section	Long. steel	Cross section	Long. steel					
EC8 M3 (9 m high)	1-3	390×390	10Ø22	390×900	18Ø22	2Ø8 @130	3Ø8 @120	375×500	6Ø16* 4Ø16+	Ø8 @90
EC8 M5 (15 m high)	1-2	450×450	16Ø20	450×1000	20Ø20	2Ø8 @120	3Ø8 @100	350×500	5Ø16* 4Ø16+	Ø8 @90
	3-5	400×400	16Ø20	400×850	20Ø20					
EC8 M10 (30 m high)	1-2	650×650	30Ø20	650×1200	34Ø20	3Ø8 @110	3Ø8 @90	350×650	8Ø16* 5Ø16+	Ø8 @90
	3-4	600×600	30Ø20	600×1100	30Ø20					
	5-7	550×550	24Ø20	550×950	28Ø20	2Ø8 @110				
	8-10	500×500	16Ø20	500×800	22Ø20					
EC8 M15 (45 m high)	1-2	850×850	30Ø25	850×1250	32Ø25	3Ø8 @90	3Ø8 @90	450×650	7Ø20* 6Ø20+	Ø8 @100
	3-4	750×750	30Ø25	750×1000	32Ø25					
	5-6	700×700	28Ø25	700×900	28Ø25					
	7-9	650×650	24Ø25	650×800	24Ø25					
	10-12	600×600	20Ø25	600×700	18Ø25					
	13-15	500×500	16Ø25	500×550	16Ø25	2Ø8 @90				

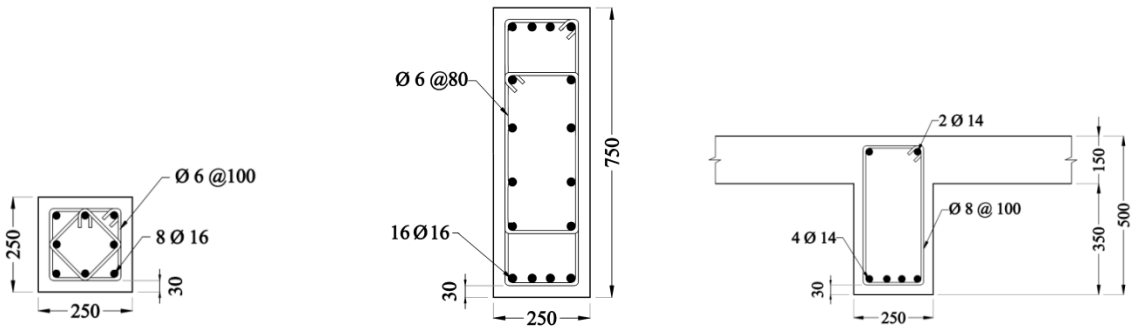

(a) (b) (c)

Figure A3-1 Cross-section details of Test 0.15 building (a) square column, (b) rectangular column, and (c) beam (all dimensions are in millimetres).

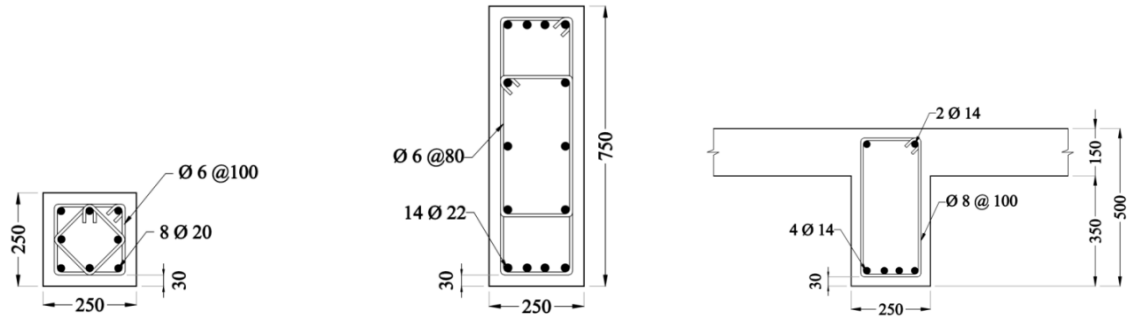

(a) (b) (c)

Figure A3-2 Cross-section details of Test 0.25 building (a) square column, (b) rectangular column, and (c) beam (all dimensions are in millimetres).

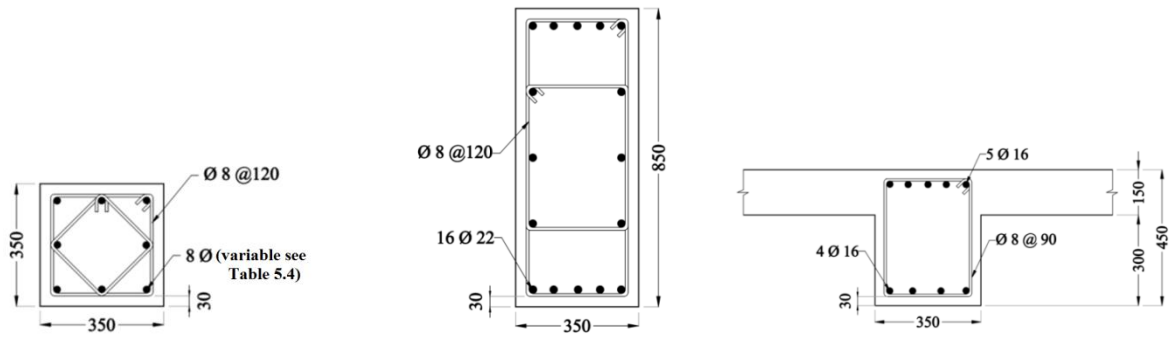

(a) (b) (c)

Figure A3-3 Cross-section details of EC8 M building (a) square column, (b) rectangular column, and (c) beam (all dimensions are in millimetres).

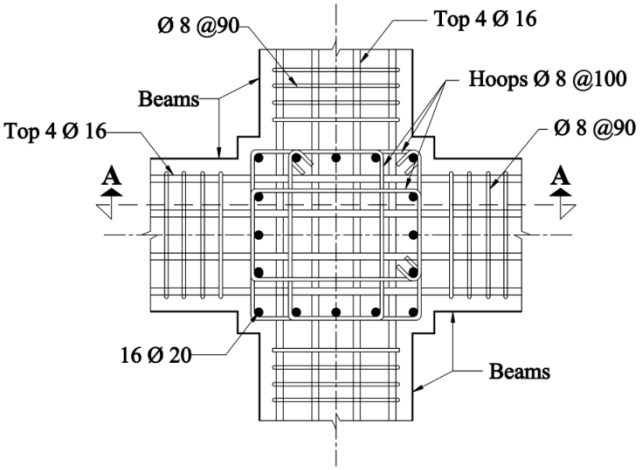

(a)

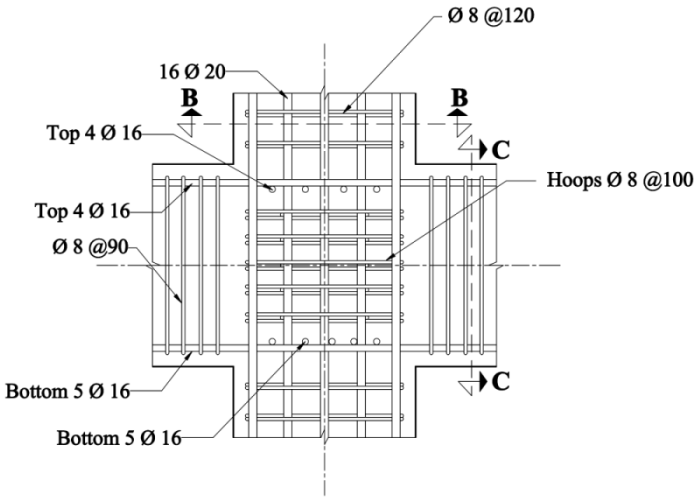

(b)

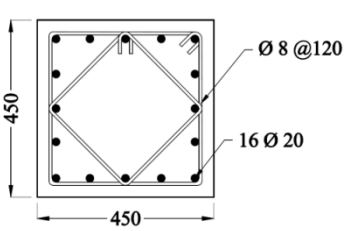

(c)

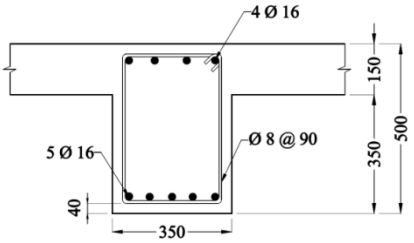

(d)

Figure A3-4 Cross-section details of the beam-column joint connection at the first floor of EC8 M5 building (a) top view, (b) elevation (section A-A) (c) section B-B in the column, and (d) section C-C in the beam (all dimensions are in millimetres).

A4: Cross-section details of eight cases of buildings presented in Chapter 6

Table A4-1 Cross-section details of one-bay three-storey RC P-structures (all dimensions are in millimetres).

Building	Column C1				Columns C2, C3, and C4			
	Cross section	Long. steel	Shear hoops (critical region)	Joint shear hoops	Cross section	Long. steel	Shear hoops (critical region)	Joint shear hoops
Reference	500×500	12Ø20	3Ø8@120	3Ø8@100	500×500	12Ø20	3Ø8@120	3Ø8@90
Modified 1	525×525	12Ø20	3Ø8@130	3Ø8@100	491×491	12Ø20	3Ø8@120	3Ø8@90
Modified 2	550×550	14Ø20	3Ø8@140	3Ø8@110	479×479	12Ø20	3Ø8@120	3Ø8@90
Modified 3	575×575	16Ø20	3Ø8@140	3Ø8@110	465×465	12Ø20	3Ø8@120	3Ø8@90
Modified 4	600×600	16Ø20	3Ø8@140	3Ø8@110	448×448	14Ø20	3Ø8@100	3Ø8@90
Modified 5	625×625	18Ø20	3Ø8@140	3Ø8@110	425×425	14Ø20	3Ø8@100	3Ø8@90
Modified 6	650×650	20Ø20	4Ø8@150	4Ø8@120	393×393	14Ø20	3Ø8@80	3Ø8@70
Modified 7	675×675	22Ø20	4Ø8@150	4Ø8@120	345×345	12Ø20	2Ø8@80	2Ø8@70

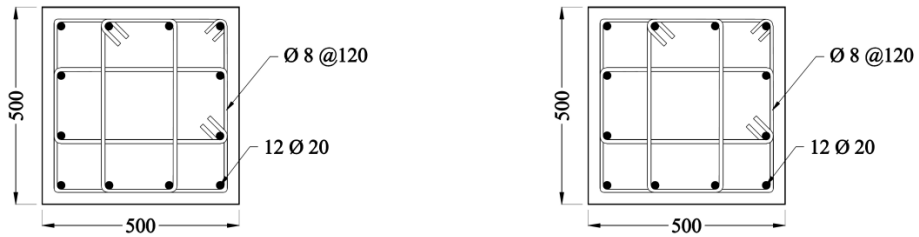

Figure A4-1 Columns cross-section details of the Reference structure without eccentricity (a) C1 and (b) C2, C3, C4 (all dimensions are in millimetres).

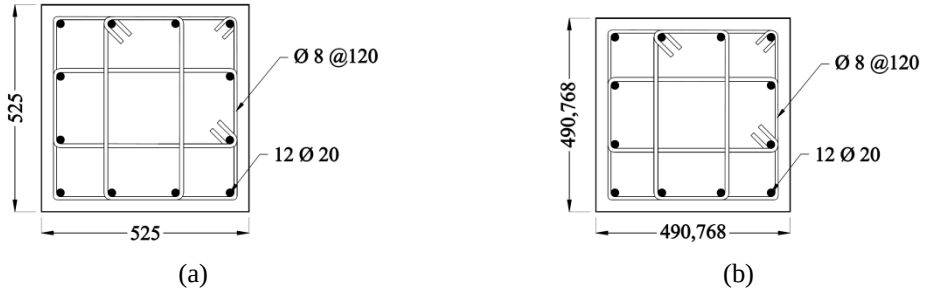

Figure A4-2 Columns cross-section details of the Modified 1 case of structure with eccentricity ratio equal to 0.026 (a) C1 and (b) C2, C3, C4 (all dimensions are in millimetres).

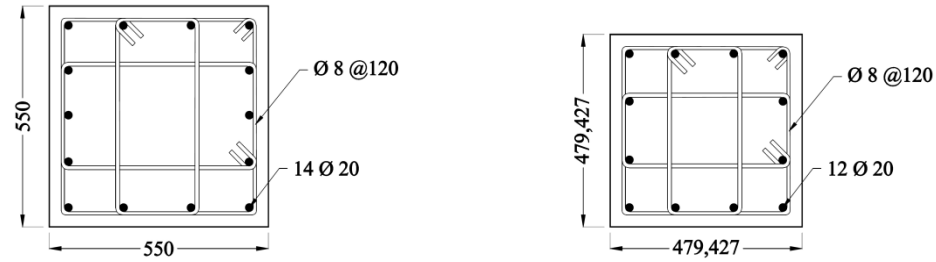

Figure A4-3 Columns cross-section details of the Modified 2 case of structure with eccentricity ratio equal to 0.06 (a) C1 and (b) C2, C3, C4 (all dimensions are in millimetres).

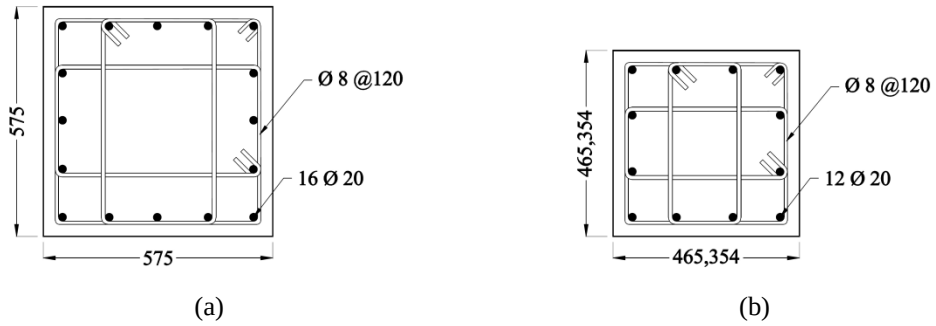

Figure A4-4 Columns cross-section details of the Modified 3 case of structure with eccentricity ratio equal to 0.098 (a) C1 and (b) C2, C3, C4 (all dimensions are in millimetres).

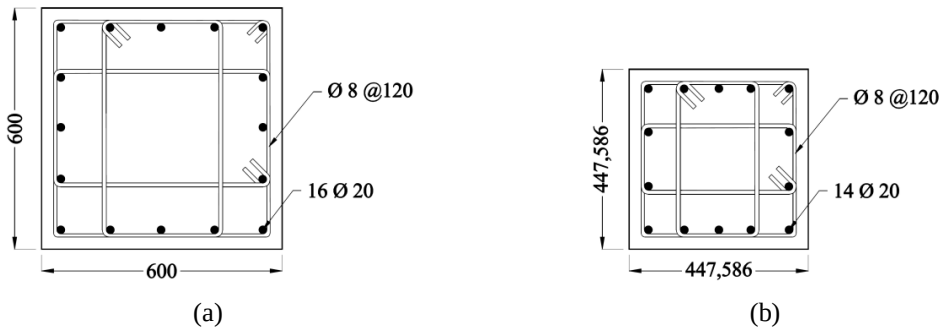

Figure A4-5 Columns cross-section details of the Modified 4 case of structure with eccentricity ratio equal to 0.143 (a) C1 and (b) C2, C3, C4 (all dimensions are in millimetres).

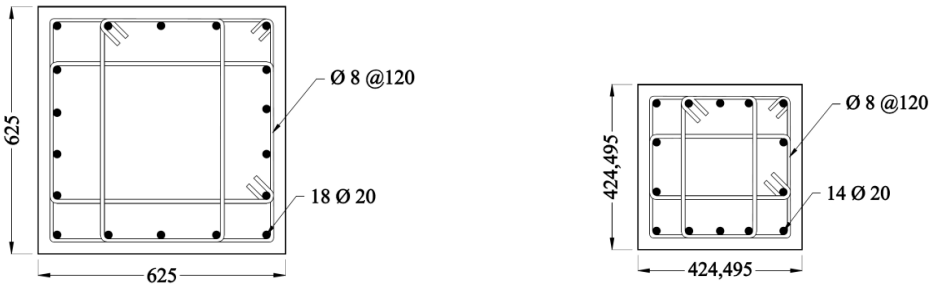

(a) (b)

Figure A4-6 Columns cross-section details of the Modified 5 case of structure with eccentricity ratio equal to 0.205 (a) C1 and (b) C2, C3, C4 (all dimensions are in millimetres).

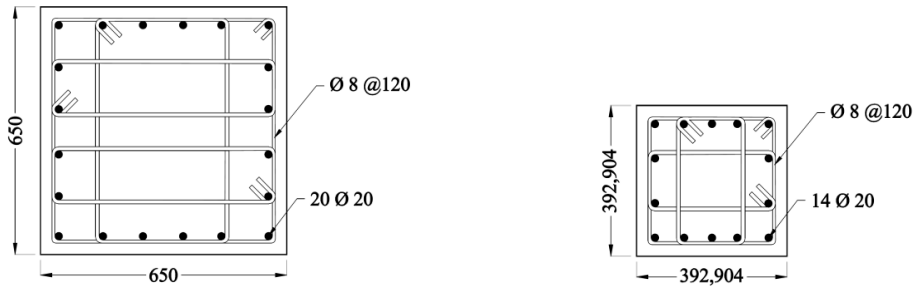

(a) (b)

Figure A4-7 Columns cross-section details of the Modified 6 case of structure with eccentricity ratio equal to 0.284 (a) C1 and (b) C2, C3, C4 (all dimensions are in millimetres).

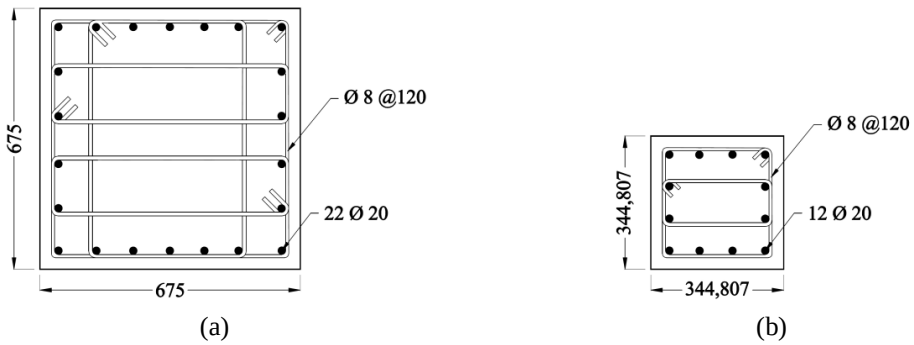

(a) (b)

Figure A4-8 Columns cross-section details of the Modified 7 case of structure with eccentricity ratio equal to 0.372 (a) C1 and (b) C2, C3, C4 (all dimensions are in millimetres).

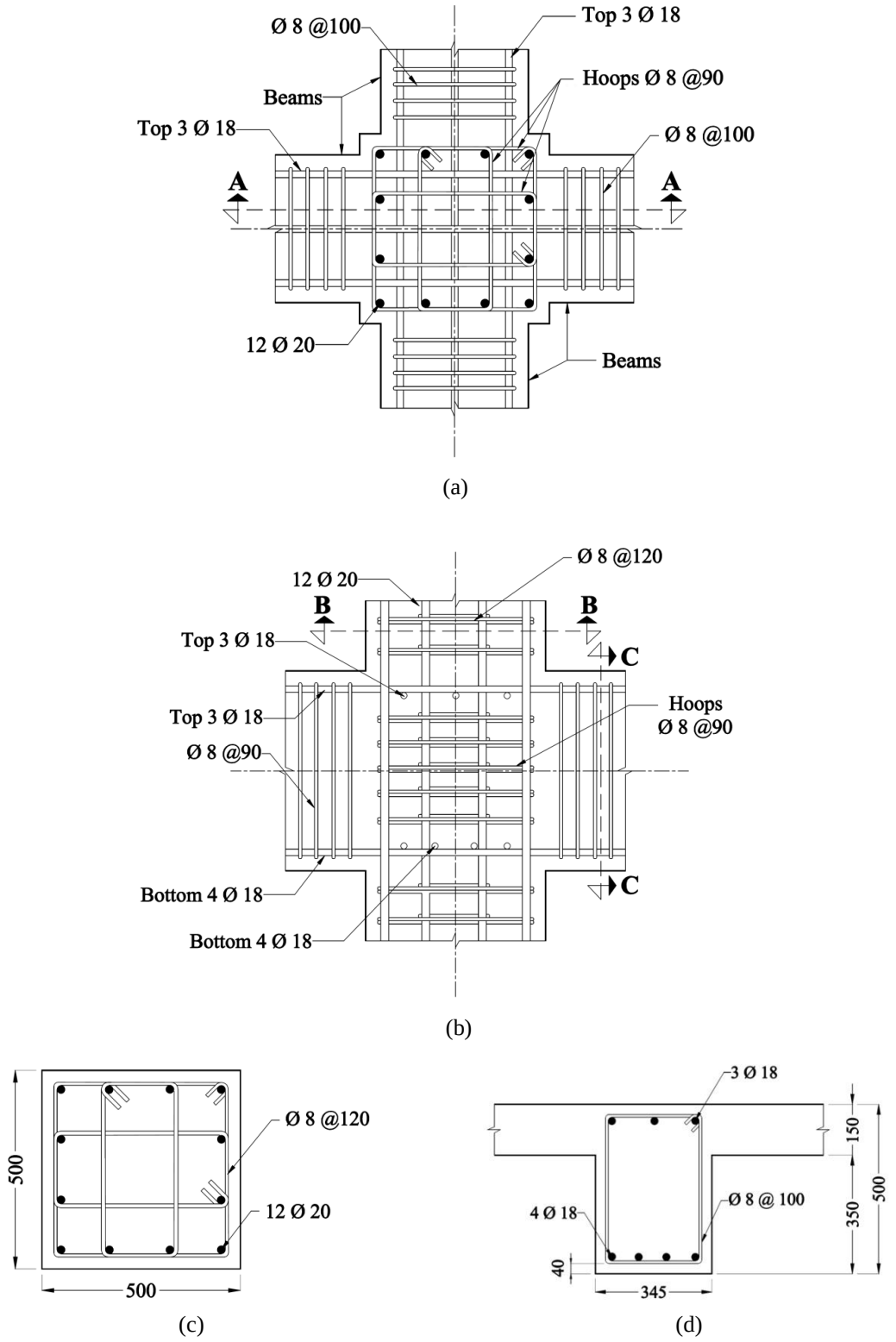

Figure A4-9 Cross-section details of the beam-column joint connection at the first floor of the Reference structure without eccentricity (a) top view, (b) elevation (section A-A), (c) section B-B in the column, and (d) section C-C in the beam (all dimensions are in millimetres).

A5: Cross-section details of complicated irregular RC P-structure presented in Chapter 7

Table A5-1 Cross-section details of the columns of the irregular 20-storey RC P-structure (all dimensions are in millimetres).

(i) Column cross-section details of the 1st storey.

Designation	Cross section	Steel reinforcement		
		Longitudinal Steel	Shear hoops (critical region)	Joint shear hoops
C1	1100×1100	28Ø40	5Ø10@150	5Ø10@130
C1A	800×1200	30Ø32	4Ø10@110	5Ø10@100
C1B	500×1800	32Ø32	4Ø10@125	5Ø10@110
C2	1200×1200	30Ø40	5Ø10@150	5Ø10@130
C3	850×850	22Ø32	4Ø10@125	4Ø10@110
C4	850×850	24Ø25	4Ø10@100	4Ø10@100
C5	850×850	26Ø32	4Ø10@125	4Ø10@110
C6	1200×1200	30Ø40	5Ø10@150	5Ø10@130
C7	1000×1000	28Ø32	5Ø10@125	5Ø10@110
C8	1200×1200	30Ø40	5Ø10@150	5Ø10@130
C9	1200×1200	30Ø40	5Ø10@150	5Ø10@130
C10	1100×1100	28Ø40	5Ø10@150	5Ø10@130
C11	1000×1000	20Ø32	5Ø10@125	5Ø10@110
C12	1000×1000	30Ø25	5Ø10@100	5Ø10@100
C13	800×800	20Ø32	4Ø10@125	4Ø10@110

(ii) Column cross-section details of the 2nd and 3rd storeys.

Designation	Cross section	Steel reinforcement		
		Longitudinal Steel	Shear hoops (critical region)	Joint shear hoops
C1	1100×1100	28Ø40	5Ø10@150	5Ø10@130
C1A	800×1200	30Ø32	4Ø10@125	4Ø10@110
C1B	500×1800	32Ø32	4Ø10@125	4Ø10@110
C2	1200×1200	30Ø40	5Ø10@150	5Ø10@130
C3	850×850	22Ø32	4Ø10@125	4Ø10@110
C4	850×850	24Ø25	4Ø10@100	4Ø10@100
C5	850×850	26Ø32	4Ø10@125	4Ø10@110
C6	1200×1200	30Ø40	5Ø10@150	5Ø10@130
C7	1000×1000	28Ø32	5Ø10@125	5Ø10@110
C8	1200×1200	30Ø40	5Ø10@150	5Ø10@130
C9	1200×1200	30Ø40	5Ø10@150	5Ø10@130
C10	1100×1100	28Ø40	5Ø10@150	5Ø10@130
C11	1000×1000	20Ø32	5Ø10@125	5Ø10@110
C12	1000×1000	30Ø25	5Ø10@100	5Ø10@100
C13	800×800	20Ø32	4Ø10@125	4Ø10@110

(iii) Column cross-section details of the 4th to 6th storeys.

Designation	Cross section	Steel reinforcement		
		Longitudinal Steel	Shear hoops (critical region)	Joint shear hoops
C1	1100×1100	28Ø40	5Ø10@150	5Ø10@130
C1A	800×1200	26Ø32	4Ø10@125	4Ø10@110
C1B	500×1800	32Ø32	4Ø10@125	4Ø10@110
C2	1200×1200	30Ø40	5Ø10@150	5Ø10@130
C3	850×850	22Ø32	4Ø10@125	4Ø10@110
C4	850×850	20Ø25	4Ø10@100	4Ø10@100
C5	850×850	26Ø32	4Ø10@125	4Ø10@110
C6	1100×1100	28Ø40	5Ø10@150	5Ø10@130
C7	1000×1000	28Ø32	5Ø10@125	5Ø10@110
C8	900×900	18Ø32	5Ø10@125	5Ø10@110
C9	900×900	28Ø32	5Ø10@125	5Ø10@110
C10	900×900	22Ø32	5Ø10@125	5Ø10@110

(iv) Column cross-section details of the 7th to 9th storeys.

Designation	Cross section	Steel reinforcement		
		Longitudinal Steel	Shear hoops (critical region)	Joint shear hoops
C1	1100×1100	28Ø40	5Ø10@150	5Ø10@130
C1A	800×1200	20Ø32	4Ø10@125	4Ø10@110
C1B	500×1800	32Ø32	4Ø10@125	4Ø10@110
C2	1200×1200	30Ø40	5Ø10@150	5Ø10@130
C3	850×850	26Ø25	4Ø10@100	4Ø10@100
C4	850×850	20Ø25	4Ø10@100	4Ø10@100
C5	850×850	28Ø25	4Ø10@100	4Ø10@100
C6	1100×1100	28Ø40	5Ø10@150	5Ø10@130
C7	1000×1000	28Ø32	5Ø10@125	5Ø10@110
C8	900×900	18Ø32	5Ø10@125	5Ø10@110
C9	900×900	24Ø32	5Ø10@125	5Ø10@110
C10	900×900	18Ø32	5Ø10@125	5Ø10@110

(v) Column cross-section details of the 10th to 12th storeys.

Designation	Cross section	Steel reinforcement		
		Longitudinal Steel	Shear hoops (critical region)	Joint shear hoops
C1	1000×1000	28Ø32	5Ø10@125	5Ø10@110
C1A	800×1200	20Ø32	4Ø10@125	4Ø10@110
C1B	500×1800	30Ø32	4Ø10@125	4Ø10@110
C2	1100×1100	26Ø40	5Ø10@150	5Ø10@130
C3	750×750	26Ø25	4Ø10@100	4Ø10@100
C4	750×750	18Ø25	4Ø10@100	4Ø10@100
C5	750×750	28Ø25	4Ø10@100	4Ø10@100
C6	1000×1000	28Ø32	5Ø10@125	5Ø10@110
C7	900×900	28Ø32	5Ø10@125	5Ø10@110
C8	800×800	24Ø25	4Ø10@100	4Ø10@100
C9	800×800	22Ø32	4Ø10@125	4Ø10@110
C10	800×800	14Ø32	4Ø10@125	4Ø10@110

(vi) Column cross-section details of the 13th to 15th storeys.

Designation	Cross section	Steel reinforcement		
		Longitudinal Steel	Shear hoops (critical region)	Joint shear hoops
C1	950×950	24Ø32	4Ø10@125	4Ø10@110
C1A	800×1000	26Ø25	4Ø10@100	4Ø10@100
C1B	500×1800	28Ø32	4Ø10@125	4Ø10@110
C2	1000×1000	20Ø40	5Ø10@150	5Ø10@130
C3	750×750	22Ø25	4Ø10@100	4Ø10@100
C4	750×750	18Ø25	4Ø10@100	4Ø10@100
C5	750×750	20Ø25	4Ø10@100	4Ø10@100
C6	950×950	20Ø32	5Ø10@125	5Ø10@110
C7	900×900	24Ø32	5Ø10@125	5Ø10@110
C8	800×800	22Ø25	4Ø10@100	4Ø10@100
C9	800×800	20Ø32	4Ø10@125	4Ø10@110
C10	800×800	14Ø32	4Ø10@125	4Ø10@110

(vii) Column cross-section details of the 16th to 18th storeys.

Designation	Cross section	Steel reinforcement		
		Longitudinal Steel	Shear hoops (critical region)	Joint shear hoops
C1	900×900	20Ø32	5Ø10@125	5Ø10@110
C1A	700×900	20Ø25	4Ø10@100	4Ø10@100
C1B	500×1800	24Ø32	4Ø10@125	4Ø10@110
C2	900×900	18Ø32	5Ø10@125	5Ø10@110
C3	650×650	20Ø25	4Ø10@100	4Ø10@100
C4	600×600	16Ø25	4Ø10@100	4Ø10@100
C5	650×650	16Ø25	4Ø10@100	4Ø10@100
C6	850×850	18Ø32	4Ø10@125	4Ø10@110
C7	800×800	20Ø32	4Ø10@125	4Ø10@110
C8	650×650	20Ø25	4Ø10@100	4Ø10@100
C9	700×700	16Ø32	4Ø10@125	4Ø10@110
C10	650×650	12Ø32	4Ø10@125	4Ø10@110

(viii) Column cross-section details of the 19th and 20th storeys.

Designation	Cross section	Steel reinforcement		
		Longitudinal Steel	Shear hoops (critical region)	Joint shear hoops
C1	750×750	24Ø25	4Ø10@100	4Ø10@100
C1A	700×900	22Ø25	4Ø10@100	4Ø10@100
C1B	500×1800	28Ø32	4Ø10@125	4Ø10@110
C2	700×700	24Ø25	4Ø10@100	4Ø10@100
C3	550×550	16Ø25	4Ø10@100	4Ø10@100
C4	550×550	16Ø25	4Ø10@100	4Ø10@100
C5	550×550	16Ø25	4Ø10@100	4Ø10@100
C6	700×700	22Ø25	4Ø10@100	4Ø10@100
C7	800×800	22Ø25	4Ø10@100	4Ø10@100
C8	550×550	16Ø25	4Ø10@100	4Ø10@100
C9	600×600	16Ø25	4Ø10@100	4Ø10@100
C10	600×600	14Ø25	4Ø10@100	4Ø10@100

Table A5-2 Cross-section details of the girders and beams of irregular 20-storey RC P-structure (all dimensions are in millimetres).

Section dimension		Steel reinforcement		
Designation	Cross section	Longitudinal Steel		Shear hoops (critical region)
		Bottom	Top	
G1	600×1000	7Ø32	6Ø25	Ø8@160
G2	600×900	6Ø32	5Ø25	Ø8@160
G3	600×1100	8Ø32	7Ø25	Ø8@160
G4	500×800	6Ø25	5Ø20	Ø8@130
G5	600×850	5Ø32	5Ø25	Ø8@150
G6	400×700	5Ø25	4Ø20	Ø8@140
G7	400×600	5Ø20	4Ø20	Ø8@110
WG	350×500	2Ø25	3Ø25	Ø8@110
B1	400×700	5Ø25	3Ø20	Ø8@140
B2	350×550	4Ø20	3Ø20	Ø8@100
B3	250×400	2Ø20	3Ø25	Ø8@80